VERSLAGEN EN VERHANDELINGEN

REPORTS AND TRANSACTIONS

NATIONAAL LUCHTVAARTLABORATORIUM

NATIONAL AERONAUTICAL RESEARCH INSTITUTE

AMSTERDAM

XXI — 1959

CONTENTS.

CCL Class. D 050 : D 031

REPORT F. 184

A Simplified Method for the Calculation of Three-Dimensional Laminar Boundary Layers

by

J. A. ZAAT.

Summary.

By aid of the assumption that the boundary layer velocities in the direction perpendicular to the local free flow are small compared with those in the direction parallel to this flow, it is possible to approximate the momentum equations for three-dimensional laminar boundary layers by two total differential equations of the first order. The boundary layer quantities in the direction of the local free flow are calculated by neglecting the boundary layer cross flow but taking into account the three-dimensional character of the potential flow. This only requires the evaluation of an integral. Thereafter, the cross flow is calculated by using the results for the main flow, which leads to an integral equation.

The simplified method has been applied to the flow about a yawed ellipsoid at zero incidence. The results agree very well with those obtained from the complete momentum equations.

This investigation has been performed under contract with the Netherlands Aircraft Development Board. (N. I. V.).

Contents.

Acknowledgements. The author acknowledges thankfully the aid of dr. VAN DE VOOREN in bringing the report in its final form. The numerical calculations have been performed at the NLL Computing Office by H. MOELEE.

List of symbols.

x, y, z	Cartesian coordinates.
ξ, η, ζ	orthogonal, curvilinear coordinates.
φ, ψ	streamline coordinates.
φ	velocity potential.
U, V, W	velocity components of the potential flow in the ξ, η, ζ-system.
$\overline{U}, \overline{V}, \overline{W}$	velocity components of the potential flow in the x, y, z-system.
u, v, w	velocity components of the boundary layer flow in the ξ, η, ζ-systeem.
h_1, h_2	see eq. (2.2).
p	pressure.
ρ^*	air density.
ν	kinematic coefficient of viscosity.
T	square of the potential flow velocity.
ρ	see Sec. 5.
δ_i, Δ_i	displacement thicknesses, see eq. (2.9).
$\vartheta_{ij}, \theta_{ij}$	momentum thicknesses, see eq. (2.9).
σ	parameter for profile in flow direction.
Ω	parameter for profile in direction perpendicular to free flow.
$\overline{\zeta}$	$\dfrac{\zeta}{\sqrt{\sigma\nu}}$
u_1	$\dfrac{u}{\sqrt{T}}$
u_2	$\dfrac{v}{\sqrt{T}}$
f, g, h	see eq. (3.2).
M, N, Λ	see eqs. (3.1) and (3.3).
$r(s)$	radius of the axially symmetric body in the section s.
g	$1 + z_x^2 + z_y^2$.

$z_x = \frac{\partial z}{\partial x}$, $z_y = \frac{\partial z}{\partial y}$, $z = z(x, y)$ is equation of the body.

$\frac{\delta}{\delta x} = \frac{\partial}{\partial x} + z_x \frac{\partial}{\partial z}$, $\frac{\delta}{\delta y} = \frac{\partial}{\partial y} + z_y \frac{\partial}{\partial z}$ are differentiations where y or x are kept constant, but z is considered as function of x and y.

1 Introduction.

In a series of reports (refs. 1—4) a method for the calculation of three-dimensional laminar boundary layers has been described and applied to the case of a three-axial ellipsoid at zero incidence. This method, which was based upon the complete momentum equations for the boundary layer in the directions parallel and perpendicular to the local potential flow, required extensive calculations since the basic equations consisted of a set of two partial differential equations with two unknown functions. These functions represented the parameters which gave the required freedom in the prescribed boundary layer profiles in the two directions mentioned above.

In the present report a simplification of the method is presented. It is assumed that in the momentum equation for the main flow the cross flow terms are small and may be neglected. There remains a total differential equation which can be solved in the form of a simple integral and which yields a result similar to the well-known formulae of Thwaites (ref. 5) and Truckenbrodt (ref. 6). With its solution, the boundary layer in the direction of the potential flow is known.

In the momentum equation for the cross flow the result obtained for the boundary layer profile in the direction of the main flow is substituted. *The remaining total differential equation can then* be solved with the aid of a relatively simple numerical procedure.

The simplified theory is applied to the case of the ellipsoid at zero angle of incidence, which has been investigated before. It appears that the differences in results between the simplified and the former, more accurate, method are quite small.

The general formulae of the present theory have been simplified further for the special cases of the yawed infinite cylinder, two-dimensional flow and axially symmetric flow.

2 The momentum equations in streamline coordinates.

The equations for the boundary layer flow about a body

$$z = z(x, y) \tag{2.1}$$

given in Cartesian coordinates $x, y, z,$ will be determined. A set of orthogonal, curvilinear coordinates ξ, η, ζ of which ξ and η are on the surface of the body and ζ along the outward normal of the body will be used. In these coordinates the line element assumes the form

$$ds^2 = h_1^2 d\xi^2 + h_2^2 d\eta^2 + h_3^2 d\zeta^2 \tag{2.2}$$

where h_1 and h_2 will be considered as functions of ξ and η only (which means that the radius of curvature is large compared with the boundary layer thickness), while h_3 will be taken equal to 1.

The equations of motion for the boundary layer can be written in the following form (see ref. 2)

$$\left.\begin{aligned} \frac{u}{h_1}\frac{\partial u}{\partial \xi} + \frac{v}{h_2}\frac{\partial u}{\partial \eta} + w\frac{\partial u}{\partial \zeta} + \frac{uv}{h_1 h_2}\frac{\partial h_1}{\partial \eta} - \frac{v^2}{h_1 h_2}\frac{\partial h_2}{\partial \xi} &= -\frac{1}{h_1}\frac{\partial\left(\frac{p}{\rho^*}\right)}{\partial \xi} + \nu\frac{\partial^2 u}{\partial \zeta^2} \\ \frac{u}{h_1}\frac{\partial v}{\partial \xi} + \frac{v}{h_2}\frac{\partial v}{\partial \eta} + w\frac{\partial v}{\partial \zeta} + \frac{uv}{h_1 h_2}\frac{\partial h_2}{\partial \xi} - \frac{u^2}{h_1 h_2}\frac{\partial h_1}{\partial \eta} &= -\frac{1}{h_2}\frac{\partial\left(\frac{p}{\rho^*}\right)}{\partial \eta} + \nu\frac{\partial^2 v}{\partial \zeta^2} \end{aligned}\right\} \tag{2.3}$$

where u, v, w are the boundary layer velocity components in ξ, η and ζ directions, p the pressure, ρ^* the air density and ν the kinematic coefficient of viscosity.

The equation of continuity is

$$\frac{1}{h_1 h_2}\frac{\partial}{\partial \xi}(h_2 u) + \frac{1}{h_1 h_2}\frac{\partial}{\partial \eta}(h_1 v) + \frac{\partial w}{\partial \zeta} = 0. \tag{2.4}$$

The pressure can be eliminated from eqs. (2.3) by aid of the free stream equations. Using the continuity equation for eliminating w and integrating with respect to ζ, the momentum equations are obtained, as has been performed by Timman in ref. 2.

A simplification of the result (also given in ref. 2) is obtained when streamline coordinates are used. Assuming that there exists no vorticity component normal to the surface, a surface potential φ and a surface streamfunction ψ may be introduced by

$$\begin{aligned} d\varphi &= U\,h_1 d\xi + V\,h_2 d\eta = \sqrt{U^2 + V^2}\,ds_1 = \sqrt{T}\,.\,ds_1\,, \\ d\psi &= \sqrt{\rho}(V\,h_1 d\xi - U\,h_2 d\eta) = \sqrt{\rho T}\,.\,ds_2\,. \end{aligned} \tag{2.5}$$

The meaning of the symbol ρ will be explained in Sec. 5. U and V are the free stream velocity components of the potential flow in ξ and η direction. ds_1 and ds_2 are the lengths of line-elements parallel and perpendicular to the streamline. The complete line element becomes equal to

$$ds^2 = \frac{d\varphi^2}{T} + \frac{d\psi^2}{\rho T} + d\zeta^2, \qquad T = U^2 + V^2. \tag{2.6}$$

This expression becomes identical to (2.2) if $d\xi$ and $d\eta$ are taken equal to $d\varphi$ and $d\psi$ respectively, while

$$h_1 = \frac{1}{\sqrt{T}} \text{ and } h_2 = \frac{1}{\sqrt{\rho T}}. \tag{2.7}$$

In the system of streamline coordinates one has $V = 0$.

The momentum equations have been derived in Appendix A and take the following form

$$\frac{\partial(\sqrt{\sigma}\theta_{11})}{\partial\varphi} + \sqrt{\rho}\,\frac{\partial(\sqrt{\sigma}\theta_{12})}{\partial\psi} + \frac{\sqrt{\sigma}}{2T}\frac{\partial T}{\partial\varphi}(\theta_{11} + \theta_{22} + \Delta_1) - \frac{\sqrt{\sigma}}{2\rho}\frac{\partial\rho}{\partial\varphi}(\theta_{11} - \theta_{22}) = \frac{1}{T\sqrt{\sigma}}\left(\frac{\partial u_1}{\partial\bar{\zeta}}\right)_{\bar{\zeta}=0}$$

$$\frac{\partial(\sqrt{\sigma}\,\theta_{21})}{\partial\varphi} + \sqrt{\rho}\,\frac{\partial(\sqrt{\sigma}\,\theta_{22})}{\partial\psi} + \frac{\sqrt{\sigma\rho}}{2T}\frac{\partial T}{\partial\psi}(\theta_{11} + \theta_{22} + \Delta_1) - \frac{\sqrt{\sigma}}{\rho}\frac{\partial\rho}{\partial\varphi}\theta_{21} = \frac{1}{T\sqrt{\sigma}}\left(\frac{\partial u_2}{\partial\bar{\zeta}}\right)_{\bar{\zeta}=0}. \tag{2.8}$$

The displacement and momentum thicknesses are given by $\delta_i = \Delta_i\sqrt{\sigma\nu}$ and $\vartheta_{ij} = \theta_{ij}\sqrt{\sigma\nu}$ respectively, where

$$\begin{aligned} \Delta_1 &= \int_0^\infty (1-u_1)\,d\bar{\zeta} & \Delta_2 &= -\int_0^\infty u_2\,d\bar{\zeta} \\ \theta_{11} &= \int_0^\infty u_1(1-u_1)\,d\bar{\zeta} & \theta_{21} &= -\int_0^\infty u_1u_2\,d\bar{\zeta} \\ \theta_{12} &= \int_0^\infty u_2(1-u_1)\,d\bar{\zeta} & \theta_{22} &= -\int_0^\infty u_2^2\,d\bar{\zeta} \end{aligned} \tag{2.9}$$

and

$$u_1 = \frac{u}{\sqrt{T}} \qquad u_2 = \frac{v}{\sqrt{T}}, \qquad \bar{\zeta} = \frac{\zeta}{\sqrt{\sigma\nu}}. \tag{2.10}$$

The coordinate ζ has been transformed into $\bar{\zeta}$ by aid of eq. (2.10) in order to be able to write the boundary layer profiles in a normalised form. $\sqrt{\sigma\nu}$ is proportional to the boundary layer thickness.

3 The boundary layer profiles.

In accordance with ref. 3, the boundary layer profiles are given by

$$\begin{aligned} u_1 &= f(\bar{\zeta}) - \Lambda\, g(\bar{\zeta}) - N h(\bar{\zeta}) \\ u_2 &= -\Omega^2 M g\left(\frac{\bar{\zeta}}{\Omega}\right) \end{aligned} \tag{3.1}$$

were

$$1 - f(\bar{\zeta}) = 2\,g(\bar{\zeta}) + e^{-\bar{\zeta}^2} = 2\,h(\bar{\zeta}) + (1+\bar{\zeta}^2)e^{-\bar{\zeta}^2} =$$

$$= \frac{2}{3\sqrt{\pi}}\,\bar{\zeta}\,e^{-\bar{\zeta}^2} + \frac{2}{\sqrt{\pi}}\int_{\bar{\zeta}}^{\infty} e^{-t^2}\,dt. \tag{3.2}$$

The functions f, g and h are represented in fig. 1.

For $\bar{\zeta} = 0$ they satisfy the conditions

$$f = g = h = f'' = h'' = f''' = g''' = h''' = f'''' = 0$$

$$f' = -2\,g' = -2\,h' = \frac{4}{3\sqrt{\pi}}$$

$$g'' = 1$$

$$g'''' = -h'''' = -6.$$

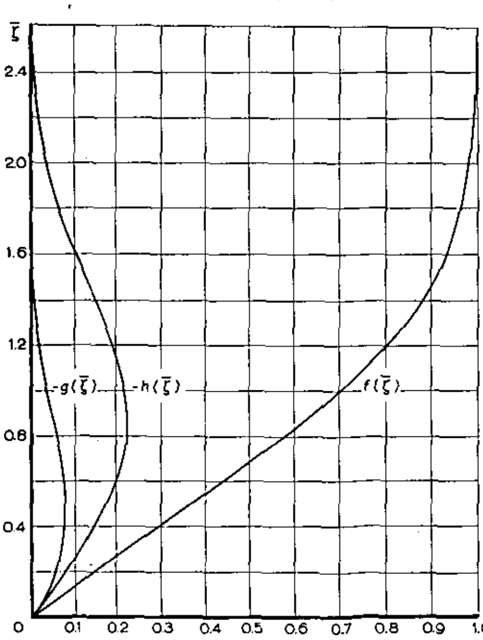

Fig. 1. The boundary layer profiles $\bar{\zeta} = \frac{\zeta}{\sqrt{\sigma\nu}} = \frac{\zeta}{l}\sqrt{\frac{Re}{\bar{\sigma}}}$ where $\bar{\sigma} = \sigma\frac{U_\infty}{l}$.

The boundary layer thickness for the cross flow (u_2) is a factor Ω larger than for the main flow (u_1). By aid of the boundary conditions at the body it can be shown (Appendix A) that

$$\Lambda = \tfrac{1}{2}\,\sigma\,\frac{\partial T}{\partial \varphi}\,, \qquad M = \tfrac{1}{2}\,\sigma\,\sqrt{\rho}\,\frac{\partial T}{\partial \psi}\,. \tag{3.3}$$

$$N = 0 \text{ if } \Lambda > 0 \text{ (accelerated flow)}, \quad N = \Lambda \text{ if } \Lambda < 0 \text{ (retarded flow)}. \tag{3.4}$$

The shear stress in flow direction at the body, $\left(\frac{\partial u_1}{\partial \bar\zeta}\right)_{\bar\zeta = 0}$, vanishes for $\Lambda = -1$. The point where $\Lambda = -1$ will be taken as the point of laminar separation.

When the potential flow is assumed to be known the momentum equations (2.8) are a set of differential equations for the quantities σ and Ω, determining the boundary layer thicknesses in the two directions.

4 Simplification of the momentum equations.

An accurate solution of the momentum equations (2.8) has been given in ref. 3 for the case of a yawed ellipsoid at zero angle of incidence. This same case will now be solved by aid of certain simplifications to be made in the equations (2.8). The fundamental assumption of the present report is that the cross flow u_2 is small of order δ with regard to the main flow u_1. It then follows that

$$\theta_{11} = 0(1),\ \ \theta_{12} = 0(\delta),\ \ \theta_{22} = 0(\delta^2),\ \ \Delta_1 = 0(1),\ \ \Delta_2 = 0(\delta).$$

The cross flow u_2 vanishes both for $\bar\zeta \to 0$ and for $\bar\zeta \to \infty$. Hence, the values of u_2 between these limits must indeed become rather large before the orders of magnitude for θ_{11} etc. as given above, no longer hold. Perhaps for swept wings at large angles of incidence, the assumption would become less accurate. It is intended to perform a separate investigation concerning this point, but in the present case, i. e. the ellipsoid under zero angle of attack, the results yield a very satisfactory confirmation of this assumption. It may be added, that the possibility of this assumption is an essential advantage of the use of streamline coordinates.

Since there is, in general, no difference in order of magnitude between the operators $\frac{\partial}{\partial \varphi}$ and $\sqrt{\rho}\,\frac{\partial}{\partial \psi}$ applied to any flow quantity, the equations (2.8) may be approximated by

$$\begin{aligned}
&\frac{\partial}{\partial \varphi}\left(\sqrt{\sigma}\,.\,\theta_{11}\right) + \frac{\sqrt{\sigma}}{2\,T}\,\frac{\partial T}{\partial \varphi}\,(\theta_{11} + \Delta_1) - \frac{\sqrt{\sigma}}{2\,\rho}\,\theta_{11}\,\frac{\partial \rho}{\partial \varphi} = \frac{1}{T\sqrt{\sigma}}\,\frac{2}{3\sqrt{\pi}}\,(2 + \Lambda + N)\\
&\frac{\partial}{\partial \varphi}\left(\sqrt{\sigma}\,.\,\theta_{21}\right) + \frac{\sqrt{\sigma\rho}}{2\,T}\,\frac{\partial T}{\partial \psi}\,(\theta_{11} + \Delta_1) - \frac{\sqrt{\sigma}}{\rho}\,\theta_{21}\,\frac{\partial \rho}{\partial \varphi} = \frac{1}{T\sqrt{\sigma}}\,\frac{2}{3\sqrt{\pi}}\,M\Omega.
\end{aligned} \tag{4.1}$$

After multiplication with $2\,T\,\theta_{11}\,\sqrt{\sigma}$ and using (3.3), the first of these equations can be brought in the form

$$\rho\,\frac{\partial}{\partial \varphi}\left(\frac{T\sigma}{\rho}\,\theta_{11}^{\,2}\right) = \frac{4}{3\sqrt{\pi}}\,\theta_{11}(2 + \Lambda + N) - 2\,\Lambda\,\theta_{11}\Delta_1\,. \tag{4.2}$$

The right hand side of this equation,

$$H(\Lambda) = \frac{4}{3\sqrt{\pi}}\,\theta_{11}(2 + \Lambda + N) - 2\,\Lambda\,\theta_{11}\Delta_1$$

as well as θ_{11} have been plotted in fig. 2 for the interval $-1 < \Lambda < 1$, which contains all prevailing values of Λ. It follows from fig. 2 that the approximations

$$H(\Lambda) = 0.436 - 2a^2\Lambda\,, \qquad \theta_{11} = a = 0.293$$

give reasonable accuracy. Inserting this in eq. (4.2) and multiplying with $\frac{T}{\rho a^2}$, one obtains

$$\frac{\partial}{\partial \varphi}\left(\frac{T^2\sigma}{\rho}\right) = \frac{0.436}{a^2}\,\frac{T}{\rho}\,. \tag{4.3}$$

Inserting the value of a and integrating, the result is

$$\sigma = 5.08\,\frac{\rho}{T^2}\left\{c_0(\varphi_0) + \int_{\varphi_0}^{\varphi} \frac{T}{\rho}\,d\varphi\right\} \tag{4.4}$$

where φ_0 is any value of φ and 5.08 $c_0(\varphi_0)$ denotes the value of $\frac{T^2\sigma}{\rho}$ for $\varphi = \varphi_0$.

Eq. (4.4) contains the final result determining the properties of the boundary layer in the direction of the main flow.

Consider now the equation for the cross flow, that is the second equation (4.1). Multiplying with $\sqrt{\sigma}$ and using eq. (3.3) brings this equation in the form

$$\frac{\rho^2}{2\,\theta_{21}}\,\frac{\partial}{\partial\varphi}\left(\frac{\sigma\theta_{21}{}^2}{\rho^2}\right)=\frac{M}{T}\left(\frac{2}{3\sqrt{\pi}}\,\Omega-a-\Delta_1\right). \tag{4.5}$$

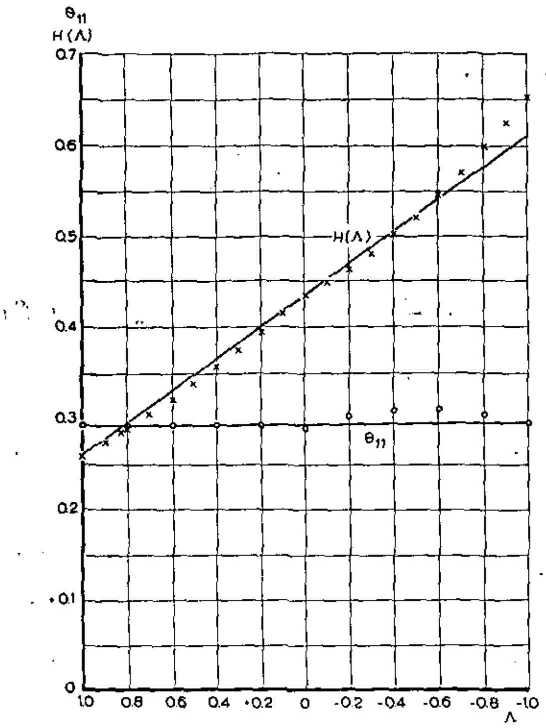

Fig. 2. $H(\Lambda)$ and ϑ_{11} as functions of Λ.
× ⊙ calculated from the given boundary layer profiles.
—— approximated.

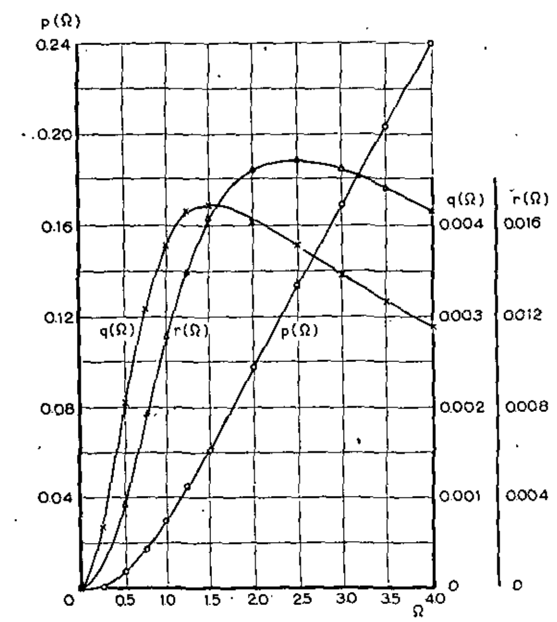

Fig. 3. The functions $p(\Omega)$, $q(\Omega)$ and $r(\Omega)$.
—— calculated from the given boundary layer profiles.
⊙ × △ approximate values.

This equation yields after integration the following relation

$$|\,\theta_{21}(\Omega)\,|=c_1(\varphi_0)\,.\,\frac{\rho}{\sqrt{\sigma}}\,e^{\int\limits_{\varphi_0}^{\varphi}\frac{M}{T\sigma\theta_{21}}\left(\frac{2}{3\sqrt{\pi}}\Omega-a-\Delta_1\right)d\varphi} \tag{4.6}$$

where $c_1(\varphi_0)$ denotes the value of $\dfrac{\sqrt{\sigma}\,|\,\theta_{21}\,|}{\rho}$ for $\varphi=\varphi_0$.

Eq. (4.6) is an equation for Ω. θ_{21} may be expressed as function of Ω, viz.

$$\theta_{21}=-\int\limits_0^{\infty}u_1u_2d\zeta=-\Omega^2M\,[p(\Omega)+\Lambda\,q(\Omega)+Nr(\Omega)\,]. \tag{4.7}$$

The functions $p(\Omega)$, $q(\Omega)$, $r(\Omega)$ can be calculated by aid of the given boundary layer profiles (3.1). However, they become very complicated functions of Ω. A satisfactory approximation is given by the expressions (fig. 3)

$$\left.\begin{aligned}p(\Omega)&=-0.00522+0.01705\,\Omega+0.01800\,\Omega^2\\q(\Omega)&=-0.00106+0.00756\,\Omega-0.00270\,\Omega^2\\r(\Omega)&=-0.00593+0.02148\,\Omega-0.00447\,\Omega^2\end{aligned}\right\}\ \text{for } 0.25<\Omega<1.5$$

$$\left.\begin{aligned}p(\Omega)&=-0.04664+0.07166\,\Omega\\q(\Omega)&=0.00603-0.00073\,\Omega-0.00108\,\frac{1}{\Omega}\\r(\Omega)&=0.03894-0.00405\,\Omega-0.02494\,\frac{1}{\Omega}\end{aligned}\right\}\ \text{for } 1.5<\Omega \tag{4.8}$$

$$\Delta_1=0.752253-0.066987\,\Lambda-0.288544\,N. \tag{4.9}$$

The functions $\sigma(\varphi)$ and $\Omega(\varphi)$ are now to be calculated from the equations (4.4) and (4.6) respectively. In order to perform this, it is necessary to determine at first the function ρ as well as $c_0(\varphi_0)$ and $c_1(\varphi_0)$. *It will be assumed throughout that the potential flow about the body is known.*

5 The function ρ.

This function is determined by the equation of continuity (2.4) applied to the potential flow. Replacing $d\xi$ and $d\eta$ by $d\varphi$ and $d\psi$ respectively, using eqs. (2.7) for h_1 and h_2 and remarking that $U = \sqrt{T}$, since $V = 0$, one obtains

$$T\sqrt{\rho}\,\frac{\partial}{\partial\varphi}\left(\frac{1}{\sqrt{\rho}}\right) + \frac{\partial W}{\partial\zeta} = 0, \qquad (5.1)$$

where W is the component of the potential flow directed normal to the body ($W = 0$ at the surface of the body $\zeta = 0$). It is seen from (5.1) that the dependence of ρ upon ψ is undetermined. In fact, ρ may be multiplied with any function of ψ. This only changes the ψ-scale as is seen from eq. (2.5) where $d\psi$ has been defined.

Eq. (5.1) can be reduced to

$$\frac{1}{\rho}\,\frac{d\rho}{d\varphi} = \frac{2}{T}\,\frac{\partial W}{\partial\zeta}. \qquad (5.2)$$

It will be assumed that the potential flow at the body surface is given by the velocity components $\overline{U}$ and $\overline{V}$ in x- and y-directions. Taking this into account, it is preferable to reduce eq. (5.2) to a form containing $\overline{U}$ and $\overline{V}$ instead of W. In Appendix B it is shown, that such a form is

$$\frac{1}{\rho g}\,\frac{\partial(\rho g)}{\partial\varphi} = -\frac{2}{T}\left(\frac{\delta\overline{U}}{\delta x} + \frac{\delta\overline{V}}{\delta y}\right), \qquad (5.3)$$

where $g = 1 + z_x^2 + z_y^2$. The symbol $\frac{\delta}{\delta x}$ denotes differentiation to x, with y constant, but z considered as function of x and y (eq. 2.1). Hence

$$\frac{\delta}{\delta x} = \frac{\partial}{\partial x} + z_x\frac{\partial}{\partial z}.$$

The differentiation in the left hand side of eq. (5.3) should be performed along a streamline (ψ constant). According to Appendix B, one has

$$T\,\frac{\partial}{\partial\varphi} = \overline{U}\,\frac{\delta}{\delta x} + \overline{V}\,\frac{\delta}{\delta y}. \qquad (5.4)$$

The function ρ is to be calculated from eq. (5.3).

6 Calculation of the thickness parameters σ and Ω.

The integration in eqs. (4.4) and (4.6) are to be performed along a streamline. Along a streamline the relations

$$\frac{dx}{\overline{U}} = \frac{dy}{\overline{V}} = \frac{dz}{\overline{W}} = \frac{ds_1}{\sqrt{T}} = \frac{d\varphi}{T},$$

$$\text{where } T = \overline{U}^2 + \overline{V}^2 + \overline{W}^2 \qquad (6.1)$$

exist. The projection of the streamline upon the x,y-plane is obtained by integration of

$$\frac{dy}{dx} = \frac{\overline{V}}{\overline{U}}.$$

The corresponding z-coordinates follow from eq. (2.1), while $\overline{W}$ follows from the condition of tangential flow as

$$\overline{W} = \overline{U}\,z_x + \overline{V}\,z_y. \qquad (6.2)$$

In the integrals occurring in (4.4) and (4.6) the integration element may be replaced by $\frac{T}{\overline{U}}\,dx$ or $\frac{T}{\overline{V}}\,dy$.

A further complication in (4.6) is the factor M, which is also determined by the potential flow as is seen from eq. (3.3). The difficulty is the differentiation to ψ. However, it is also shown in Appendix B that

$$T\sqrt{\rho g}\,\frac{\partial}{\partial\psi} = \frac{\delta\varphi}{\delta y}\,\frac{\delta}{\delta x} - \frac{\delta\varphi}{\delta x}\,\frac{\delta}{\delta y}, \qquad (6.3)$$

$$\text{where } \frac{\delta\varphi}{\delta x} = \overline{U}(1 + z_x^2) + \overline{V}\,z_x z_y$$

$$\text{and } \frac{\delta\varphi}{\delta y} = \overline{V}\,(1 + z_y^2) + \overline{U} z_x z_y. \qquad (6.4)$$

Finally, there remains the determination of the integration constants c_0 and c_1. For a body of small thickness there will be near the leading edge (equator) a streamline, separating the flow passing along the one side from that passing along the other side of the body. For sake of convenience this dividing line will be called henceforth equator, also if the body is at incidence. The streamlines have in the stagnation point a contact of very high order with the equator (fig. 4 and ref. 1). The calculation of σ and Ω along the equator and along streamlines in the immediate vicinity of the equator occurs by an iteration procedure (ref. 3), using eqs. (4.3) and (4.5) in the form

$$\sigma\,\frac{\partial}{\partial\varphi}\left(\frac{T^2}{\rho}\right) + \frac{T^2}{\rho}\,\frac{\partial\sigma}{\partial\varphi} = \frac{0.436}{a^2}\,\frac{T}{\rho}$$

$$\tfrac{1}{2}\,\rho^2\,\theta_{21}\,\frac{\partial}{\partial\varphi}\left(\frac{\sigma}{\rho^2}\right) + \sigma\,\frac{\partial\theta_{21}}{\partial\varphi} =$$

$$= \frac{M}{T}\left(\frac{2}{3\sqrt{\pi}}\,\Omega - a - \Delta_1\right). \qquad (6.5)$$

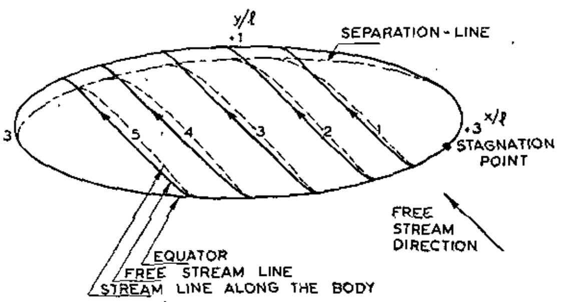

Fig. 4. The projections on the x,y-plane of
(i) potential flow streamlines ————
(ii) streamlines along the body — — — —
(iii) separation line —·—·—

The iteration is based upon the physical consideration that σ and Ω cannot change rapidly along that part of the equator, where the flow is accelerated. Therefore: initial values for σ and Ω are obtained from eqs. (6.5) by neglecting $\frac{\partial\sigma}{\partial\varphi}$ and $\frac{\partial\Omega}{\partial\varphi}$. By numerical differentiation of the values of σ and Ω, a first approximation is obtained for $\frac{\partial\sigma}{\partial\varphi}$ and $\frac{\partial\Omega}{\partial\varphi}$. The latter values are substituted in eq. (6.5) and new values for σ and Ω are calculated. This is repeated until the values no longer change[1]).

Only for a streamline along which the flow is moving away from the equator, larger values of $\frac{\partial\sigma}{\partial\varphi}$ and $\frac{\partial\Omega}{\partial\varphi}$ are possible.

The iteration procedure has the advantage that the values of σ and Ω in the stagnation point itself are not required. These values can only be determined after difficult limiting transitions.

For calculating the flow along the point of the streamline, that is not near the equator, eqs. (4.4) and (4.6) are used, where now $c_0(\varphi_0)$ and $c_1(\varphi_0)$ are known. Eq. (4.4) offers no difficulties. Eq. (4.6) is solved as follows.

Let the values of Ω be known up to a certain value $\Omega_{i-1} = \Omega(\varphi_{i-1})$. The problem is then to find Ω_i. The value Ω_i has to satisfy the relation

$$\theta_{21}(\Omega_i) = \gamma\, e^{\int_{\varphi_{i-1}}^{\varphi_i} I\, d\varphi}$$

where
$$\gamma = c_1(\varphi_0)\, \frac{p}{\sqrt{\sigma}}\, e^{\int_{\varphi_0}^{\varphi_{i-1}} I\, d\varphi}$$

and I denotes the integrand, also occurring in eq. (4.6).

For the numerical calculation the interval has to be taken so small that the trapezoidal rule for integration may be applied. If now for Ω_i the guess $\bar{\Omega}_i$ is made, so that $\Omega_i = \bar{\Omega}_i + \Delta\Omega$, then

$$\theta_{21}(\bar{\Omega}_i) + \Delta\Omega\, \left(\frac{d\theta_{21}}{d\Omega}\right)_{\Omega=\bar{\Omega}_i} = \gamma\, e^{\frac{1}{2}\Delta\varphi \left\{ I(\Omega_{i-1}) + I(\Omega_i) \right\}}$$

or

$$\theta_{21}(\bar{\Omega}_i) + \Delta\Omega\, \left(\frac{d\theta_{21}}{d\Omega}\right)_{\Omega=\bar{\Omega}_i} =$$
$$= \gamma\, e^{\frac{1}{2}\Delta\varphi\, \left\{ I(\Omega_{i-1}) + I(\bar{\Omega}_i) \right\}} \left\{ 1 + \tfrac{1}{2}\, \Delta\varphi\Delta\Omega\, \left(\frac{dI}{d\Omega}\right)_{\Omega=\bar{\Omega}_i} \right\}.$$

The latter equation allows the determination of $\Delta\Omega$ and hence, the improvement of the guessed value $\bar{\Omega}_i$.

[1]) This procedure is possible since the equator forms a *singular line for the differential equation.* If along the equator the integration of eqs. (6.5) would be started with values of σ and Ω for which $\frac{\partial\sigma}{\partial\varphi}$ and $\frac{\partial\Omega}{\partial\varphi}$ are not small, the result is that σ and Ω would rapidly change as functions of φ until the same values as obtained in the procedure described above would be reached.

It appears in the calculation that near the highest point of each streamline Ω becomes infinitely large. Since θ_{21} should remain finite, it follows *from eqs. (4.7) and (4.8) that* M vanishes at least as $\frac{1}{\Omega^3}$. Hence

$$u_2 = -\,\Omega^2 M\, g\left(\frac{\zeta}{\Omega}\right) \approx -\,\frac{1}{\Omega}\, g\left(\frac{\zeta}{\Omega}\right) \rightarrow 0$$
$$\text{if}\ \ \Omega \rightarrow \infty\,.$$

The point where $M = 0$ is determined by the condition $\frac{\partial T}{\partial\psi} = 0$. The cross flow vanishes together with the gradient of the velocity vector in the direction perpendicular to the streamlines. Beyond the point where $M = 0$, $\frac{\partial T}{\partial\psi}$ changes sign. This makes that the sign of $c_1(\varphi_1)$ in eq. (4.6) should also be changed.

Eq. (4.4) is *the most important equation for the calculation of three dimensional flows.* This equation yields the value of σ, determining the boundary layer thickness as well as the point of laminar separation where $N = \Lambda = \frac{1}{2}\,\sigma T_{\varphi} = -1$. Eq. (4.6) serves for the calculation of the cross flow.

Finally, it may be mentioned that the criterion for laminar separation $\Lambda = -1$ is not exact. The separation line is, in fact, the envelope of the streamlines, infinitely close to the body. Since this envelope will, in general, not be perpendicular to the streamlines of the potential flow, there will remain a component of the shear stress in the direction of the potential flow streamlines. This component, however, is small and changes rapidly near *separation.* Hence, the criterion $\Lambda = -1$ *yields a good approximation for separation.*

7 The boundary layer flow about a three-axial ellipsoid.

In two former reports (ref. 3, 4) a solution has been given for the boundary layer flow about the ellipsoid

$$\frac{x^2}{a^2} + \frac{y^2}{b^2} + \frac{z^2}{c^2} = 1,$$
$$a = 3\,l,\ \ b = l,\ \ c = 0.15\,l$$

which was placed in a flow, which at infinity had the direction $(-1,\ -1,0)$.

Five streamlines of the potential flow near the body have been calculated. Their projections on the x, y-plane are shown in fig. 4.

Results for the dimensionless values $\sqrt{\sigma\, \frac{U_\infty}{l}}$ and Ω (U_∞ = speed of undisturbed flow) obtained in ref. 3 by aid of the complete differential equations (2.8) are shown in figs. 5 and 6 as drawn lines for the five streamlines. The approximate solutions obtained from eqs. (4.4) and (4.6) have also been plotted in figs. 5 and 6 as separate points. It is seen that the agreement is highly satisfactory. In comparing the results for Ω (fig. 6), it should be kept in mind that in the present calculation a better approximation for θ_{21} has been used, viz. eqs. (4.7) and (4.8). Therefore Ω has also been calculated with the approximate method of this report but using the former approximation for θ_{21}. This result is also shown in fig. 6, which is seen to agree slightly better with the drawn lines then

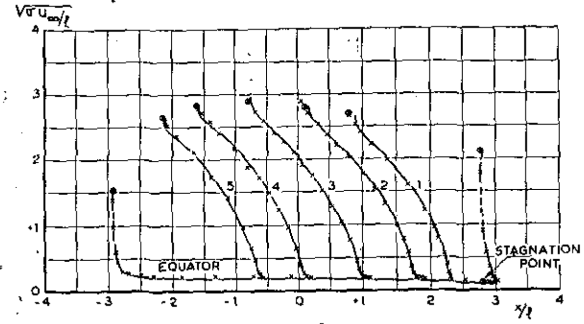

Fig. 5. $\sqrt{\sigma \frac{U_\infty}{l}}$ parameter for boundary layer thickness in main flow direction along the equator and the streamlines.
—— calculated by aid of the complete momentum equations (2.8).
× calculated by aid of the simplified equation (4.4).
⊙ points of separation.

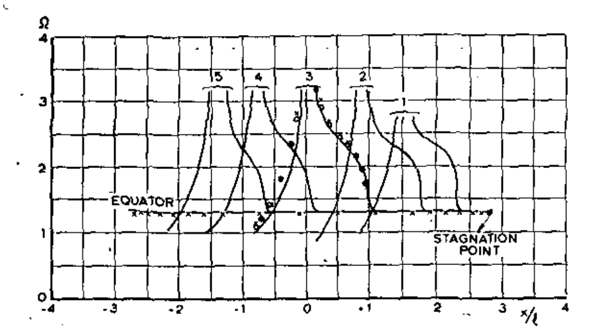

Fig. 6. Ω (ratio of boundary layer thicknesses of cross flow and main flow) as function of x/l along the equator *and along the streamlines.*
—— calculated by aid of the complete momentum equations (2.8).
× calculated from (4.6) with θ according to (4.7).
⊙ calculated from (4.6) with θ according to refs. 3 and 4.

the result obtained with the improved expression for θ_{21}.

The boundary layer profiles for the central streamline are given by figs. 7 and 8. They are calculated from eqs. (3.1) with the values obtained for Λ, N, M, σ and Ω. It is seen that separation occurs for $x/l \sim -0.780$, since for this value of x/l $\left(\frac{\partial u_1}{\partial \zeta}\right)_{\zeta=0}$ vanishes. The cross flow vanishes for values of x/l near zero. It is seen from fig. 8 that the cross flow obtained by the approximate method is slightly larger than that obtained by the more exact method, although the difference may be due to the different approximation for θ_{21}.

Fig. 9 shows the displacement thickness in dimensionless form along the aequator and the streamlines.

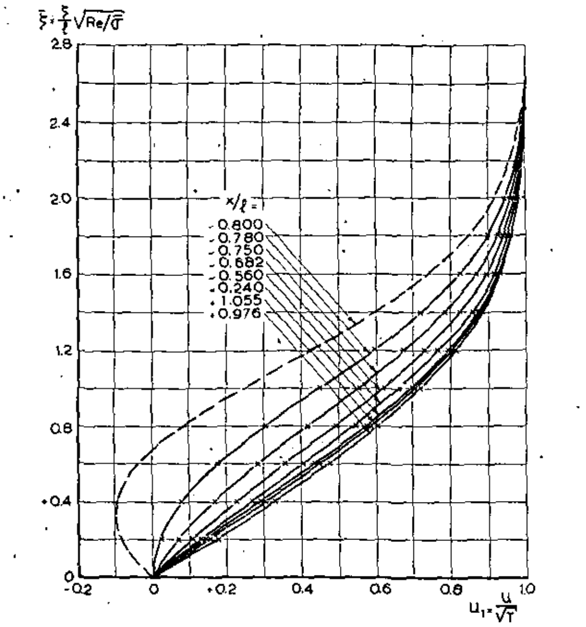

Fig. 7. The boundary layer profiles in main flow direction for various points of the central streamline.
—— calculated from the simplified method.
× calculated from the complete momentum equations.

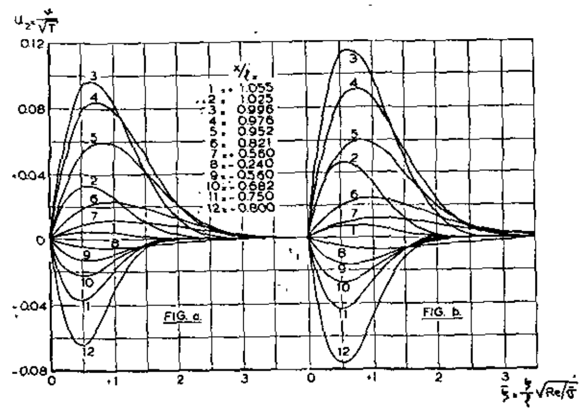

Fig. 8. The boundary layer profiles of the cross flow in various points of the central streamline.
a) calculated from the complete momentum equations.
b) calculated from the simplified method.

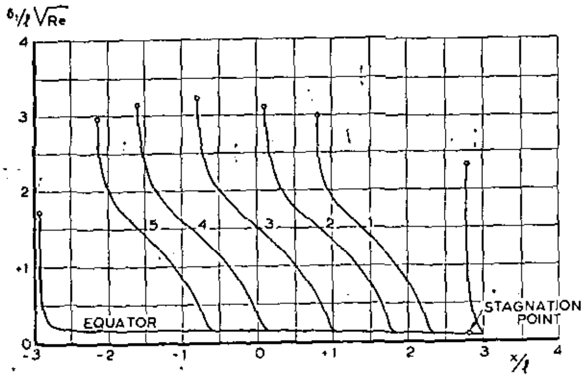

Fig. 9. The dimensionless thickness $\frac{\delta_1}{l} \sqrt{\frac{U_\infty l}{\nu}}$ as function of $\frac{x}{l}$.
⊙ Points of separation.

The direction of the streamlines in the boundary layer near the body is given by

$$\lim_{\zeta \to 0} \frac{u_2}{u_1} = \left(\frac{\partial u_2}{\partial \zeta} \Big/ \frac{\partial u_1}{\partial \zeta} \right)_{\zeta=0} = \frac{\Omega M}{2 + \Lambda + N}.$$

These streamlines as well as the line of separation have also been drawn in fig. 4.

8 Some special cases.

8.1 *The flow about a yawed, infinite cylinder.*

In the case of a yawed infinite cylinder, the y-axis will be taken in the direction of the axis of the cylinder. All quantities then are independent of y.

The function ρ is calculated from eqs. (5.3) and (5.4). The differential equation for ρ becomes

$$\frac{\delta}{\delta x} (ln\, \rho\, g) = -2 \frac{\delta}{\delta x} (ln\, \overline{U})$$

with the solution

$$\rho = \frac{A}{\overline{U}^2(1 + z_x^2)}$$

where A is an arbitrary constant.

Since

$$T = \overline{U}^2 + \overline{V}^2 + \overline{W}^2 \text{ and } \overline{W} = \overline{U} z_x \qquad \text{(see eq. (6.2))}$$

one may write also

$$\rho = \frac{A}{T - \overline{V}^2}.$$

Considering now eq. (4.4), the integration element $d\varphi$ may be replaced, when using eq. (6.1), by

$$d\varphi = \frac{T}{\sqrt{T - \overline{V}^2}} ds,$$

where $ds = \sqrt{dx^2 + dz^2}$ is the line element in a section $y =$ constant. Taking for φ_0 the velocity in a point of the stagnation line, it follows that

$$5.08\, c_0(\varphi_0) = \left(\frac{T^2 \sigma}{\rho} \right)_{\varphi_0} = 0,$$

since $\rho = \infty$ $(T - \overline{V}^2 = 0)$ along the stagnation line.

Hence, eq. (4.4) becomes

$$\sigma = \frac{5.08\, \nu}{T^2(T - \overline{V}^2)} \int_0^s T^2 \sqrt{T - \overline{V}^2}\, ds \qquad (8.1)$$

where $s = 0$ is at the stagnation point. The value of σ for $s \neq 0$ does not vanish as follows when $T - \overline{V}^2$ is expanded near $s = 0$.

In order to calculate the cross flow, eqs. (6.3) and (6.4) are used. They yield

$$T \sqrt{\rho g} \frac{\partial}{\partial \psi} = \overline{V} \frac{\delta}{\delta x}$$

or $\sqrt{\rho} \dfrac{\partial}{\partial \psi} = \dfrac{\overline{V}}{T} \dfrac{\partial}{\partial s}$, since $ds = dx \sqrt{1 + z_x^2}$.

Substituting the values for ρ and M into eq. (4.6), the result is

$$\frac{\theta_{21}(\Omega)}{M} = \frac{C\, T}{\sigma^{3/2} (T - \overline{V}^2) \dfrac{\partial T}{\partial s}}\, e^{\int_0^s \frac{1}{\sigma \sqrt{T - \overline{V}^2}} \frac{M}{\vartheta_{21}} \left(\frac{2}{3\sqrt{\pi}} \Omega - \alpha - \Delta_1 \right) ds} \qquad (8.2)$$

8.2 *Two-dimensional flow.*

For two-dimensional flow one has

$$\overline{V} = 0, \; T = \overline{U}^2 + \overline{W}^2 = U^2$$

and eq. (8.1) becomes

$$\sigma = 5.08 \frac{1}{U^6} \int_0^s U^5(s) ds. \qquad (8.3)$$

After introduction of

$$\theta^2 = \left\{ \int_0^\infty \frac{u}{U} \left(1 - \frac{u}{U} \right) d\zeta \right\}^2 = \sigma \nu \theta_{11}^2 = \sigma \nu a^2$$

where $a = 0.293$, eq. (8.3) can be brought in the form

$$\theta^2 = 0.436\, U^{-6} \nu \int_0^s U^5 ds \qquad (8.4)$$

which is identical to THWAITES' equation (ref. 5).

8.3 *Axial-symmetric flow.*

The potential flow in the direction of the axis of an axially symmetric body depends only upon the coordinate s_1 along a streamline. The function ρ could again be calculated from eq. (5.3), but it is much simpler to consider eq. (2.6). Taking the azimuth angle ψ in a circular section perpendicular to the axis as streamfunction it follows that

$$ds^2 = ds_1^2 + r^2(s_1)\, d\psi^2 = \frac{d\varphi^2}{U^2(s_1)} + r^2\, d\psi^2. \qquad (8.5)$$

By comparison of eqs. (2.6) and (8.5) it is seen that

$$\rho = \frac{1}{r^2 U^2}.$$

Eq. (4.4) then becomes

$$\sigma = \frac{5.08}{r^2 U^6} \int_0^{s_1} r^2 U^5 ds_1 \qquad (8.6)$$

which is similar to a result of TRUCKENBRODT (ref. 6).

Due to the symmetry, there exists no cross flow in this case.

9 Conclusions.

The main equation in the simplified method for the calculation of three-dimensional laminar boundary layers is eq. (4.4)

$$\sigma = 5.08 \frac{\rho}{T^2} \left\{ c_0(\varphi_0) + \int_{\varphi_0}^{\varphi} \frac{T}{\rho} d\varphi \right\}. \qquad (4.4)$$

This equation determines the boundary layer thickness $\sqrt{\sigma\nu}$ in the direction of the local free flow. The displacement and momentum thicknesses are proportional to $\sqrt{\sigma\nu}$, see eqs. (2.9), with the proportionality factors depending upon the prescribed boundary layer profiles.

In eq. (4.4) T is the square of the potential flow velocity and ρ is a function depending upon the divergence of the potential flow velocity along the body surface (see Sec. 5). This function introduces generally the three-dimensional character of the flow. As seen from eq. (5.2) ρ depends on $\partial W/d\zeta$. Assuming in a point of the surface a system of Cartesian coordinate axes ξ, η, ζ falling along the φ and ψ directions and the direction of the body normal, one has for three-dimensional flow

$$\frac{\partial W}{\partial \zeta} = -\frac{\partial U}{\partial \xi} - \frac{\partial V}{\partial \eta}.$$

For two-dimensional flow the term $\partial V/d\eta$ vanishes and eq. (4.4) may be replaced by eq. (8.3). Hence, eq. (8.3) will also yield an approximate result for the three-dimensional boundary layer provided $\partial V/d\eta$ is small. This occurs for the ellipsoid at zero incidence if the flow not too near to the equator is considered. Along the equator, however, $dV/d\eta$ is large (although $V=0$) and here, eq. (4.4) should be used, resulting in a value of σ which is much smaller than it would be for two-dimensional flow. Due to the cross flow the streamlines in the boundary layer are not parallel to those of the potential flow (see fig. 4). The boundary layer streamlines deviate from the potential flow streamlines towards the side of the center of curvature of the latter streamlines.

The envelope of the boundary layer streamlines near the body surface is the line of separation. Separation occurs in the region of decelerated flow. Approximately, separation takes place if the shear stress in the local direction of free flow vanishes, that is if $N = \Lambda = -1$. However, exactly, the shear stress perpendicular to the separation-line should vanish and since this line is not perpendicular to the free flow streamlines, the criterion $\Lambda = -1$ is indeed an approximate criterion for separation. The difference ,however, will usually be negligible.

10 References.

1. TIMMAN, R. A Calculation Method for Threedimensional Laminar Boundary Layers. NLL Report F. 66, 1951.
2. TIMMAN, R. The Theory of Threedimensional Boundary Layers. Symposium on Boundary Layer Effects in Aerodynamics. Nat. Phys. Lab. Teddington, England 1955. Paper No. 1.
3. ZAAT, J. A., SPIEGEL, E. VAN, TIMMAN, R. The Threedimensional Laminar Boundary Layer Flow about a Yawed Ellipsoid at Zero Incidence. NLL Report F. 165, 1955.
4. TIMMAN, R. und ZAAT, J. A. Eine Rechenmethode für dreidimensionale laminare Grenzschichte. 50 Jahre Grenzschichtforschung 1955. Friedr. Vieweg u. Sohn Braunschweig.
5. THWAITES, B. Approximate Calculation of the Laminar Boundary Layer. Aeron. Quart. Vol. 1 (Nov. 1949), p. 245—280.
6. TRUCKENBRODT, E. Ein Quadraturverfahren zur Berechnung der laminaren und turbulenten Reibungsschicht bei ebener und rotationssymmetrischer Strömung. Ing. Arch. Bd 20, Heft 14 (1952), p. 211—228.

APPENDIX A.

Derivation of the momentum equations in streamline coordinates.

1. Introducing streamline coordinates into the equations of motion (2.3) by putting

$$\xi = \varphi, \quad \eta = \psi, \quad h_1 = \frac{1}{U}, \quad h_2 = \frac{1}{U\sqrt{\rho}}$$

these equations become

$$uU\frac{\partial u}{\partial \varphi} + vU\sqrt{\rho}\frac{\partial u}{\partial \psi} + w\frac{\partial u}{\partial \zeta} - uv\sqrt{\rho}\frac{\partial U}{\partial \psi} + v^2\frac{\partial U}{\partial \varphi} + \frac{1}{2}\frac{v^2 U}{\rho}\frac{\partial \rho}{\partial \varphi} = -U\frac{\partial\left(\frac{p}{\rho^*}\right)}{\partial \varphi} + \nu\frac{\partial^2 u}{\partial \zeta^2}$$

$$uU\frac{\partial v}{\partial \varphi} + vU\sqrt{\rho}\frac{\partial v}{\partial \psi} + w\frac{\partial v}{\partial \zeta} - uv\frac{\partial U}{\partial \varphi} - \frac{1}{2}\frac{uvU}{\rho}\frac{\partial \rho}{\partial \varphi} + u^2\sqrt{\rho}\frac{\partial U}{\partial \psi} = -U\sqrt{\rho}\,\frac{\partial\left(\frac{p}{\rho^*}\right)}{\partial \psi} + \nu^2\frac{\partial^2 v}{\partial \zeta^2}$$

$$0 = \frac{\partial\left(\frac{p}{\rho^*}\right)}{\partial \zeta}. \tag{A.1}$$

The corresponding equations for the free stream are obtained by taking $u=U$, $v=V=0$ and omitting all derivatives of U and V to ζ. Hence, they are

$$U^2\frac{\partial U}{\partial \varphi} = -U\frac{\partial\left(\frac{p}{\rho^*}\right)}{\partial \varphi} \tag{A.2}$$

$$U^2\sqrt{\rho}\,\frac{\partial U}{\partial \psi} = -U\sqrt{\rho}\,\frac{\partial\left(\frac{p}{\rho^*}\right)}{\partial \psi}$$

Elimination of the pressure from (A. 1) and (A. 2) yields

$$U\left(u\frac{\partial u}{\partial\varphi}-U\frac{\partial U}{\partial\varphi}\right)+vU\sqrt{\rho}\,\frac{\partial u}{\partial\psi}+w\frac{\partial u}{\partial\zeta}-uv\sqrt{\rho}\,\frac{\partial U}{\partial\psi}+v^2\frac{\partial U}{\partial\varphi}+\frac{v^2U}{2\rho}\frac{\partial p}{\partial\varphi}=\nu\frac{\partial^2U}{\partial\zeta^2}$$

$$uU\frac{\partial v}{\partial\varphi}+vU\sqrt{\rho}\,\frac{\partial v}{\partial\psi}+w\frac{\partial v}{\partial\zeta}-uv\frac{\partial U}{\partial\varphi}-\frac{uvU}{2\rho}\frac{\partial\rho}{\partial\varphi}+(u^2-U^2)\sqrt{\rho}\,\frac{\partial U}{\partial\psi}=\nu\frac{\partial^2v}{\partial\zeta^2}. \tag{A. 3}$$

The momentum equations are now obtained by an integration over ζ from 0 to ∞. As preliminary steps it is remarked that

$$\int_0^\infty w\frac{\partial u}{\partial\zeta}d\zeta=\int_0^\infty(U-u)\frac{\partial w}{\partial\zeta}d\zeta\quad\text{and}\quad\int_0^\infty w\frac{\partial v}{\partial\zeta}d\zeta=-\int_0^\infty v\frac{\partial w}{\partial\zeta}d\zeta \tag{A. 4}$$

$\frac{\partial w}{\partial\zeta}$ follows from the continuity equation (2.4) as

$$\frac{\partial w}{\partial\zeta}=-U\frac{\partial u}{\partial\varphi}+u\frac{\partial U}{\partial\varphi}+\frac{uU}{2\rho}\frac{\partial\rho}{\partial\varphi}-U\sqrt{\rho}\,\frac{\partial v}{\partial\psi}+v\sqrt{\rho}\,\frac{\partial U}{\partial\psi}. \tag{A. 5}$$

Performing now the integration of (A. 3) over ζ, the result is

$$\int_0^\infty\Big[U\frac{\partial(U-u)u}{\partial\varphi}+\sqrt{\rho}\,U\frac{\partial(U-u)v}{\partial\psi}+U(U-u)\frac{\partial U}{\partial\varphi}-\sqrt{\rho}\,vU\frac{\partial U}{\partial\psi}+$$

$$-\left(\frac{1}{2\rho}\frac{\partial\rho}{\partial\varphi}+\frac{1}{U}\frac{\partial U}{\partial\varphi}\right)U\{(U-u)u+v^2\}-\sqrt{\rho}\,\frac{\partial U}{\partial\psi}\{(U-u)v-uv\}\Big]d\zeta=\nu\left(\frac{\partial u}{\partial\zeta}\right)_{\zeta=0}$$

$$\int_0^\infty\Big[-\sqrt{\rho}\,U\frac{\partial v^2}{\partial\psi}-U\frac{\partial(uv)}{\partial\varphi}+\sqrt{\rho}\,\frac{\partial U}{\partial\psi}(v^2+U^2-u^2)+2uvU\left(\frac{1}{2\rho}\frac{\partial\rho}{\partial\varphi}+\frac{1}{U}\frac{\partial U}{\partial\varphi}\right)\Big]d\zeta=\nu\left(\frac{\partial v}{\partial\zeta}\right)_{\zeta=0}.$$

After introduction of the expressions given in (2.9) these equations become

$$\frac{1}{T}\frac{\partial}{\partial\varphi}(T\sqrt{\sigma}\,\theta_{11})+\frac{\sqrt{\rho}}{T}\frac{\partial}{\partial\psi}(T\sqrt{\sigma}\,\theta_{12})+\frac{\sqrt{\sigma}}{2T}\Delta_1\frac{\partial T}{\partial\varphi}+\frac{\sqrt{\sigma\rho}}{2T}\Delta_2\frac{\partial T}{\partial\psi}+$$

$$-\sqrt{\sigma}(\theta_{11}-\theta_{22})\left(\frac{1}{2\rho}\frac{\partial\rho}{\partial\varphi}+\frac{1}{2T}\frac{\partial T}{\partial\varphi}\right)-\frac{\sqrt{\sigma\rho}}{2T}(\theta_{12}+\theta_{21})\frac{\partial T}{\partial\psi}=\frac{1}{T\sqrt{\sigma}}\left\{\frac{\partial}{\partial\zeta}\left(\frac{u}{\sqrt{T}}\right)\right\}_{\zeta=0}$$

$$\frac{\sqrt{\rho}}{T}\frac{\partial}{\partial\psi}(T\sqrt{\sigma}\,\theta_{22})+\frac{1}{T}\frac{\partial}{\partial\varphi}(T\sqrt{\sigma}\,\theta_{21})-\frac{\sqrt{\sigma\rho}}{2T}(\theta_{22}-\theta_{11}-\Delta_1)\frac{\partial T}{\partial\psi}+$$

$$-\sqrt{\sigma}(\theta_{21}+\theta_{12}+\Delta_2)\left(\frac{1}{2\rho}\frac{\partial\rho}{\partial\varphi}+\frac{1}{2T}\frac{\partial T}{\partial\varphi}\right)=\frac{1}{T\sqrt{\sigma}}\left\{\frac{\partial}{\partial\zeta}\left(\frac{v}{\sqrt{T}}\right)\right\}_{\zeta=0}.$$

These equations appear to be equivalent to the equation (2.8) given in the main text.

2. The boundary conditions at the body ($\zeta=0$) are $u=v=0$. Also all derivatives of u and v with respect to φ and ψ vanish.

$w=0$ and according to (2.4) also $\frac{\partial w}{\partial\zeta}=0$.

From (A. 3) it follows that for $\zeta=0$

$$\frac{\nu}{U}\frac{\partial^2u}{\partial\zeta^2}=\frac{1}{\sigma}\frac{\partial^2}{\partial\zeta^2}\left(\frac{u}{\sqrt{T}}\right)=-U\frac{\partial U}{\partial\varphi}=-\frac{1}{2}\frac{\partial T}{\partial\varphi}.$$

It follows from (3.1) and the boundary condition $g''=1$, $f''=h''=0$ that $\Lambda=\frac{1}{2}\sigma\frac{\partial T}{\partial\varphi}$.

From (A. 4) for $\zeta=0$:

$$\frac{\nu}{U}\frac{\partial^2v}{\partial\zeta^2}=\frac{1}{\sigma}\frac{\partial^2}{\partial\zeta^2}\left(\frac{v}{\sqrt{T}}\right)=-\sqrt{\rho}\,U\frac{\partial U}{\partial\psi}=-\frac{1}{2}\sqrt{\rho}\,\frac{\partial T}{\partial\psi}$$

or, with (3.1)

$$M=\frac{1}{2}\sigma\sqrt{\rho}\,\frac{\partial T}{\partial\psi}.$$

By differentiation, from (A. 3) with respect to ζ it follows

$$\frac{\partial^3}{\partial\zeta^3}\left(\frac{u}{\sqrt{T}}\right)=\frac{\partial^3}{\partial\zeta^3}\left(\frac{v}{\sqrt{T}}\right)=0 \quad \text{for} \quad \zeta=0.$$

The following boundary conditions contain derivatives of unknown functions as is seen by differentiating (A. 3) once more with respect to ζ and putting $\zeta=0$. Hence these cannot be taken into account without greatly complicating the calculations.

APPENDIX B.

The differential equation for the function ρ.

1. As has been mentioned in Sec. 5 the function ρ is to be calculated from the equation of continuity. Let $\vec{i}_1$, $\vec{i}_2$, $\vec{i}_3$ be unit vectors in the directions of the cartesian coordinate axes x, y, z. A vector along the body surface can then be decomposed as

$$\vec{dr}=\vec{i}_1 dx+\vec{i}_2 dy+\vec{i}_3 dz=(\vec{i}_1+\vec{i}_3 z_x)dx+(\vec{i}_2+\vec{i}_3 z_y)dy=$$
$$\vec{\mu}_1\sqrt{1+z_x^2}\,dx+\vec{\mu}_2\sqrt{1+z_y^2}\,dy=\vec{\mu}_1 p_1 dx+\vec{\mu}_2 p_2 dy.$$

$\vec{\mu}_1$ and $\vec{\mu}_2$ are unit vectors which are tangent to the body surface. $\vec{\mu}_1$ lies in a plane y = constant and $\vec{\mu}_2$ in a plane x = constant. The vectors $\vec{\mu}_1$ and $\vec{\mu}_2$ make an angle α, determined by

$$\cos\alpha=\vec{\mu}_1\cdot\vec{\mu}_2=\frac{z_x z_y}{p_1 p_2},\ \sin\alpha=\frac{\sqrt{1+z_x^2+z_y^2}}{p_1 p_2}=\frac{\sqrt{g}}{p_1 p_2}.$$

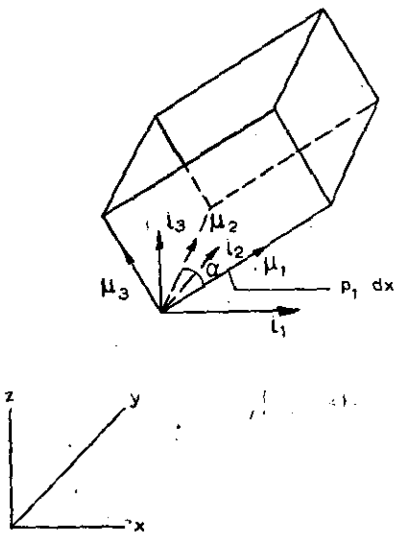

SKETCH "a"

When $\overline{U}$ and $\overline{V}$ denote the velocity components in the x and y directions, it is clear that $p_1\overline{U}$ and $p_2\overline{V}$ are the velocity components in the directions of the vectors $\vec{\mu}_1$ and $\vec{\mu}_2$. For a small volume with sides $\vec{\mu}_1 p_1 dx$, $\vec{\mu}_2 p_2 dy$ and $\vec{\mu}_3 d\zeta$ the mass excess entering in the direction of the side $\vec{\mu}_1 p_1 dx$ (see sketch "a") is given by

$$\rho^*\frac{\delta}{\delta x}(p_1 p_2\overline{U}\sin\alpha)dx\,dy\,d\zeta\,dt=\rho^*\frac{\delta}{\delta x}(\sqrt{g}\,\overline{U})dx\,dy\,d\zeta\,dt,$$

where ρ^* is the density. For the mass entering in the other directions, similar expressions are obtained and the equation of continuity becomes

$$\frac{\delta}{\delta x}(\sqrt{g}\,\overline{U})+\frac{\delta}{\delta y}(\sqrt{g}\,\overline{V})+\frac{\delta}{\delta\zeta}(\sqrt{g}\,\mathrm{W})=0.$$

Hence

$$\frac{\partial W}{\partial\zeta}=-\left(\frac{\delta\overline{U}}{\delta x}+\frac{\delta\overline{V}}{\delta y}+\frac{\overline{U}}{\sqrt{g}}\frac{\delta\sqrt{g}}{\delta x}+\frac{\overline{V}}{\sqrt{g}}\frac{\delta\sqrt{g}}{\delta y}\right). \tag{B.1}$$

Furthermore

$$\frac{\partial}{\partial\varphi}=\frac{\partial x}{\partial\varphi}\frac{\delta}{\delta x}+\frac{\partial y}{\partial\varphi}\frac{\delta}{\partial y}$$

and, according to eq. (6.2), one has along a streamline

$$\frac{\partial x}{\partial\varphi}=\frac{\overline{U}}{T}\quad\text{and}\quad\frac{\partial y}{\partial\varphi}=\frac{\overline{V}}{T}.$$

Hence

$$T\frac{\partial}{\partial\varphi}=\overline{U}\frac{\delta}{\delta x}+\overline{V}\frac{\delta}{\partial y}, \tag{B.2}$$

which is identical to eq. (5.4). Using eq. (B.2), eq. (B.1) becomes

$$\frac{\partial W}{\partial \zeta} = -\left(\frac{\delta \overline{U}}{\delta x} + \frac{\delta \overline{V}}{\delta y} + \frac{T}{\sqrt{g}} \frac{\partial \sqrt{g}}{\partial \varphi}\right).$$

Substituting this in eq. (5.2), the result is easily seen to be identical to eq. (5.3).

2. An alternative method is as follows

$$\begin{aligned} \frac{\delta \varphi}{\delta x} &= \frac{\partial \varphi}{\partial x} + \frac{\partial \varphi}{\partial z} z_x = \overline{U}(1 + z_x^2) + \overline{V} z_x z_y \\ \frac{\delta \varphi}{\delta y} &= \frac{\partial \varphi}{\partial y} + \frac{\partial \varphi}{\partial z} z_y = \overline{U} z_x z_y + \overline{V}(1 + z_y^2), \end{aligned} \tag{B.3}$$

where use is made of eq. (6.2) for $\frac{\partial \varphi}{\partial z} = \overline{W}$.

The line element along the body surface is seen from sketch "a" to be

$$ds^2 = p_1^2 dx^2 + p_2^2 dy^2 + 2\, p_1 p_2 \cos \alpha\, dx\, dy$$

or

$$ds^2 = (1 + z_x^2) dx^2 + 2\, z_x z_y\, dx\, dy + (1 + z_y^2) dy. \tag{B.4}$$

On the other hand, also

$$ds^2 = \frac{1}{T}\left((d\varphi^2 + \frac{1}{\rho} d\psi^2) \right). \tag{B.5}$$

With

$$d\varphi = \{ \overline{U}(1 + z_x^2) + \overline{V} z_x z_y \} dx + \{ \overline{U} z_x z_y + \overline{V}(1 + z_y^2) \} dy$$

and

$$T = \overline{U}^2 + \overline{V}^2 + \overline{W}^2 = \overline{U}^2 (1 + z_x^2) + \overline{V}^2(1 + z_y^2) + 2\, \overline{U}\, \overline{V} z_x z_y$$

it follows that (B.4) and (B.5) are in agreement, provided

$$\frac{1}{\sqrt{\rho}} d\psi = \overline{V} \sqrt{g}\, dx - \overline{U} \sqrt{g}\, dy.$$

Hence

$$\frac{\delta \psi}{\delta x} = \overline{V} \sqrt{\rho\, g}\,, \quad \frac{\delta \psi}{\delta y} = -\overline{U} \sqrt{\rho\, g}\,. \tag{B.6}$$

Since two ways in which $\frac{\delta^2 \psi}{\delta x \delta y}$ can be formed, must be identical, one finds

$$\sqrt{\rho\, g} \left(\frac{\delta \overline{U}}{\delta x} + \frac{\delta \overline{V}}{\delta y}\right) + \overline{U} \frac{\delta(\sqrt{\rho g})}{\delta x} + \overline{V} \frac{\delta(\sqrt{\rho g})}{\delta y} = 0$$

which is seen to yield eq. (5.3), if (B.2) is used.
It follows from eqs. (B.3) and (B.6) that

$$\sqrt{\rho g}\, T = -\frac{\delta \varphi}{\delta x} \frac{\delta \psi}{\delta y} + \frac{\delta \varphi}{\delta y} \frac{\delta \psi}{\delta x}.$$

Finally,

$$\begin{aligned} \frac{\delta}{\delta x} &= \frac{\delta \varphi}{\delta x} \frac{\partial}{\partial \varphi} + \frac{\delta \psi}{\delta x} \frac{\partial}{\partial \psi} \\ \frac{\delta}{\delta y} &= \frac{\delta \varphi}{\delta y} \frac{\partial}{\partial \varphi} + \frac{\delta \psi}{\delta y} \frac{\partial}{\partial \psi} \end{aligned}$$

which leads to

$$\begin{aligned} T \frac{\partial}{\partial \varphi} &= \overline{U} \frac{\delta}{\delta x} + \overline{V} \frac{\delta}{\delta y} \\ T \sqrt{\rho g} \frac{\partial}{\partial \psi} &= \frac{\delta \varphi}{\delta y} \frac{\delta}{\delta x} - \frac{\delta \varphi}{\delta x} \frac{\delta}{\partial y}. \end{aligned}$$

The last equation is identical to eq. (6.3).

C.C.L. Class. D 43

REPORT TN - F. 192.

Calculation of aerodynamic forces on slowly oscillating rectangular wings in subsonic flow

by

A. I. VAN DE VOOREN and E. M. DE JAGER.

Summary.

A method is presented for the calculation of the aerodynamic forces on a slowly oscillating airfoil. The method is essentially a lifting surface theory which takes into account the unsteady effects due to the wake. Results are given as series containing terms of increasing powers in reduced frequency. The method has been applied to rectangular airfoils. It is shown that if the axis of rotation is ahead of the airfoil, the aerodynamic damping is much less than it would be according to quasi-steady theory. Instability is possible if the aspect ratio is larger than a certain value. This limiting aspect ratio decreases with increasing Mach number.

Contents.

The research reported in this document was sponsored by the AIR RESEARCH AND DEVELOPMENT COMMAND, UNITED STATES AIR FORCE, under Contract AF 61(514)-879 through the European Office, ARDC.

Symbols.

b	semi-span.
c_{l_α}	sectional lift-curve slope.
el	position of sectional center of pressure aft of leading edge.
$g_0(\eta)$	function determining the lift distribution along the span.
$g_1(\eta)$	function determining the moment distribution along the span.
k	reduced frequency.
k_a, k_b	aerodynamic force derivatives defined by eq. (6.1).
l	semi-chord.
m_a, m_b	aerodynamic moment derivatives defined by eq. (6.1).
p	pressure (positive in upward direction).
s	aspect radio of wing (b/l).
t	time.
w	downwash (positive downward).
x, y, z	coordinates made dimensionless by aid of l, see sec. 2.
x_0, y_0	$x-\xi$ and $y-\eta$, respectively.
Al	amplitude of translation of mid-chord point (positive downward).
B	amplitude of rotation (positive if trailing edge is more downward than leading edge).
C_{l_α}	lift-curve slope for complete wing.
El	position of center of pressure of complete wing aft of leading edge.
K	kernel in eq. (2.1).
$\overline{K}$	force, defined by eq. (6.1), positive downward.
$\overline{M}$	moment about mid-chord axis, defined by eq. (6.1), positive if it tends to increase the angle of attack.
M	Mach number.
M_ε	moment about axis which lies εl aft of mid-chord axis.

U forward speed.
AR aspect ratio.
β $\sqrt{1-M^2}$.
εl distance of pitching axis aft of mid-chord axis.
ϑ angular chordwise coordinate, eq. (3.1).
φ angular spanwise coordinate, eq. (3.2).
ξ, η x and y coordinates of an arbitrary point of the wing.
ρ air density.
ν frequency of oscillation.

Subscripts R and T denote the cases of rotation and translation respectively.

Superscripts (0), (1), (2) and (3) denote 0th, 1st, 2nd or 3rd approximation.

1 Introduction.

It is normal practice to perform stability calculations for airplanes on the basis of quasi-steady airfoil theory. Only for the downwash at the horizontal tailplane due to the wing, a time-lag is sometimes introduced, which expresses the fact that this downwash was generated at the wing a little sooner.

A few years ago it was remarked by MILES (ref. 1) and SMILG (ref. 2) that oscillations of a two-dimensional airfoil about a pitching axis may become unstable for low values of the reduced frequency if the axis lies in a certain region ahead of the quarter chord axis and if the moment of inertia about this axis is sufficiently large. This instability follows from exact unsteady theory but is not revealed by quasi-steady theory. RUNYAN (ref. 3) has shown that this instability occurs in a much larger range of reduced frequencies, pitching axes and moments of inertia, if compressibility is taken into account. In the case of snaking, where a vertical tailplane is oscillating about the airplane's top axis, the reduced frequency, axis of rotation and moment of inertia about this axis are within or near the range, where RUNYAN obtains instability. This makes it opportune to consider the question whether it is allowed to calculate snaking of airplanes, especially at high subsonic Mach numbers, by aid of quasi-steady theory.

Part I of the investigation performed under contract AF 61(514)-879 is concerned with the extension of RUNYAN's two-dimensional results to three-dimensional flow. Part II, about the results of which will be reported in a sequel paper, deals with the practical consequences of a decreased damping due to the unsteady effect upon the snaking motion of an airplane with rudder fixed.

In the past there were some investigations of the effect of finite span unsteady airfoil theory on stability calculations. VAN DE VOOREN and YFF (ref. 4) introduced a reduced value for the lift curve slope, while BIRD, FISHER and HUBBARD (ref. 5) applied the method of BIOT and BÖHNLEIN as well as that of REISSNER for calculating finite span corrections. Although these methods are valid as approximations for large aspect-ratio wings, they were used for aspect-ratio 2. Moreover, the investigations of refs. 4 and 5 were restricted to incompressible flow. ASHLEY and co-authors (ref. 6) also applied REISSNER's method for introducing finite span effects and also confined their investigation mainly to incompressible flow. Finally, GOLAND, HAGER and LUKE (ref. 7) calculated oscillatory forces from indicial functions by aid of DUHAMEL's integral. The indicial functions were modified for both finite span and compressibility.

In view of the results of refs. 5 and 6, it seems fairly certain that the difference between unsteady and quasi-steady incompresisble theory is much less important for finite span configurations than for the two-dimensional case. Hence, unsteady effects for the snaking problem will be relatively unimportant for incompressible flow. This can also be made plausible by considering the vortex pattern behind a slowly oscillating wing. For the case of snaking the wing should be identified with the vertical tailplane. The vortices near A (sketch a) with axes parallel to the wing span

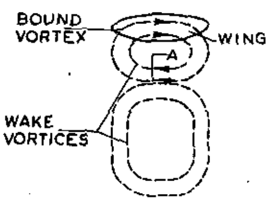

Sketch a

are responsible for the posible instability in the two-dimensional case. In order to estimate in the three-dimensional case their influence as compared with the influence of the tip vortices, the distances of both vortices to the wing are compared. In sketch a the pitching wing is at the position of maximum angle of incidence. The "starting" vortices at A were formed one quarter of a period before and hence the distance from it to the wing is of the order of $\pi U/2\nu$, where U = airspeed and ν = frequency of oscillation (rad/sec). The distance of the tip vortices to the wing is of the order b, where b = semispan. Hence, the ratio of the two distances is as

$$\pi U/2\,\nu : b = \pi : 2\,k\,AR$$

where $k = \nu l/U$ reduced frequency, l = semichord and $AR = b/l$ (aspect-ratio). Since it follows from two-dimensional unsteady theory that instability may occur for k smaller than 0.04 it is clear that for all usual values of AR, the distance of the starting vortices is much larger than that of the tip vortices. This means that the change in the pressure distribution of the wing, due to the unsteady effect will be small for the low values of k, which are of importance in stability calculations.

It is seen that $k \times AR$ is the relevant parameter, if the wing planform is left out of account. For two-dimensional flow this parameter assumes the value ∞ whatever the value of k; for stability considerations in three-dimensional flow it has a small value unless AR becomes excessively large.

For compressible flow the picture is different.

It is stated in ref. 7 that the unsteady effects on the snaking motion are generally significant at $M = 0.7$. The reasoning given above for incompressible flow is quantitatively modified since for the two-dimensional case instability may occur for values of k as high as 0.1 (at $M = 0.7$); moreover, there is the more fundamental modification of the finite speed of propagation of disturbances. What consequences this modification has, is somewhat difficult to assess. In any case it is known that in the transonic region the range of k-values where the flow may be considered as quasi-steady becomes very small for large aspect ratio wings. This suggests that also for high subsonic Mach numbers the differences between quasi-steady and unsteady theory will become of increasing importance.

For these reasons it was considered desirable to investigate the influence of finite span effects on a slowly oscillating airfoil placed in a subsonic flow. The approximate theory which has to be used for this purpose is not based upon the assumption of large aspect ratio like BIOT and BÖHNLEIN's and REISSNER's theories, but upon that of low frequency. The new theory uses as a starting point the integral equation between downwash w and pressure p at the wing, viz.

$$w(x, y) = \frac{1}{4\pi\rho U} \iint_{\text{wing}} K(x-\xi, y-\eta) p(\xi, \eta)\, d\xi\, d\eta,$$

where the kernel K has been given for subsonic compressible flow by WATKINS, RUNYAN and WOOLSTON (ref. 8). These authors have also given the expansion of K towards the reduced frequency k. Since the expansion of w towards k is also known, it is possible to obtain by an iterative procedure of lifting surface theory the corresponding expansion for the pressure p.

In the present report lift and moment are calculated for rectangular wings of aspect ratios 4, 8 and 16 at $M = 0.7$, performing a translation or a pitching rotation. Results are also presented for $M = 0.9$ and wings of different aspect ratio. By identifying a semi-wing with the vertical tailplane, the results can be applied for snaking calculations. In the case of $M = 0.7$ the aspect ratio of the tailplane then takes the values 2, 4 and 8.

2 Description of the iteration process.

The fundamental integral equation between downwash w (positive in downward direction) and pressure p (positive in upward direction) can be written in the form

$$w(x, y) = \frac{1}{4\pi\rho U} \iint_{\text{wing}} K(x-\xi,\, y-\eta) p(\xi, \eta)\, d\xi\, d\eta. \tag{2.1}$$

The system of coordinates is fixed to the wing (sketch b). All coordinates are made dimensionless by aid of a reference length l.

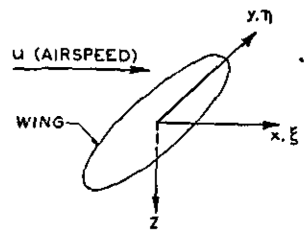

Sketch b

In ref. 8 an expansion of the kernel $K(x-\xi, y-\eta)$ towards the reduced frequency $k = \nu l/U$, up to and including k^5, has been given. The first terms of this expansion, which are relevant for the present investigation, are

$$K = K^{(0)} + kK^{(1)} + k^2 \log k \,.\, K^{(2)} + k^2 K^{(3)} + 0(k^3) \tag{2.2}$$

where

$$\left.\begin{aligned}
K^{(0)} &= -\frac{\sqrt{x_0^2+\beta^2 y_0^2}+x_0}{y_0^2\sqrt{x_0^2+\beta^2 y_0^2}}\\
K^{(1)} &= i\,\frac{x_0\sqrt{x_0^2+\beta^2 y_0^2}+x_0^2+y_0^2}{y_0^2\sqrt{x_0^2+\beta^2 y_0^2}}\\
K^{(2)} &= -\frac{1}{2}\\
K^{(3)} &= -\frac{1}{2}\log\frac{\sqrt{x_0^2+\beta^2 y_0^2}-x_0}{2(1-M)} + \frac{x_0^2\sqrt{x_0^2+\beta^2 y_0^2}+x_0(x_0^2+2y_0^2)}{2y_0^2\sqrt{x_0^2+\beta^2 y_0^2}} +\\
&\quad + \frac{1}{2\beta^2}\left\{M - \frac{x_0}{\sqrt{x_0^2+\beta^2 y_0^2}} - \beta^2\left(\gamma-\frac{1}{2}\right) - i\,\frac{\pi\beta^2}{2}\right\}
\end{aligned}\right\} \tag{2.3}$$

and where $x_0 = x - \xi$, $y_0 = y - \eta$, $\beta^2 = 1 - M^2$ and $M =$ Mach number.

The convergence of the series (2.2) becomes slower for increasing values of y_0. This means that the range of k-values for which (2.2), neglecting terms of order k^3, can be used becomes smaller with increasing aspect ratio. In the two-dimensional case it is known that the expansion of the kernel is different. In fact, it then contains a term $k \log k$ which is the term giving rise to the pitching instability.

The pressure distribution will be considered for the cases of translation and rotation about the mid-chord axis. By linear superposition the pressure distribution for rotation about any spanwise axis can then be obtained.

The downwash is given by (z is dimensionless)

$$w = l \frac{dz}{dt} = l \frac{\partial z}{\partial t} + U \frac{\partial z}{\partial x}.$$

For translation one has

$$z = A\, e^{i\nu t}$$

and hence $w_T = i\,\nu\, l\, A\, e^{i\nu t} = i\, A\, U\, k\, e^{i\nu t}$ where the suffix T denotes translation.

For rotation

$$z = B\, x\, e^{i\nu t}$$

and hence $w_R = UB(1 + ikx)e^{i\nu t}$.

From the definition given above, it is clear that a translation is positive in downward direction, while a rotation is positive if the trailing edge is more downward than the leading edge.

For both translation and rotation the downwash can be written in the form

$$w = (w^{(0)} + kw^{(1)})e^{i\nu t} \tag{2.4}$$

with

$$\left.\begin{aligned} w_T^{(0)} &= 0 \qquad & w_T^{(1)} &= iAU \\ w_R^{(0)} &= BU \qquad & w_R^{(1)} &= iBUx \end{aligned}\right\} \tag{2.5}$$

Introducing eqs. (2.2) and (2.4) into (2.1) yields

$$(w^{(0)} + kw^{(1)})e^{i\nu t} = \frac{1}{4\,\pi\rho U} \iint\limits_{\text{wing}} \{ K^{(0)} + kK^{(1)} + k^2 \log k - K^{(2)} + k^2 K^{(3)} \}\, p(\xi, \eta) d\xi\, d\eta \tag{2.6}$$

Hence, the pressure distribution can be written as

$$p = (p^{(0)} + kp^{(1)} + k^2 \log k\,.\, p^{(2)} + k^2 p^{(3)})e^{i\nu t} \tag{2.7}$$

Inserting (2.7) into (2.6) and equating corresponding powers of k, the original integral equation is separated into the four following equations

$$\left.\begin{aligned} w^{(0)} &= \frac{1}{4\,\pi\rho U} \iint\limits_{\text{wing}} K^{(0)} p^{(0)}\, d\xi\, d\eta \\ w^{(1)} &= \frac{1}{4\,\pi\rho U} \iint\limits_{\text{wing}} (K^{(1)} p^{(0)} + K^{(0)} p^{(1)})\, d\xi\, d\eta \\ 0 &= \iint\limits_{\text{wing}} (K^{(2)} p^{(0)} + K^{(0)} p^{(2)})\, d\xi\, d\eta \\ 0 &= \iint\limits_{\text{wing}} (K^{(3)} p^{(0)} + K^{(1)} p^{(1)} + K^{(0)} p^{(3)}\, d\xi\, d\eta \end{aligned}\right\} \tag{2.8}$$

The equations of this set can be solved consecutively by a numerical procedure. The first equation involves the calculation of the pressure distribution $p^{(0)}(\xi, \eta)$ by application of steady state lifting surface theory. After having determined $p^{(0)}$, the first term of the right hand side of the second equation (2.8) is calculated and the resulting equation can be used for solving $p^{(1)}$. This is again performed by steady state lifting surface theory, since $p^{(1)}$ occurs in combination with the same kernel $K^{(0)}$. Similarly, the third and fourth equation yield $p^{(2)}$ and $p^{(3)}$ respectively.

It is seen that by this procedure the solution of the unsteady lifting surface problem is reduced to the solution of a series of steady lifting surface problems.

Physically, the terms in a certain equation which can be evaluated by aid of the solutions of previous equations represent a downwash due to unsteady wake vortices. In quasi-steady theory, the pressure distribution would be given by

$$p = (p^{(0)} + kp^{(1)})\, e^{i\nu t} \tag{2.9}$$

where $p^{(0)}$ and $p^{(1)}$ are determined by

$$\left.\begin{aligned} w^{(0)} &= \frac{1}{4\,\pi\rho U} \iint_{\text{wing}} K^{(0)} p^{(0)}\, d\xi\, d\eta \\ w^{(1)} &= \frac{1}{4\,\pi\rho U} \iint_{\text{wing}} K^{(0)} p^{(1)}\, d\xi\, d\eta \end{aligned}\right\} \tag{2.10}$$

By inspection of the expressions for w and K, it follows immediately that $p^{(0)}$ and $p^{(2)}$ are real, $p^{(1)}$ is pure imaginary and $p^{(3)}$ is complex. Hence, for the damping $p^{(1)}$ and the imaginary part of $p^{(3)}$ are of importance. Since it may be expected that the contributions of $k^2 \log k \,.\, p^{(2)}$ and the real part of $k^2 p^{(3)}$ to the total real part of the pressure are only small in comparison with $p^{(0)}$ for the low values of k concerned, these will not be calculated. They would only lead to a minor change in the frequency of oscillation, but do not affect the stability of the system directly. The imaginary part of $p^{(3)}$ will be evaluated since this is a damping component which, moreover, might furnish an appreciable correction to the damping $kp^{(1)}$.

Hence, the real part of the aerodynamic forces will be approximated by $p^{(0)}$ and the imaginary part by $Im(kp^{(1)} + k^2 p^{(3)})$. This means that the third equation (2.8) may be left out of account, while the fourth equation may be simplified.

Since the numerical solution will be performed for a series of rectangular airfoils, the final set of integral equations to be solved is

$$\left.\begin{aligned} & w^{(0)}(x,y) = \frac{1}{4\,\pi\rho U} \int_{-1}^{1}\int_{-s}^{s} K^{(0)}(x-\xi,\ y-\eta)\, p^{(0)}(\xi,\eta)\, d\xi\, d\eta, \\ & w^{(1)}(x,y) - \frac{1}{4\,\pi\rho U} \int_{-1}^{1}\int_{-s}^{s} K^{(1)}(x-\xi,\ y-\eta)\, p^{(0)}(\xi,\eta)\, d\xi\, d\eta = \\ & = \frac{1}{4\,\pi\rho U} \int_{-1}^{1}\int_{-s}^{s} K^{(0)}(x-\xi,\ y-\eta)\, p^{(1)}(\xi,\eta)\, d\xi\, d\eta, \\ & - \frac{1}{4\,\pi\rho U} \int_{-1}^{1}\int_{-s}^{s} Im\, K^{(3)}(x-\xi,\ y-\eta)\, p^{(0)}(\xi,\eta)\, d\xi\, d\eta = \\ & \qquad = \frac{1}{4\,\pi\rho U} \int_{-1}^{1}\int_{-s}^{s} K^{(0)}(x-\xi,\ y-\eta)\, Im\, p^{(3)}(\xi,\eta)\, d\xi\, d\eta. \end{aligned}\right\} \tag{2.11}$$

where $s = b/l = AR$.

3 Results for the steady state pressure ditribution.

The method which is followed for the solution of the first equation (2.11) is the one which has been described by the first author in ref. 9 and which is presented in detail in Appendix A for the present case. The chordwise pressure distribution is prescribed in the form, eq. (A.5)

$$p^{(0)}(\xi,\eta) = \frac{1}{\pi}\, g_1{}^{(0)}(\eta) \cot\frac{\vartheta}{2} + \frac{2}{\pi}\{\, g_0{}^{(0)}(\eta) - g_1{}^{(0)}(\eta)\} \sin\vartheta, \tag{3.1}$$

where $\xi = -\cos\vartheta$ is the chordwise coordinate.

The lift per unit span appears to become equal to $l\, g_0{}^{(0)}(\eta)$, while the moment per unit span about the mid-chord axis becomes equal to $\frac{1}{2} l^2 g_1{}^{(0)}(\eta)$, positive tailheavy.

The functions p, g_0 and g_1 are provided in the case of translation with a suffix T and in the case of rotation with a suffix R. From the first equation of (2.11) and (2.5) follows immediately, that $p_T{}^{(0)}(\xi,\eta)$ and hence $g^{(0)}_{0,T}(\eta)$ and $g^{(0)}_{1,T}(\eta)$ equal zero; therefore the first integral equation of (2.11) needs only to be solved for the case of rotation.

The assumption (3.1) allows the approximate evaluation of the chordwise integrals. By multiplying the equation with two suitable weight functions (functions of x) and integrating, two simultaneous integral equations for $g_0(\eta)$ and $g_1(\eta)$ are obtained. The integrations to x are approximated in a similar way as the integrations to ξ, viz. by aid of 2 chordwise pivotal points (Appendix A. 2).

The integral equations are transformed into a set of linear algebraic equations by a procedure which is an extension of MULTHOPP's method (Appendix A. 3). This leads to the set of equations (A. 28) for the unknowns $g_{0,R}^{(0)\nu}$ and $g_{1,R}^{(0)\nu}$. These denote the values of the functions $g_{0,R}^{(0)}(\eta)$ and $g_{1,R}^{(0)}(\eta)$ in the sections

$$\eta = s \cos \varphi_\nu \,, \text{ where } \varphi_\nu = \frac{\pi}{2} - \frac{\nu\pi}{m+1} \,, \; \nu = 0,1, \ldots \frac{m-1}{2} \tag{3.2}$$

For the present calculations m has been taken equal to 15.

It follows from eqs. (A. 28) that if βs is kept constant, the values of $\beta g_{0,R}^{(0)}(\eta)$ and $\beta g_{1,R}^{(0)}(\eta)$ and also those of $g_{0,R}^{(0)}(\eta)/s$ and $g_{1,R}^{(0)}(\eta)/s$ remain invariant, which is in agreement with the PRANDTL-GLAUERT rule.

Calculations have been performed for the following cases

$\beta s = 2.8566$,	correspoding	to $M = 0.7$,	$s = 4$	or	to	$M = 0.9$,	$s = 6.553$
$\beta s = 5.7131$,	,,	,,	,,	$s = 8$	,,	,,	,,	$s = 13.106$
$\beta s = 11.4263$,	,,	,,	,,	$s = 16$	,,	,,	,,	$s = 26.20$

The results are shown in fig. 1.

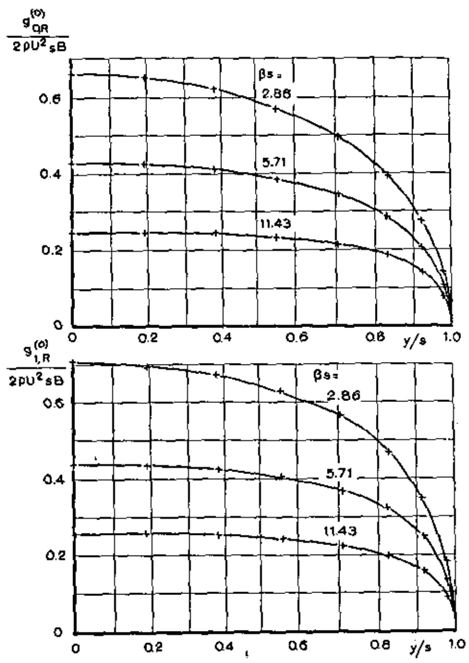

Fig. 1. Distribution of lift and pitching moment in spanwise direction.

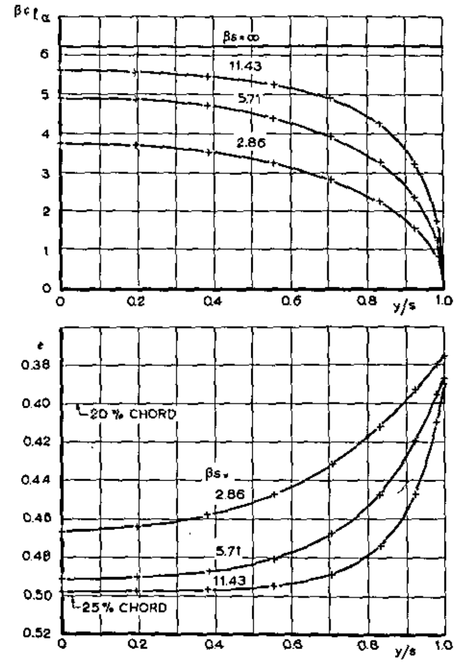

Fig. 2. Sectional lift curve slope and sectional position of the center of pressure aft of leading edge.

The same results are also presented (fig. 2) in the form of sectional lift curve slope c_{l_α} and sectional position el of the center of pressure aft of the leading edge. They are obtained from the relations

$$\beta c_{l_\alpha} = 2\,\beta s \,. \frac{g_{0,R}^{(0)}}{2\,\rho U^2 sB} \text{ and } e = 1 - \frac{g_{1,R}^{(0)}}{2 g_{0,R}^{(0)}} \,. \tag{3.3}$$

An expression for the value of e at the tip is derived in Appendix C.

The lift curve slope for the whole wing is equal to

$$C_{l_\alpha} = \frac{1}{s} \int_0^s c_{l_\alpha} \, d\eta$$

which can be evaluated by aid of the trapezoidal rule with the result that

$$C_{l_\alpha} = \frac{\pi}{m+1} \left\{ \tfrac{1}{2} c_{l_\alpha}^{0} + \sum_{\nu=1}^{\frac{m-1}{2}} c_{l_\alpha}^{\nu} \sin \varphi_\nu \right\} \tag{3.4}$$

where $c_{l_\alpha}^{\nu}$ denotes the sectional lift curve slope in the section $\eta = s \cos \varphi_\nu$, see (3.2).

The position of the center of pressure of the whole wing is in the middle section at a distance El aft of the leading edge, where

$$E = 1 - \frac{\frac{1}{2} g_{1,R}^{(0)0} + \sum_{\nu=1}^{\frac{m-1}{2}} g_{1,R}^{(0)\nu} \sin \varphi_\nu}{2 \left\{ \frac{1}{2} g_{0,R}^{(0)0} + \sum_{\nu=1}^{\frac{m-1}{2}} g_{0,R}^{(0)\nu} \sin \varphi_\nu \right\}}. \tag{3.5}$$

The values of βC_{l_α} and E are plotted in fig. 3 as functions of βs. For $\beta s \to \infty$ the two-dimensional

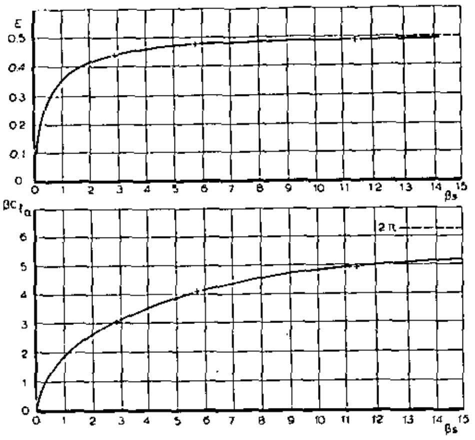

Fig. 3. Lift curve slope and position of center of pressure for total wing.

values 2π and 0.5 are obtained, while for $\beta s \to 0$ the curves have been drawn to the origins, in agreement with slender wing theory.

4 Results for the aerodynamic damping at low frequency.

The first approximation for the aerodynamic damping at low frequency is given by the pressure distribution $p^{(1)}$. This is determined by the second of the equations (2.11). When for $p^{(1)}$ the substitution

$$p^{(1)}(\xi, \eta) = \frac{1}{\pi} g_1^{(1)}(\eta) \cot \frac{\vartheta}{2} + \frac{2}{\pi} \{ g_0^{(1)}(\eta) - g_1^{(1)}(\eta) \} \sin \vartheta \tag{4.1}$$

is made, this equation can be solved in a similar way as the first equation (2.11). The second term of the left hand side in the second equation (2.11) is evaluated by aid of the results of Sec. 3. The detailed procedure is described in Appendix B.

The final set of algebraic equations determining $g_0^{(1)\nu}$ and $g_1^{(1)\nu}$, which denote the values of $g_0^{(1)}(\eta)$ and $g_1^{(1)}(\eta)$ in the sections $\eta = s \cos \varphi_\nu$, see eq. (3.2), is given by (B. 16) and (B. 17). It follows from these equations and from the expressions (2.5), that in the case of translation the solution can be written down immediately as

$$g_{0,T}^{(1)}(\eta) = i \frac{A}{B} g_{0,R}^{(0)}(\eta), \; g_{1,T}^{(1)}(\eta) = i \frac{A}{B} g_{1,R}^{(0)}(\eta). \tag{4.2}$$

This correspondence is due to the fact that a wing performing a harmonic translation, has a dynamic angle of incidence which is constant over the wing area. Since the wake effects, being of order k^2 for the case of translation, are neglected, the pressure distribution will be proportional to that of the flat plate at constant angle of incidence.

The solutions for the case of rotation are found by solving eq. (B. 16) and (B. 17). They are shown in figs. (4) and (5).

The second approximation for the aerodynamic damping is obtained by solving also the third equation (2.11). The unknown function in this equation is $Im\, p^{(3)}$, for which a similar substitution as in (3.1) and (4.1) is made. Because $Im\, K^{(3)}(x-\xi, y-\eta)$ is independent of $x-\xi$ and $y-\eta$ (see eq. 2.3), it follows that $Im\, p^{(3)}$ is proportional to $p^{(0)}$.

5 Results for the aerodynamic damping from quasi-steady theory.

Using quasi-steady theory the aerodynamic damping follows from the second equation (2.10) instead of the second equation (2.11). The quasi-steady values of $g^{(1)}_{0,R}$ and $g^{(1)}_{1,R}$ for the case of rotation are determined by eqs. (B. 16) and (B. 17) with the simplification that all terms of the left hand side of these equations are to be omitted with the exception of the term $\rho U^2 sBi$ in eq. (B. 16). For the case of translation the quasi-steady values are identical to the unsteady values, which are given by (4.2).

The quasi-steady values for rotation have been added to fig. 4, where they are shown by the dotted lines.

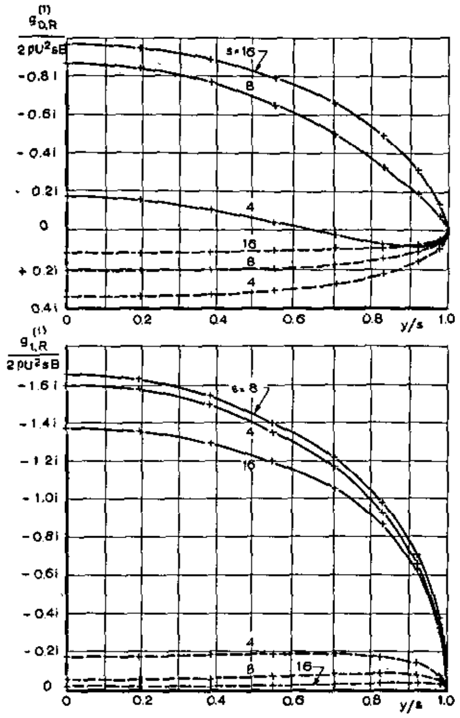

Fig. 4. The functions $g^{(1)}_{0,R}$ and $g^{(1)}_{1,R}$ for $M = 0.7$.

$s = 4$ is identical to $\beta s = 2.86$
$s = 8$ is identical to $\beta s = 5.71$
$s = 16$ is identical to $\beta s = 11.43$

—— unsteady values
- - - quasi steady values

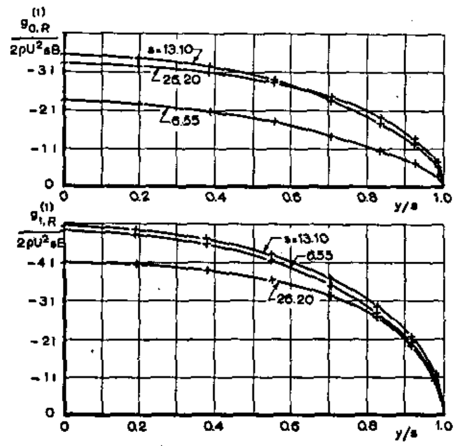

Fig. 5. The unsteady values of the functions $g^{(1)}_{0,R}$ and $g^{(1)}_{1,R}$ for $M = 0.9$.

$s = 6.55$ is identical to $\beta s = 2.86$
$s = 13.10$ „ „ „ $\beta s = 5.71$
$s = 26.20$ „ „ „ $\beta s = 11.43$

6 Transformation of results to the form of flutter derivatives.

In Küssner's notation, the flutter derivatives are defined by

$$\begin{aligned}\overline{K} &= \pi\rho U^2 l\, e^{i\nu t}(k_a A + k_b B)\\ \overline{M} &= \pi\rho U^2 l^2\, e^{i\nu t}(m_a A + m_b B)\end{aligned} \tag{6.1}$$

where $\overline{K}$ and $\overline{M}$ denote the force and the moment about the mid-chord point per unit span due to harmonic motions of frequency ν. $\overline{K}$ is positive in downward direction (like A) and $\overline{M}$ is positive if the moment tends to increase the angle of attack. The derivatives k_a, k_b, m_a and m_b are complex functions of the reduced frequency k. They are separated into a real and an imaginary part by writing

$$k_a = k_a' + i\,k_a'', \text{ etc.}$$

According to Secs. 3 and 4, the force per unit span in downward direction is in the approximation used equal to

$$\overline{K} = -l\, e^{i\nu t}\{\, g^{(0)}_0(\eta) + k\, g^{(1)}_0(\eta) + i\,k^2 Im\, g^{(3)}_0(\eta)\,\} \tag{6.2}$$

Comparing the first equation (6.1) with (6.2), it follows that

$$\begin{aligned}k_a &= -\frac{1}{\pi\rho U^2 A}\{\, g^{(0)}_{0,T}(\eta) + k\, g^{(1)}_{0,T}(\eta) + i\,k^2 Im\, g^{(3)}_{0,T}(\eta)\,\}\\ k_b &= -\frac{1}{\pi\rho U^2 B}\{\, g^{(0)}_{0,R}(\eta) + k\, g^{(1)}_{0,R}(\eta) + i\,k^2 Im\, g^{(3)}_{0,R}(\eta)\,\}.\end{aligned} \tag{6.3}$$

Similarly

$$\overline{M} = \tfrac{1}{2}\, l^2 e^{i\nu t}\, \{\, g_1^{(0)}(\eta) + k\, g_1^{(1)}(\eta) + i\, k^2 Im\, g_1^{(3)}(\eta)\,\}$$

which leads to

$$m_a = \frac{1}{2\,\pi\rho U^2 A}\,\{\, g_{1,T}^{(0)}(\eta) + k\, g_{1,T}^{(1)}(\eta) + i\, k^2 Im\, g_{1,T}^{(3)}(\eta)\,\}$$

$$m_b = \frac{1}{2\,\pi\rho U^2 B}\,\{\, g_{1,R}^{(0)}(\eta) + k\, g_{1,R}^{(1)}(\eta) + i\, k^2 Im\, g_{1,R}^{(3)}(\eta)\,\}. \tag{6.4}$$

Separating into real and imaginary part and using also (4.2) the various coefficients are given by

$$k_a' = 0, \qquad k_a'' = -\frac{\dot{g}_{0,R}^{(0)}}{\pi\rho U^2 B}\, k = -\frac{1}{\pi}\, c_{l\,\alpha}\, k,$$

$$k_b' = -\frac{g_{0,R}^{(0)}}{\pi\rho U^2 B} = -\frac{1}{\pi}\, c_{l\,\alpha}, \qquad k_b'' = -Im\left\{\frac{g_{0,R}^{(1)} k + g_{0,R}^{(3)} k^2}{\pi\rho U^2 B}\right\},$$

$$m_a' = 0, \qquad m_a'' = \frac{g_{1,R}^{(0)}\, k}{2\,\pi\rho U^2 B},$$

$$m_b' = \frac{g_{1,R}^{(0)}}{2\,\pi\rho U^2 B}, \qquad m_b'' = Im\left\{\frac{g_{1,R}^{(1)} k + g_{1,R}^{(3)} k^2}{2\,\pi\rho U^2 B}\right\}.$$

The values of $\beta k_b'$, $\beta m_b'$, $\lim\limits_{k\to 0} \dfrac{k_b''}{k}$ and $\lim\limits_{k\to 0} \dfrac{m_b''}{k}$ are given in figs. 6, 7, 8a, 8b, 9a and 9b and in tables 1, 2, 3. The coefficients of k^2 in k_b'' and m_b'' are proportional to $\beta k_b'$ and $\beta m_b'$, the proportionality factor following from eq. (B. 18) and tabulated in table 8. The values $\dfrac{\beta k_a''}{k}$ and $\dfrac{\beta m_a''}{k}$ are identical with $\beta k_b'$ and $\beta m_b'$ respectively.

The results for the whole wing follow from the sectional values by formulae of the type (3.4). These overall values are denoted by K_a, K_b, M_a and M_b. They are tabulated in tables 5, 6 and 7. The values of K_b'' and M_b'' are given in the figs. 12 and 13 as functions of the reduced frequency parameter k. The two-dimensional values have been added for comparison.

Table 4 and figs. 10 and 11 give similar results for the quasi-steady appriximation.

7 Unstable oscillations with one degree of freedom.

The motion about an arbitrary pitching axis of the wing is determined by the equation

$$I\,\ddot{\varphi} = \overline{M},$$

where I is the mass moment of inertia and M the aerodynamic moment both taken about the pitching axis. φ is the angle of deflection. If it is assumed that φ is of the type

$$\varphi = \varphi_0\, e^{i\nu t}$$

it follows that

$$\nu^2\, I\, \varphi = -\overline{M}.$$

Hence, a harmonic oscillation will occur if $\overline{M}'' = 0$ and $\overline{M}' < 0$, since then a real value of ν will result. If $\overline{M}'' > 0$ and $\overline{M}' < 0$, ν becomes complex with a negative imaginary part, which means that the oscillation is unstable. The solution is complicated by the fact that M itself is a function of the reduced frequency k and that the value of k must be compatible with those of ν and $U (k = \nu l/U)$.

Let it now be assumed that the pitching axis lies at a distance εl aft of the mid-chord axis. The motion then can be decomposed into a rotation B about the mid-chord axis and a translation $-\varepsilon B$ of the mid-chord axis. The moment about the pitching axis is given by

$$M_\varepsilon = \overline{M} - \varepsilon l\, \overline{K}.$$

Substituting eq. (6.1) as well as the value $A = -\varepsilon B$ for the translational amplitude, the result is

$$M_\varepsilon = \pi\,\rho\, U^2\, l^2\, B\, e^{i\nu t}\,\{\, M_b - \varepsilon(M_a + K_b) + \varepsilon^2 K_a\,\}. \tag{7.1}$$

The two conditions $M_\varepsilon'' > 0$ and $M_\varepsilon' < 0$ then become

$$\begin{aligned} &M_b'' - \varepsilon(M_a'' + K_b'') + \varepsilon^2 K_a'' > 0 \\ &M_b' - \varepsilon\, K_b' \qquad\qquad\qquad < 0 \end{aligned} \tag{7.2}$$

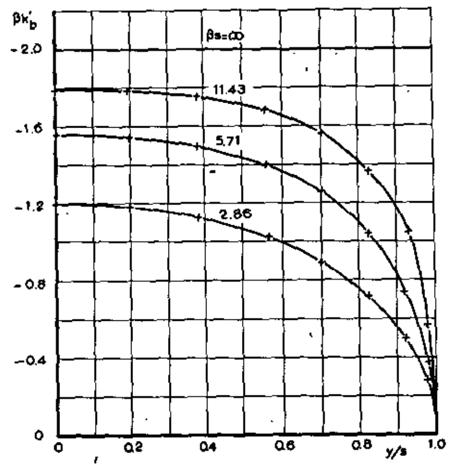

Fig. 6. The values of $\beta k'_b$ as function of the spanwise coordinate.

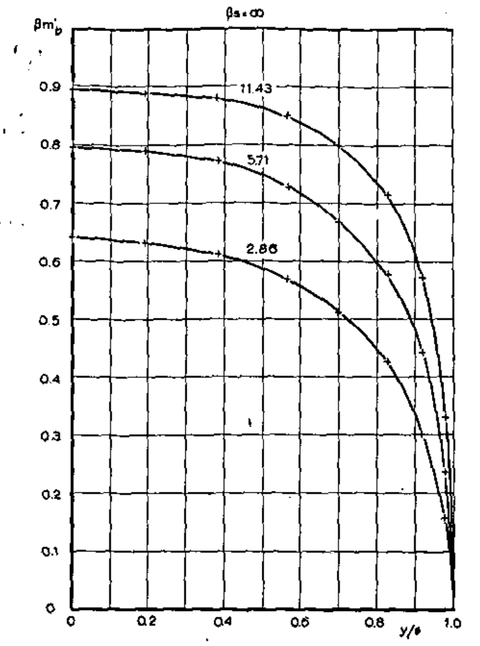

Fig. 7. The values of $\beta m'_b$ as function of the spanwise coordinate.

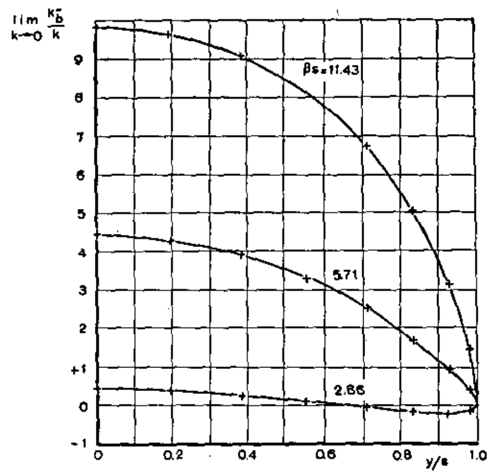

Fig. 8a. The values of $\lim\limits_{k \to 0} \dfrac{k''_b}{k}$ as function of the spanwise coordinate for $M = 0.7$.

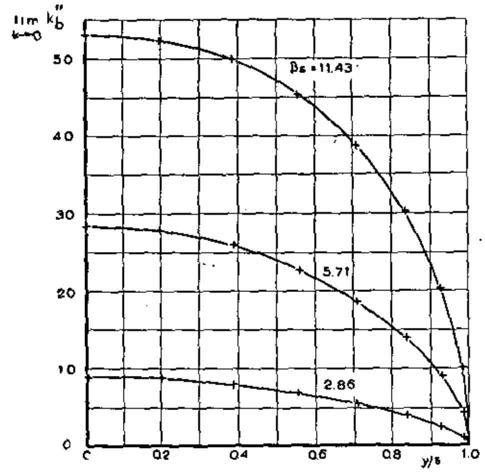

Fig. 8b. The values of $\lim\limits_{k \to 0} \dfrac{k''_b}{k}$ as function of the spanwise coordinate for $M = 0.9$.

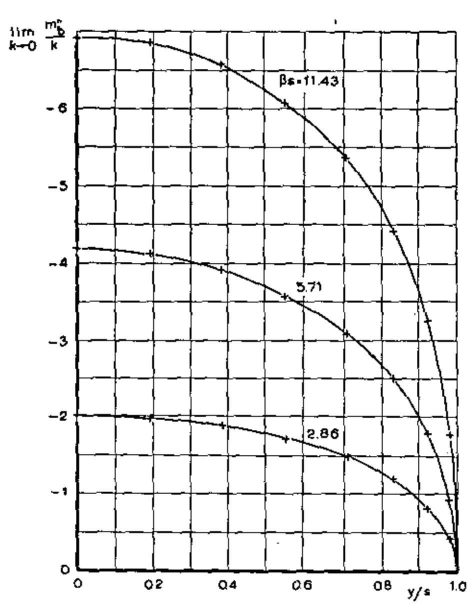

Fig. 9a. The values of $\lim\limits_{k \to 0} \dfrac{m''_b}{k}$ as function of the spanwise coordinate for $M = 0.7$.

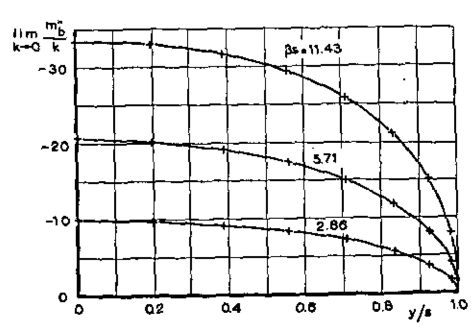

Fig. 9b. The values of $\lim\limits_{k \to 0} \dfrac{m''_b}{k}$ as function of the spanwise coordinate for $M = 0.9$.

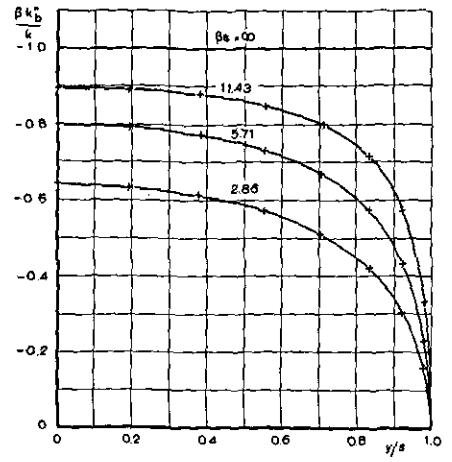

Fig. 10. Quasi-steady approximation of $\beta \frac{k_b''}{k}$ against spanwise coordinate.

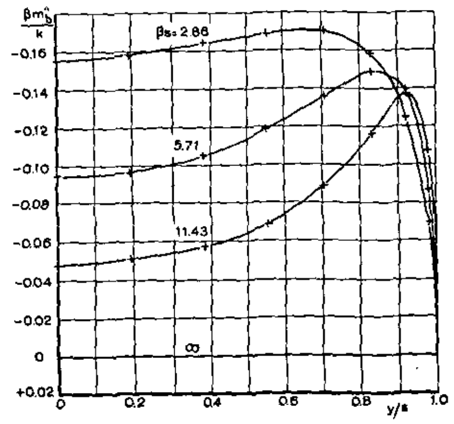

Fig. 11. Quasi-steady approximation of $\beta \frac{m_b''}{k}$ against spanwise coordinate.

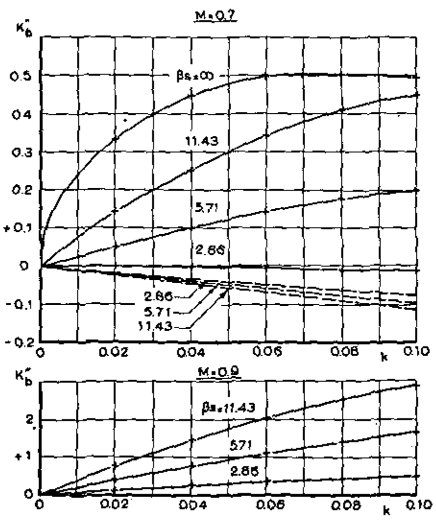

Fig. 12. K'' as function of the reduced frequency for $M = 0.7$ and $M = 0.9$.
—— unsteady values.
– – – quasi-steady values.

Quasi-steady curves for $M = 0.9$ are straight lines from the origin to the points

$k = 0.1$	$K'' = -0.12$	for $\beta s =$	2.86
id	-0.16		5.71
id	-0.18		11.43

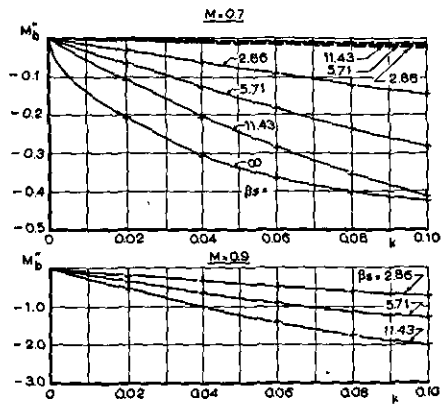

Fig. 13. M'' as function of the reduced frequency for $M = 0.7$ and $M = 0.9$.
—— unsteady values
– – – quasi-steady values

Quasi-steady curves for $M = 0.9$ are straight lines from the origin to the points

$k = 0.1$	$M'' = -0.036$	for $\beta s =$	2.86
id	-0.026		5.71
id	-0.017		11.43

The last of these two conditions indicates that the pitching axis should lie in front of the center of pressure of the whole wing. Otherwise, the aerodynamic moment resulting from a deflection B will induce a still larger deflection. Instead of an oscillation, a divergence of the wing would occur. Hence, the most backward position of the pitching axis which is allowed is at a distance El aft of the leading edge, where E is given in fig. 3.

When solving ε from the first condition (7.2), the positions of the pitching axis are obtained for which unstable oscillations are possible. They are given in figs. 14 and 15 as functions of k with s and M as parameters. For $M = 0.7$ no instability is possible for $\beta s = 5.71$ and $\beta s = 2.86$; likewise for $M = 0.9$ and $\beta s = 2.86$.

It follows by interpolation that for $M = 0.7$ unstable oscillations are only possible if $s > 11.5$ and for $M = 0.9$ if $s > 6.9$; see also fig. 16.

Finally, figs. 17 and 18 show that the damping coefficient M_ε'' is quite different whether the calculations have been made by unsteady or by quasi-steady theory. It follows from these figures that for forward positions of the axis of rotation the damping according to the unsteady theory is much smaller than according to quasi-steady theory.

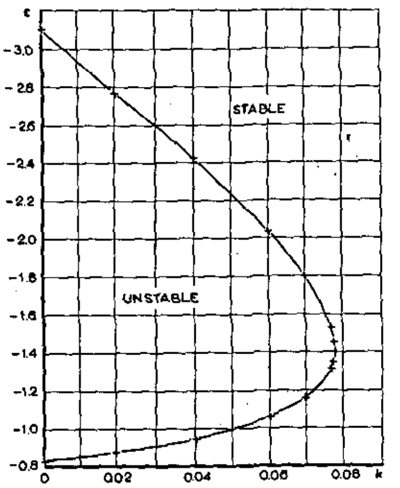

Fig. 14. Possible positions of pitching axis to cause unstable oscillations; $M = 0.7$, $\beta s = 11.43$.

For $\beta s = 5.71$ and 2.86 the oscillations are always stable.

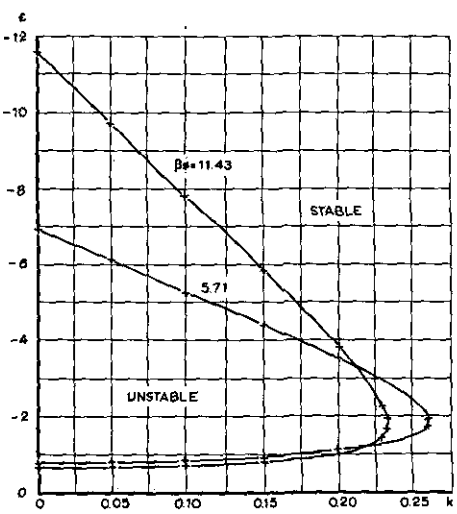

Fig. 15. Possible positions of pitching axis to cause unstable motions, $M = 0.9$.

For $\beta s = 2.86$ the oscillations are always stable.

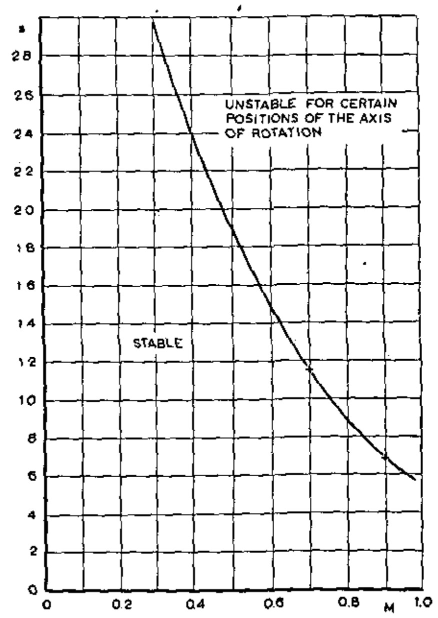

Fig. 16. Stability diagram; above the curve instability is possible.

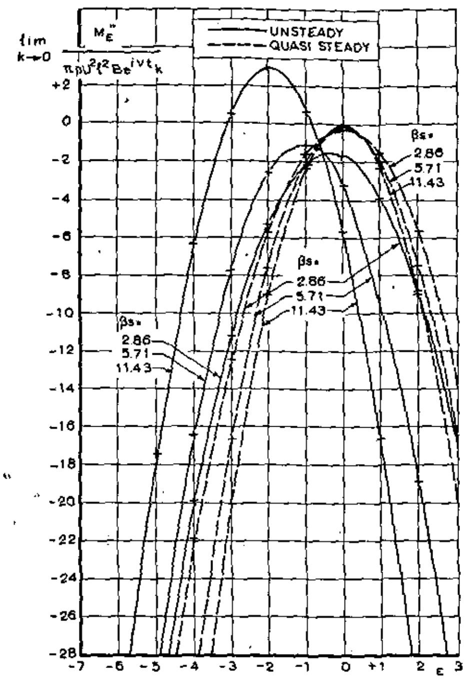

Fig. 17. The unsteady and quasi-steady values of the damping moment for $M = 0.7$ and various positions of the pitching axis (εl is distance aft of mid-chord).

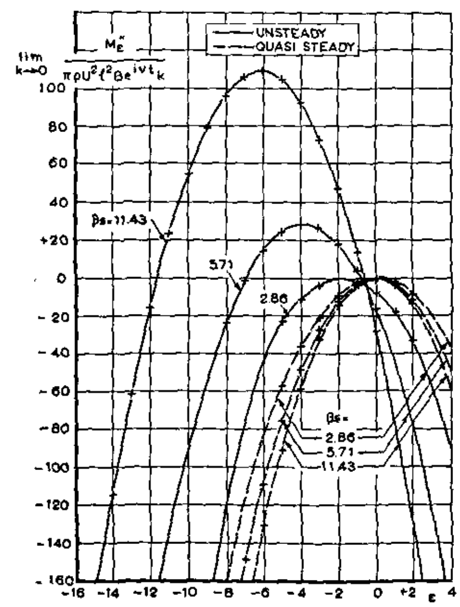

Fig. 18. The unsteady and quasi-steady values of the damping moment for $M = 0.9$ and various positions of the pitching axis (εl is distance aft of mid-chord).

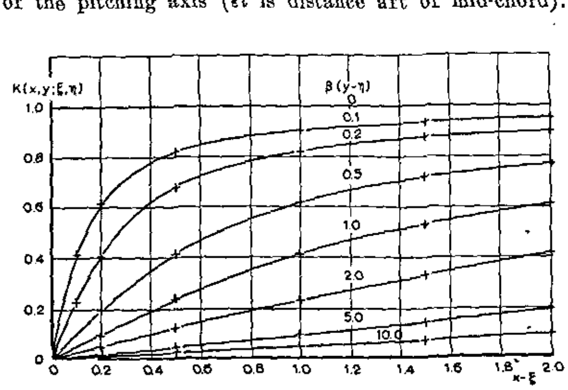

Fig. 19. The function $K(x, y;\ \xi, \eta)$.

8 Conclusions.

(i) A method has been presented which allows the calculation of the in-phase and out-of-phase components of lift and moment distribution on rectangular wings in subsonic flow. The method could, in principle, be extended to wings of any planform.

(ii) For compressible flow there is an important difference between the out-of-phase (damping) components calculated by aid of quasi-steady and by unsteady aerodynamic theory. It may be doubtful whether quasi-steady values are useful for stability calculations if compressibility has to be taken into account.

(iii) Oscillations about a pitching axis which is ahead of the quarterchord axis may become unstable according to unsteady theory. The range within which the pitching axis must lie in order that instability occurs, decreases with decreasing aspect ratio but increases with increasing Mach number.

(iv) Although the snaking motion for usual airplanes will not become unstable on potential-theoretical grounds (even at $M = 0.9$ the aspect ratio of the vertical tail-plane should exceed 3.5 in order that this happens), a considerable reduction of the damping in comparison with the quasi-steady results occurs for large aspect ratios. For smaller aspect ratio this reduction decreases. This will be shown in more details in a subsequent report.

Recommendation for future research.

It would be of interest to investigate how the relation between aspect ratio and Mach number, for which unstable pitching oscillations are possible, continues into the transonic and supersonic ranges. This means the extension of fig. 16 toward higher Mach numbers.

9 List of references.

1. Miles, J. W. Quasi-stationary thin airfoil theory. J. Aer. Sci. **16** (1949) 440.
2. Smilg, B. The instability of pitching oscillations of an airfoil in subsonic incompressible potential flow. J. Aer. Sci. **16** (1949) 691—696.
3. Runyan, H. L. *Single-degree-of-freedom-flutter calculations for a wing in subsonic potential flow and comparison with an experiment.* NACA Tech. Rep. 1089, 1952.
4. Van de Vooren, A. I. and Yff, J. *The effect of aerodynamic lag on the snaking motion of aeroplanes.* NLL Rep. F. 107, 1952.
5. Bird, J. D., Fisher, L. R. and Hubbard, S. M. *Some effects of frequency on the contribution of a vertical tail to the free aerodynamic damping of a model oscillating in yaw.* NACA Tech. Rep. 1130, 1953.
6. Ashley, H., Codik, A., Pratt, R. M. and Campbell, H. J. *Investigation of unsteady aerodynamic and friction effects on rudder-free yawing oscillations of aircraft.* WADC Tech. Rep. 53—273, 1953.
7. Goland, M., Hager, R. G. and Luke, Y. L. Aerodynamic lag in lateral control-free dynamic stability. WADC Tech. Rep. 54—259, 1954.
8. Watkins, Ch. E., Runyan, H. L. and Woolston, D. S. On the kernel function of the integral equation relating the lift and downwash distributions of oscillating finite wings in subsonic flow. NACA Tech. Note 3131, 1954.
9. Van de Vooren, A. I. An approach to lifting surface theory. NLL Rep. F. 129, 1953.
10. Flax, A. H. *General reverse flow and variational theorems in lifting-surface theory.* J. Aer. Sci. **19** (1952) 361—374.
11. Multhopp, H. *Die Berechnung der Auftriebsverteilung von Tragflügeln. Luftfahrtforschung,* Vol. 15, p. 153—169, 1938.
12. Multhopp, H. Methods for calculating the lift distribution of wings (Subsonic lifting surface theory). R. and M. 2884, 1950.
13. De Young, J. and Harper, Ch. E. Theoretical symmetric span loading at subsonic speeds for wings having arbitrary plan form. NACA Tech. Rep. 921, 1948.
14. De Leeuw, J. H., Eckhaus, W. and van de Vooren, A. I. The solution of the generalized Prandtl-equation for swept wings. NLL Rep. F. 156, 1954.

APPENDIX A.

Reduction of the integral equation for steady lifting surface theory.

1 Reduction of the integral equation to two one-variable integral equations.

According to eqs. (2.11) and (2.3) the integral equation for the steady pressure distribution $p^{(0)}$ due to the steady downwash $w^{(0)}$ can be written in the form

$$w^{(0)}(x,y) = -\frac{1}{4\pi\rho U}\int_{-1}^{1}\int_{-s}^{s}\frac{\sqrt{(x-\xi)^2+\beta^2(y-\eta)^2}+x-\xi}{(y-\eta)^2\sqrt{(x-\xi)^2+\beta^2(y-\eta)^2}}\,p^{(0)}(\xi,\eta)\,d\xi\,d\eta \qquad (A.1)$$

where the integration should be taken in the sense of Hadamard. In order to get rid of the improper integral, a partial integration with respect to η is performed resulting in

$$w^{(0)}(x,y) = \frac{1}{4\pi\rho U}\int_{-1}^{1}\int_{-s}^{s}\frac{1}{y-\eta}\left\{1+\frac{\sqrt{(x-\xi)^2+\beta^2(y-\eta)^2}}{x-\xi}\right\}\frac{\partial p^{(0)}(\xi,\eta)}{\partial\eta}\,d\xi\,d\eta. \qquad (A.2)$$

Since the integrations in chordwise direction will be performed by a numerical approximation method, it is logical to split off the singularity at $\xi = x$ in the integrand.

We write

$$\left.\begin{aligned}&\frac{\sqrt{(x-\xi^2)+\beta^2(y-\eta)^2}}{x-\xi} = \beta\,\frac{|y-\eta|}{x-\xi} + K(x,y;\,\xi,\eta)\\ &\text{where } K(x,y;\,\xi,\eta) = \frac{\sqrt{(x-\xi)^2+\beta^2(y-\eta)^2}-\beta\,|y-\eta|}{x-\xi}.\end{aligned}\right\} \qquad (A.3)$$

The term containing the singularity at $\xi = x$ can be integrated to η by writing:

$$\int_{-s}^{s}\frac{|y-\eta|}{y-\eta}\,\frac{\partial p^{(0)}}{\partial\eta}\,d\eta = \int_{-s}^{y}\frac{\partial p^{(0)}}{\partial\eta}\,d\eta - \int_{y}^{s}\frac{\partial p^{(0)}}{\partial\eta}\,d\eta = 2\,p^{(0)}(\xi,y).$$

Hence the integral equation becomes

$$\begin{aligned}w^{(0)}(x,y) = {}&\frac{\beta}{2\pi\rho U}\int_{-1}^{1}\frac{p^{(0)}(\xi,y)}{x-\xi}\,d\xi\,+\\ &+\frac{1}{4\pi\rho U}\int_{-1}^{1}\int_{-s}^{s}\frac{1}{y-\eta}\,\{1+K(x,y;\,\xi,\eta)\}\,\frac{\partial p^{(0)}(\xi,\eta)}{\partial\eta}\,d\xi\,d\eta.\end{aligned} \qquad (A.4)$$

The first term of the right hand side of this equation denotes the two-dimensional downwash, the second term denotes the part of the downwash already familiar from the Prandtl equation while the term with K gives the correction to the Prandtl equation.

Eq. (A.4) is solved by aid of the following assumption

$$p^{(0)}(\xi,\eta) = \frac{1}{\pi}\,g_1^{(0)}(\eta)\cot\frac{\vartheta}{2} + \frac{2}{\pi}\{\,g_0^{(0)}(\eta) - g_1^{(0)}(\eta)\,\}\sin\vartheta \qquad (A.5)$$

where $\xi = -\cos\vartheta$.

It follows from (A.5) that the lift per unit span is equal to $lg^{(0)}(\eta)$ positive upward and the moment per unit span about the mid-chord axis equal to $\frac{1}{2}\,l^2 g_1^{(0)}(\eta)$, positive tailheavy.

After substitution of (A.5) into (A.4), the first term of the right hand side of (A.4) becomes

$$\frac{\beta}{2\pi\rho U}\int_{-1}^{1}\frac{p^{(0)}(\xi,y)}{x-\xi}\,d\xi = \frac{\beta}{2\pi\rho U}\,[g_1^{(0)}(y) - 2\,\{\,g_0^{(0)}(y) - g_1^{(0)}(y)\}\cos\vartheta_0]$$

where $x = -\cos\vartheta_0$.

In the second term of the right hand side of (A.4) the integration to ξ is performed as follows

$$\int_{-1}^{1}\frac{\partial p^{(0)}(\xi,\eta)}{\partial\eta}\,d\xi = g_0^{(0)\prime}(\eta),$$

the prime denoting differentiation to the argument.

For the last term one has

$$\int_{-1}^{1} K(x, y;\ \xi, \eta)\ \frac{\partial p^{(0)}(\xi, \eta)}{\partial \eta}\, d\xi = g_1^{(0)\prime}(\eta)\ .\ K_0(x, y;\ \eta) + \{ g_0^{(0)\prime}(\eta) - g_1^{(0)\prime}(\eta)\}\, K_1(x, y;\ \eta)$$

where

$$\left. \begin{aligned} K_0(x, y;\ \eta) &= \frac{1}{\pi} \int_0^{\pi} K(x, y;\ \xi, \eta) \cot \frac{\vartheta}{2} \sin \vartheta\, d\vartheta \\ K_1(x, y;\ \eta) &= \frac{2}{\pi} \int_0^{\pi} K(x, y;\ \xi, \eta) \sin^2 \vartheta\, d\vartheta. \end{aligned} \right. \tag{A. 6}$$

The integral equation then becomes

$$w^{(0)}(x, y) = \frac{\beta}{2\pi\rho U} [g_1^{(0)}(y) - 2\{ g_0^{(0)}(y) - g_1^{(0)}(y)\} \cos \vartheta_0] + \frac{1}{4\pi\rho U} \int_{-s}^{s} \frac{g_0^{(0)\prime}(\eta)}{y - \eta}\, d\eta +$$

$$+ \frac{1}{4\pi\rho U} \int_{-s}^{s} \frac{g_1^{(0)\prime}(\eta)}{y - \eta} K_0(x, y;\ \eta) d\eta + \frac{1}{4\pi\rho U} \int_{-s}^{s} \frac{g_0^{(0)\prime}(\eta) - g_1^{(0)\prime}(\eta)}{y - \eta} K_1(x, y;\ \eta) d\eta. \tag{A. 7}$$

Since the chordwise distribution of the pressure has been represented by the two-term approximation (A. 5), it is impossible to satisfy (A. 7) for more than 2 values of x. The best procedure, as suggested by FLAX, ref. 10, is to multiply (A. 7) with the weight functions

$$\tan \frac{\vartheta_0}{2} \quad \text{and} \quad 2 \sin \vartheta_0$$

and integrate to x from -1 to $+1$. This leads to two integral equations for the two unknown functions $g_0^{(0)}(\eta)$ and $g_1^{(0)}(\eta)$. In the case of translation $w_T^{(0)}(x, y) = 0$ and hence $g_{0,T}^{(0)}(\eta)$ and $g_{1,T}^{(0)}(\eta)$ equal zero. Therefore the case of rotation needs only to be considered, where $w_R^{(0)} = BU$ and the equations become

$$\left. \begin{aligned} \pi\rho U^2 B &= \tfrac{1}{2} \beta\, g_{0,R}^{(0)}(y) + \tfrac{1}{4} \int_{-s}^{s} \frac{g_{0,R}^{(0)\prime}(\eta)}{y - \eta}\, d\eta + \tfrac{1}{4} \int_{-s}^{s} \frac{g_{1,R}^{(0)\prime}(\eta)}{y - \eta} K_{00}(y, \eta) d\eta + \\ &\qquad + \tfrac{1}{4} \int_{-s}^{s} \frac{g_{0,R}^{(0)\prime}(\eta) - g_{1,R}^{(0)\prime}(\eta)}{y - \eta} K_{10}(y, \eta) d\eta \\ \pi\rho U^2 B &= \tfrac{1}{2} \beta\, g_{1,R}^{(0)}(y) + \tfrac{1}{4} \int_{-s}^{s} \frac{g_{0,R}^{(0)\prime}(\eta)}{y - \eta}\, d\eta + \tfrac{1}{4} \int_{-s}^{s} \frac{g_{1,R}^{(0)\prime}(\eta)}{y - \eta} K_{01}(y, \eta) d\eta + \\ &\qquad + \tfrac{1}{4} \int_{-s}^{s} \frac{g_{0,R}^{(0)\prime}(\eta) - g_{1,R}^{(0)\prime}(\eta)}{y - \eta} K_{11}(y, \eta) d\eta, \end{aligned} \right\} \tag{A. 8}$$

where

$$\left. \begin{aligned} K_{00}(y, \eta) &= \frac{1}{\pi} \int_0^{\pi} K_0(x, y; \eta) \tan \frac{\vartheta_0}{2} \sin \vartheta_0 d\vartheta_0 = \\ &= \frac{1}{\pi^2} \int_0^{\pi}\!\! \int_0^{\pi} K(x, y; \xi, \eta) \tan \frac{\vartheta_0}{2} \sin \vartheta_0 \cot \frac{\vartheta}{2} \sin \vartheta d\vartheta_0 d\vartheta \\ K_{10}(y, \eta) &= \frac{1}{\pi} \int_0^{\pi} K_1(x, y; \eta) \tan \frac{\vartheta_0}{2} \sin \vartheta_0 d\vartheta_0 = \frac{2}{\pi^2} \int_0^{\pi}\!\! \int_0^{\pi} K(x, y; \xi, \eta) \tan \frac{\vartheta_0}{2} \sin \vartheta_0 \sin^2 \vartheta d\vartheta_0 d\vartheta \\ K_{01}(y, \eta) &= \frac{2}{\pi} \int_0^{\pi} K_0(x, y; \eta) \sin^2 \vartheta_0 d\vartheta_0 = \frac{2}{\pi^2} \int_0^{\pi}\!\! \int_0^{\pi} K(x, y; \xi, \eta) \sin^2 \vartheta_0 \cot \frac{\vartheta}{2} \sin \vartheta d\vartheta_0 d\vartheta \\ K_{11}(y, \eta) &= \frac{2}{\pi} \int_0^{\pi} K_1(x, y; \eta) \sin^2 \vartheta_0 d\vartheta_0 = \frac{4}{\pi^2} \int_0^{\pi}\!\! \int_0^{\pi} K(x, y; \xi, \eta) \sin^2 \vartheta_0 \sin^2 \vartheta d\vartheta_0 d\vartheta. \end{aligned} \right\} \tag{A. 9}$$

According to (A.3) $K(x,y;\xi,\eta)$ is in fact a function of the form $K(x-\xi, y-\eta)$ which, moreover, is an odd function of $x-\xi$. This means that

$$K(x,y;\xi,\eta) = -K(\xi,y;x,\eta) \text{ and hence } K_{11}(y,\eta)=0.$$

Furthermore, if in the double integral for $K_{01}(y,\eta)$, $\vartheta_0 = \pi - \vartheta$ and $\vartheta = \pi - \vartheta_0$ is substituted (and, what is the same, x replaced by $-\xi$ and ξ by $-x$), then the expression for $K_{01}(y,\eta)$ transforms into that for $K_{10}(y,\eta)$ and hence $K_{01}(y,\eta) = K_{10}(y,\eta)$.

Eqs. (A.8) then become

$$\left.\begin{aligned}
\pi\rho U^2 B &= \tfrac{1}{2}\beta\, g^{(0)}_{0,R}(y) + \tfrac{1}{4}\int_{-s}^{s}\frac{g^{(0)\prime}_{0,R}(\eta)}{y-\eta}d\eta + \tfrac{1}{4}\int_{-s}^{s}\frac{K_{10}(y,\eta)}{y-\eta}\, g^{(0)\prime}_{0,R}(\eta)d\eta + \\
&\qquad + \tfrac{1}{4}\int_{-s}^{s}\frac{K_{00}(y,\eta)-K_{10}(y,\eta)}{y-\eta}\, g^{(0)\prime}_{1,R}(\eta)d\eta \\
\pi\rho U^2 B &= \tfrac{1}{2}\beta\, g^{(0)}_{1,R}(y) + \tfrac{1}{4}\int_{-s}^{s}\frac{g^{(0)\prime}_{0,R}(\eta)}{y-\eta}d\eta + \tfrac{1}{4}\int_{-s}^{s}\frac{K_{10}(y,\eta)}{y-\eta}\, g^{(0)\prime}_{1,R}(\eta)d\eta.
\end{aligned}\right\} \quad (A.10)$$

The integrals without a K-function will be calculated by aid of the standard MULTHOPP-procedure (ref. 11); the other integrals can be reduced as follows

$$\int_{-s}^{s}\frac{K_{10}(y,\eta)}{y-\eta}\, g^{(0)\prime}_{0,R}(\eta)d\eta = K_{10}(y,y)\int_{-s}^{s}\frac{g^{(0)\prime}_{0,R}(\eta)}{y-\eta}d\eta + \int_{-s}^{s}\frac{K_{10}(y,\eta)-K_{10}(y,y)}{y-\eta}\, g^{(0)\prime}_{0,R}(\eta)d\eta,$$

where the first integral can again be evaluated by aid of MULTHOPP's procedure while the second integral can be calculated by aid of the trapezoidal rule since the integrand is no longer singular.

Putting

$$\left.\begin{aligned}
\frac{K_{10}(y,\eta)-K_{10}(y,y)}{y-\eta} &= \frac{1}{s}L_0(y,\eta) \\
\frac{K_{00}(y,\eta)-K_{10}(y,\eta)-K_{00}(y,y)+K_{10}(y,y)}{y-\eta} &= \frac{1}{s}L_1(y,\eta)
\end{aligned}\right\} \quad (A.11)$$

the integral equations can finally be written as follows

$$\left.\begin{aligned}
2\pi\rho U^2 B &= \beta\, g^{(0)}_{0,R}(y) + \tfrac{1}{2}\{1+K_{10}(y,y)\}\int_{-s}^{s}\frac{g^{(0)\prime}_{0,R}(\eta)}{y-\eta}d\eta + \\
&\quad + \tfrac{1}{2}\{K_{00}(y,y)-K_{10}(y,y)\}\int_{-s}^{s}\frac{g^{(0)\prime}_{1,R}(\eta)}{y-\eta}d\eta + \\
&\quad + \frac{1}{2s}\int_{-s}^{s}L_0(y,\eta)g^{(0)\prime}_{0,R}(\eta)d\eta + \frac{1}{2s}\int_{-s}^{s}L_1(y,\eta)g^{(0)\prime}_{1,R}(\eta)d\eta \\
2\pi\rho U^2 B &= \beta\, g^{(0)}_{1,R}(y) + \tfrac{1}{2}\int_{-s}^{s}\frac{g^{(0)\prime}_{0,R}(\eta)}{y-\eta}d\eta + \tfrac{1}{2}K_{10}(y,y)\int_{-s}^{s}\frac{g^{(0)\prime}_{1,R}(\eta)}{y-\eta}d\eta + \frac{1}{2s}\int_{-s}^{s}L_0(y,\eta)g^{(0)\prime}_{1,R}(\eta)d\eta.
\end{aligned}\right\} \quad (A.12)$$

The advantage of adding a factor $\frac{1}{s}$ in the right hand sides of (A.11) is that L_0 and L_1 depend upon βs, but not upon s separately.

2 The chordwise integration of the function $K(x,y;\xi,\eta)$ and the calculation of the functions $L_0(y,\eta)$ and $L_1(y,\eta)$.

The integrations occurring in eqs. (A.6) and (A.9) are approximated by a method due to MULTHOPP (ref. 12), which has also been applied to the present case by VAN DE VOOREN in ref. 9. For the integration to ξ (or ϑ) the function $K(x,y;\xi,\eta)$ is expanded into a FOURIER series of $\cos m\vartheta$, viz.

$$K(x,y;\xi,\eta) = \sum_{m=0}^{\infty}\lambda_m\cos m\vartheta.$$

If the function $K(x, y; \xi, \eta)$ is given for two values $\xi = \xi_1$ and $\xi = \xi_2$, it is possible to use a FOURIER series consisting of two terms. With this approximation $K_0(x, y; \eta)$ and $K_1(x, y; \eta)$ can be calculated according to eq. (A. 6). However, by a special choice of ξ_1 and ξ_2, it appears possible to use a three-term FOURIER series, which is not completely determined, but of which the uncertainty has no influence upon the values for K_0 and K_1. These values of ξ_1 and ξ_2 (pivotal points) are, see ref. 9, table 8.1

$$\xi_1 = -\cos\frac{1}{5}\pi = -0.8090$$

$$\xi_2 = -\cos\frac{3}{5}\pi = \quad 0.3090$$

and the expressions for K_0 and K_1 become

$$K_0(x, y; \eta) = \frac{1}{\pi}\sum_{h=1}^{2} q_{0h}\, K(x, y; \xi_h, \eta)$$

$$K_1(x, y; \eta) = \frac{2}{\pi}\sum_{h=1}^{2} q_{1h}\, K(x, y; \xi_h, \eta),$$

where $q_{01} = 2.2733$, $q_{02} = 0.8683$, $q_{11} = 0.4342$, $q_{12} = 1.1367$.

For the calculation of K_{00} and K_{10} according to (A. 9), the same method is used, but due to the difference of the factor $\tan\frac{\vartheta_0}{2}$ as compared with $\cot\frac{\vartheta}{2}$ in the integrals (A. 6), the pivotal points are different. They are now (ref. 9, table 8.2)

$$x_1 = -\cos\frac{2}{5}\pi = -0.3090$$

$$x_2 = -\cos\frac{4}{5}\pi = \quad 0.8090.$$

The results for K_{00} and K_{10} are

$$K_{00}(y, \eta) = \frac{1}{\pi}\sum_{i=1}^{2} p_{0i} K_0(x_i, y; \eta) = \frac{1}{\pi^2}\sum_{i=1}^{2}\sum_{h=1}^{2} p_{0i} q_{0h} K(x_i, y; \xi_h, \eta)$$

$$K_{10}(y, \eta) = \frac{1}{\pi}\sum_{i=1}^{2} p_{0i} K_1(x_i, y; \eta) = \frac{2}{\pi^2}\sum_{i=1}^{2}\sum_{h=1}^{2} p_{0i} q_{1h} K(x_i, y; \xi_h, \eta)$$

where $p_{01} = 0.8683$ and $p_{02} = 2.2733$ (ref. 9, table 8.2).

The function $K(x, y; \xi, \eta)$, which is a function of $x - \xi$ and $\beta(y - \eta)$ only, is shown in fig. 19. It may be expected that the representation by a short FOURIER series is better if $\beta(y - \eta)$ is larger. For $\beta(y - \eta) = 0$ the function is discontinuous in $x - \xi = 0$. This will probably give the worst results for the integrated functions K_{00} and K_{10}. To investigate the accuracy of the approximation, the values for $K_{00}(y, y)$ and $K_{10}(y, y)$ are compared with the exact results. For the special case $\eta = y$ the integrals in (A. 9) can be calculated exactly. The results are

	exact	approximated
$\pi^2 K_{00}(y, y)$	8	8.36
$\pi^2 K_{10}(y, y)$	$\frac{16}{3}$ $(= 5.33)$	5.92

For $\eta \neq y$ the agreement may be expected to improve. Since for wings of large aspect ratio $y - \eta$ will be large over the greater part of the wing, the approximation is thought to be sufficiently accurate. Moreover, the term with K in (A. 4) is only the correction to the Prandtl equation.

It follows from (A. 3) that $K(x, y; \xi, \eta)$ is an even function of $y - \eta$. Hence, the same holds for $K_{00}(y, \eta)$ and $K_{10}(y, \eta)$. Due to the term $-\beta\,|y - \eta|$ in (A.3) the functions K, K_{00} and K_{10} have a discontinuous tangent in $\eta = y$ when considered as functions of $y - \eta$. The functions $L_0(y, \eta)$ and $L_1(y, \eta)$ then have a discontinuity for $\eta = y$, such that for $\delta \to 0$

$$L_0(y, y + \delta) = -L_0(y, y - \delta) \quad \text{and} \quad L_1(y, y + \delta) = -L_1(y, y - \delta).$$

3 Transformation of the one-variable integral equations to a set of linear algebraic equations.

For the further reduction of eqs. (A. 12) the standard MULTHOPP procedure (ref. 11) is used. Let

$$y = s\cos\varphi\ ; \quad -s \leqq y \leqq s\,, \quad 0 \leqq \varphi \leqq \pi. \tag{A. 13}$$

For the functions $g^{(0)}_{0,R}$ and $g^{(0)}_{1,R}$ the following FOURIER series is introduced

$$g(y) = g(s\cos\varphi) = \sum_{\lambda=1}^{m} c_\lambda \sin\lambda\varphi \tag{A. 14}$$

with

$$c_\lambda = \frac{2}{\pi}\int_0^\pi g\,(s\cos\varphi)\,\sin\lambda\varphi\,d\varphi.$$

The latter integral is approximated by applying the trapezoidal rule with a division of the integration interval in $m+1$ equal parts. This gives

$$c_\lambda = \frac{2}{m+1}\sum_{n=-\frac{m-1}{2}}^{\frac{m-1}{2}} g^n \sin\lambda\varphi_n\,, \tag{A. 15}$$

where $g^n = g(s\cos\varphi_n)$ and $\varphi_n = \frac{\pi}{2} - \frac{n\pi}{m+1}$ with $n = 0, \pm 1, \pm 2, \ldots, \pm\frac{m+1}{2}$, m is odd. (A. 16)

Substitution of (A. 15) into (A. 14) yields the well-known MULHTOPP formula

$$g(s\cos\varphi) = \frac{2}{m+1}\sum_{n=-\frac{m-1}{2}}^{\frac{m-1}{2}} g^n \sum_{\lambda=1}^{m} \sin\lambda\varphi_n \sin\lambda\varphi. \tag{A. 17}$$

This formula is quite satisfactory since one can show that

$$\frac{2}{m+1}\sum_{\lambda=1}^{m} \sin\lambda\varphi_n \sin\lambda\varphi_k = \begin{cases} 1 & \text{if } n = k \\ 0 & \text{if } n \neq k \end{cases}$$

and hence the interpolation formula (A. 17) yields exactly the right values of $g(s\cos\varphi)$ in the points $y_n = s\cos\varphi_n$.

Series of the type (A. 17) are now substituted for the functions $g^{(0)}_{0,R}(y)$ and $g^{(0)}_{1,R}(y)$ in the integral-equations (A. 12). These equations can then be satisfied no longer for all values of y. They will be satisfied for the m spanwise pivotal points $y_n = s\cos\varphi_n$, where φ_n is given by (A. 16) and $n = 0$, $\pm 1 \ldots\ldots \pm\frac{m-1}{2}$.

In (A. 12) two types of integrals appear, viz.

$$\int_{-s}^{s} \frac{g'(\eta)}{y-\eta}\,d\eta \quad\text{and}\quad \int_{-s}^{s} L(y,\eta)\,g'(\eta)\,d\eta.$$

The reduction of the first integral has been given by MULTHOPP in ref. 11 and also by DE YOUNG and HARPER in ref. 13. The result for the pivotal point $y = y_\nu$ is

$$\int_{-s}^{s} \frac{g'(\eta)}{y_\nu-\eta}\,d\eta = \frac{2\pi}{s}\left\{ b_{\nu\nu} g^\nu - \sum_{\mu=-\frac{m-1}{2}}^{\frac{m-1}{2}}{}' b_{\nu\mu} g^\mu \right\},\ \nu = 0, \pm 1, \ldots \pm\frac{m-1}{2} \tag{A. 18}$$

where

$$\left.\begin{aligned} b_{\nu\nu} &= \frac{m+1}{4\sin\varphi_\nu} \\ b_{\nu\mu} &= \frac{\sin\varphi_\mu}{(\cos\varphi_\mu - \cos\varphi_\nu)^2}\cdot\frac{1-(-1)^{\mu-\nu}}{2(m+1)}. \end{aligned}\right\} \tag{A. 19}$$

The prime at the summation sign denotes that $\mu = \nu$ is excluded from the summation.

For a symmetrical load distribution one has $g^{\nu} = g^{-\nu}$. In this case eqs. (A. 18) and (A. 19) can be simplified as follows

$$\int_{-s}^{s} \frac{g'(\eta)}{y_\nu - \eta} d\eta = \frac{2\pi}{s} \sum_{\mu=0}^{\frac{m-1}{2}} b^{\star}_{\nu\mu} g^{\mu}, \quad \nu = 0,1 \ldots \frac{m-1}{2} \tag{A. 20}$$

where

$$\begin{aligned} b^{\star}_{\nu\mu} &= -(b_{\nu\mu} + b_{\nu,-\mu}) && \text{if } \nu \neq \mu \text{ and } \mu \neq 0 \\ b^{\star}_{\nu\nu} &= \quad b_{\nu\nu} - b_{\nu,-\nu} = b_{\nu\nu} && \text{if } \nu \neq 0 \\ b^{\star}_{\nu 0} &= -b_{\nu 0} && \text{if } \nu \neq 0 \\ b^{\star}_{00} &= \quad b_{00} \end{aligned} \tag{A. 21}$$

For the calculation of the second integral one writes

$$\frac{dg(s\cos\varphi)}{d\varphi} = \frac{2}{m+1} \sum_{n=-\frac{m-1}{2}}^{\frac{m-1}{2}} g^n \sum_{\lambda=1}^{m} \lambda \sin\lambda\varphi_n \cos\lambda\varphi = \sum_{n=-\frac{m-1}{2}}^{\frac{m-1}{2}} g^n f_n(\varphi)$$

where

$$f_n(\varphi) = \frac{2}{m+1} \sum_{\lambda=1}^{m} \lambda \sin\lambda\varphi_n \cos\lambda\varphi. \tag{A. 22}$$

This summation can be performed in a similar way as the summations occurring in $b_{\nu\nu}$ and $b_{\nu\mu}$ have been performed by MULTHOPP (ref. 11). The result is (see ref. 14)

$$f_n(\varphi_\rho) = (-1)^{n-\rho} \frac{\sin\varphi_n}{\cos\varphi_n - \cos\varphi_\rho} \quad \text{if } n \neq \rho,\ \rho = 0, \pm 1, \pm 2, \ldots \pm \frac{m+1}{2} \tag{A. 23}$$

$$f_n(\varphi_n) = -\frac{\cos\varphi_n}{2\sin\varphi_n}.$$

The integral is now reduced as follows

$$\int_{-s}^{s} L(y_\nu, \eta) g'(\eta) d\eta = -\int_{0}^{\pi} L(s\cos\varphi_\nu, s\cos\varphi) \frac{dg(s\cos\varphi)}{d\varphi} d\varphi =$$

$$= -\sum_{\mu=-\frac{m-1}{2}}^{\frac{m-1}{2}} g^{\mu} \int_{0}^{\pi} L(s\cos\varphi_\nu, s\cos\varphi) f_\mu(\varphi) d\varphi.$$

For symmetrical load distributions this becomes

$$-\sum_{\mu=0}^{\frac{m-1}{2}} g^{\mu} \int_{0}^{\pi} L(s\cos\varphi_\nu, s\cos\varphi) f^{\star}_{\mu}(\varphi) d\varphi$$

where

$$f^{\star}_{\mu}(\varphi) = f_\mu(\varphi) + f_{-\mu}(\varphi) \quad \text{if } \mu \neq 0$$

and

$$f^{\star}_{0}(\varphi) = f_0(\varphi).$$

In the pivotal points φ_ρ these functions become:

$$\left.\begin{aligned} f^{\star}_{\mu}(\varphi_\rho) &= f_\mu(\varphi_\rho) + f_{-\mu}(\varphi_\rho) = 4(-1)^{\mu-\rho} \frac{\sin\varphi_\mu \cos\varphi_\rho}{\cos 2\varphi_\mu - \cos 2\varphi_\rho} && \text{if } \mu \neq \pm\rho \text{ and } \mu \neq 0 \\ f^{\star}_{\mu}(\varphi_{\pm\mu}) &= f_\mu(\varphi_{\pm\mu}) + f_{-\mu}(\varphi_{\pm\mu}) = \mp \frac{1}{\sin 2\varphi_\mu} && \text{if } \mu \neq 0 \\ f^{\star}_{0}(\varphi_\rho) &= f_0(\varphi_\rho) = -(-1)^{\rho} \frac{1}{\cos\varphi_\rho} && \text{if } \rho \neq 0 \\ f^{\star}_{0}(\varphi_0) &= f_0(\varphi_0) = 0,\ \varphi_0 = \frac{\pi}{2}. \end{aligned}\right\} \tag{A. 24}$$

Writing now

$$c_{i,\nu,\mu} = -\frac{1}{2\pi}\int_0^\pi L_i(s\cos\varphi_\nu,\ s\cos\varphi)\, f_\mu^\star(\varphi)d\varphi, \tag{A.25}$$

it is obtained finally that

$$\int_{-s}^{+s} L_i(y_\nu,\eta)g'(\eta)d\eta = 2\pi\sum_{\mu=0}^{\frac{m-1}{2}} c_{i,\nu,\mu}\, g^\mu . \tag{A.26}$$

The coefficients $c_{i,\nu,\mu}$ are calculated by aid of the trapezoidal rule. This leads to

$$c_{i,\nu,\mu} = -\frac{1}{2(m+1)}\left\{\frac{L_i(s\cos\varphi_\nu, s)f_\mu^\star(0) + L_i(s\cos\varphi_\nu, -s)f_\mu^\star(\pi)}{2} + \sum_{\rho=-\frac{m-1}{2}}^{\frac{m-1}{2}} L_i(s\cos\varphi_\nu, s\cos\varphi_\rho)f_\mu^\star(\varphi_\rho)\right\}. \tag{A.27}$$

Returning now to eqs. (A.12) and applying them for the pivotal points $y=y_\nu$, the integrals can be reduced by aid of eqs. (A.20) and (A.26). Inserting, moreover, the values of $K_{00}(y,y)$ and $K_{10}(y,y)$ as calculated in Appendix A.2, the result becomes

$$\left.\begin{aligned}
2\rho U^2 s\dot{B} &= \frac{\beta s}{\pi} g_{0,R}^{(0)\nu} + 1.6\sum_{\mu=0}^{\frac{m-1}{2}} b_{\nu\mu}^\star g_{0,R}^{(0)\mu} + 0.24723\sum_{\mu=0}^{\frac{m-1}{2}} b_{\nu\mu}^\star g_{1,R}^{(0)\mu} + \\
&\qquad + \sum_{\mu=0}^{\frac{m-1}{2}} c_{0,\nu,\mu}\, g_{0,R}^{(0)\mu} + \sum_{\mu=0}^{\frac{m-1}{2}} c_{1,\nu,\mu}\, g_{1,R}^{(0)\mu} \\
2\rho U^2 s B &= \frac{\beta s}{\pi} g_{1,R}^{(0)\nu} + \sum_{\mu=0}^{\frac{m-1}{2}} b_{\nu\mu}^\star g_{0,R}^{(0)\mu} + 0.6\sum_{\mu=0}^{\frac{m-1}{2}} b_{\nu\mu}^\star g_{1,R}^{(0)\mu} + \sum_{\mu=0}^{\frac{m-1}{2}} c_{0,\nu,\mu}\, g_{1,R}^{(0)\mu}
\end{aligned}\right\} \tag{A.28}$$

if $\nu = 0, 1, \dots \frac{m-1}{2}$.

It follows from these equations that if βs is kept constant, the values of $\beta g_{0,R}^{(0)}$ and $\beta g_{1,R}^{(0)}$ will remain invariant, which is in agreement with the PRANDTL-GLAUERT rule.

APPENDIX B.

Reduction of the integral equation for the aerodynamic damping.

1 Reduction of the integral equation to two one-variable integral equations.

The integral equation for the pressure distribution $p^{(1)}$ which determines the aerodynamic damping for very low values of the reduced frequency k is, according to eq. (2.11)

$$w^{(1)}(x,y) - \frac{1}{4\pi\rho U}\int_{-1}^{1}\int_{-s}^{s} K^{(1)}(x-\xi, y-\eta)p^{(0)}(\xi,\eta)d\xi d\eta = \frac{1}{4\pi\rho U}\int_{-1}^{1}\int_{-s}^{s} K^{(0)}(x-\xi, y-\eta)p^{(1)}(\xi,\eta)d\xi d\eta. \tag{B.1}$$

The second term on the left hand side of this equation will be evaluated by aid of the results of the previous sections. Substituting for $K^{(1)}$ the expression (2.3), this term becomes

$$-\frac{i}{4\pi\rho U}\int_{-1}^{1}\int_{-s}^{s}\frac{(x-\xi)\sqrt{(x-\xi)^2+\beta^2(y-\eta)^2}+(x-\xi)^2+(y-\eta)^2}{(y-\eta)^2\sqrt{(x-\xi)^2+\beta^2(y-\eta)^2}}\, p^{(0)}(\xi,\eta)d\xi d\eta.$$

Improper integrals can be avoided by partial integration to η of the first two terms. This leads to

$$\frac{i}{4\pi\rho U}\int_{-1}^{1}\int_{-s}^{s}\left\{\frac{x-\xi+\sqrt{(x-\xi)^2+\beta^2(y-\eta)^2}}{y-\eta}\,\frac{\partial p^{(0)}(\xi,\eta)}{\partial\eta} - \frac{p^{(0)}(\xi,\eta)}{\sqrt{(x-\xi)^2+\beta^2(y-\eta)^2}}\right\} d\xi d\eta.$$

The following three terms will now be considered consecutively

a) $$\frac{i}{4\pi\rho U}\int_{-1}^{1}\int_{-s}^{s}\frac{x-\xi}{y-\eta}\,\frac{\partial p^{(0)}(\xi,\eta)}{\partial\eta}\,d\xi\,d\eta;$$

b) $$\frac{i}{4\pi\rho U}\int_{-1}^{1}\int_{-s}^{s}\frac{\sqrt{(x-\xi)^2+\beta^2(y-\eta)^2}}{y-\eta}\,\frac{\partial p^{(0)}(\xi,\eta)}{\partial\eta}\,d\xi\,d\eta;$$

c) $$-\frac{i}{4\pi\rho U}\int_{-1}^{1}\int_{-s}^{s}\frac{p^{(0)}(\xi,\eta)}{\sqrt{(x-\xi)^2+\beta^2(y-\eta)^2}}\,d\xi\,d\eta.$$

When the assumption (A. 5) is substituted for $p^{(0)}(\xi,\eta)$, the integrations to ξ can be performed. Since the integral equation (B. 1) is solved by multiplication with the weight functions $\tan\frac{\vartheta_0}{2}$ and $2\sin\vartheta_0$, where $x=-\cos\vartheta_0$, followed by integration to x between the limits -1 and $+1$, this operation will also be performed on each of the terms a), b) and c).

a) Reduction of $\frac{i}{4\pi\rho U}\int_{-1}^{1}\int_{-s}^{s}\frac{x-\xi}{y-\eta}\,\frac{\partial p^{(0)}(\xi,\eta)}{\partial\eta}\,d\xi\,d\eta.$

Substituting (A. 5) and performing the integration to ξ yields

$$\frac{i}{4\pi\rho U}\int_{-s}^{s}\frac{\frac{1}{2}g_1^{(0)\prime}(\eta)-\cos\vartheta_0\cdot g_0^{(0)\prime}(\eta)}{y-\eta}\,d\eta.$$

Multiplication with the weight functions $\tan\frac{\vartheta_0}{2}$ and $2\sin\vartheta_0$ and integration to x yields

$$\frac{i}{8\rho U}\int_{-s}^{s}\frac{g_1^{(0)\prime}(\eta)+g_0^{(0)\prime}(\eta)}{y-\eta}\,d\eta \text{ and } \frac{i}{8\rho U}\int_{-s}^{s}\frac{g_1^{(0)\prime}(\eta)}{y-\eta}\,d\eta, \qquad \text{(B. 2)}$$

b) Reduction of $\frac{i}{4\pi\rho U}\int_{-1}^{1}\int_{-s}^{s}\frac{\sqrt{(x-\xi)^2+\beta^2(y-\eta)^2}}{y-\eta}\,\frac{\partial p^{(0)}(\xi,\eta)}{\partial\eta}\,d\xi\,d\eta.$

Putting

$$\sqrt{(x-\xi)^2+\beta^2(y-\eta)^2}=J(x,y;\xi,\eta) \qquad \text{(B. 3)}$$

this integral becomes identical to the third term of the right hand side of eq. (A. 4) provided

$K(x,y;\xi,\eta)$ is replaced by $i\,J(x,y;\xi,\eta)$.

Hence, it follows that the final contributions of this term to the two one-variable integral equations are, in analogy to (A. 8), given by

$$\left.\begin{aligned}&\frac{i}{4\rho U}\int_{-s}^{s}\frac{J_{10}(y,\eta)}{y-\eta}\,g_0^{(0)\prime}(\eta)d\eta+\frac{i}{4\rho U}\int_{-s}^{s}\frac{J_{00}(y,\eta)-J_{10}(y,\eta)}{y-\eta}\,g_1^{(0)\prime}(\eta)d\eta\\ &\text{and}\\ &\frac{i}{4\rho U}\int_{-s}^{s}\frac{J_{11}(y,\eta)}{y-\eta}\,g_0^{(0)\prime}(\eta)d\eta+\frac{i}{4\rho U}\int_{-s}^{s}\frac{J_{01}(y,\eta)-J_{11}(y,\eta)}{y-\eta}\,g_1^{(0)\prime}(\eta)d\eta\end{aligned}\right\} \qquad \text{(B. 4)}$$

where the relations between $J_{00}(y,\eta)$, $J_{01}(y,\eta)=J_{10}(y,\eta)$, $J_{11}(y,\eta)$ and $J(x,y;\,\xi,\eta)$ are similar to those between the corresponding K-functions, see eq. (A. 9). Since J is always positive or zero, $J_{11}(y,\eta)$ does not vanish.

It is to be remarked, that $J_{11}(y,\eta)=\frac{2}{\pi}\sum_{i=1}^{2}p_{1i}J_1(x_i,y;\eta)=$

$$=\frac{4}{\pi^2}\sum_{i=1}^{2}\sum_{h=1}^{2}p_{1i}\,q_{1h}\,J(x_i,y;\xi_h,\eta)$$ where $p_{11}=1.1367$ and $p_{12}=0.4342$ (ref. 9, table 8.2).

c) Reduction of $-\frac{i}{4\pi\rho U}\int_{-1}^{1}\int_{-s}^{s}\frac{p^{(0)}(\xi,\eta)}{\sqrt{(x-\xi)^2+\beta^2(y-\eta)^2}}\,d\xi\,d\eta.$

Direct application of the method of pivotal points for the integration to ξ leads to difficulties since the integrand becomes infinite for $x = \xi$ and $y = \eta$. Therefore the singularity at $y = \eta$ is isolated by writing

$$-\frac{i}{4\pi\rho U}\int_{-1}^{1}\int_{-s}^{s}\frac{p^{(0)}(\xi,\eta)-p^{(0)}(\xi,y)}{\sqrt{(x-\xi)^2+\beta^2(y-\eta)^2}}\,d\xi\,d\eta-\frac{i}{4\pi\rho U}\int_{-1}^{1}\int_{-s}^{s}\frac{p^{(0)}(\xi,y)}{\sqrt{(x-\xi)^2+\beta^2(y-\eta)^2}}\,d\xi\,d\eta. \tag{B.5}$$

Since the integrand of the first term remains finite, this term can be reduced by aid of the pivotal points method. Putting

$$\frac{1}{\sqrt{(x-\xi)^2+\beta^2(y-\eta)^2}}=M(x,y;\xi,\eta) \tag{B.6}$$

this term gives, in analogy to (A.8), the following contributions to the one-variable integral equations

$$-\frac{i}{4\rho U}\left[\int_{-s}^{s}\{g_0^{(0)}(\eta)-g_0^{(0)}(y)\}\,M_{10}(y,\eta)d\eta+\int_{-s}^{s}\{g_1^{(0)}(\eta)-g_1^{(0)}(y)\}\,\{M_{00}(y,\eta)-M_{10}(y,\eta)\}d\eta\right]$$

and (B.7)

$$-\frac{i}{4\rho U}\left[\int_{-s}^{s}\{g_0^{(0)}(\eta)-g_0^{(0)}(y)\}\,M_{11}(y,\eta)d\eta+\int_{-s}^{s}\{g_1^{(0)}(\eta)-g_1^{(0)}(y)\}\,\{M_{01}(y,\eta)-M_{11}(y,\eta)\}\,d\eta\right]$$

where the relations between $M_{00}(y,\eta)$, $M_{10}(y,\eta)=M_{01}(y,\eta)$, $M_{11}(y,\eta)$ and $M(x,y;\xi,\eta)$ are again similar to those between the corresponding K-functions.

In the second term of (B.5) the integration to η can be performed, leading to

$$-\frac{i}{4\pi\beta\rho U}\int_{-1}^{1}p^{(0)}(\xi,y)\log\frac{\beta(y+s)+\sqrt{(x-\xi)^2+\beta^2(y+s)^2}}{\beta(y-s)+\sqrt{(x-\xi)^2+\beta^2(y-s)^2}}\,d\xi. \tag{B.8}$$

Since for all points on the wing $y \leq s$, the integrand contains a logarithmic singularity for $x=\xi$. This can be isolated by writing

$$\beta(y-s)+\sqrt{(x-\xi)^2+\beta^2(y-s)^2}=\frac{(x-\xi)^2}{-\beta(y-s)+\sqrt{(x-\xi)^2+\beta^2(y-s)^2}}.$$

Hence, (B.8) may be replaced by

$$-\frac{i}{4\pi\beta\rho U}\int_{-1}^{1}p^{(0)}(\xi,y)\log\left[\{\beta(y+s)+\sqrt{(x-\xi)^2+\beta^2(y+s)^2}\}\{-\beta(y-s)+\right.$$

$$\left.+\sqrt{(x-\xi)^2+\beta^2(y-s)^2}\}\right]d\xi+\frac{i}{4\pi\beta\rho U}\int_{-1}^{1}p^{(0)}(\xi,y)\log(x-\xi)^2d\xi. \tag{B.9}$$

In the first term of (B.9) the pivotal point method can again be used since the integrand remains finite.

Putting

$$\log\{\beta(y+s)+\sqrt{(x-\xi)^2+\beta^2(y+s)^2}\}\{-\beta(y-s)+\sqrt{(x-\xi)^2+\beta^2(y-s)^2}\}=P(x,y;\xi), \tag{B.10}$$

this term yields in analogy to (A.8), the following contributions to the one-variable integral equations

$$-\frac{i}{4\beta\rho U}[g_0^{(0)}(y)\,.\,P_{10}(y)+g_1^{(0)}(y)\,.\,\{P_{00}(y)-P_{10}(y)\}]$$

and (B.11)

$$-\frac{i}{4\beta\rho U}[g_0^{(0)}(y)\,.\,P_{11}(y)+g_1^{(0)}(y)\,.\,\{P_{01}(y)-P_{11}(y)\}]$$

where the relations between $P_{00}(y)$, $P_{10}(y)=P_{01}(y)$, $P_{11}(y)$ and $P(x,y;\xi)$ are again similar to those between the corresponding K-functions.

Substituting into the second term of (B.9) the expression (A.5) for $p^{(0)}(\xi,y)$ the following integrations to ϑ appear

$$\int_{-1}^{1}\cot\frac{\vartheta}{2}\log(x-\xi)^2\,d\xi=-2\pi\log 2-2\pi\cos\vartheta_0$$

$$\int_{-1}^{1} \sin \vartheta \log (x-\xi)^2 \, d\xi = -\pi \log 2 + \tfrac{1}{2}\pi \cos 2\vartheta_0 ,$$

which are derived in Appendix D. Hence

$$+\frac{i}{4\pi\beta\rho U}\int_{-1}^{1} p^{(0)}(\xi, y) \log (x-\xi)^2 d\xi =$$

$$= -\frac{i}{4\pi\beta\rho U}\{ (2\log 2 - \cos 2\vartheta_0) g_0{}^{(0)}(y) + (2\cos\vartheta_0 + \cos 2\vartheta_0) g_1{}^{(0)}(y) \} . \tag{B. 13}$$

Multiplication with the weight functions $\tan \frac{\vartheta_0}{2}$ and $2\sin\vartheta_0$, followed by integration to x from -1 to 1, yields as contributions to the one-variable integral equations

$$-\frac{i}{4\beta\rho U}\{ 2\log 2 \, . \, g_0{}^{(0)}(y) - g_1{}^{(0)}(y) \}$$

and (B. 14)

$$-\frac{i}{4\beta\rho U}\{ (2\log 2 + \tfrac{1}{2}) g_0{}^{(0)}(y) - \tfrac{1}{2} g_1{}^{(0)}(y) \} .$$

Finally, the term $w^{(1)}(x,y)$ must also be multiplied with the weight functions $\tan\frac{\vartheta_0}{2}$ and $2\sin\vartheta_0$, followed by integration to x from -1 to $+1$. Considering first the case of rotation, according to (2.5) $w_R{}^{(1)}(x,y)$ is given by

$$w^{(1)}_R(x,y) = i\,B\,U\,x.$$

Hence, this term yields the following contributions to the one-variable integral equations

$$iBU\frac{\pi}{2} \text{ and } 0.$$

Making use of (B. 2), (B. 4), (B. 7), (B. 11), (B. 14), and (A. 10) the two one-variable integral equations become

$$\frac{i}{2}\pi\rho U^2 B + Q_0(y) + R_0(y) + S_0(y) = \frac{1}{2}\beta g^{(1)}_{0,R}(y) + \frac{1}{4}\int_{-s}^{s}\frac{g^{(1)\prime}_{0,R}(\eta)}{y-\eta}d\eta +$$

$$+\frac{1}{4}\int_{-s}^{s}\frac{K_{10}(y,\eta)}{y-\eta} g^{(1)\prime}_{0,R}(\eta)d\eta + \frac{1}{4}\int_{-s}^{s}\frac{K_{00}(y,\eta)-K_{10}(y,\eta)}{y-\eta} g^{(1)\prime}_{1,R}(\eta)d\eta,$$

$$Q_1(y) + R_1(y) + S_1(y) = \frac{1}{2}\beta g^{(1)}_{1,R}(y) + \frac{1}{4}\int_{-s}^{s}\frac{g^{(1)\prime}_{0,R}(\eta)}{y-\eta}d\eta + \frac{1}{4}\int_{-s}^{s}\frac{K_{10}(y,\eta)}{y-\eta} g^{(1)\prime}_{1,R}(\eta)d\eta.$$

The expressions valid for Q, R and S are as follows

$$Q_0(y) = \frac{1}{8} i \int_{-s}^{s}\frac{g^{(0)\prime}_{0,R}(\eta) + g^{(0)\prime}_{1,R}(\eta)}{y-\eta}d\eta$$

$$R_0(y) = \frac{1}{4} i \left\{ \int_{-s}^{s}\frac{J_{10}(y,\eta)}{y-\eta} g^{(0)\prime}_{0,R}(\eta)d\eta + \int_{-s}^{s}\frac{J_{00}(y,\eta)-J_{10}(y,\eta)}{y-\eta} g^{(0)\prime}_{1,R}(\eta)d\eta \right\}$$

$$S_0(y) = -\frac{1}{4} i \left[\int_{-s}^{s} M_{10}(y,\eta)\{ g^{(0)}_{0,R}(\eta) - g^{(0)}_{0,R}(y) \} d\eta + \int_{-s}^{s}\{ M_{00}(y,\eta) - M_{10}(y,\eta) \}\{ g^{(0)}_{1,R}(\eta) - g^{(0)}_{1,R}(y) \} d\eta \right]$$

$$-\frac{1}{4\beta} i [P_{10}(y) g^{(0)}_{0,R}(y) + \{ P_{00}(y) - P_{10}(y) \} g^{(0)}_{1,R}(y)] - \frac{1}{4\beta} i [(2\log 2) g^{(0)}_{0,R}(y) - g^{(0)}_{1,R}(y)]$$

$$Q_1(y) = \frac{1}{8} i \int_{-s}^{s}\frac{g^{(0)\prime}_{1,R}(\eta)}{y-\eta} d\eta$$

$$R_1(y) = \frac{1}{4} i \left\{ \int_{-s}^{s} \frac{J_{11}(y,\eta)}{y-\eta}\, g_{0,R}^{(0)\prime}(\eta) d\eta + \int_{-s}^{s} \frac{J_{01}(y,\eta) - J_{11}(y,\eta)}{y-\eta}\, g_{1,R}^{(0)\prime}(\eta) d\eta \right\}$$

$$S_1(y) = -\frac{1}{4} i \left[\int_{-s}^{s} M_{11}(y,\eta) \{ g_{0,R}^{(0)}(\eta) - g_{0,R}^{(0)}(y) \} d\eta + \right.$$

$$\left. + \int_{-s}^{s} \{ M_{01}(y,\eta) - M_{11}(y,\eta) \} \{ g_{1,R}^{(0)}(\eta) - g_{1,R}^{(0)}(y) \} d\eta \right] -$$

$$- \frac{1}{4\beta} i [P_{11}(y) g_{0,R}^{(0)}(y) + \{ P_{01}(y) - P_{11}(y) \} g_{1,R}^{(0)}(y)] - \frac{1}{4\beta} i [\{ 2 \log 2 + \tfrac{1}{2} \} g_{0,R}^{(0)}(y) - \tfrac{1}{2} g_{1,R}^{(0)}(y)].$$

For translation the equations are given immediately by (A. 10) with the following modifications

$$B \rightarrow iA, \quad g_{0,R}^{(0)} \rightarrow g_{0,T}^{(1)}, \quad g_{1,R}^{(0)} \rightarrow g_{1,T}^{(1)}.$$

Before the integrations to η are performed by aid of the MULTHOPP procedure, the expressions for $R_0(y)$ and $R_1(y)$ are brought into another form, similar to the reduction given by (A. 11).
Introduce

$$\frac{J_{10}(y,\eta) - J_{10}(y,y)}{y-\eta} = \frac{1}{s} G_1(y,\eta)$$

$$\frac{J_{00}(y,\eta) - J_{10}(y,\eta) - J_{00}(y,y) + J_{10}(y,y)}{y-\eta} = \frac{1}{s} G_2(y,\eta)$$

$$\frac{J_{11}(y,\eta) - J_{11}(y,y)}{y-\eta} = \frac{1}{s} G_3(y,\eta)$$

$$\frac{J_{01}(y,\eta) - J_{11}(y,\eta) - J_{01}(y,y) + J_{11}(y,y)}{y-\eta} = \frac{1}{s} G_4(y,\eta).$$

Since $J_{01} = J_{10}$, it follows that $G_4 = G_1 - G_3$.
Then

$$R_0(y) = \frac{1}{4} i \left[J_{10}(y,y) \int_{-s}^{s} \frac{g_{0,R}^{(0)\prime}(\eta)}{y-\eta} d\eta + \{ J_{00}(y,y) - J_{10}(y,y) \} \int_{-s}^{s} \frac{g_{1,R}^{(0)\prime}(\eta)}{y-\eta} d\eta + \right.$$

$$\left. + \frac{1}{s} \int_{-s}^{s} G_1(y,\eta) g_{0,R}^{(0)\prime}(\eta) d\eta + \frac{1}{s} \int_{-s}^{s} G_2(y,\eta) g_{1,R}^{(0)\prime}(\eta) d\eta \right]$$

$$R_1(y) = \frac{1}{4} i \left[J_{11}(y,y) \int_{-s}^{s} \frac{g_{0,R}^{(0)\prime}(\eta)}{y-\eta} d\eta + \{ J_{01}(y,y) - J_{11}(y,y) \} \int_{-s}^{s} \frac{g_{1,R}^{(0)\prime}(\eta)}{y-\eta} d\eta + \right.$$

$$\left. + \frac{1}{s} \int_{-s}^{s} G_3(y,\eta) g_{0,R}^{(0)\prime}(\eta) d\eta + \frac{1}{s} \int_{-s}^{s} G_4(y,\eta) g_{1,R}^{(0)\prime}(\eta) d\eta \right].$$

The values of $J_{00}(y,y)$, $J_{01}(y,y)$ and $J_{11}(y,y)$ as calculated by aid of the pivotal points method can be compared with the exact values. The result is

	exact	approximated
$\pi^2 J_{00}(y,y)$	$10^2/_3$ $(= 10.67)$	10.80
$\pi^2 J_{01}(y,y) = \pi^2 J_{10}(y,y)$	$7^1/_9$ $(= 7.11)$	7.37
$\pi^2 J_{11}(y,y)$	$5^{31}/_{45}$ $(= 5.69)$	6.39

The final integral equations now become in analogy to (A. 12)

$$\left.\begin{aligned}
&\pi\rho U^2 Bi + 2\,Q_0(y) + 2\,R_0(y) + 2\,S_0(y) = \\
&\quad = \beta\, g^{(1)}_{0,R}(y) + \tfrac{1}{2}\{1 + K_{10}(y,y)\} \int\limits_{-s}^{s} \frac{g^{(1)\prime}_{0,R}(\eta)}{y-\eta}\,d\eta + \\
&\quad + \tfrac{1}{2}\{K_{00}(y,y) - K_{10}(y,y)\} \int\limits_{-s}^{s} \frac{g^{(1)\prime}_{1,R}(\eta)}{y-\eta}\,d\eta + \frac{1}{2\,s}\int\limits_{-s}^{s} L_0(y,\eta)\, g^{(1)\prime}_{0,R}(\eta)\,d\eta + \\
&\quad + \frac{1}{2s}\int\limits_{-s}^{s} L_1(y,\eta)\, g^{(1)\prime}_{1,R}(\eta)\,d\eta \\
&\quad 2Q_1(y) + 2R_1(y) + 2S_1(y) = \beta\, g^{(1)}_{1,R}(y) + \tfrac{1}{2}\int\limits_{-s}^{s} \frac{g^{(1)\prime}_{0,R}(\eta)}{y-\eta}\,d\eta + \\
&\quad\quad + \tfrac{1}{2} K_{10}(y,y) \int\limits_{-s}^{s} \frac{g^{(1)\prime}_{1,R}(\eta)}{y-\eta}\,d\eta + \frac{1}{2s}\int\limits_{-s}^{s} L_0(y,\eta)\, g^{(1)\prime}_{1,R}(\eta)\,d\eta
\end{aligned}\right\} \quad \text{(B. 15*)}$$

2 Transformation of the one-variable integral equations to a set of linear algebraic equations.

The reduction of the integral equations (B. 15*) to algebraic equations occurs again by aid of the MULTHOPP procedure. Since the right hand sides of these equations are identical with those of (A. 12), provided $g^{(0)}$ is replaced by $g^{(1)}$, the reduction for these terms has already been performed in Appendix A 3. In the present section the reduction of the terms Q, R and S will be given.

In agreement with eq. (A. 20), it follows that

$$2Q_0(y\nu) = \frac{1}{2\,s}\,\pi\, i \sum_{\mu=0}^{\frac{m-1}{2}} b^{\star}_{\nu\mu}\,(g^{(0)\mu}_{0,R} + g^{(0)\mu}_{1,R})$$

$$2Q_1(y\nu) = \frac{1}{2\,s}\,\pi\, i \sum_{\mu=0}^{\frac{m-1}{2}} b^{\star}_{\nu\mu}\, g^{(0)\mu}.$$

In analogy with (A. 25), (A. 26) and (A. 27) certain integrals occurring in the expressions for R_0 and R_1 are evaluated as follows

$$\int\limits_{-s}^{s} G_i(y_\nu,\eta)\, g'(\eta)\,d\eta = 2\pi \sum_{\mu=0}^{\frac{m-1}{2}} d_{i,\nu,\mu}\, g^{\mu},$$

where

$$d_{i,\nu,\mu} = -\frac{1}{2(m+1)}\left\{\frac{G_i(s\cos\varphi_\nu, s) f^{\star}_{\mu}(0) + G_i(s\cos\varphi_\nu, -s) f^{\star}_{\mu}(\pi)}{2} + \right.$$
$$\left. + \sum_{\rho=-\frac{m-1}{2}}^{\frac{m-1}{2}} G_i(s\cos\varphi_\nu,\ s\cos\varphi_\rho) f^{\star}_{\mu}(\varphi_\rho)\right\}$$

and $f^{\star}_{\mu}(\varphi_\rho)$ is given by (A. 24).

Hence

$$2R_0(y_\nu) = \frac{\pi i}{s}\left[0.7472 \sum_{\mu=0}^{\frac{m-1}{2}} b^{\star}_{\nu\mu} g^{(0)\mu}_{0,R} + 0.3472 \sum_{\mu=0}^{\frac{m-1}{2}} b^{\star}_{\nu\mu} g^{(0)\mu}_{1,R} + \sum_{\mu=0}^{\frac{m-1}{2}} d_{1,\nu,\mu}\, g^{(0)\mu}_{0,R} + \sum_{\mu=0}^{\frac{m-1}{2}} d_{2,\nu,\mu}\, g^{(0)\mu}_{1,R}\right]$$

$$2R_1(y_\nu) = \frac{\pi i}{s}\left[0.6472 \sum_{\mu=0}^{\frac{m-1}{2}} b^{\star}_{\nu\mu} g^{(0)\mu}_{0,R} + 0.1 \sum_{\mu=0}^{\frac{m-1}{2}} b^{\star}_{\nu\mu} g^{(0)\mu}_{1,R} + \sum_{\mu=0}^{\frac{m-1}{2}} d_{3,\nu,\mu}\, g^{(0)\mu}_{0,R} + \sum_{\mu=0}^{\frac{m-1}{2}} d_{4,\nu,\mu}\, g^{(0)\mu}_{1,R}\right].$$

The integrals occurring in the expressions for S_0 and S_1 are also evaluated by aid of the trapezoidal rule. For instance,

$$\int_{-s}^{s} M_{10}(y_\nu,\eta)g(\eta)d\eta = s\int_0^{\pi} M_{10}(s\cos\varphi_\nu,\ s\cos\varphi)g\,(s\cos\varphi)\sin\ \varphi\, d\varphi =$$

$$\frac{\pi s}{m+1}\sum_{\mu=-\frac{m-1}{2}}^{\frac{m-1}{2}} M_{10}(s\cos\varphi_\nu, s\cos\varphi'_\mu)\sin\varphi_\mu \,.\, g^\mu = \frac{\pi s}{m+1}\sum_{\mu=-\frac{m-1}{2}}^{\frac{m-1}{2}} M_{10}^{\nu\mu}\,.\sin\varphi_\mu\,.\,g^\mu$$

where $M_{ij}^{\nu\mu} = M_{ij}(s\cos\varphi_\nu,\ s\cos\varphi_\mu)$.

Hence

$$2S_0(y_\nu) = -\frac{\pi s}{2(m+1)}\,i\sum_{\mu=-\frac{m-1}{2}}^{\frac{m-1}{2}}\left\{M_{10}^{\nu\mu}\ \sin\varphi_\mu(g_{0,R}^{(0)\mu}-g_{0,R}^{(0)\nu}) + (M_{00}^{\nu,\mu}-M_{10}^{\nu,\mu})\ \sin\varphi_\mu(g_{1,R}^{(0)\mu}-g_{1,R}^{(0)\nu})\right\} -$$

$$-\frac{1}{2\beta}\,i\left\{P_{10}^{\nu}g_{0,R}^{(0)\nu} + (P_{00}^{\nu}-P_{10}^{\nu})g_{1,R}^{(0)\nu}\right\} - \frac{1}{2\beta}\,i\left\{(2\log 2)g_{0,R}^{(0)\nu} - g_{1,R}^{(0)\nu}\right\}$$

$$2S_1(y_\nu) = -\frac{\pi s}{2(m+1)}\,i\sum_{\mu=-\frac{m-1}{2}}^{\frac{m-1}{2}}\left\{M_{11}^{\nu,\mu}\ \sin\varphi_\mu(g_{0,R}^{(0)\mu}-g_{0,R}^{(0)\nu}) + (M_{01}^{\nu,\mu}-M_{11}^{\nu,\mu})\sin\varphi_\mu(g_{1,R}^{(0)\mu}-g_{1,R}^{(0)\nu})\right\} -$$

$$-\frac{1}{2\beta}\,i\,P_{11}^{\nu}g_{0,R}^{(0)\nu} + (P_{01}-P_{11})g_{1,R}^{(0)\nu} - \frac{1}{2\beta}\,i\left\{(2\log 2+\tfrac{1}{2})g_{0,R}^{(0)\nu} - \tfrac{1}{2}\,g_{1,R}^{(0)\nu}\right\}$$

where $P_{i,j}\ (s\cos\varphi_\nu) = P_{i,j}^{\nu}$.

Finally, the set of algebraic equations is

$$\rho U^2 sBi + 1.2472\,i\sum_{\mu=0}^{\frac{m-1}{2}} b_\mu^{\star}\,g_{0,R}^{(0)\mu} + 0.8472\,i\sum_{\mu=0}^{\frac{m-1}{2}} b_\mu^{\star}\,g_{1,R}^{(0)\mu} + i\sum_{\mu=0}^{\frac{m-1}{2}} d_{1,\nu,\mu}\,g_{0,R}^{(0)\mu} + i\sum_{\mu=0}^{\frac{m-1}{2}} d_{2,\nu,\mu}\,g_{1,R}^{(0)\mu} -$$

$$-\frac{s^2}{2(m+1)}\,i\sum_{\mu=-\frac{m-1}{2}}^{\frac{m-1}{2}}\left\{M_{10}^{\nu\mu}(g_{0,R}^{(0)\mu}-g_{0,R}^{(0)\nu}) + (M_{00}^{\nu\mu}-M_{10}^{\nu\mu})(g_{1,R}^{(0)\mu}-g_{1,R}^{(0)\nu})\right\}\sin\varphi_\mu -$$

$$-\frac{s}{2\pi\beta}\,i\left\{(P_{10}^{\nu}+2\log 2)g_{0,R}^{(0)\nu} + (P_{00}^{\nu}-P_{10}^{\nu}-1)g_{1,R}^{(0)\nu}\right\} =$$

$$= \frac{\beta s}{\pi}g_{0,R}^{(1)\nu} + 1.6\sum_{\mu=0}^{\frac{m-1}{2}} b_{\nu\mu}^{\star}\,g_{0,R}^{(1)\mu} + 0.24723\sum_{\mu=0}^{\frac{m-1}{2}} b_{\nu\mu}^{\star}\,g_{1,R}^{(1)\mu} + \sum_{\mu=0}^{\frac{m-1}{2}} c_{0,\nu,\mu}\,g_{0,R}^{(1)\mu} + \sum_{\mu=0}^{\frac{m-1}{2}} c_{1,\nu,\mu}\,g_{1,R}^{(1)\mu}. \tag{B. 16}$$

and

$$0.6472\,i\sum_{\mu=0}^{\frac{m-1}{2}} b_{\nu\mu}^{\star}\,g_{0,R}^{(0)\mu} + 0.6\,i\sum_{\mu=0}^{\frac{m-1}{2}} b_{\nu\mu}^{\star}\,g_{1,R}^{(0)\mu} + i\sum_{\mu=0}^{\frac{m-1}{2}} d_{3,\nu,\mu}\,g_{0,R}^{(0)\mu} + i\sum_{\mu=0}^{\frac{m-1}{2}} d_{4,\nu,\mu}\,g_{1,R}^{(0)\mu} -$$

$$-\frac{s^2}{2(m+1)}\,i\sum_{\mu=-\frac{m-1}{2}}^{\frac{m-1}{2}}\left\{M_{11}^{\nu\mu}(g_{0,R}^{(0)\mu}-g_{0,R}^{(0)\nu}) + (M_{01}^{\nu\mu}-M_{11}^{\nu\mu})(g_{1,R}^{(0)\mu}-g_{1,R}^{(0)\nu})\right\}\sin\varphi_\mu -$$

$$-\frac{s}{2\pi\beta}\,i\left\{(P_{11}^{\nu}+2\log 2+\tfrac{1}{2})g_{0,R}^{(0)\nu} + (P_{01}^{\nu}-P_{11}^{\nu}-\tfrac{1}{2})g_{1,R}^{(0)\nu}\right\} =$$

$$= \frac{\beta s}{\pi}g_{1,R}^{(1)\nu} + \sum_{\mu=0}^{\frac{m-1}{2}} b_{\nu\mu}^{\star}\,g_{0,R}^{(1)\mu} + 0.6\sum_{\mu=0}^{\frac{m-1}{2}} b_{\nu\mu}^{\star}\,g_{1,R}^{(1)\mu} + \sum_{\mu=0}^{\frac{m-1}{2}} c_{0,\nu,\mu}\,g_{1,R}^{(1)\mu}. \tag{B. 17}$$

In these equations, the left hand sides are known, while the quantities $g_{0,R}^{(1)\nu}$ and $g_{1,R}^{(1)\nu}$, $\nu = 0, 1 \ldots \frac{m-1}{2}$ are the unknowns. They differ from eqs. (A. 28) only in the known terms.

The property of $g_{0,R}^{(0)}(\eta)$ and $g_{1,R}^{(0)}(\eta)$, that $\beta g_{0,R}^{(0)}(\eta)$ and $\beta g_{1,R}^{(0)}(\eta)$ remain invariant if βs is hold constant (See sec. 3) is no longer valid for $g_{0,R}^{(1)}(\eta)$ and $g_{1,R}^{(1)}(\eta)$, because the left-handsides of eqs. (B. 16) and (B. 17) are not proportional to s.

3 The two-dimensional case.

It follows from eqs. (A 28) that for $s \to \infty$,

$$g_{0,R}^{(0)\nu} = \frac{2\pi}{\beta}\rho U^2 B \quad \text{and} \quad g_{1,R}^{(0)\nu} = \frac{2\pi}{\beta}\rho U^2 B.$$

Dividing eqs. (B. 16) and (B. 17) through s, these equations become in the limit $s \to \infty$,

$$\rho U^2 Bi + \frac{i}{s}\sum_{\mu=0}^{\frac{m-1}{2}} d_{1,\nu,\mu}\, g_{0,R}^{(0)\mu} + \frac{i}{s}\sum_{\mu=0}^{\frac{m-1}{2}} d_{2,\nu,\mu}\, g_{1,R}^{(0)\mu} -$$

$$-\frac{s}{2(m+1)}\, i \sum_{\mu=-\frac{m-1}{2}}^{\frac{m-1}{2}} \left\{ M_{10}^{\nu\mu}(g_{0,R}^{(0)\mu} - g_{0,R}^{(0)\nu}) + (M_{00}^{\nu\mu} - M_{10}^{\nu\mu})(g_{1,R}^{(0)\mu} - g_{1,R}^{(0)\nu}) \right\} \sin\varphi_\mu -$$

$$-\frac{i}{2\pi\beta}\left\{ (P_{10}^{\nu} + 2\log 2) g_{0,R}^{(0)\nu} + (P_{00}^{\nu} - P_{10}^{\nu} - 1) g_{1,R}^{(0)\nu} \right\} = \frac{\beta}{\pi}\, g_{0,R}^{(1)\nu}, \text{ and}$$

$$+\frac{i}{s}\sum_{\mu=0}^{\frac{m-1}{2}} d_{3,\nu,\mu}\, g_{0,R}^{(0)\mu} + \frac{i}{s}\sum_{\mu=0}^{\frac{m-1}{2}} d_{4,\nu,\mu}\, g_{1,R}^{(0)\mu} -$$

$$-\frac{s}{2(m+1)}\, i \sum_{\mu=-\frac{m-1}{2}}^{\frac{m-1}{2}} \left\{ M_{11}^{\nu\mu}(g_{0,R}^{(0)\mu} - g_{0,R}^{(0)\nu}) + (M_{01}^{\nu\mu} - M_{11}^{\nu\mu})(g_{1,R}^{(0)\mu} - g_{1,R}^{(0)\nu}) \right\} \sin\varphi_\mu -$$

$$-\frac{i}{2\pi\beta}\left\{ (P_{11}^{\nu} + 2\log 2 + \tfrac{1}{2}) g_{0,R}^{(0)\nu} + (P_{01}^{\nu} - P_{11}^{\nu} - \tfrac{1}{2}) g_{1,R}^{(0)\nu} \right\} = \frac{\beta}{\pi}\, g_{1,R}^{(1)\nu}.$$

Since the function M for large s is of order $\frac{1}{s}$ and since $g_{0,R}^{(0)}$ and $g_{1,R}^{(0)}$ are constant along the wing, the summations containing M vanish.

Furthermore the function P is of order $\log s$ forlarge values of s. It follows from eqs. (A. 9) that if P is independent of x and ξ

$$P_{00} = P_{10} = P_{01} = P_{11} = P \text{ and hence, also } 0\,(\log s).$$

As the remaining terms at the left hand side are of order 1, $g_{0,R}^{(1)}$ and $g_{1,R}^{(1)}$ become also of order $\log s$ for $s \to \infty$.

The quantities $\frac{g_{0,R}^{(1)}}{s}$ and $\frac{g_{1,R}^{(1)}}{s}$ vanish for $s \to \infty$.

4 The integral equation for the pressure distribution $Im\, p^{(3)}$.

The third equation (2.11) reads

$$-\frac{1}{4\pi\rho U}\int_{-1}^{1}\int_{-s}^{s} Im\, K^{(3)}(x-\xi,\ y-\eta) p^{(0)}(\xi,\eta)\, d\xi\, d\eta = \frac{1}{4\pi\rho U}\int_{-1}^{1}\int_{-s}^{s} K^{(0)}(x-\xi,\ y-\eta) Im\, p^{(3)}(\xi,\eta)\, d\xi\, d\eta$$

where $Im\, K^{(3)}\,(x-\xi,\ y-\eta) = -\frac{\pi}{4}$.

After substitution of (A. 5) for $p^{(0)}(\xi,\eta)$ it follows that

$$-\frac{1}{4\pi\rho U}\int_{-1}^{1}\int_{-s}^{s} Im\, K^{(3)}(x-\xi,\ y-\eta) p^{(0)}(\xi,\eta)\, d\xi\, d\eta = \frac{1}{16\rho U}\int_{-s}^{s} g_0^{(0)}(\eta)\, d\eta.$$

By aid of eqs. (A. 14) and (A. 15), this becomes equal to

$$\frac{\pi s}{32\rho U}\, c_1 = \frac{\pi s}{16(m+1)\rho U}\left(g_0^{(0)\nu} + 2\sum_{\nu=1}^{\frac{m-1}{2}} g_0^{(0)\nu} \sin\varphi_\nu\right).$$

Hence, the integral equation becomes

$$\frac{\pi s}{16(m+1)\rho U}\left(g_0^{(0)0}+2\sum_{\nu=1}^{\frac{m-1}{2}} g_0^{(0)\nu}\sin\varphi_\nu\right)=\frac{1}{4\pi\rho U}\int_{-1}^{1}\int_{-s}^{s}K^{(0)}(x-\xi,\ y-\eta)Im\,p^{(3)}(\xi,\eta)\,d\xi d\eta.$$

The left hand side of this equation is independent of x and y. If the left hand side is replaced by UB, the equation is identical to the one which has been solved in Appendix A. Hence the solution of the present equation is for the case of rotation given by

$$\left.\begin{aligned} Im\,g_{0,R}^{(3)}&=\frac{\pi s}{16(m+1)\rho U^2 B}\left(g_{0,R}^{(0)0}+2\sum_{\nu=1}^{\frac{m-1}{2}} g_{0,R}^{(0)\nu}\sin\varphi_\nu\right)g_{0,R}^{(0)}\\ Im\,g_{1,R}^{(3)}&=\frac{\pi s}{16(m+1)\rho U^2 B}\left(g_{0,R}^{(0)0}+2\sum_{\nu=1}^{\frac{m-1}{2}} g_{0,R}^{(0)\nu}\sin\varphi_\nu\right)g_{1,R}^{(0)} \end{aligned}\right\} \qquad (B.18)$$

with $p^{(3)}(\xi,\eta)=\frac{1}{\pi}g_1^{(3)}(\eta)\cot\frac{\vartheta}{2}+\frac{2}{\pi}\{g_0^{(3)}(\eta)-g_1^{(3)}(\eta)\}\sin\vartheta.$

For the case of translation $Im\,g_{0,T}^{(3)}=Im g_{1,T}^{(3)}=0$, because $g_{0,T}^{(0)}$ equals zero.

APPENDIX C.

The position of the sectional center of pressure at the tip.

The sectional center of pressure lies at a distance el aft of the leading edge, where according to eq. (3.3), e is given by

$$e=1-\frac{g_1^{(0)}}{2\,g_0^{(0)}}.$$

Since both $g_0^{(0)}$ and $g_1^{(0)}$ vanish at the tip, the following limiting procedure must be performed

$$\lim_{y\to s}\frac{g_1^{(0)}}{g_0^{(0)}}=\lim_{\varphi\to 0}\frac{g_1^{(0)}}{g_0^{(0)}}=\lim_{\varphi\to 0}\frac{dg_1^{(0)}/d\varphi}{dg_0^{(0)}/d\varphi}.$$

Using eq. (A.17), this becomes equal to

$$\frac{\displaystyle\sum_{n=-\frac{m-1}{2}}^{\frac{m-1}{2}} g_1^{(0)n}\sum_{\lambda=1}^{m}\lambda\sin\lambda\varphi_n}{\displaystyle\sum_{n=-\frac{m-1}{2}}^{\frac{m-1}{2}} g_0^{(0)n}\sum_{\lambda=1}^{m}\lambda\sin\lambda\varphi_n}.$$

According to ref. 14, one has

$$\sum_{\lambda=1}^{m}\lambda\sin\lambda\varphi_n=\frac{m\sin(m+1)\varphi_n-(m+1)\sin m\varphi_n}{2(\cos\varphi_n-1)}.$$

With $\varphi_n=\frac{\pi}{2}-\frac{n\pi}{m+1}$, eq. (A.16), and m being an odd number, one has

$$\sin(m+1)\varphi_n=0,\ \cos(m+1)\varphi_n=(-1)^{-n+\frac{m+1}{2}}$$

Hence, $\sin m\varphi_n=\sin(m+1)\varphi_n\cos\varphi_n-\cos(m+1)\varphi_n\sin\varphi_n=-(-1)^{-n+\frac{m+1}{2}}\sin\varphi_n$

and $\displaystyle\sum_{\lambda=1}^{m}\lambda\sin\lambda\varphi_n=\frac{m+1}{2}(-1)^{-n+\frac{m+1}{2}}\frac{\sin\varphi_n}{\cos\varphi_n-1}.$

Thus

$$\lim_{y \to s} \frac{g_1^{(0)}}{g_0^{(0)}} \frac{\sum_{n=-\frac{m-1}{2}}^{\frac{m-1}{2}} g_1^{(0)n} (-1)^n \frac{\sin\varphi_n}{\cos\varphi_n - 1}}{\sum_{n=-\frac{m-1}{2}}^{\frac{m-1}{2}} g_0^{(0)n} (-1)^n \frac{\sin\varphi_n}{\cos\varphi_n - 1}}.$$

For symmetric load distributions, the values of n and $-n$ can be taken together. For $n \neq 0$

$$\frac{\sin\varphi_n}{\cos\varphi_n - 1} + \frac{\sin\varphi_{-n}}{\cos\varphi_{-n} - 1} = \frac{\sin\varphi_n}{\cos\varphi_n - 1} - \frac{\sin\varphi_n}{\cos\varphi_n + 1} = \frac{2\sin\varphi_n}{\cos^2\varphi_n - 1} = -\frac{2}{\sin\varphi_n}$$

while for $n = 0$, $\frac{\sin\varphi_n}{\cos\varphi_n - 1} = -1$.

Hence

$$\lim_{y \to s} \frac{g_1^{(0)}}{g_0^{(0)}} = \frac{g_1^{(0)0} + 2\sum_{\nu=1}^{\frac{m-1}{2}} g_1^{(0)\nu} \frac{(-1)^\nu}{\sin\varphi_\nu}}{g_0^{(0)0} + 2\sum_{\nu=1}^{\frac{m-1}{2}} g_0^{(0)\nu} \frac{(-1)^\nu}{\sin\varphi_\nu}}.$$

Thus, at the tip section

$$e = 1 - \tfrac{1}{2} \cdot \frac{g_1^{(0)0} + 2\sum_{\nu=1}^{\frac{m-1}{2}} g_1^{(0)\nu} \frac{(-1)^\nu}{\sin\varphi_\nu}}{g_0^{(0)0} + 2\sum_{\nu=1}^{\frac{m-1}{2}} g_0^{(0)\nu} \frac{(-1)^\nu}{\sin\varphi_\nu}}.$$

APPENDIX D.

Reduction of two integrals.

Calculation of the integrals $\int_{-1}^{+1} \operatorname{cotg} \frac{\vartheta}{2} \log (x-\xi)^2 d\xi$ and $\int_{-1}^{+1} \sin\vartheta \log (x-\xi)^2 d\xi$.

Substituting $x = -\cos\vartheta_0$ and $\xi = -\cos\vartheta$, the first integral becomes

$$\int_{-1}^{+1} \operatorname{cotg} \frac{\vartheta}{2} \log (x-\xi)^2 d\xi = \int_0^\pi \operatorname{cotg} \frac{\vartheta}{2} \sin\vartheta \log (\cos\vartheta - \cos\vartheta_0)^2 d\vartheta = \int_0^\pi (1+\cos\vartheta) \log (\cos\vartheta - \cos\vartheta_0)^2 d\vartheta.$$

Integration by parts yields

$$\int_{-1}^{+1} \operatorname{cotg} \frac{\vartheta}{2} \log (x-\xi)^2 d\xi = (\vartheta + \sin\vartheta) \log (\cos\vartheta - \cos\vartheta_0)^2 \Big|_0^\pi + 2\int_0^\pi (\vartheta + \sin\vartheta) \frac{\sin\vartheta}{\cos\vartheta - \cos\vartheta_0} d\vartheta =$$

$$+ 2\pi \log (1 + \cos\vartheta_0) + 2\int_0^\pi \frac{\vartheta \sin\vartheta}{\cos\vartheta - \cos\vartheta_0} d\vartheta + \int_0^\pi \frac{1 - \cos 2\vartheta}{\cos\vartheta - \cos\vartheta_0} d\vartheta.$$

The first integral is calculated by integrating by parts and using the formula

$$\int_0^{\frac{\pi}{2}} \log \sin \vartheta \, d\vartheta = -\frac{\pi}{2} \log 2 \ \ldots$$

and the result is $$\int_0^{\pi} \frac{\vartheta \sin \vartheta}{\cos \vartheta - \cos \vartheta_0} d\vartheta = -\pi \log (1 + \cos \vartheta_0) - \pi \log 2. \qquad \text{(D. 1)}$$

(See also ref. 14)

The second integral is of the well-known Glauert-form and

$$\int_0^{\pi} \frac{1 - \cos 2\vartheta}{\cos \vartheta - \cos \vartheta_0} d\vartheta = -2\pi \cos \vartheta_0 .$$

Finally the total integral becomes

$$\int_{-1}^{+1} \operatorname{cotg} \frac{\vartheta}{2} \log (x - \xi)^2 \, d\xi = -2\pi \log 2 - 2\pi \cos \vartheta_0 . \qquad \text{(D. 2)}$$

The integral

$$\int_{-1}^{+1} \sin \vartheta \log (x - \xi)^2 \cdot d\xi = \frac{1}{2} \int_0^{\pi} (1 - \cos 2\vartheta) \log (\cos \vartheta - \cos \vartheta_0)^2 d\vartheta$$

can be handled in the same manner.

Integrating by parts yields

$$\int_{-1}^{+1} \sin \vartheta \log (x - \xi)^2 d\xi = \pi \log (1 + \cos \vartheta_0) + \int_0^{\pi} \vartheta \frac{\sin \vartheta}{\cos \vartheta - \cos \vartheta_0} d\vartheta - \tfrac{1}{2} \int_0^{\pi} \frac{\sin \vartheta \sin 2\vartheta}{\cos \vartheta - \cos \vartheta_0} d\vartheta .$$

The first integral at the right hand side has been already calculated and equals $-\pi \log (1 + \cos \vartheta_0) - \pi \log 2$ (D. 1).

The second integral

$$-\tfrac{1}{2} \int_0^{\pi} \frac{\sin \vartheta \sin 2\vartheta}{\cos \vartheta - \cos \vartheta_0} d\vartheta = +\tfrac{1}{4} \int_0^{\pi} \frac{\cos 3\vartheta - \cos \vartheta}{\cos \vartheta - \cos \vartheta_0} d\vartheta$$

is again of the well-known Glauert-form and equals

$$\tfrac{1}{4}\pi \frac{\sin 3\vartheta_0 - \sin \vartheta_0}{\sin \vartheta_0} = \tfrac{1}{2}\pi \cos 2\vartheta_0 .$$

Hence the total integral becomes

$$\int_{-1}^{+1} \sin \vartheta \log (x - \xi)^2 d\xi = -\pi \log 2 + \tfrac{1}{2}\pi \cos 2\vartheta_0 .$$

Values of the local aerodynamic derivatives at various spanwise positions.

TABLE 1. $\beta s = 2.86$

	M \ y/s	0	0.1951	0.3827	0.5556	0.7071	0.8315	0.9239	0.9808
$\beta k_b'$	$0 < M < 1$	−1.2009	−1.1844	−1.1304	−1.0356	−0.89894	−0.72030	−0.50404	−0.25949
$\beta m_b'$	$0 < M < 1$	0.64045	0.63433	0.61251	0.57245	0.51122	0.42370	0.30607	0.16105
$\lim_{k \to 0} \frac{k_b''}{k}$	0.7	0.44019	0.39254	0.26723	0.096917	−0.075415	−0.19451	−0.21787	−0.14007
	0.9	0.3532	9.0766	8.2739	7.0528	5.5769	4.0309	2.5645	1.2351
$\lim_{k \to 0} \frac{m_b''}{k}$	0.7	−2.0264	−1.9977	−1.8964	−1.7228	−1.4877	−1.1915	−0.83458	−0.42846
	0.9	−10.104	−9.9310	−9.3509	−8.3803	−7.0935	−5.5439	−3.7917	−1.9139

TABLE 2. $\beta s = 5.71$

	M \ y/s	0	0.1951	0.3827	0.5556	0.7071	0.8315	0.9239	0.9808
$\beta k_b'$	$0 < M < 1$	−1.5675	−1.5516	−1.5014	−1.4090	−1.2617	−1.0457	−0.75389	−0.39575
$\beta m_b'$	$0 < M < 1$	0.79756	0.79092	0.77006	0.73215	0.67143	0.57826	0.43759	0.23933
$\lim_{k \to 0} \frac{k_b''}{k}$	0.7	4.4290	4.2954	3.9039	3.2890	2.5156	1.6923	0.95443	0.40202
	0.9	28.721	28.056	26.091	22.940	18.825	14.108	9.2237	4.5078
$\lim_{k \to 0} \frac{m_b''}{k}$	0.7	−4.2105	−4.1299	−3.9152	−3.5615	−3.0889	−2.5027	−1.7927	−0.94083
	0.9	−20.800	−20.438	−19.341	−17.520	−15.051	−11.988	−8.3903	−4.3157

TABLE 3. $\beta s = 11.43$

	M \ y/s	0	0.1951	0.3827	0.5556	0.7071	0.8315	0.9239	0.9808
$\beta k_b'$	$0 < M < 1$	−1.7855	−1.7801	−1.7509	−1.6867	−1.5711	−1.3702	−1.0434	−0.57079
$\beta m_b'$	$0 < M < 1$	0.89707	0.89427	0.88092	0.85295	0.80410	0.72093	0.57803	0.33762
$\lim_{k \to 0} \frac{k_b''}{k}$	0.7	9.8133	9.6485	9.0936	8.1204	6.7462	5.0304	3.1684	1.4451
	0.9	53.519	52.783	50.201	45.589	38.967	30.435	20.575	10.213
$\lim_{k \to 0} \frac{m_b''}{k}$	0.7	−6.9372	−6.8598	−6.5796	−6.0785	−5.3609	−4.4251	−3.2582	−1.7834
	0.9	−33.585	−33.217	−31.881	−29.470	−25.952	−21.271	−15.389	−8.2251

TABLE 4. Quasi steady values of the local aerodynamic derivatives at various spanwise positions $(0 < M < 1)$.

y/s	0	0.1951	0.3827	0.5556	0.7071	0.8315	0.9239	0.9808
$\beta s = 2.86$								
$\frac{\beta k_b''}{k}$	−0.64166	−0.63557	−0.61342	−0.57250	−0.51027	−0.42189	−0.30406	−0.15975
$\frac{\beta m_b''}{k}$	−0.15475	−0.15815	−0.16404	−0.16924	−0.17007	−0.15819	−0.12535	−0.09825
$\beta s = 5.71$								
$\frac{\beta k_b''}{k}$	−0.79905	−0.79241	−0.77134	−0.73278	−0.67072	−0.57565	−0.43365	−0.23623
$\frac{\beta m_b''}{k}$	−0.093981	−0.096666	−0.10483	−0.11845	−0.13567	−0.14877	−0.13929	−0.087411
$\beta s = 11.43$								
$\frac{\beta k_b''}{k}$	−0.89739	−0.89503	−0.88196	−0.85375	−0.80434	−0.71935	−0.57398	−0.33285
$\frac{\beta m_b''}{k}$	−0.047497	−0.050378	−0.057008	−0.068672	−0.088489	−0.11629	−0.13773	−0.10727

The aerodynamic derivatives for various values of the reduced frequency k.

TABLE 5. $\beta s = 2.86$

	M \ k	0	0.02	0.04	0.06	0.08	0.10
$\beta K_a'$	$0 < M < 1$	0	0	0	0	0	0
$\beta K_b'$	id	— 0.97132	— 0.97132	— 0.97132	— 0.97132	— 0.97132	— 0.97132
$\beta M_a'$	id	0	0	0	0	0	0
$\beta M_b'$	id	+ 0.53597	+ 0.53597	+ 0.53597	+ 0.53597	+ 0.53597	+ 0.53597
$\beta K_a''$	id	0	— 0.019426	— 0.038853	— 0.058279	— 0.077706	— 0.097132
K_b''	0.7	0	+ 0.0014313	+ 0.00053810	— 0.0026802	— 0.0082220	— 0.016089
	0.9	0	0.13034	0.25046	0.36035	0.46002	0.54948
$\beta M_a''$	$0 < M < 1$	0	0.010719	0.021439	0.032158	0.042851	0.053597
M_b''	0.7	0	— 0.031851	— 0.062419	— 0.091704	— 0.11971	— 0.14643
	0.9	0	— 0.15551	— 0.30539	— 0.44962	— 0.58822	— 0.72117

TABLE 6. $\beta s = 5.71$

	M \ k	0	0.02	0.04	0.06	0.08	0.10
$\beta K_a'$	$0 < M < 1$	0	0	0	0	0	0
$\beta K_b'$	id	— 1.3161	— 1.3161	— 1.3161	— 1.3161	— 1.3161	— 1.3161
$\beta M_a'$	id	0	0	0	0	0	0
$\beta M_b'$	id	0.68821	0.68821	0.68821	0.68821	0.68821	0.68821
$\beta K_a''$	id	0	— 0.026322	— 0.052644	— 0.078966	— 0.10529	— 0.13161
K_b''	0.7	0	0.058294	0.10805	0.14928	0.18196	0.20611
	0.9	0	0.41562	0.79370	1.1342	1.4373	1.7028
$\beta M_a''$	$0 < M < 1$	0	0.013764	0.027528	0.041293	0.055057	0.068821
M_b''	0.7	0	0.065210	— 0.12595	— 0.18225	— 0.23406	— 0.28142
	0.9	0	— 0.32099	— 0.62235	— 0.90409	— 1.1662	— 1.4087

TABLE 7. $\beta s = 11.43$

	M \ k	0	0.02	0.04	0.06	0.08	0.10
$\beta K_a'$	$0 < M < 1$	0	0	0	0	0	0
$\beta K_b'$	id	— 1.5789	— 1.5789	— 1.5789	— 1.5789	— 1.5789	— 1.5789
$\beta M_a'$	id	0	0	0	0	0	0
$\beta M_b'$	id	0.80596	0.80596	0.80596	0.80596	0.80596	0.80596
$\beta K_a''$	id	0	— 0.031578	— 0.063156	— 0.094734	— 0.12631	— 0.15789
K_b''	0.7	0	0.13922	0.25388	0.34397	0.40947	0.45041
	0.9	0	0.79870	1.4893	2.0720	2.5466	2.9131
$\beta M_a''$	$0 < M < 1$	0	0.016119	0.032238	0.048358	0.064477	0.080596
M_b''	0.7	0	— 0.10829	— 0.20403	— 0.28725	— 0.35790	— 0.41602
	0.9	0	— 0.52611	— 0.99710	— 1.4128	— 1.7735	— 2.0791

TABLE 8. Factors of proportionality.

M \ βs	2.86	5.71	11.43
0.7	2.9917	8.1070	19.453
0.9	13.154	35.646	85.534

The unsteady and quasi steady values of $\lim\limits_{k \to 0} \dfrac{M_\varepsilon''}{\pi \rho U^2 l^2 B e^{i\nu t} k}$ (damping moment) for various positions of the pitching axis.

TABLE 9. $\beta s = 2.86$

M \ ε		−5	−4	−3	−2	−1	0	+1	+2
0.7	unsteady	−31.227	−19.866	−11.225	−5.3046	−2.1045	−1.6246	−3.8649	−8.8254
0.7	quasisteady	−34.221	−21.980	−12.459	−5.6589	−1.5786	−0.21845	−1.5786	−5.6589
0.9	unsteady	−23.612	−11.560	−3.9647	−0.82550	−2.143	−7.9167	−18.147	−32.834
0.9	quasisteady	−56.063	−36.009	−20.412	−9.2707	−2.5861	−0.35787	−2.5861	−9.2707

TABLE 10. $\beta s = 5.71$

M	$\varepsilon \rightarrow$	−8	−7	−6	−5	−4	−3	−2	−1	0	+1	+2
0.7	unsteady	−88.588	−65.032	−45.166	−28.986	−16.491	−7.6831	−2.5602	−1.1233	−3.3721	−9.3067	−18.927
0.7	quasisteady	−118.11	−90.463	−66.505	−46.234	−29.647	−16.747	−7.5327	−2.0040	−0.16114	−2.0040	−7.5327
0.9	unsteady	−23.380	−1.400	+14.560	+24.472	+28.345	+26.181	+17.980	+3.7389	−16.540	−42.857	−75.212
0.9	quasisteady	−193.48	−148.20	−108.95	−75.742	−48.570	−27.436	−12.340	−3.2831	−0.26398	−3.2831	−12.340

TABLE 11. $\beta s = 11.43$

M	$\varepsilon \rightarrow$	−14	−13	−12	−11	−10	−9	−8	−7	−6
0.7	unsteady	−317.23	−266.24	−219.66	−177.51	−139.79	−106.48	−77.595	−53.139	−33.099
0.7	quasisteady	−433.47	−373.77	−318.49	−267.64	−221.21	−179.20	−141.61	−108.45	−79.702
0.9	unsteady	−114.82	−61.504	−15.444	+23.386	+54.956	+79.296	+96.386	+106.24	+108.83
0.9	quasisteady	−710.10	−612.30	−521.75	−438.44	−362.38	−293.56	−231.98	−177.65	−130.57

M	$\varepsilon \rightarrow$	−5	−4	−3	−2	−1	0	+1	+2
0.7	unsteady	−17.482	−6.2881	+0.48490	+2.8359	+0.76500	−5.7281	−16.643	−31.980
0.7	quasisteady	−55.381	−35.482	−20.005	−8.9495	−2.3165	−0.10551	−2.3165	−8.9495
0.9	unsteady	+104.19	+92.302	+73.177	+46.798	+13.179	−27.684	−75.791	−131.14
0.9	quasisteady	−90.726	−58.127	−32.772	−14.661	−3.7950	−0.17285	−3.7950	−14.661

C.C.L. Class. D 43 : E 030

REPORT NLL-TR F. 208

The influence of non-stationary stability derivatives on the snaking motion at high subsonic speed*)

by

J. YFF.

Summary.

Some lateral stability calculations with two degrees of freedom for flight at high subsonic speed have been performed in order to study the influence of the non-stationary stability derivatives $C_{n_{\dot\beta}}$, $C_{y_{\dot\beta}}$, $C_{n_{\dot r}}$ and $C_{y_{\dot r}}$ on the damping of the snaking motion. These derivatives can be determined theoretically for the case of small aspect ratios and with compressibility taken into account.

It is found that only $C_{n_{\dot\beta}}$ has a small influence on the damping in yaw, the influence of the other non-stationary derivatives being negligible. Whether the introduction of $C_{n_{\dot\beta}}$ causes a decrease or an increase of the damping in yaw depends mainly on the aspect ratio of the vertical tail. For nearly all practical tail designs, however, an increase of the damping in yaw will result. Furthermore it is found that the theoretical non-stationary stability derivatives for vertical tails are practically independent of the reduced frequency.

Contents.

Symbols.

A	amplitude of translation of mid-chord point of vertical tail, made dimensionless by aid of $\frac{c_v}{2}$
B	amplitude of rotation of vertical tail
C_L	lift coefficient (Lift/q.S)
K	force acting on the vertical tail
K_a, K_b	aerodynamic force derivatives defined by eq. A-1
$K^{(i)}$	coeffcients of the series expansion of the kernel of the integral equation relating downwash and pressure distribution
L	rolling moment
M	moment about mid-chord axis of the vertical tail
M_a, M_b	aerodynamic moment derivatives defined by eq. A-1
Ma	MACH number
N	yawing moment

*) The research reported in this document was sponsored by the Air Research and Development Command, United States Air Force, under Contract AF 51(514)-879 through the European Office-ARDC.

N_β'	in phase component of yawing moment due to sideslip
N_β''	out of phase component of yawing moment due to sideslip
N_r'	in phase component of yawing moment due to yawing velocity
N_r''	out of phase component of yawing moment due to yawing velocity
P	period of the lateral oscillation
S	wing area
S_v	vertical tail area
$T_{1/2}$	time to damp to one-half amplitude
V	airspeed
W	weight of airplane
Y	lateral force
Y_β'	in phase component of lateral force due to side slip
Y_β''	out of phase component of lateral force due to side slip
Y_r'	in phase component of lateral force due to yawing velocity
Y_r''	out of phase component of lateral force due to yawing velocity
b	wing span
b_v	vertical tail span
c_v	mean aerodynamic chord of vertical tail
$g_0^{(i)}$	coefficients of series expansion of the function determining the lift distribution along the span of the vertical tail
$g_1^{(i)}$	coefficients of series expansion of the function determining the moment distribution along the span of the vertical tail
k	reduced frequency $k = \frac{\nu \cdot c_v}{2\,V}$
k_x	radius of gyration about X-axis
k_z	radius of gyration about Z-axis
k_{xz}	product of inertia factor
m	mass of airplane
p	angular rolling velocity $(p = \dot{\varphi})$
$p^{(i)}$	coefficients of series expansion of pressure
q	dynamic pressure
r	angular yawing velocity $(r = \dot{\psi})$
s	$\frac{2\,b_v}{c_v}$
t	time
w	downwash
x, y, z	coordinates made dimensionless by $c_v/2$
α	angle of attack of body reference axis
β	angle of sideslip
γ	angle of rotation of vertical tail about y-axis
$\varepsilon \frac{c_v}{2}$	distance of c. g. to mid-chord axis of vertical tail
ϑ	angular chordwise coordinate $(\xi = -\cos\vartheta)$
λ	roots of characteristic equation
μ	relative density factor, $\mu = \frac{m}{\rho S b}$
ν	angular frequency of lateral oscillation
ξ, η	x and y coordinates of an arbitrary point of the wing
ρ	air density
σ	non-dimensional time factor $\sigma = \frac{t}{\tau}$
τ	time conversion factor $\tau = \frac{m}{\rho S V}$
ψ	angle of yaw
φ	angle of bank
Λ	sweepback of wing quarter-chord line
Λ_v	sweepback of vertical tail quarter chord line

$$C_{L_\alpha} = \frac{\partial C_L}{\partial \alpha},\; C_l = \frac{L}{qSb},\; C_n = \frac{N}{qSb},\; C_y = \frac{Y}{qS}$$

$$K_x = \frac{k_x}{b},\; K_z = \frac{k_z}{b},\; K_{xz} = \frac{k_{xz}}{b}$$

$$K_1 = \frac{K_{xz}}{K_x^2},\; K_2 = \frac{K_{xz}}{K_z^2}$$

Stationary stability derivatives

$$C_{l_p} = \frac{\partial C_l}{\partial \frac{pb}{2V}} \qquad C_{n_p} = \frac{\partial C_n}{\partial \frac{pb}{2V}} \qquad C_{y_p} = \frac{\partial C_y}{\partial \frac{pb}{2V}}$$

$$C_{l_r} = \frac{\partial C_l}{\partial \frac{rb}{2V}} \qquad C_{n_r} = \frac{\partial C_n}{\partial \frac{rb}{2V}} \qquad C_{y_r} = \frac{\partial C_y}{\partial \frac{rb}{2V}}$$

$$C_{l_\beta} = \frac{\partial C_l}{\partial \beta} \qquad C_{n_\beta} = \frac{\partial C_n}{\partial \beta} \qquad C_{y_\beta} = \frac{\partial C_y}{\partial \beta}$$

Non-stationary stability derivatives

$$C_{n_\beta} = \frac{N'_\beta}{qSb}, \; C_{y_\beta} = \frac{Y'_\beta}{qS}$$

$$C_{n_{\dot\beta}} = \frac{c_v \,.\, N''_\beta}{qSb^2k}, \; C_{y_{\dot\beta}} = \frac{c_v \,.\, Y''_\beta}{qSbk}$$

$$C_{n_r} = \frac{N'_r}{qSb}, \; C_{y_n} = \frac{Y'_r}{qS}$$

$$C_{n_{\dot r}} = \frac{c_v N''_r}{qSb^2 \,.\, k}, \; C_{y_{\dot r}} = \frac{c_v Y''_r}{qSb \,.\, k}$$

$$l_p = \frac{C_{l_p}}{4K_x^2}, \; n_p = \frac{C_{n_\beta}}{4K_z^2}, \; y_r = \frac{1}{4\mu} C_{y_p}$$

$$l_r = \frac{C_{l_r}}{4K_x^2}, \; n_r = \frac{C_{n_r}}{4K_z^2}, \; y_r = \frac{1}{4\mu} C_{y_r}$$

$$l_\beta = \frac{\mu C_{l_\beta}}{2K_x^2}, \; n_\beta = \frac{\mu C_{n_\beta}}{2K_z^2}, \; y_\beta = \frac{1}{2} C_{y_\beta}$$

$$n_{\dot\beta} = \frac{Cn_{\dot\beta}}{4K_z^2}, \; y_{\dot\beta} = \frac{1}{4\mu} C_{y_{\dot\beta}}$$

$$n_{\dot r} = \frac{C_{n_{\dot r}}}{8\mu K_z^2}, \; y_{\dot r} = \frac{1}{8\mu^2} C_{y_{\dot r}}$$

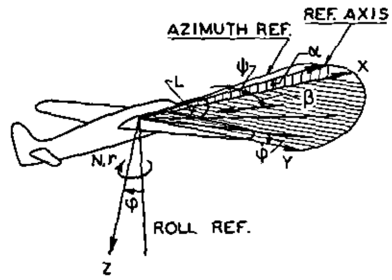

Stability system of axes.

1 Introduction.

In view of the uncertainty which exists concerning the influence of unsteady aerodynamic effects upon stability calculations, an investigation was performed with the purpose of clarifying this question for the snaking motion at high subsonic speeds.

Hitherto it has been very difficult to take into account in a proper way the unsteady flow effects because accurate measurements of the non-stationary stability derivatives are hard to obtain and the theoretical determination of these derivatives was hampered by the fact that an unsteady finite span theory for the calculation of the aerodynamic loads on the low aspect ratio tail did not exist.

Therefore the results of former investigations are not very accurate due to inadequate representation of the aerodynamic forces. E. g., VAN DE VOOREN and YFF (ref. 1) used two-dimensional unsteady aerodynamic coefficients and only a reduced value of the lift slope curve was used to take into account the three-dimensional effects. BIRD, FISHER and HUBBARD (ref. 2) applied the finite span method of BIOT and BÖHNLEIN as well as that of REISSNER which was used also by ASHLEY and co-authors (ref. 3). These finite span methods of BIOT and BÖHNLEIN as well as of REISSNER were applied, however, to aspect ratios of about 2 while they are only valid for relatively large aspect ratios. Moreover they are valid only in incompressible flow while RUNYAN (ref. 4) has shown that for two-dimensional flow pitching or yawing instability occurs for a much larger range of parameters when compressibility is taken into account.

As the first part of the present investigation a theory has been developed therefore by VAN DE VOOREN and DE JAGER (ref. 5) for the calculation of the aerodynamic forces acting upon a slowly oscillating finite span airfoil which takes into account also compressibility effects. The present report deals with the introduction in the stability calculations of the unsteady aerodynamic forces obtained in ref. 5 while, moreover, some examples are given of calculations with and without the non-stationary stability derivatives. These calculations refer to snaking motions with two degrees of freedom viz. yawing and side-slipping, at MACH numbers of 0.7 and 0.9, because it was reasoned in ref. 5 that at the high speeds at which snaking occurs the influence of the non-stationary derivatives would be much larger than at lower speeds.

For the case of yawing motions which is studied here the airfoil for which the unsteady effects should be taken into account is the vertical tail.

A similar investigation for three degrees of freedom which used measured non-stationary stability derivatives has been carried out by CAMPBELL and WOODLING (ref. 6). This investigation however, was restricted to low speeds and high angles of attack, thus representing the landing condition. Therefore it is impossible to compare the results with these of the present investigation. It was found in ref. 6 that for large angles of attack the introduction of non-stationary stability derivatives caused large differences for the calculated damping in yaw.

2 Analysis.

The linearized equations of motion for the lateral motion of an aeroplane in level flight, referred to the stability axes, are given by:

$$\begin{aligned} I_{xx}\ddot{\varphi} + I_{xz}\ddot{\psi} &= L \\ I_{xz}\ddot{\varphi} + I_{zz}\ddot{\psi} &= N \\ -W\varphi + mV(\dot{\psi} + \dot{\beta}) &= Y \end{aligned} \tag{2.1}$$

in which a dot denotes a differentiation with respect to time and I_{xx} and I_{zz} denote mass moments of inertia about the x and the z axis while I_{xz} gives the product of inertia. According to the classical stability theory the aerodynamic roll and yawing moments L and N as well as the lateral force Y depend only on the instantaneous values of the angle of side slip β, the yawing velocity $\dot{\psi}$ and the rolling velocity $\dot{\varphi}$. Thus it is possible to write:

$$\begin{aligned} L &= \frac{\partial L}{\partial \beta}\beta + \frac{\partial L}{\partial \frac{\dot{\psi}b}{2V}}\frac{\dot{\psi}b}{2V} + \frac{\partial L}{\partial \frac{\dot{\varphi}b}{2V}}\frac{\dot{\varphi}b}{2V} \\ N &= \frac{\partial N}{\partial \beta}\beta + \frac{\partial N}{\partial \frac{\dot{\psi}b}{2V}}\frac{\dot{\psi}b}{2V} + \frac{\partial N}{\partial \frac{\dot{\varphi}b}{2V}}\frac{\dot{\varphi}b}{2V} \\ Y &= \frac{\partial Y}{\partial \beta}\beta + \frac{\partial Y}{\partial \frac{\dot{\psi}b}{2V}}\frac{\dot{\psi}b}{2V} + \frac{\partial Y}{\partial \frac{\dot{\varphi}b}{2V}}\frac{\dot{\varphi}b}{2V}. \end{aligned} \tag{2.2}$$

When eqs. (2.1) are made dimensionless they become in the notation of ref. 6, after substitution of (2.2) in (2.1):

$$\begin{aligned} \varphi'' - l_p\varphi' + K_1\psi'' - l_r\psi' - l_\beta \, . \, \beta &= 0 \\ K_2\varphi'' - n_p\varphi' + \psi'' - n_r\psi' - n_\beta \, . \, \beta &= 0 \\ -y_p \, . \, \varphi' - \frac{C_L}{2}\varphi + (1 - y_r)\psi' + \beta' - y_\beta \, . \, \beta &= 0 \end{aligned} \tag{2.3}$$

where a dash denotes a differentiation with respect to $\sigma = \dfrac{t}{\tau}$ where $\tau = \dfrac{m}{\rho S V}$. Eqs. (2.3) were used for the calculations with three degrees of freedom.

However, snaking is a motion which consists mainly of two degrees of freedom viz. yawing and sideslipping. The calculations which have been performed to illustrate the influence of the non-stationary derivatives therefore take into account only these two degrees of freedom. For that case the non-stationary stability derivatives can be derived from ref. 5 in which the unsteady forces acting on airfoils of finite span are calculated for low frequency pitching and heaving motions. It has been derived in Appendix A, in which the results of ref. 5 are transformed to stability derivatives, that the following expressions for N and Y are valid for harmonic motions when unsteady flow effects are taken into account (compare eq. A. 3)):

$$\begin{aligned} N &= (N_\beta' + iN_\beta'')\beta + (N_r' + iN_r'')\frac{rb}{2V} \\ Y &= (Y_\beta' + iY_\beta'')\beta + (Y_r' + iY_r'')\frac{rb}{2V}. \end{aligned} \tag{2.4}$$

In these expressions the stability derivatives have a somewhat different meaning from that in eq. 2.2, as has been explained in App. A.

Here they express the components of the moment and the force which are in-, resp. out of phase with the motion. When eqs. 2.4 are substituted in the last two equations of eqs. 2.1 in which $\varphi = 0$ and use is made of the non-dimensional notation of ref. 6 then the following equations of motion for the flat yawing motion with the degrees of freedom: yawing and side-slipping, are obtained:

$$\psi''(1-n_{\dot r})-\psi' n_r-\beta\, n_\beta-\beta' n_{\dot\beta}=0$$
$$-\psi''.\, y_{\dot r}+\psi'(1-y_r)-\beta\, y_\beta+\beta'(1-y_{\dot\beta})=0.$$

The solution of these equations can be found from the following characteristic determinant:

$$\begin{vmatrix} \lambda^2(1-n_{\dot r})-\lambda n_r & -\lambda n_{\dot\beta}-n_\beta \\ -\lambda^2 y_{\dot r}+\lambda(1-y_r) & \lambda(1-y_{\dot\beta})-y_\beta \end{vmatrix}=0$$

which can be written as

$$\lambda^2\{(1-y_{\dot\beta})(1-n_{\dot r})-y_{\dot r}n_{\dot\beta}\}-\lambda\{y_\beta(1-n_{\dot r})+n_r(1-y_{\dot\beta})+n_\beta y_{\dot r}-n_{\dot\beta}(1-y_r)\}+$$
$$+\{n_r y_\beta+n_\beta(1-y_r)\}=0. \tag{2.5}$$

The period of the oscillation P and the time to damp to one-half amplitude $T_{1/2}$ are related as follows to the complex root $\lambda=R\pm iI$ of the complex quadratic equation in λ:

$$T_{1/2}=\frac{ln\frac{1}{2}}{R/\tau} \text{ and } P=\frac{2\pi}{I/\tau}. \tag{2.6}$$

The in-phase and out-of-phase aerodynamic coefficients can be derived from Appendix A where the following expressions are obtained in which k is the reduced frequency $k=\frac{\nu c_v}{2V}$ and K_z is the non-dimensional radius of gyration, $K_z=\frac{k_z}{b}$ while $\mu=$ defined by $\mu=\frac{m}{\rho Sb}$:

$$y_\beta=\frac{1}{2}\,C_{y_\beta}=2\pi\,\frac{S_v}{S}\,\frac{1}{4}\,\frac{K_a''}{k}$$

$$n_\beta=\frac{\mu}{2K_z^2}\,C_{n_\beta}=-2\pi\,\frac{S_v c_v}{Sb}\,\frac{\mu}{K_z^2}\,\frac{1}{8}\,\frac{M_a''+\varepsilon K_a''}{k}$$

$$y_r=\frac{1}{4\mu}\,C_{y_r}=-2\pi\,\frac{S_v c_v}{Sb}\,\frac{1}{8\mu}\left\{\varepsilon\frac{K_a''}{k}+\frac{K_b''}{k}+\frac{K_a'}{k^2}\right\}$$

$$n_r=\frac{1}{4K_z^2}\,C_{n_r}=2\pi\,\frac{S_v c_v}{Sb^2}\,\frac{1}{16K_z^2}\left\{\frac{\varepsilon M_a''+\varepsilon^2K_a''+M_b''+\varepsilon K_b''}{k}+\frac{M_a'+\varepsilon K_a'}{k^2}\right\}$$

$$y_{\dot\beta}=\frac{1}{4\mu}\,C_{y_{\dot\beta}}=-2\pi\,\frac{S_v c_v}{Sb}\,\frac{1}{8\mu}\,\frac{K_a'}{k^2}$$

$$n_{\dot\beta}=\frac{1}{4K_z^2}\,C_{n_{\dot\beta}}=2\pi\,\frac{S_v c_v^2}{Sb^2}\,\frac{1}{16K_z^2}\,\frac{M_a'+\varepsilon K_a'}{k^2}$$

$$y_{\dot r}=\frac{1}{8\mu^2}\,C_{y_{\dot r}}=2\pi\,\frac{S_v c_v^2}{Sb^2}\,\frac{1}{16\mu^2}\left\{\varepsilon\frac{K_a'}{k^2}+\frac{K_b'}{k^2}-\frac{K_a''}{k^3}\right\}$$

$$n_{\dot r}=\frac{1}{8\mu K_z^2}\,C_{n_{\dot r}}=-2\pi\,\frac{S_v c_v^3}{Sb^3}\,\frac{1}{32\mu K_z^2}\left\{\frac{\varepsilon^2K_a'+\varepsilon(M_a'+K_b')+M_b'}{k^2}-\frac{M_a''+\varepsilon K_a''}{k^3}\right\}.$$

When using the results of ref. 5 it is found however that K_a' and M_a' are zero, thus indicating that the most important non-stationary derivatives $C_{n_{\dot\beta}}$ and $C_{y_{\dot\beta}}$ are zero. This is due to the fact that in ref. 5 for the real parts of the flutter derivatives also the terms of second order of k are neglected as it was thought that with the low values of k concerned these terms are negligible in comparison with the steady term. The real parts of the translational derivatives, however, do not contain steady terms. Moreover, these derivatives influence also the damping derivatives. Therefore the derivatives K_a' and M_a' are needed more accurately than they are given in ref. 5. It is possible, however, to obtain these derivatives accurate to the third power of k from the results which are given already in ref. 5. This is outlined in Appendix B. The results are given in table 1 and fig. 1 as a function of the quantity $\frac{b_v}{c_v}\sqrt{1-Ma^2}$.

The results of ref. 5 for the other derivatives are repeated here for completeness. They are given in table 2 and in figs. 2—3 in which they are given as a function of $\frac{b_v}{c_v}\sqrt{1-Ma^2}$. This gives the possibility of obtaining, by means of interpolation, values of the stability derivatives for other values of the aspect ratio then the few cases which have been calculated.

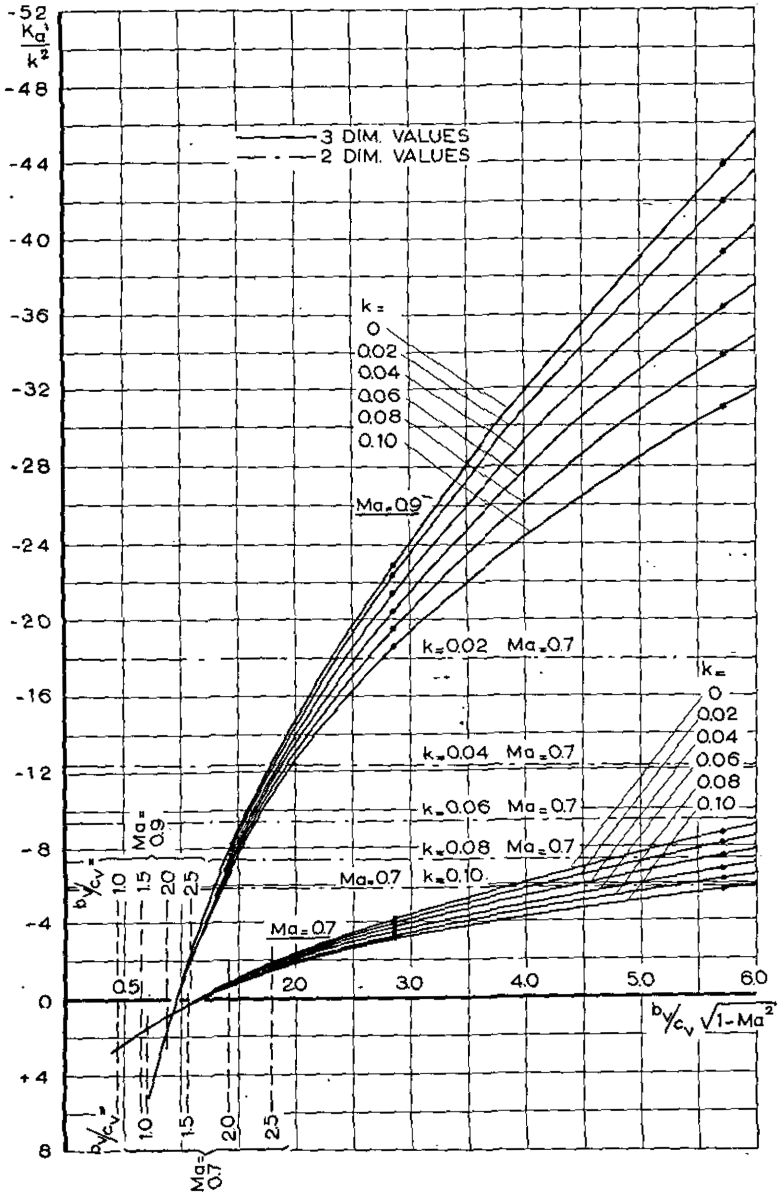

Fig. 1a. $\frac{K'_a}{k^2}$ as function of $\frac{b_v}{c_v}\sqrt{1-Ma^2}$ for various values of the reduced frequency k.

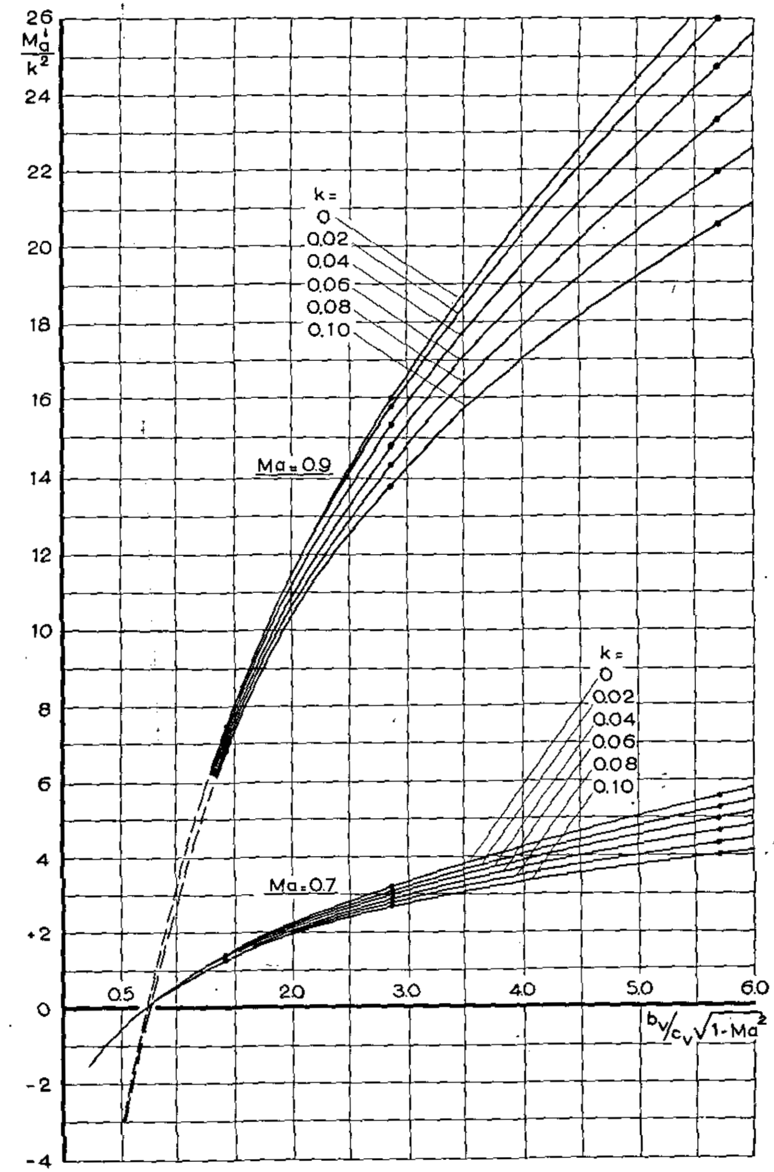

Fig. 1b. $\frac{M'_a}{k^2}$ as function of $b_v/c_v\sqrt{1-Ma^2}$ for various values of the reduced frequency k.

Because in ref. 5 the forces and moments have been calculated for complete wings while the results of ref. 5 are used here *only* for vertical tails which are treated as semi-wings, the scale of $\frac{b_v}{c_v}\sqrt{1-Ma^2}$ in figs. 1—3 and in table 1 and 2 is halved in comparison with ref. 5.

The derivatives K_b' and M_b' are not repeated here because they occur only in the expressions for the stability derivatives $C_{y_{\dot r}}$ and $C_{n_{\dot r}}$ of which it is concluded in section 4 that the are negligible. The results of section 4 are obtained with values of the derivatives $C_{y_{\dot r}}$ and $C_{n_{\dot r}}$ which were derived from ref. 5. In Appendix B it is derived that these expressions are not quite correct but that the order of magnitude of these derivatives is not changed when the correct expressions are used. Therefore the results which are obtained in section 4 will remain unchanged because it is found that the influence of $C_{n_{\dot r}}$ and $C_{y_{\dot r}}$ on the stability of the airplane motion is completely negligible.

3 Calculations.

Calculations were made to determine the period and the damping of the oscillatory yawing motion in order to study the influence of the non-stationary derivatives $C_{y_{\dot\beta}}$, $C_{n_{\dot\beta}}$, $C_{y_{\dot r}}$ and $C_{n_{\dot r}}$ for the case of flight with high subsonic speeds at zero altitude.

The calculations have been performed for two different examples. The first, example A, is a conventional straight wing high subsonic fighter design which is identical with configuration 5 of ref. 8,

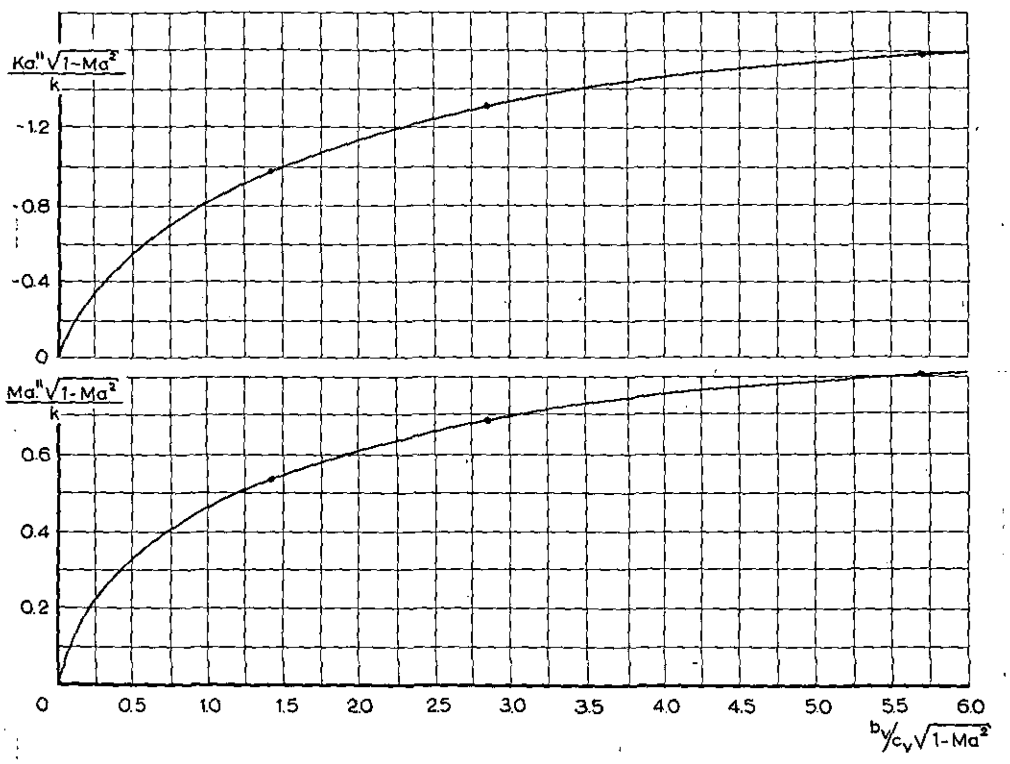

Fig. 2. $K_a''\sqrt{\frac{1-M_a^2}{k}}$ and $M_a''\sqrt{\frac{1-M_a^2}{k}}$ as a function of $\frac{b_v}{c_v}\sqrt{1-Ma^2}$.

a sketch of which is given in fig. 4. Most data could be derived directly from ref. 8 although the stability derivatives must be adapted to the lift coefficient corresponding to the Mach number Ma = 0.7 and Ma = 0.9 for which the calculations have been performed. This could be done easily because the stability derivatives were given for several values of the lift coefficient and thus the proper values of the stability derivatives could be found by interpolation for the lift coefficient belonging to the chosen Mach number. Moreover, the stability derivatives had to be corrected for compressibility effects because the theoretical determined non-stationary stability derivatives $C_{y_{\dot\beta}}$, $C_{n_{\dot\beta}}$, $C_{y_{\dot r}}$ and $C_{n_{\dot r}}$ depend upon the Mach number. These corrections have been determined according to ref. 9.

All non-stationary stability derivatives have been calculated for a rectangular vertical tail of aspect ratio 2 which possesses the same area as the vertical tail of configuration 5 of ref. 8. These theoretically determined non-stationary derivatives depend on the reduced frequency $k = \frac{\nu c_v}{2V}$ and thus an iteration procedure should have been used in order to determine the frequency ν. However, it can be seen from figs. 1 and 3 that for the small tail aspect ratios involved there is hardly any dependency on k of the

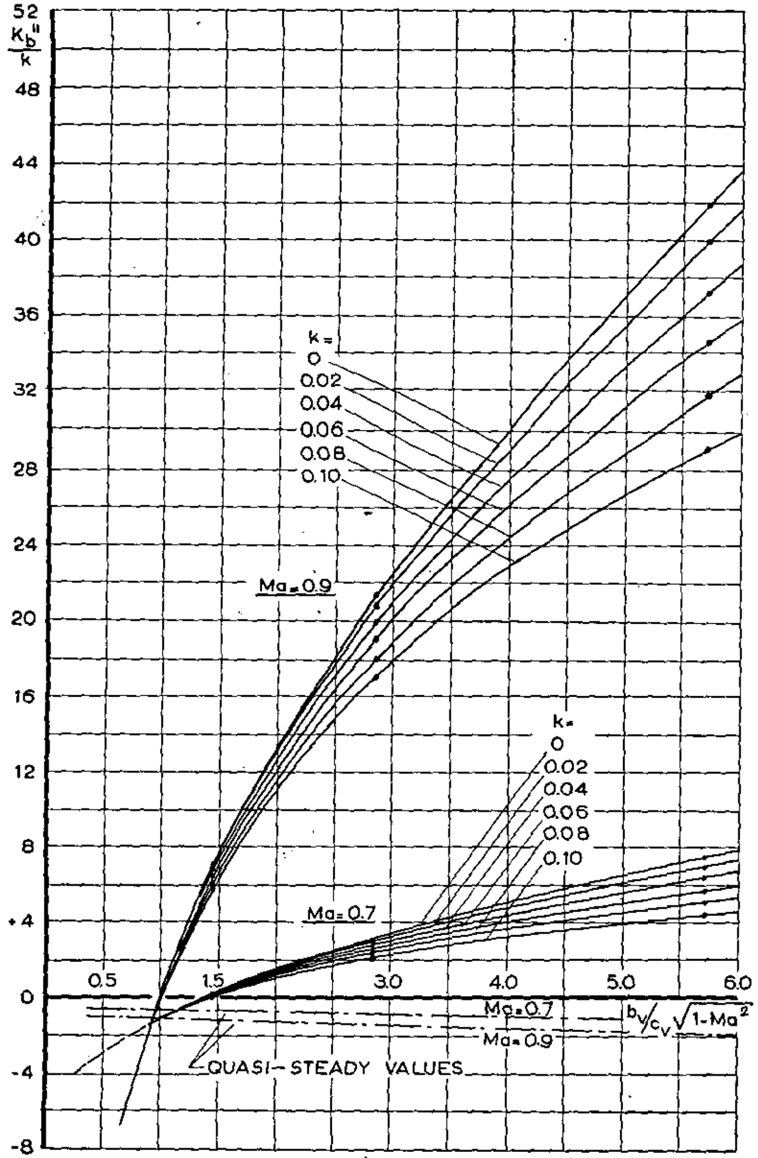

Fig. 3a. $\frac{K_b''}{k}$ as function of $\frac{b_v}{c_v}\sqrt{1-Ma^2}$ for various values of the reduced frequency k.

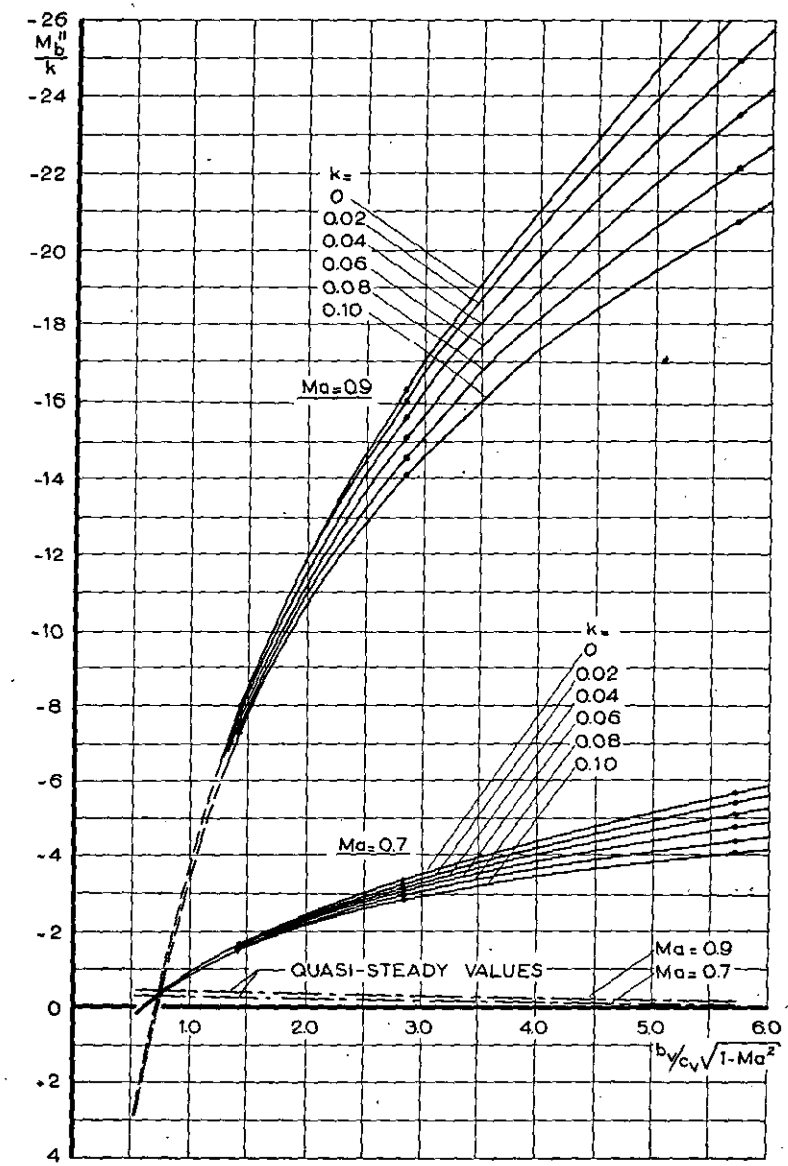

Fig. 3b. $\frac{M_b''}{k}$ as function of $\frac{b_v}{c_v}\sqrt{1-Ma^2}$ for various values of the reduced frequency k.

non-stationary derivatives and therefore the frequency of the motion can be found directly, thus simplifying the calculations considerably.

All data concerning example A, derived from ref. 8 as well as theoretically determined, are collected in tables 3 and 4. The following calculations have been performed with example A.

a) Three degrees of freedom, rolling, yawing and sideslipping. Without non-stationary stability derivatives, $Ma = 0.7$.

b) Two degrees of freedom; yawing and sideslipping. Without non-stationary stability derivatives, $Ma = 0.7$.

c) Two degrees of freedom; yawing and sideslipping. Without non-stationary stability derivatives, $C_{y_r} = 0$, $Ma = 0.7$.

d) Two degrees of freedom; yawing and sideslipping. Without non-stationary stability derivatives, $C_{y_r} = 0$, $Ma = 0.9$. Radius of gyration k_z has been varied.

e) Two degrees of freedom; yawing and sideslipping. With the non-stationary stability derivatives $C_{y_{\dot\beta}}$, $C_{y_{\dot r}}$, $C_{n_{\dot\beta}}$ and $C_{n_{\dot r}}$ included. $C_{y_r} = 0$, $Ma = 0.9$. Radius of gyration k_z has been varied.

f) Two degrees of freedom; yawing and sideslipping. With $C_{n_{\dot\beta}}$ but without $C_{y_{\dot\beta}}$, $C_{y_{\dot r}}$ and $C_{n_{\dot r}} = C_{y_r} = 0$. $Ma = 0.9$. Radius of gyration k_z has been varied.

g) Two degrees of freedom; yawing and sideslipping. With $C_{n_{\dot\beta}}$ but without $C_{y_{\dot\beta}}$, $C_{y_{\dot r}}$ and $C_{n_{\dot r}} = C_{y_r} = 0$. $Ma = 0.9$. Radius of gyration k_z has been varied. The value of $C_{n_{\dot\beta}}$ has been taken equal to ½ of the theoretical value of $C_{n_{\dot\beta}}$.

Example B is derived from ref. 10 and it represents a semi-tailess airplane with small tail length as shown in fig. 4. In ref. 10 all aerodynamic data are given for two values of the tail length and there-

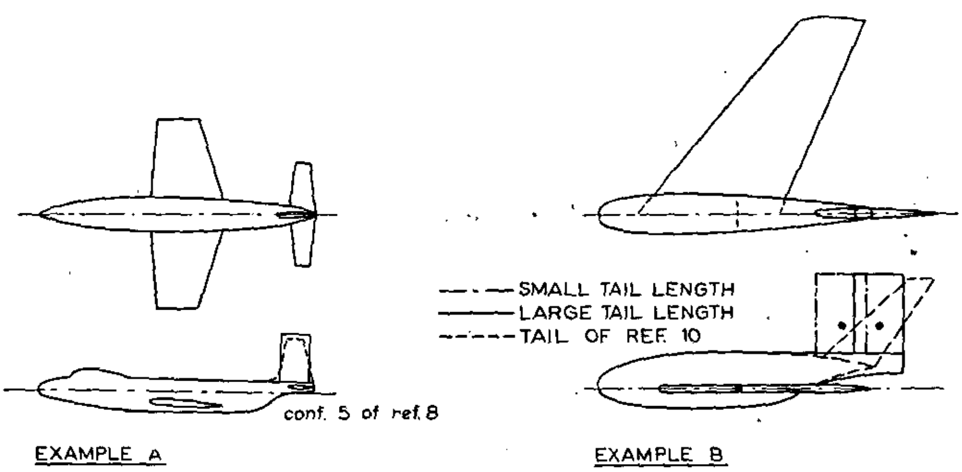

Fig. 4. Basic configurations for which calculations were made.

fore the stability calculations have been performed also for both cases. The mass of the airplane has been chosen after comparison with airplanes comparable in size and configuration. All relevant data can be found in tables 4 and 5.

The calculations have been performed for different values of the radius of gyration as well as for three different values of $C_{n_{\dot\beta}}$, viz. $C_{n_{\dot\beta}}$ equal to the theoretically determined value of $C_{n_{\dot\beta}}$, equal to half that value and equal to zero. $C_{n_{\dot\beta}}$ has been calculated for a rectangular vertical tail of aspect ratio 1,70 with the same area as the swept back vertical tail of the original model while $C_{y_{\dot\beta}}$, $C_{y_{\dot r}}$, C_{n_r} and C_{y_r} are neglected. The other stability derivatives have been corrected for compressibility effects by aid of ref. 9.

4 Results and discussion.

The results of the calculations concerning example A are collected in table 4 while those of example B are given in table 5.

Influence of number of degrees of freedom.

By comparing the results of the calculations of example A with two and with three degrees of freedom (calculations 1 and 2) it will be seen that the period of the oscillation remains nearly the same but that the calculation with two degrees of freedom overestimates the damping of the motion by about 10 %.

Yet the subsequent calculations have been performed with two degrees of freedom only because all essential properties of the oscillatory motion are found with such a calculation.

Moreover, it has been found possible to neglect the stability derivatives C_{y_r} as will be clear from a comparison of calculations 2 and 3. The results of both calculations are exactly the same. Thus in the subsequent calculations the derivative C_{y_r} is neglected.

Influence of Mach-number.

The calculations 1, 2 and 3 have been performed for $Ma = 0.7$. The influence of the MACH number can be studied by comparing the calculations 3 and 5. The latter calculation is exactly the same as calculation 3 except for the MACH number which is chosen as $Ma = 0.9$. It is seen that both frequency and damping are increased by increasing the MACH number. The result is not very conclusive, however, because compressibility effects have been taken into account only in a rather simple manner so that e. g. shock waves have not been taken into account. The results of ref. 5 show however that for $Ma = 0.9$ the non-stationary derivatives become much larger and thus the influence of the non-stationary derivatives will be more important for $Ma = 0.9$. Therefore the subsequent calculations were performed for $Ma = 0.9$ only.

Effects of the non-stationary stability derivatives $C_{y_{\dot r}}$, $C_{n_{\dot r}}$, $C_{y_{\dot\beta}}$ and $C_{n_{\dot\beta}}$.

In order to investigate the influence of the non-stationary stability derivatives on the results of the stability calculations, some calculations have been performed with and without these derivatives. The results can be found in table 4 by comparing the calculations 4 through 9 and 10 through 15 where for several values of the radius of gyration the damping and the period of the oscillatory motion of airplane A flying at $Ma = 0.9$ are given. By comparing the results of the calculations with and without the non-stationary stability derivatives for a certain value of the radius of gyration it is seen that again the period of the oscillation is hardly affected while the damping is increased by about 10 %.

Influence of different non-stationary derivatives.

Another question which can be posed here, is, which is the influence of each of the different non-stationary derivatives. In order to investigate this question some calculations have been performed in which $C_{y_{\dot\beta}} = C_{y_{\dot r}} = C_{n_{\dot r}} = 0$. By comparing the results of calculations 10—15 with these calculations (16—21) it will be clear that the derivatives $C_{y_{\dot\beta}}$, $C_{y_{\dot r}}$ and $C_{n_{\dot r}}$ can be safely neglected for the results of calculations with and without these derivatives are exactly the same.

Thus the non-stationary effects in lateral stability calculations with two degrees of freedom are due to the derivative $C_{n_{\dot\beta}}$.

Dependance of non-stationary effect on $C_{n_{\dot\beta}}$.

The accuracy by which $C_{n_{\dot\beta}}$ is determined is not known because up till now it is impossible to compare the theoretically determined value of $C_{n_{\dot\beta}}$ with the results of unsteady measurements. It seems however that the theoretically determined values of $C_{n_{\dot\beta}}$ are too large for it is found by calculating other stability derivatives for which experimental verification is possible that large differences exist between the theoretically determined and the measured values of the derivatives. Though the theory of ref. 5, which is used here, is valid for small aspect ratios and though it takes into account compressibility effects it is found e. g. that the theoretically determined value of C_{n_r} is twice as big as the value given in ref. 8. The main reason for this difference will be the uncertainty about the effective aspect ratio of the vertical tail. It is assumed in this theoretical investigation that the pressure distribution of the vertical tail is equal to that of a semi wing thus assuming the horizontal tail to act as an infinitely large plate. For this case the effective aspect ratio is twice the geometrical aspect ratio of the vertical tail.

This value will not be reached in practical cases because there is always a decrease in the pressure difference on the vertical tail towards the horizontal tail.

Because this uncertainty about the magnitude of $C_{n_{\dot\beta}}$ some calculations have been performed with values of $C_{n_{\dot\beta}}$ which are one-half the theoretical values. The results of these calculations are numbered 22—27 in table 4. It is shown by these results that the difference in the damping of the oscillatory motion due to the introduction of $C_{n_{\dot\beta}}$ is about proportional to $C_{n_{\dot\beta}}$.

Influence of different parameters determining $C_{n_{\dot\beta}}$.

Up till now the introduction of $C_{n_{\dot\beta}}$ in the stability calculations has led to increased damping of the oscillatory motion. The question arises on which parameters the sign and magnitude of $C_{n_{\dot\beta}}$ depend and if a decrease of the damping of the oscillatory motion is also possible. The theoretical expression for $C_{n_{\dot\beta}}$ is given by

$$C_{n_{\dot\beta}} = \frac{S_v c_v^2}{S b^2} 2\pi \cdot \frac{1}{4} \left\{ \varepsilon \frac{K_a'}{k^2} + \frac{M_a'}{k^2} \right\}.$$

The values of $\frac{K_a'}{k^2}$ and $\frac{M_a'}{k^2}$ are given in fig. 1 as a function of $\frac{b_v}{c_v} \sqrt{1-\mathrm{Ma}^2}$ for several values of the Mach number. It is seen, in the first place that for practical values of ε (5 to 10) the term $\varepsilon \frac{K_a'}{k^2}$ is much more important than $\frac{M_a'}{k^2}$. A point of great interest is that for practical values of the vertical tail aspect ratio there is practically no influence of the reduced frequency k.

The most important feature of fig. 1 is however that for both Mach-numbers 0.7 and 0.9 $\frac{K_a'}{k^2}$ changes sign between aspect ratios 1.5 and 2.5. This means that only for tailplanes of very high aspect ratio the introduction of $C_{n_{\dot\beta}}$ will cause a reduction of the damping of the oscillatory motion. Most present day tailplane designs, however, have aspect ratios which are less then the values at which $\frac{K_a'}{k^2}$ changes sign and therefore in most cases the introduction of $C_{n_{\dot\beta}}$ in stability calculations will lead to increased damping of the oscillatory motion.

Influence of radius of gyration.

As can be seen from table 4 most calculations have been performed for several values of the radius of gyration. The value $K_z^2 = 0{,}101$ is the value given in ref. 8. For large values of the radius of gyration the motion will be governed more by inertia forces then by aerodynamic forces and therefore also the influence of $C_{n_{\dot\beta}}$ will diminish when K_z becomes larger. This is what is actually shown by the results of the calculations as they are given in table 4.

Influence of tail length.

In order to study also the influence of the tail length on the behaviour of $C_{n_{\dot\beta}}$ in stability calculations the calculations referring to example B have been performed. The results of these calculations are given in table 5.

As it is found in the previous sections that $C_{y_{\dot\beta}}$, $C_{y_{\dot r}}$ and $C_{n_{\dot r}}$ as well as C_{y_r} can be neglected, this has been done in this case.

By comparing the calculations for both cases of example B, which have tail lengths of $\varepsilon = 3{,}95$ and 5,56 resp. (calculations 28—42 and 43—57), it is seen that for the larger tail length the motion is damped heavier than for the small tail length as could be expected. The same is found when the results of the calculations of example B are compared with those of example A ($\varepsilon = 10{,}75$).

As has been found already with example A it is found here too that for both tail lengths of example B the introduction of $C_{n_{\dot\beta}}$ causes an increase of the damping of the motion. This is shown by comparing the results of calculations 28—32 and 38—42 as well as 43—47 and 53—57. The difference in the damping of calculations with and without $C_{n_{\dot\beta}}$, is much larger than for example A, viz. 20—50 % depending on the value of the radius of gyration. This percentage however is nearly the same for both tail lengths and thus it cannot be attributed to the influence of the tail length. The only further parameter of the vertical tail which is found to be different for examples A and B is the aspect ratio of the vertical tail which is 1.7 for example B and 2 for example A. From fig. 1 it will be clear that this is very important for the magnitude of $C_{n_{\dot\beta}}$

Thus it can be concluded that the influence of $C_{n_{\dot\beta}}$ on the damping of the motion is nearly independent of the tail length but dependent on the aspect ratio of the vertical tail.

As in the case of example A it is found that the difference in the damping of the oscillation due to the introduction of $C_{n_{\dot\beta}}$ in the calculations is almost proportional to the value of $C_{n_{\dot\beta}}$ as is shown by the results of the calculations 33—37 and 48—52.

Also with regard to the influence of the radius of gyration the same results are obtained as with example A. The influence of the aerodynamic forces and thus of $C_{n_{\dot\beta}}$ becomes relatively smaller when K_z is increased.

5 Conclusions.

From the calculations for the period and the damping of the oscillatory motion of an airplane flying at high subsonic speed and possessing two degrees of freedom, viz. yawing and side slipping the following conclusions can be drawn with regard to the influence of the non-stationary stability derivatives $C_{y_{\dot\beta}}$, $C_{n_{\dot r}}$, $C_{y_{\dot r}}$ and $C_{n_{\dot r}}$.

a) The only non-stationary stability derivative which has any influence on the calculated damping of the oscillatory flat yawing motion is $C_{n_{\dot{\beta}}}$.

b) The influence of $C_{n_{\dot{\beta}}}$ becomes only noteworthy at high subsonic MACH numbers.

c) The derivative $C_{n_{\dot{\beta}}}$ can cause a decrease as well as an increase of the damping of the oscillatory motion depending on the aspect ratio of the vertical tail. For all practical tailplane designs with aspect ratios between 1 and 2 an increase of the damping will result.

d) For the small aspect ratios involved in practical tailplane design the derivative $C_{n_{\dot{\beta}}}$ is independent of the reduced frequency k.

e) The influence of $C_{n_{\dot{\beta}}}$ on the damping of the oscillatory motion is about proportional to the value of $C_{n_{\dot{\beta}}}$.

f) Changes in both tail length and radius of gyration do not change the conclusions given above.

6 List of references.

1. VOOREN, A. I. VAN DE and YFF, J. The effect of aerodynamic lag on the snaking motion of aeroplanes. NLL Report F. 107; 1952.
2. BIRD, J. D., FISHER, L. R. and HUBBARD, S. M. Some effects of frequency on the contribution of a vertical tail to the free aerodynamic damping of a model oscillating in yaw. NACA TR 1130; 1953.
3. ASHLEY, H., CODIC, A., PRATT, R. M. and CAMPBELL, H. J. Investigation of unsteady aerodynamic and friction effects on rudder free yawing oscillations of aircraft. WADC Technical Report 53—273; 1953.
4. RUNYAN, H. L. Single degree of freedom flutter calculations for a wing in subsonic potential flow and comparison with an experiment. NACA TR 1089; 1952.
5. VOOREN, A. I. VAN DE and JAGER, E. M. DE. Calculation of aerodynamic forces on slowly oscillating rectangular wings in subsonic flow. NLL TN F. 192; 1956.
6. CAMPBELL, J. P. and WOODLING, C. H. Calculated effects of the lateral acceleration derivatives on the dynamic lateral stability of a delta-wing airplane. NACA RM-L 54 K 26; 1954.
7. CAMPBELL, J. P. and MCKINNEY, M. O. Summary of methods for calculating dynamic lateral stability and response and for estimating lateral stability derivatives. NACA TR 1098; 1950.
8. CAMPBELL, J. P. and MCKINNEY, M. O. A study of the problem of designing airplanes with satisfactory inherent damping of the Dutch roll oscillation. NACA TR 1199; 1953.
9. FISHER, L. R. Approximate corrections for the effects of compressibility on the subsonic stability derivatives of swept wings. NACA TN 1854; 1949.
10. FISHER, L. R. and MICHAEL, W. H. An investigation of the effect of vertical-fin location and area on low-speed lateral stability derivatives of a semi-tailless airplane model. NACA RM L 51 A 10; 1951.

APPENDIX A.

Relations between flutter and stability derivatives.

In linearized unsteady aerodynamic theory the expressions for the moment about the mid-chord axis and the force acting at a harmonically oscillating rigid airfoil can be written in the form

$$
\begin{aligned}
K &= \pi \rho V^2 \frac{S_v}{2} \{ (K_a' + iK_a'')A + (K_b' + iK_b'')B \} e^{i\nu t} \\
M &= \pi \rho V^2 \frac{S_v}{2} \frac{c_v}{2} \{ (M_a' + iM_a'')A + (M_b' + iM_b'')B \} e^{i\nu t}
\end{aligned} \qquad (A.1)
$$

in which A is the non-dimensional translational amplitude of the mid-chord axis and B is the rotational amplitude. While eqs. A.1 are defined with respect to fixed coordinate axes, in stability theory use is made of axes which are fixed to the moving body. Then it is supposed that the lateral force Y and the yawing moment N can be expressed as functions of the angle of side slip β and the angular velocity r and of their time derivatives. Hence:

$$
\begin{aligned}
Y &= \frac{\partial Y}{\partial \beta}\beta + \frac{\partial Y}{\partial \dot{\beta}}\dot{\beta} + \frac{\partial Y}{\partial \ddot{\beta}}\ddot{\beta} + \ldots\ldots \frac{\partial Y}{\partial r} r + \frac{\partial Y}{\partial \dot{r}}\dot{r} + \ldots\ldots \\
N &= \frac{\partial N}{\partial \beta}\beta + \frac{\partial N}{\partial \dot{\beta}}\dot{\beta} + \frac{\partial N}{\partial \ddot{\beta}}\ddot{\beta} + \ldots\ldots \frac{\partial N}{\partial r} r + \frac{\partial N}{\partial \dot{r}}\dot{r} + \ldots\ldots
\end{aligned}
$$

which can be written for the case of harmonic oscillations when $\beta = \beta_0 e^{i\nu t}$ and $r = r_0 e^{i\nu t}$ as

$$Y = \left\{ \frac{\partial Y}{\partial \beta} - k^2 \frac{b^2}{c_v^2} \frac{\partial Y}{\partial \frac{\ddot{\beta} b^2}{4V^2}} + \ldots i \left(k \frac{b}{c_v} \frac{\partial Y}{\partial \frac{\dot{\beta} b}{2V}} \ldots \right) \right\} \beta + \left\{ \frac{\partial Y}{\partial \frac{rb}{2V}} \ldots + i \left(k \frac{b}{c_v} \frac{\partial Y}{\partial \frac{\dot{r} b^2}{4V^2}} \ldots \right) \right\} \frac{rb}{2V}$$

$$N = \left\{ \frac{\partial N}{\partial \beta} - k^2 \frac{b^2}{c_v^2} \frac{\partial N}{\partial \frac{\ddot{\beta} b^2}{4V^2}} + \ldots i \left(k \frac{b}{c_v} \frac{\partial N}{\partial \frac{\dot{\beta} b}{2V}} \ldots \right) \right\} \beta + \left\{ \frac{\partial N}{\partial \frac{rb}{2V}} \ldots + i \left(k \frac{b}{c_v} \frac{\partial N}{\partial \frac{\dot{r} b^2}{4V^2}} \ldots \right) \right\} \frac{rb}{2V} \qquad \text{(A. 2)}$$

In the foregoing expressions for Y and N it is assumed that it is possible to expand these quantities in power series of the reduced frequency $k = \frac{\nu c_v}{2V}$. It follows however from ref. 5 that for the case of low frequency harmonic oscillations of finite aspect ratio wings, the force and moment cannot be identified with a power series of k because also terms with $k^2 \log k$, $k^3 \log k$ etc. occur and thus it is impossible to identify the different partial derivatives in eq. A. 2 with certain terms of the theoretical expressions for Y and N as they are derived in ref. 5. From a theoretical point of view it seems more appropriate therefore to write e. g.

$$Y = (Y_\beta' + i\, Y_\beta'')\beta + (Y_r' + i Y_r'') \frac{rb}{2V} \qquad \text{(A.3)}$$

in which Y_β' and Y_β'' denote the in phase and out of phase components of the force Y due to the angle of side slip β. Comparing eq. A. 3 with the first of eqs. A. 2 it is seen that e. g. the following identifications may be made

$$Y_\beta' = \frac{\partial Y}{\partial \beta} - k^2 \frac{b^2}{c_v^2} \frac{\partial Y}{\partial \frac{\ddot{\beta} b^2}{4V^2}} \ \ldots\ldots$$

$$Y_\beta'' = k \frac{b}{c_v} \frac{\partial Y}{\partial \frac{\dot{\beta} b}{2V}} + \ldots\ldots .$$

In general, the contributions of the higher derivatives to e. g. Y_β' and Y_β'' will be very small. Therefore the symbols of the non-dimensional values of e. g. Y_β' and Y_β'', viz. C_{y_β} and $k \frac{b}{c_v} C_{y_{\dot{\beta}}}$ have been chosen identical to the symbols of the non-dimensional values of $\frac{\partial Y}{\partial \beta}$ and $k \frac{b}{c_v} \frac{\partial Y}{\partial \frac{\dot{\beta} b}{2V}}$.

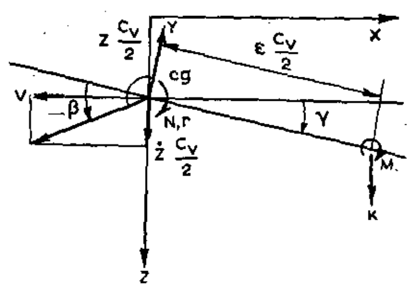

Sketch a.

As can be seen from sketch a the following relations exist between K, M and Y, N when linearisation is allowed.

$$Y = -K \qquad \text{(A. 4)}$$

$$N = M + \varepsilon \frac{c_v}{2} . K$$

In order to express the stability derivatives as functions of the flutter derivatives the relations between A, B and β, r have to be derived. It follows at once from sketch a that

$$\gamma = \gamma_0 e^{i\nu t} = B e^{i\nu t}$$

and

$$\dot{\gamma} = r = i\nu \beta e^{i\nu t} \ \text{or} \ B e^{i\nu t} = -i \frac{r}{\nu} = -i \frac{\frac{rb}{2V}}{k} \frac{c_v}{b} = \gamma. \qquad \text{(A. 5)}$$

In the same way it follows from sketch a that

$$Ae^{i\nu t} = \varepsilon\gamma + z.$$

and

$$i\nu A e^{i\nu t} = \varepsilon\dot{\gamma} + \dot{z}\,. \tag{A. 6}$$

Moreover $\dot{z} = -\dfrac{V}{c_v/2}(\beta+\gamma)$ and $\gamma = -i\dfrac{r}{\nu}$.

After substitution of these expressions in (A. 6) the following result can be derived:

$$Ae^{i\nu t} = -i\left(\varepsilon + \frac{i}{k}\right)\frac{\frac{rb}{2V}}{k}\cdot\frac{c_v}{b} + i\frac{\beta}{k}. \tag{A. 7}$$

When eqs. A. 1 are substituted in A. 4 and use is made of A. 7 and A. 5 it follows that

$$Y = -\pi\rho V^2\frac{S_v}{2}\left[-i(K_a' + iK_a'')\left\{\left(\frac{\varepsilon}{k} + \frac{i}{k^2}\right)\frac{rb}{2V}\cdot\frac{c_v}{b} - \frac{\beta}{k}\right\} - \frac{i}{k}(K_b' + iK_b'')\frac{rb}{2V}\frac{c_v}{b}\right]$$

$$N = \pi\rho V^2\frac{S_v}{2}\frac{c_v}{2}\left[-i\left\{(M_a' + \varepsilon K_a' + i(M_a'' + \varepsilon K_a'')\right\}\left\{\left(\frac{\varepsilon}{k} + \frac{i}{k^2}\right)\frac{rb}{2V}\cdot\frac{c_v}{b} - \frac{\beta}{k}\right\} - \right.$$

$$\left. - \frac{i}{k}\left\{M_b' + \varepsilon K_b' + i(M_b'' + iK_b'')\right\}\frac{rb}{2V}\frac{c_v}{b}\right]$$

which can be written as:

$$Y = -\pi\rho V^2\frac{S_v}{2}\left[\left(-\frac{K_a''}{k} + i\frac{K_a'}{k}\right)\beta + \left\{\left(\frac{K_b''}{k} + \frac{K_a'}{k^2} + \varepsilon\frac{K_a''}{k}\right) + \right.\right.$$

$$\left.\left. + i\left(-\frac{K_b'}{k} - \varepsilon\frac{K_a'}{k} + \frac{K_a''}{k^2}\right)\right\}\frac{rb}{2V}\cdot\frac{c_v}{b}\right] \tag{A. 8}$$

$$N = \pi\rho V^2\frac{S_v}{2}\frac{c_v}{2}\left[\left(-\frac{M_a'' + \varepsilon K_a''}{k} + i\frac{M_a' + \varepsilon K_a'}{k}\right)\beta + \left\{\left(\frac{M_b'' + \varepsilon K_b''}{k} + \frac{M_a' + \varepsilon K_a'}{k^2} + \varepsilon\frac{M_a'' + \varepsilon K_a''}{k}\right) + \right.\right.$$

$$\left.\left. + i\left(-\frac{M_b' + \varepsilon K_b'}{k} - \varepsilon\frac{M_a' + \varepsilon K_a'}{k} + \frac{M_a'' + \varepsilon K_a''}{k^2}\right)\right\}\frac{rb}{2V}\frac{c_v}{b}\right].$$

From eqs. A. 8 the expressions for the stability quantities as they are given in eq. A. 3 follow at once and are given by:

$$C_{y_\beta} \approx \frac{Y'_\beta}{qS} = 2\pi\frac{S_v}{S}\frac{1}{2}\frac{K_a''}{k}. \qquad C_{n_\beta} \approx \frac{N'_\beta}{qSb} = -2\pi\frac{S_v c_v}{Sb}\frac{1}{4}\frac{M_a'' + \varepsilon K_a''}{k}.$$

$$C_{y_{\dot\beta}} \approx \frac{Y''_\beta\,.\,c_v}{qSbk} = -2\pi\frac{S_v c_v}{Sb}\frac{1}{2}\frac{K_a'}{k^2}. \qquad C_{n_{\dot\beta}} \approx \frac{N''_\beta\,.\,c_v}{qSb^2k} = 2\pi\frac{S_v c_v^2}{Sb^2}\frac{1}{4}\frac{M_a' + \varepsilon K_a'}{k^2}.$$

$$C_{y_r} \approx \frac{Y'_r}{qS} = -2\pi\frac{S_v c_v}{Sb}\frac{1}{2}\left(\varepsilon\frac{K_a''}{k} + \frac{K_b''}{k} + \frac{K_a'}{k^2}\right).$$

$$C_{n_r} \approx \frac{N'_r}{qSb} = 2\pi\frac{S_v c_v^2}{Sb^2}\frac{1}{4}\left(\frac{\varepsilon M_a'' + \varepsilon^2 K_a''}{k} + \frac{M_b'' + \varepsilon K_b''}{k} + \frac{M_a' + \varepsilon K_a'}{k^2}\right).$$

$$C_{y_{\dot r}} \approx \frac{Y''_r\,.\,c_v}{q\,.\,Sbk} = 2\pi\frac{S_v c_v^2}{Sb^2}\frac{1}{2}\left(\varepsilon\frac{K_a'}{k^2} + \frac{K_b'}{k^2} - \frac{K_a''}{k^3}\right).$$

$$C_{n_{\dot r}} \approx \frac{N''_r\,.\,C_v}{qSb^2k} = -2\pi\frac{S_v c_v^3}{Sb^3}\frac{1}{4}\left(\frac{\varepsilon M_a' + \varepsilon^2 K_a'}{k^2} + \frac{M_b' + \varepsilon K_b'}{k^2} - \frac{M_a'' + \varepsilon K_a''}{k^3}\right).$$

APPENDIX B.

B. 1 *Determination of the flutter derivatives K_a' and M_a'.*

In ref. 5 the pressure distribution on an airfoil is determined from the following integral equation

$$w = (w^{(0)} + k\,w^{(1)})e^{i\nu t} =$$
$$= \frac{1}{4\pi\rho V}\iint_v \{ K^{(0)} + kK^{(1)} + k^2 \log k \,.\, K^{(2)} + k^2K^{(3)} + k^3 \log k K^{(4)} + k^3K^{(5)} + \ldots \} \tag{B. 1}$$
$$\{ p^{(0)} + kp^{(1)} + k^2 \log k\, p^{(2)} + k^2p^{(3)} + k^3 \log k \,.\, p^{(4)} + k^3p^{(5)} + \ldots \}\, e^{i\nu t}\, d\xi d\eta,$$

where the integration should be taken over the vertical tailplane V.

By equating corresponding powers of k, the following series of equations is obtained

$$\begin{aligned}
w^{(0)} &= \frac{1}{4\pi\rho V}\iint_v K^{(0)}p^{(0)}\, d\xi d\eta \\
w^{(1)} &= \frac{1}{4\pi\rho V}\iint_v \{ K^{(1)}p^{(0)} + K^{(0)}p^{(1)}\}\, d\xi d\eta \\
0 &= \iint_v \{ K^{(2)}p^{(0)} + K^{(0)}p^{(2)}\}\, d\xi d\eta \\
0 &= \iint_v \{ K^{(3)}p^{(0)} + K^{(1)}p^{(1)} + K^{(0)}p^{(3)}\}\, d\xi d\eta \\
0 &= \iint_v \{ K^{(4)}p^{(0)} + K^{(2)}p^{(1)} + K^{(1)}p^{(2)} + K^{(0)}p^{(4)}\}\, d\xi d\eta \\
0 &= \iint_v \{ K^{(5)}p^{(0)} + K^{(3)}p^{(1)} + K^{(1)}p^{(3)} + K^{(0)}p^{(5)}\}\, d\xi d\eta \\
&\text{etc.}
\end{aligned} \tag{B. 2}$$

As the downwash is different for translation and rotation, separate calculations are necessary for both cases. For translation one has $z_T = Ae^{i\nu t}$ and hence:

$$w = \frac{c_v}{2} \cdot \frac{dz}{dt} = \frac{c_v}{2}\ \frac{\partial z}{\partial t} + V\frac{\partial z}{\partial x} = iAVke^{i\nu t}.$$

Thus it is found that for the case of translation $w_T^{(0)} = 0$ and $w_T^{(1)} = iAV$. In the same way it is found that for rotation $z = Bxe^{i\nu t}$ and thus $w_R^{(0)} = BV$ and $w_R^{(1)} = i.B.V.x.$

From the fact that $K^{(0)}$ and $K^{(2)}$ are real and $K^{(1)}$ and $K^{(4)}$ are purely imaginary while $K^{(3)}$ and $K^{(5)}$ are complex it follows at once from (B. 2) that $p^{(1)}$ and $p^{(4)}$ are always purely imaginary and $p^{(0)}$ and $p^{(2)}$ are real while $p^{(3)}$ and $p^{(5)}$ are complex. Because $w_T^{(0)} = 0$ it follows moreover that $p_T^{(0)}$ and $p_T^{(2)}$ are zero and that $p_T^{(3)}$ is real.

In ref. 5 the coefficients $p^{(i)}$ are determined by prescribing the chordwise distribution in the form:

$$p^{(i)} = \frac{1}{\pi}\, g_1^{(i)} \cot\, \frac{\vartheta}{2} + \frac{2}{\pi}\{ g_0^{(i)} - g_1^{(i)}\} \sin \vartheta, \tag{B. 3}$$

in which ϑ is a coordinate in chordwise direction being determined by

$$\xi = -\cos \vartheta.$$

From this expression for $p^{(i)}$ it follows that $g_0^{(i)}$ is proportional to the lift per unit span while $g_1^{(i)}$ is proportional to the moment per unit span about the mid-chord axis. Then the expressions for the total force K and the total moment M of the rectangular airfoil become:

$$\begin{aligned}
K &= -\frac{c_v}{2}\, e^{i\nu t} \int_0^s \{ g_0^{(0)} + kg_0^{(1)} + k^2 \log k\, g_0^{(2)} + k^2g_0^{(3)} + k^3 \log k\, g_0^{(4)} + k^3g_0^{(5)} + \ldots \}\, d\eta \\
M &= \frac{c_v^2}{8}\, e^{i\nu t} \int_0^s \{ g_1^{(0)} + kg_1^{(1)} + k^2 \log k\, g_1^{(2)} + k^2g_1^{(3)} + k^3 \log kg_1^{(4)} + k^3g_1^{(5)} + \ldots \}d\eta
\end{aligned} \tag{B. 4}$$

and thus

$$K_a' = -\frac{1}{\pi\rho V^2 As}\int_0^s \{ k^2 g^{(3)}_{0.T} + k^3 Re\, g^{(5)}_{0.T} + \dots \}\, d\eta$$

$$K_a'' = +\frac{i}{\pi\rho V^2 As}\int_0^s \{ k\, g^{(1)}_{0.T} + k^3 \log k\, g^{(4)}_{0.T} + k^3 Im\, g^{(5)}_{0.T} + \dots \}\, d\eta$$

$$K_b' = -\frac{1}{\pi\rho V^2 Bs}\int_0^s \{ g^{(0)}_{0.R} + k^2 \log\, k\, g^{(2)}_{0.R} + k^2 Re\, g^{(3)}_{0.R} + k^3\, Re\, g^{(5)}_{0.R} + \dots \}\, d\eta \qquad \text{(B. 5)}$$

$$K_b'' = +\frac{i}{\pi\rho V^2 Bs}\int_0^s \{ k\, g^{(1)}_{0.R} + k^2 Im\, g^{(3)}_{0.R} + k^3 \log k\, g^{(4)}_{0.R} + k^3 Im\, g^{(5)}_{0.R} + \dots \}\, d\eta.$$

Similar expressions are found for M_a and M_b.

It will be shown now that there exists a relation between K_a' and K_b'' which enables the determination of K_a' without additional calculations. Therefore it will be shown that there exist several relations between the different coefficients $g_T^{(i)}$ and $g_R^{(i)}$.

When e.g. the first equation of eqs. B. 2 for the case of rotation is compared with the second equation of B. 2 for the case of translation it is found that

$$\frac{1}{iA}\iint_v K^{(0)}(x.y.\xi.\eta).p_T{}^{(1)}.\,d\xi d\eta = \frac{1}{B}\iint_v K^{(0)}(x.y.\xi.\eta)\,p_R{}^{(0)}\,d\xi d\eta.$$

As this relation must be valid for any point $x.y$ of the lifting surface, it follows that $p_T{}^{(1)}$ is identical to $i\dfrac{A}{B}\,p_R{}^{(0)}$.

From this relation it follows immediately that

$$g^{(1)}_{0.T} = i\frac{A}{B} g^{(0)}_{0.R} \text{ and } g^{(1)}_{1.T} = i\frac{A}{B} g^{(0)}_{1.R}. \qquad \text{B. 6}$$

In the same way it is possible to compare the fourth equation of B. 2 for translation with the second equation for rotation. These equations are

$$0 = \iint_v \{ K^{(1)} p_T{}^{(1)} + K^{(0)} p_T{}^{(3)} \}\, d\xi d\eta = \iint_v \{ K^{(1)} p_R{}^{(0)} - iK^{(0)}\,.\,\frac{B}{A} p_T{}^{(3)} \}\, d\xi d\eta \qquad \text{B. 7}$$

$$w_R{}^{(1)} = \frac{1}{4\pi\rho V}\iint_v \{ K^{(1)} p_R{}^{(0)} + K^{(0)} p_R{}^{(1)} \}\, d\xi d\eta = \frac{1}{4\pi\rho V}\iint_v \{ K^{(1)} p_R{}^{(0)} + K^{(0)}(p^{(1)}_{R_{q.s}} + p^{(1)}_{R_{n.s}}) \}\, d\xi d\eta.$$

Thus $p^{(1)}_R$ is divided into a part $p^{(1)}_{R_{n.s}}$ which is due to the unsteady wake effect and a part $p^{(1)}_{R_{q.s}}$ which gives the pressure distribution for the quasi-steady case in which the unsteady wake effects are absent. For this case the following relation is valid

$$w^{(1)}_R = \frac{1}{4\pi\rho V}\iint_v K^{(0)} p^{(1)}_{R_{q.s}}\, d\xi d\eta.$$

By subtracting this equation from the foregoing one it is seen that

$$0 = \iint_v \{ k^{(1)} p_R{}^{(0)} + K^{(0)} p^{(1)}_{R_{n.s}} \}\, d\xi d\eta.$$

Comparing B. 7 with this equation gives

$$-i\frac{B}{A}\iint_v K^{(0)} p_T{}^{(3)}\,.\,d\xi\,.\,d\eta = \iint_v K^{(0)} p^{(1)}_{R_{n.s}}\, d\xi d\eta$$

and thus

$$-i\,\frac{B}{A}\; p_T{}^{(3)} = p^{(1)}_{R_{n.s}}$$

from which it follows that

$$-i\frac{B}{A} g^{(3)}_{0.T} = g^{(1)}_{0.R_{n.s}} \text{ and } -i\frac{B}{A} g^{(3)}_{1.T} = g^{(1)}_{1.R_{n.s}}. \qquad \text{(B. 8)}$$

At last the real part of the sixth equation of B. 2 for the case of translation must be compared with the imaginary part of the fourth equation for the case of rotation. The two equations are given by the following expressions

$$0 = \iint\limits_{v} \{ ImK^{(3)} . p_T{}^{(1)} + K^{(0)} . Re\, p_T{}^{(5)} \} \, d\xi d\eta$$

$$0 = \iint\limits_{v} \{ ImK^{(3)} . p_R{}^{(0)} + K^{(0)} . Im\, p_R{}^{(3)} \} \, d\xi d\eta.$$

By aid of the relation $p_T^{(1)} = i \dfrac{A}{B} \, p_R^{(0)}$ the first equation becomes

$$0 = \iint\limits_{v} \{ ImK^{(3)} p_R{}^{(0)} - i \frac{B}{A} K^{(0)} . Re\, p_T{}^{(5)} \} \, d\xi d\eta.$$

Thus it follows that $Re\, p_T{}^{(5)} = \dfrac{iA}{B} Im\, p_R{}^{(3)}$ and

$$Re\, g_{0.T}^{(5)} = i \frac{A}{B} \, Im\, g_{0.R}^{(3)} \text{ and } Re_{1.T}^{(5)} = i \frac{A}{B} \, Im\, g_{1.R}^{(3)}. \tag{B. 9}$$

When now the eqs. B. 8 and B. 9 are substituted in the expression for K_a' the following relation is obtained

$$K_a' = -\frac{i}{\pi \rho V^2 A s} \int\limits_0^s \{ k^2 g_{0.T}^{(3)} + k^3 Re\, g_{0.T}^{(5)} + \ldots \} \, d\eta = -\frac{i}{\pi \rho V^2 B s} \int\limits_0^s \{ k^2 g_{0.R_{n.s}}^{(1)} + k^3 \, Im\, g_{0.R}^{(3)} + \ldots \} \, d\eta.$$

in which $s = \dfrac{2b_v}{c_v}$.

Now $g_{0.R_{n.s}}^{(1)} = g_{0.R}^{(1)} - g_{0.R_{q.s}}^{(1)}$ as has been derived above and hence it is possible to write

$$K_a' = -\frac{ik}{\pi \rho V^2 B s} \int\limits_0^s \{ k\, g_{0.R}^{(1)} + k^2 Im\, g_{0.R}^{(3)} + \ldots - k\, g_{0.R_{q.s}}^{(1)} \} \, d\eta. \tag{B. 10}$$

In ref. 5 the derivative K_b'' has been calculated by taking into account terms up to the second power of k. Thus in the approximation of ref. 5

$$K_b'' = -\frac{i}{\pi \rho V^2 B s} \int\limits_0^s \{ k\, g_{0.R}^{(1)} + k^2 \, Im\, g_{0.R}^{(3)} \} \, d\eta. \tag{B. 11}$$

The relation between K_b'' and K_a' follows now immediately by comparing this expression with B. 10. The result is

$$K_a' = -k(K_b'' - K_b''{}_{q.s}) \tag{B. 12}$$

in which K_a' is accurate to the third power of k. As K_b'' and $K_b''{}_{q.s}$ have been calculated in ref. 5 the results of K_a' are directly obtainable from ref. 5. The same derivation and thus also the same result is valid for M_a'. Thus

$$M_a' = -K(M_b'' - M_b''{}_{q.s}) \tag{B. 13}$$

From these results it follows also that the non-stationary effects of $\dfrac{Y_r'}{qs}$ and $\dfrac{N_r'}{qsb}$ which are denoted also by the symbols C_{y_r} and C_{n_r} are small of the third power in k.

Considering e.g. C_{y_r} the following expression is given in eq. A. 9:

$$C_{y_r} = -2\pi \frac{S_v c_v}{Sb} \, \frac{1}{2} \left(\varepsilon \frac{K_a''}{k} + \frac{K_b''}{k} + \frac{K_a'}{k^2} \right).$$

From eqs. B. 10 and B. 11 it follows that

$$\frac{K_b''}{k} + \frac{K_a'}{k^2} = \frac{i}{\pi \rho V^2 B s} \int\limits_0^s \left\{ g_{0.R_{q.s}}^{(1)} + \frac{0(k^3)}{k} + \ldots \right\} d\eta$$

while it follows from eq. B. 5 that

$$\frac{K_a''}{k} = -\frac{1}{\pi\rho V^2 Bs}\int\limits_0^s \left\{ g^{(0)}_{0.R} + \frac{0(k^3)}{k} + \dots \right\} d\eta.$$

Thus C_{y_r} (a similar derivation is valid for C_{n_r}), consists of a quasi steady part denoted by $g^{(1)}_{0.R_{q.s}}$ and $g^{(0)}_{0.R}$ and further of terms of third order of k. When considering eqs. A. 2 and A. 3 this result can be given also in the statement that $\frac{\partial Y}{\partial r}$ and $\frac{\partial N}{\partial r}$ indeed are quasi steady quantities while the higher order terms of Y_r' and N_r' can be identified with $\frac{\partial Y}{\partial \frac{\ddot{r}\, b^2}{4V^2}}$ and $\frac{\partial N}{\partial \frac{\ddot{r}\, b^2}{4V^2}}$.

B. 2 *Further consideration of the stability derivatives $C_{y_{\dot r}}$ and $C_{n_{\dot r}}$.*

When the expressions B. 5 are substituted in eq. A. 9 the following expression for e.g. $C_{y_{\dot r}}$ is obtained

$$C_{y_{\dot r}} = -\frac{1}{q}\,\frac{S_v c_v^2}{Sb^2}\,\frac{1}{2s}\left[\frac{\varepsilon}{A}\int\limits_0^s (g^{(3)}_{0.T} + k\, Re\, g^{(5)}_{0.T} + \dots)d\eta + \right.$$

$$+\frac{1}{B}\int\limits_0^s \left(\frac{g^{(0)}_{0.R}}{k^2} + \log k\,.\,g^{(2)}_{0.R} + Re\,.\,g^{(3)}_{0.R} + k\,.\,Re\, g^{(5)}_{0.R} + \dots\right) d\eta -$$

$$\left. -\frac{1}{iA}\int\limits_0^s \left(\frac{g^{(1)}_{0.T}}{k^2} + \log k\, g^{(4)}_{0.T} + Im\, g^{(5)}_{0.T} + \dots\right) d\eta\right]. \qquad \text{(B. 13)}$$

At first sight it would appear from B. 13 that for $k=0$ the expression for $C_{y_{\dot r}}$ would become infinitely large. However when B. 6 is substituted in B. 13 and when a similar relation between $g^{(4)}_{0.T}$ and $g^{(2)}_{0.T}$ could be derived the terms which cause the singularity for $k=0$ would disappear. Therefore the fifth equation of B. 2 for the case of translation will be compared with the third equation for the case of rotation. These equations are:

$$0 = \iint\limits_v \{K^{(2)} p_R^{(0)} + K^{(0)}\,.\,p_R^{(2)}\}\, d\xi d\eta$$

$$0 = \iint\limits_v \{K^{(2)} p_T^{(1)} + K^{(0)}\, p_T^{(4)}\}\, d\xi d\eta.$$

By substituting the relation $p_T^{(1)} = i\,\frac{A}{B}\,p_R^{(0)}$ in the first of the equations given above and subtracting both equations it follows that

$$\iint\limits_v \left\{ K^{(0)}\,.\,i\,\frac{A}{B}\,.\,p_R^{(2)} \right\} d\xi d\eta = \iint\limits_v \{K^{(0)} p_T^{(4)}\}\, d\xi d\eta.$$

Because this relation must be valid for any point of the lifting surface it is possible to write

$$p_T^{(4)} = i\,\frac{A}{B}\,p_R^{(2)}$$

and thus

$$g^{(4)}_{0.T} = i\,\frac{A}{B}\,g^{(2)}_{0.R} \text{ and } g^{(4)}_{1.T} = i\,\frac{A}{B}\,g^{(2)}_{1.R}. \qquad \text{(B. 14)}$$

When B. 6 and B. 14 are substituted in B. 13 the following expression is obtained

$$C_{y_{\dot r}} = -\frac{1}{q}\,\frac{S_v c_v^2}{Sb^2}\,\frac{1}{2s}\int\limits_0^s \left[\frac{\varepsilon}{A}\,(g^{(3)}_{0.T} + k\, Re\, g^{(5)}_{0.T} + \dots) + \right.$$

$$\left. + \frac{1}{B}\,(Re\,.\,g^{(3)}_{0.R} + k\, Re\, g^{(5)}_{0.R} + \dots) + \frac{i}{A}\,(Im\, g^{(5)}_{0.T} + \dots)\right] d\eta. \qquad \text{(B. 15)}$$

It is seen hat the singularity has been removed. When investigating $C_{n_{\dot r}}$ the same derivation is valid and the same conclusion will be reached.

The formula which has been derived from ref. 5 is given by

$$C_{y_{\dot r}} = -\frac{1}{q}\;\frac{S_v c_v^2}{Sb^2}\;\frac{1}{2s}\int_0^s \frac{\varepsilon}{A}\, g^{(3)}_{0.T}\, d\eta \tag{B.16}$$

so that not only all terms containing k have been neglected but also

$$\frac{1}{B}\; Re\, g^{(3)}_{0.R} + \frac{i}{A}\; Im\, g^{(5)}_{0.T}.$$

Although this expression is not zero it will be shown that indeed it is very small compared with $\frac{\varepsilon}{A}\cdot g^{(3)}_{0.T}$. Therefore the imaginary part of the 6th eq. of B. 2 for translation must be compared with the real part of the 4th eq. of B. 2 for rotation. These equations yield

$$0 = \iint_v \{ Re\, K^{(3)} p_T{}^{(1)} + K^{(1)} p_T{}^{(3)} + K^{(0)}\, Im\, p_T{}^{(5)} \}\, d\xi d\eta$$

$$0 = \iint_v \{ Re\, K^{(3)} p_R{}^{(0)} + K^{(1)} p_R{}^{(1)} + K^{(0)}.\, Re\, p_R{}^{(3)} \}\, d\xi d\eta.$$

Since it has been shown already that

$$p_T{}^{(1)} = i\frac{A}{B}\, p_R{}^{(0)} \quad \text{and} \quad p_T{}^{(3)} = i\frac{A}{B}\, \{ p_R{}^{(1)} - p_{R}{}^{(1)}_{R_{q.s}} \}$$

it follows that

$$\iint_v K^{(0)} \left\{ Im\, p_T{}^{(5)} - i\frac{A}{B}\; Re\, p_R{}^{(3)} \right\}\, d\xi d\eta = i\frac{A}{B}\iint_v K^{(1)}\, p_{R_{q.s}}\, d\xi d\eta. \tag{B.17}$$

When a quantity $\bar{p}_R{}^{(3)}$ is defined by the relation

$$\iint_v \left(K^{(1)} p^{(1)}_{R_{q.s}} + K^{(0)} \bar{p}^{(3)} \right) d\xi d\eta = 0 \tag{B.18}$$

it is possible by substituting eq. B. 18 in eq. B. 17 to obtain:

$$Im\, p_T{}^{(5)} = i\frac{A}{B} Re\, \{ p_R{}^{(3)} - \bar{p}_R{}^{(3)} \} \tag{B.19}$$

and hence

$$\frac{1}{B}\; Re\, g^{(3)}_{0.R} + \frac{i}{A}\; Im\, g^{(5)}_{0.T} = \frac{1}{B}\; \bar{g}^{(3)}_{0.R} \quad \text{and} \quad \frac{1}{B}\; Re\, g^{(3)}_{1.R} + \frac{i}{A}\; Im\, g^{(5)}_{1.5} = \frac{1}{B}\; \bar{g}^{(3)}_{1.R}$$

which are very small indeed, as they are determined by $p^{(1)}_{R_{q.s}}$ in (B. 18).

Since it is shown in sec. 4 that the influence of $C_{y_{\dot r}}$ and $C_{n_{\dot r}}$ on the stability is already very small when using eq. B. 16 the neglect of the term $\frac{1}{B}\,\bar{g}^{(3)}_{0.R}$ is certainly allowed.

TABLE 1. The aerodynamic derivatives K_a' and M_a' for various values of the reduced frequency k.

	Ma	0.7			0.9		
	$\frac{b_v}{c_v}\sqrt{1-Ma^2}$	1.43	2.85^5	5.71^5	1.43	2.85^5	5.71^5
$\frac{K_a'}{k^2}$	$k=0$	−0.88	−4.07	−8.66	−7.89	−22.95	−43.80
	0.02	−0.82	−3.87	−8.09	−7.75	−22.36	−41.79
	0.04	−0.76	−3.66	−7.48	−7.49	−21.42	−39.08
	0.06	−0.71	−3.45	−6.86	−7.24	−20.48	−36.38
	0.08	−0.65	−3.23	−6.25	−6.98	−19.55	−33.68
	0.10	−0.59	−3.02	−5.63	−6.72	−18.61	−30.98
$\frac{M_a'}{k^2}$	0	1.40	3.19	5.59	7.43	16.01	27.06
	0.02	1.37	3.10	5.31	7.42	15.79	26.13
	0.04	1.34	2.99	5.00	7.28	15.30	24.76
	0.06	1.31	2.88	4.68	7.14	14.80	23.37
	0.08	1.28	2.77	4.37	7.00	14.31	22.00
	0.10	1.25	2.65	4.05	6.85	13.82	20.63

TABLE 2. The aerodynamic derivatives K_a'', M_a'', K_b'' and M_b'' for various values of $\frac{b_v}{c_v}\sqrt{1-Ma^2}$.

$\frac{b_v}{c_v}\sqrt{1-Ma^2}$	1.43	2.85^5	5.71^5
$\frac{\beta K_a''}{k}$	−0.97132	−1.3161	−1.5789
$\frac{\beta M_a''}{k}$	0.53597	0.68821	0.80596

	Ma	0.7			0.9		
	$\frac{b_v}{c_v}\sqrt{1-Ma^2}$	1.43	2.85^5	5.71^5	1.43	2.85^5	5.71^5
$\frac{K_b''}{k}$	$k=0$	0.1289	3.108	7.572	6.663	21.37	41.95
	0.02	0.0716	2.915	6.961	6.517	20.78	39.94
	0.04	0.0135	2.701	6.347	6.261	19.84	37.23
	0.06	−0.0447	2.448	5.733	6.006	18.90	34.53
	0.08	−0.1028	2.275	5.118	5.750	17.97	31.83
	0.10	−0.1609	2.061	4.504	5.495	17.03	29.13
$\frac{M_b''}{k}$	0	−1.614	−3.350	−5.691	−7.789	−16.27	−27.24
	0.02	−1.593	−3.260	−5.414	−7.775	−16.05	−26.31
	0.04	−1.560	−3.149	−5.101	−7.635	−15.56	−24.93
	0.06	−1.528	−3.037	−4.787	−7.494	−15.07	−23.55
	0.08	−1.496	−2.926	−4.474	−7.353	−14.58	−22.17
	0.10	−1.464	−2.814	−4.160	−7.212	−14.09	−20.79

TABLE 3. Dimensional and mass characteristics of example airplanes.

	Example A conf. 5 of ref. 8	Example B (ref. 10)	
		small taillength	large taillength
W lb	20.833	20.000	20.000
W/S lb/sq.ft	50	64	64
μ $(h=0)$	18.4	24.9	24.9
S sq.ft	417	313	313
b ft	35.4	33.6	33.6
AR	3	3.6	3.6
Λ degrees	0°	37.5°	37.5°
taper ratio	0.5	0.455	0.455
S_v sq.ft	45.5	30	30
AR_v	2	1.7	1.7
c_v ft	4.78	4.2	4.2
Λ_v degrees	0°	0°	0°
taper ratio of vertical tail	1	1	1
ε	10.75	3.95	5.56

TABLE 4.

Conditions for which calculations were made, derivatives used in calculations and results of calculations for example A.

No.	C_L	Ma	α°	K_x^2	K_z^2	K_{xz}	C_{y_β}	C_{n_β}	C_{l_β}	C_{y_p}	C_{n_p}	C_{l_p}	C_{y_r}	C_{n_r}	C_{l_r}	Aperiodic modes		Oscillatory mode	
																$T_{1/2}$	$T_{1/2}$	p	$T_{1/2}$
1	0.07	0.7	+0.7	0.0237	0.101	—0.00128	—0.51	0.145	—0.058	0.024	—0.0087	—0.29	0.39	—0.29	0.092	156	0.143	1.13	1.03

No.	C_L	Ma	α°	K_z^2	C_{y_β}	C_{n_β}	C_{y_r}	C_{n_r}	$C_{y_{\dot\beta}}$	$C_{n_{\dot\beta}}$	$C_{y_{\dot r}}$	$C_{n_{\dot r}}$	Oscillatory mode	
													p_{sec}	$T_{1/2}$ sec
2	0.07	0.7	+ 0.7	0.101	— 0.51	0.145	0.39	— 0.29	0	0	0	0	1.14	0.92
3													1.14	0.92
4	0.04	0.9	+ 0.3	0.050	— 0.55	0.172	0	— 0.33	0	0	0	0	0.73	0.46
5				0.101									1.04	0.82
6				0.159									1.30	1.13
7				0.201									1.46	1.31
8				0.258									1.65	1.31
9				0.328									1.86	1.71
10				0.050					— 0.074	0.059	0.108	— 0.086	0.73	0.40
11				0.101									1.04	0.73
12				0.159									1.31	1.02
13				0.201									1.47	1.19
14				0.258									1.66	1.38
15				0.328									1.87	1.58
16				0.050					0	0.059	0	0	0.73	0.40
17				0.101									1.04	0.73
18				0.159									1.30	1.02
19				0.201									1.46	1.19
20				0.258									1.65	1.38
21				0.328									1.87	1.58
22				0.050					0	0.0295	0	0	0.73	0.43
23				0.101									1.04	0.77
24				0.159									1.30	1.07
25				0.201									1.46	1.25
26				0.258									1.65	1.45
27				0.328									1.87	1.64

TABLE 5.

Conditions for which calculations were made, derivatives used in calculations and results of calculations for example B.

$H = 0$ ft, $C_{y_{\dot{\beta}}} = C_{y_{\dot{r}}} = C_{n_{\dot{r}}} = C_{y_r} = 0$

No.	C_L	Ma	K_z^2	C_{y_β}	C_{n_β}	C_{n_r}	$C_{n_{\dot{\beta}}}$	Oscillatory mode p_{sec}	Oscillatory mode $T_{1/2}$ sec
				$\varepsilon = 3.95$					
28	0.054	0.9	0.04	— 0.57	0.096	— 0.057	0.046	0.96	1.25
29			0.0625					1.20	1.66
30			0.09					1.44	2.03
31			0.1225					1.69	2.34
32			0.16					1.93	2.60
33			0.04				0.023	0.96	1.48
34			0.0625					1.20	1.92
35			0.09					1.44	2.29
36			0.1225					1.68	2.59
37			0.16					1.93	2.83
38			0.04				0	0.96	1.81
39			0.0625					1.20	2.26
40			0.09					1.44	2.62
41			0.1225					1.68	2.89
42			0.16					1.92	3.10
				$\varepsilon = 5.56$					
43			0.04	— 0.54	0.125	— 0.084	0.064	0.85	0.97
44			0.0625					1.06	1.35
45			0.09					1.27	1.70
46			0.1225					1.48	2.03
47			0.16					1.69	2.31
48			0.04				0.032	0.84	1.17
49			0.0625					1.05	1.58
50			0.09					1.27	1.96
51			0.1225					1.48	2.29
52			0.16					1.69	2.57
53			0.04				0	0.84	1.46
54			0.0625					1.05	1.91
55			0.09					1.26	2.30
56			0.1225					1.48	2.63
57			0.16					1.69	2.89

C.C.L. Class. D 050

NLL-TN F. 193

Stability diagrams for laminar boundary layer flow

by

R. TIMMAN, J. A. ZAAT and TH. J. BURGERHOUT.

Summary

For a one-parameter family of boundary layer velocity profiles stability diagrams are given. The method of calculation applied, starts from the asymptotic behaviour of the inviscid differential equation of disturbance. This method makes use of only one solution in the complete domain of integration.

This investigation was performed under contract with the Netherlands Aircraft Development Board (N. I. V.).

Contents.

List of symbols.

x, y	coordinates along and normal to the wall
$\bar{\omega}$	velocity in the boundary layer
W	free stream velocity
$w = \frac{\bar{\omega}}{W} = f(y/\delta, \lambda)$	velocity profile for $x =$ const.
δ	boundary layer thickness
$\lambda = \frac{5}{7} b^2 - \frac{12}{7} b$	profile form-parameter
b	velocity profile parameter
$\psi(x, y, t) = \varphi(y) e^{i\bar{\alpha}(x - \bar{c}t)}$	stream function of the disturbance
$\varphi(y)$	amplitude of the disturbance
$\bar{c}$	velocity of propagation of the disturbance
t	time
$\bar{\alpha}/2\pi$	the reciprocal wave length
$c = \frac{\bar{c}}{W}$, $\eta = \frac{y}{\delta}$, $\alpha = \bar{\alpha}\delta$	dimensionless quantities
$\eta = \eta_0$ for $w = f(\eta_0) = c$	
ν	kinematic viscosity
$R = \frac{W\delta}{\nu}$	Reynolds number
$\varphi_1, \varphi_2, \varphi_3, \varphi_4$	particular solutions of eq. (2.4)
$z = \left(\alpha R \frac{dw}{d\eta}\right)^{1/3}_{\eta=\eta_0} (\eta - \eta_0)$	
$A_i, \alpha_i, \beta_i, a_i, c_i, d_i$	coefficients
$\Delta_1 = \frac{\delta^*}{\delta}$	displacement thickness
Δ_2	momentum thickness
$\zeta = \eta - \eta_0$	in sec. 4
$\zeta = \eta + i\nu$, $\varphi = \chi + i\psi$	see Appendix A
$g(\zeta), G(\zeta)$	functions of ζ
$D(z) = -\frac{\varphi_3(z)}{d\varphi_3/dz}$	function of Tietjens ref. 5, p. 38
$\beta_r = \bar{\alpha}\bar{c}$	circular frequency
$A_3 = -\frac{\varphi_1(0)}{\varphi_3(0)}$	coefficient, see eq. (6.2)
k	arbitrary intensity factor
f', f'', φ''	denoting differentiations to η
subscripts η, ν	denoting derivatives to η, ν

1 Introduction.

In ref. 1 a one parameter method for the calculation of laminar boundary layers is given. As unstability of the laminar boundary layer is an important feature in the transition to turbulence, it is useful to complete this calculation method by designing a stability diagram, giving the stability limit of the boundary layer profile corresponding to different values of the parameter. As the theory of this subject has been exposed comprehensively in several papers (refs. 2, 3, 4) it is not repeated here. As the numerical method is different from the method followed in other papers, only an exposition of the numerical methods will be given, starting from the well-known differential equations, which describe the phenomenon.

2 Results of the theory of the stability of laminar boundary flow.

We consider a two-dimensional laminar boundary layer flow along a plane wall. Introducing coordinates x and y along and normal to the wall, the velocity profile in a section $x = \text{const.}$ is assumed to be given by an equation

$$w = \frac{\overline{w}}{W} = f(y/\delta, \lambda) \tag{1}$$

where W is the local free stream velocity and δ is a length, corresponding to the boundary layer thickness.

We assume an infinitesimal disturbance, with periodic time dependence, determined by a stream function

$$\psi(x, y, t) = \varphi(y) \,.\, e^{i\overline{\alpha}(x - \overline{c}t)} \tag{2}$$

where $\overline{\alpha}$ and $\overline{c}$ are real. $\overline{c}$ is the velocity of propagation of the disturbance, which at a certain instant t represents a wave with constant amplitude. The function $\varphi(y)$ satisfies the SOMMERFELD equation (ref. 2, p. 282)

$$(\overline{w} - \overline{c}) \left(\frac{d^2\varphi}{dy^2} - \overline{\alpha}^2\varphi\right) - \varphi \,.\, \frac{d^2\overline{w}}{dy^2} = - \frac{i\nu}{\overline{\alpha}}\left(\frac{d^4\varphi}{dy^4} - 2\overline{\alpha}^2\,\frac{d^2\varphi}{dy^2} + \overline{\alpha}^4\varphi\right), \tag{3}$$

where ν is the kinematic viscosity.

Introducing dimensionless quantities

$$c = \frac{\overline{c}}{W}, \quad \eta = \frac{y}{\delta}, \quad \alpha = \overline{\alpha}\,\delta$$

we obtain the equation

$$(w - c)(\varphi'' - \alpha^2\varphi) - w''\varphi = - \frac{i}{\alpha R}\,(\varphi^{\text{IV}} - 2\alpha^2\varphi'' + \alpha^4\varphi), \tag{4}$$

where $R = \dfrac{W\delta}{\nu}$ is the REYNOLDS' number referred to free stream velocity and boundary layer thickness.

The boundary conditions for the stream function $\varphi(y)$ are

$$\eta = 0 \qquad \varphi = 0, \qquad \varphi' = 0 \tag{5}$$

$$\eta \to \infty \qquad \varphi \to 0, \qquad \varphi' \to 0. \tag{6}$$

Any solution of the linear homogeneous equation (4) can be obtained from a set of particular independent solutions φ_1, φ_2, φ_3 and φ_4.

It is shown in the theory, that a good approximation for large values of R is obtained by choosing for φ_1 and φ_2 two independent solutions of the "inviscid" equation

$$(w - c)(\varphi'' - \alpha^2\varphi) - w''\varphi = 0 \tag{7}$$

if necessary corrected for viscosity effects.

The functions φ_3 and φ_4 are represented asymptotically for large values of R by solutions of a simplified equation, representing the behaviour of eq. (4) in the neighbourhood of the point $\eta = \eta_0$, where $w = c$. Here, $w \approx (\eta - \eta_0)w_0'$ and the approximating equation is, on introducing a new variable (ref. 5)

$$z = (\alpha R w_0')^{1/3}\,(\eta - \eta_0), \tag{8}$$

$$i\,\frac{d^4\varphi}{dz^4} + z\,\frac{d^2\varphi}{dz^2} = 0. \tag{9}$$

The function φ_3, which is finite at infinity, then is taken as the solution

$$\varphi_3(z) = \int_{\infty}^{z} dz_1 \int_{\infty}^{z_1} \eta^{1/2}\, H_{1/3}^{(1)}\left[\frac{2}{3}\,(i\eta)^{3/2}\right] d\eta. \tag{10}$$

Any other solution φ_4 is infinite for $z \to \infty$.

Regarding the boundary condition (6) it is obvious, that φ_4 cannot contribute to the solution. Hence we put

$$\varphi = A_1\varphi_1 + A_2\varphi_2 + A_3\varphi_3 \tag{11}$$

and A_1, A_2, A_3 are determined from

$$\left.\begin{aligned} A_1\varphi_1(0) + A_2\varphi_2(0) + A_3\varphi_3(0) &= 0 \\ A_1\varphi_1'(0) + A_2\varphi_2'(0) + A_3\varphi_3'(0) &= 0 \\ A_1\varphi_1(\infty) + A_2\varphi_2(\infty) &= 0. \end{aligned}\right\} \tag{12}$$

If, moreover, we choose φ_1 so, that $\varphi_1(\infty) = 0$, then $A_2 = 0$ and the system becomes

$$\left.\begin{aligned} A_1\varphi_1(0) + A_3\varphi_3(0) &= 0 \\ A_1\varphi_1'(0) + A_3\varphi_3'(0) &= 0. \end{aligned}\right\} \tag{13}$$

This is only possible for non-vanishing coefficients $A_{1,3}$ if c and α have values, which make

$$\begin{vmatrix} \varphi_1(0) & \varphi_3(0) \\ \varphi_1'(0) & \varphi_3'(0) \end{vmatrix} = 0. \tag{14}$$

The values of c and α satisfying this equation can be plotted as functions of R to give the stability curve.

3 The inviscid solution.

The inviscid solution φ_1 is a solution of the equation

$$\varphi'' = \left\{\alpha^2 + \frac{f''}{f(\eta) - f(\eta_0)}\right\}\varphi,$$

where η_0 is the value of η for which $f(\eta_0) = c$, which tends to zero if $\eta \to \infty$.

The function $f(\eta)$ is a modification of the velocity profile, chosen in ref. 1.

$$f(\eta) = (1 - b)f_1(\eta) + b\,f_2(\eta) - d\,f_3(\eta)$$

where the third term has been added to remove the discontinuity in the passage from accelerated to retarded flow.

The functions $f_1(\eta)$, $f_2(\eta)$ and $f_3(\eta)$ are given by

$$f_1(\eta) = \frac{4}{3\sqrt{\pi}} \int_0^\eta (1 + t^2) e^{-t^2}\, dt = -$$

$$- \frac{2}{3\sqrt{\pi}} \eta e^{-\eta^2} + \frac{2}{\sqrt{\pi}} \int_0^\eta e^{-t^2} dt$$

$$f_2(\eta) = 1 - e^{-\eta^2}$$

$$f_3(\eta) = \eta^2 e^{-\eta^2}$$

and $d = \frac{1}{14}(2b + 5b^2)$.

The value of b in the stagnation point follows from:

$$\frac{4}{3\sqrt{\pi}}(1 - b) + 2(b - d)(\Delta_1 + 2\Delta_2) = 0,$$

where Δ_1 the displacement thickness, is

$$\Delta_1 = \int_0^\infty (1 - f)\, d\eta =$$

$$= 0{,}752253 + 0{,}133974\, b + 0{,}443114\, d$$

and Δ_2 the momentum thickness:

$$\Delta_2 = \int_0^\infty f(1 - f)\, d\eta =$$

$$0{,}289430 - 0{,}014670\, b - 0{,}015190\, b^2 + d(0{,}188063 - 0{,}058279\, b) + 0{,}117498\, d^2$$

in the stagnation point

$$b = -\,0{,}412.$$

Hence, for sufficiently large values of η_1 the term $\frac{f''}{f - c}$ may be neglected and the differential equation simplifies to

$$\varphi'' = \alpha^2 \varphi.$$

The solution φ_1, which, for $\eta \to \infty$ must vanish together with its derivative, hence it can be approximated by

$$\varphi_1(\eta) = e^{-\alpha\eta}$$

$$\varphi_1'(\eta) = -\alpha\, e^{-\alpha\eta}.$$

These values can, in the region, where they are valid, be taken as starting values for the numerical integration. This numerical integration was performed by ADAM's method, operating with central differences and extrapolation.

This method was useful up to the neighbourhood of the pole $\eta = \eta_0$ of the coefficient of φ in the differential equation.

4 The integration through the pole.

The equation for the inviscid solutions

$$\varphi'' - \left(\alpha^2 + \frac{f''}{f - c}\right)\varphi = 0 \qquad (1)$$

has a singular point for $\eta = \eta_0$, where $f(\eta_0) = c$.

It is known from the general theory, that the differential equation has two solutions, the first one is regular in η_0, the second has a logarithmic singularity and as the function $\varphi_1(\eta)$, calculated here, is a linear composition of these two solutions, it will also contain a logarithmic part.

Introducing a new variable

$$\zeta = \eta - \eta_0 \qquad (2)$$

and putting

$$g(\zeta) = \alpha^2\zeta + \frac{\zeta f''(\eta_0 + \zeta)}{f(\eta_0 + \zeta) - f(\eta_0)}$$

we write the differential equation as follows

$$\zeta \,.\, \varphi'' = g(\zeta)\varphi.$$

Assuming, that the zero of $f(\eta_0 + \zeta) - f(\eta_0)$ is simple in ζ, the function $g(\zeta)$ is regular in a neighbourhood of $\zeta = 0$ and

$$g(0) = \frac{f''(\eta_0)}{f'(\eta_0)}.$$

Hence, we assume a power series for $g(\zeta)$

$$g(\zeta) = a_0 + a_1\zeta + a_2\zeta^2 + \ldots\ldots .$$

The coefficients a_n, which are the successive derivatives of $g(\zeta)$, can be determined from a difference-scheme for the tabulated function.

We now assume, from the general theory a series for φ_1

$$\varphi(\zeta) = (\alpha_1\zeta + \alpha_2\zeta^2 + \ldots)\, ln\, \zeta + (\beta_0 + \beta_1\zeta + \ldots)$$

valid in a neighbourhood of $\zeta = 0$.

Substitution in the differential equation gives the following scheme for the computation of the unknown coefficients α_k and β_k:

$$1.2.\,\alpha_2 = a_0\alpha_1 \qquad\qquad \alpha_1 = a_0\beta_0$$

$$2.3.\,\alpha_3 = a_0\alpha_2 + a_1\alpha_1 \qquad\qquad 3\,\alpha_2 + 1.2.\beta_2 = a_0\beta_1 + a_1\beta_0$$

$$5\,\alpha_3 + 2.3.\beta_3 = a_0\beta_2 + a_1\beta_1 + a_2\beta_0$$

— — — — — — — — — — — — — — — — —

$$n(n-1)\alpha_n = \sum_{k=1}^{n-1} a_{k-1}\alpha_{n-k} \qquad\qquad (2\,n - 1)\alpha_n + n(n-1)\beta_n = \sum_{k=1}^{n} a_{k-1}\beta_{n-k}.$$

From this scheme the coefficients α_n and β_n can be expressed into α_1 and β_1. Putting

$$\alpha_n = c_n \cdot \alpha_1$$
$$\beta_n = c_n\beta_1 + d_n\alpha_1$$

we find for c_n and d_n the set of formulae

$$\begin{cases} n(n-1)c_n = \sum_{k=1}^{n-1} a_{k-1} c_{n-k} \\ n(n-1)d_n = \sum_{k=1}^{n} a_{k-1} d_{n-k} - (2n-1)c_n . \end{cases} \qquad c_0 = 0,\ c_1 = 1,\ d_0 = \frac{1}{a_0},\ d_1 = 0$$

Substitution gives:

$$\varphi = \left[\sum_{n=0}^{\infty} d_n \zeta^n + \left(\sum_{n=0}^{\infty} c_n \zeta^n \right) \log \zeta \right] \alpha_1 + \left(\sum_{n=0}^{\infty} c_n \zeta^n \right) \beta_1 .$$

The values of α_1 and β_1 are determined by fitting the solution for small positive values of $\zeta = \eta - \eta_0$ to the values, obtained by numerical integration for φ and φ'. Here a check on the accuracy of the numerical integration can be given by comparing the results in two neighbouring points η and $\eta + \Delta\eta$.

If the coefficients in the series expansion are known, the functions $\varphi(\eta)$ and $\varphi'(\eta)$ at the other side of the pole can be determined. Here $\eta = \eta - \eta_0$ is negative and the logarithm becomes complex. The ambiguity in sign of the imaginary part is removed in the general theory by a consideration of the viscosity correction (ref. 2, p. 292). The logarithm must be chosen as

$$\ln \zeta = \ln |\zeta| - \pi i.$$

Now, the numerical integration must be pursued; as starting values different values of η are chosen and again a check on the accuracy is obtained by comparison of the values of φ and φ', computed from the series expansion and the numerical integration. The numerical integration is pursued up to $\eta = 0$ or $\zeta = -\eta_0$, where the quotient $\frac{\varphi'}{\varphi}$ is calculated [1]).

5 The determination of the neutral oscillations.

The values of $\frac{\varphi_1'(0)}{\varphi_1(0)}$ were calculated for each velocity profile, characterized by a value of b, for several values of c and α.

The determination of the pair of values (c, α), corresponding to neutral oscillations, was made from

$$\frac{\varphi_1'(0)}{\varphi_1(0)} = \frac{\varphi_3'(0)}{\varphi_3(0)} .$$

The function φ_3 is given as a function of $z = (\alpha R w_0')^{1/3} (\eta - \eta_0)$ (ref. 5).

Usually, tables and graphs are given of the function

$$\frac{D(z)}{z} = - \frac{\varphi_3(z)}{z d\varphi_3/dz} .$$

We plot a diagram with the real and imaginary part of this function as coordinate axes with $z_0 = -\eta_0(\alpha R w_0')^{1/3}$ as a parameter. Now we must solve the equation

$$\frac{\varphi_1(0)}{\eta_0 \varphi_1'(0)} = \frac{D(z_0)}{z_0} .$$

For different values of α the curves $\frac{\varphi_1(0)}{\eta_0 \varphi_1'(0)}$ are plotted on the same diagram with η_0 (or c) as parameter. The intersection of the two curves gives a set of values α, c and z. From the latter the Reynolds' number can be found

$$R = \left(\frac{z}{-\eta_0} \right)^3 \cdot \frac{1}{\alpha \left(\frac{dw}{d\eta} \right)_0} .$$

6 Discussion of results.

The diagrams were computed for several values of the velocity profile parameter b

$$b = 0{,}8;\ 0{,}4;\ 0;\ -0{,}4.$$

The corresponding velocity profiles are given in fig. 1.

The indifference curves are given in fig. 2 for these profiles in the form of a plot of disturbance wave length $\bar{\alpha}\delta^*$ against Reynolds' number $Re_\delta^* = \frac{W\delta^*}{\nu}$. The corresponding frequencies

$$\frac{\beta_r \nu}{W^2} = \frac{\bar{\alpha}\, \bar{c} \nu}{W^2} = \bar{\alpha}\, \delta^* \frac{\bar{c}}{Re_\delta^*} \tag{1}$$

and velocities of propagation $c = \frac{\bar{c}}{W}$ are given in fig. 3 and 4 (dotted lines are obtained by extrapolation from computed values).

The regions enclosed by the indifference curves increase in the region of adverse pressure gradient, in particular in the neigbourhood of the point of separation.

For $b = 0$ (corresponding to the Blasius profile) the results are compared with those of Schlichting and Lin (figs. 5 and 6).

The values computed here correspond mostly to those of Lin. The agreement with the measurements of Schubauer and Skramstad is even somewhat better.

[1]) A second method of integration using the principle of analytical continuation is given in Appendix A.

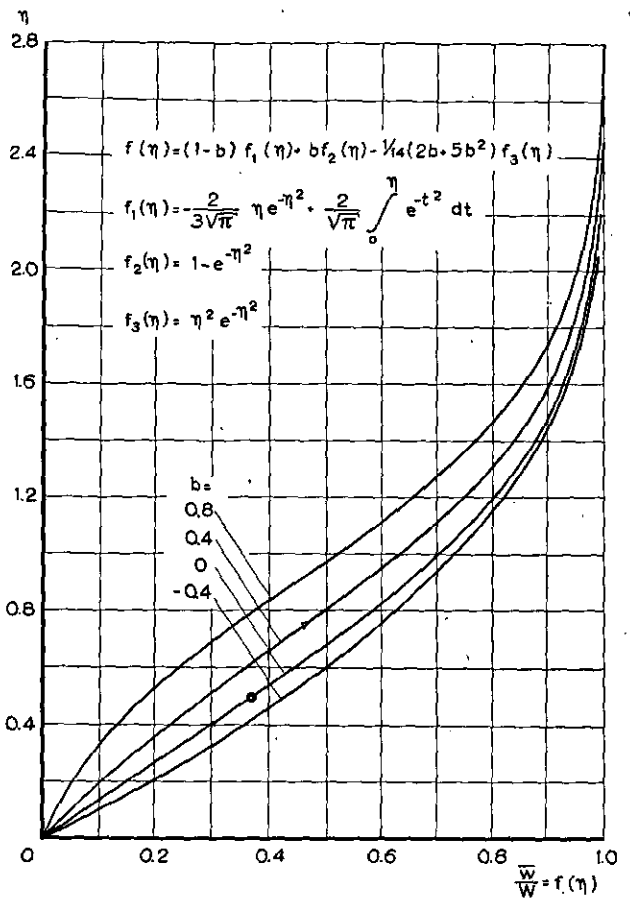

Fig. 1 The laminar boundary layer profiles for which the indifference-curves are calculated.

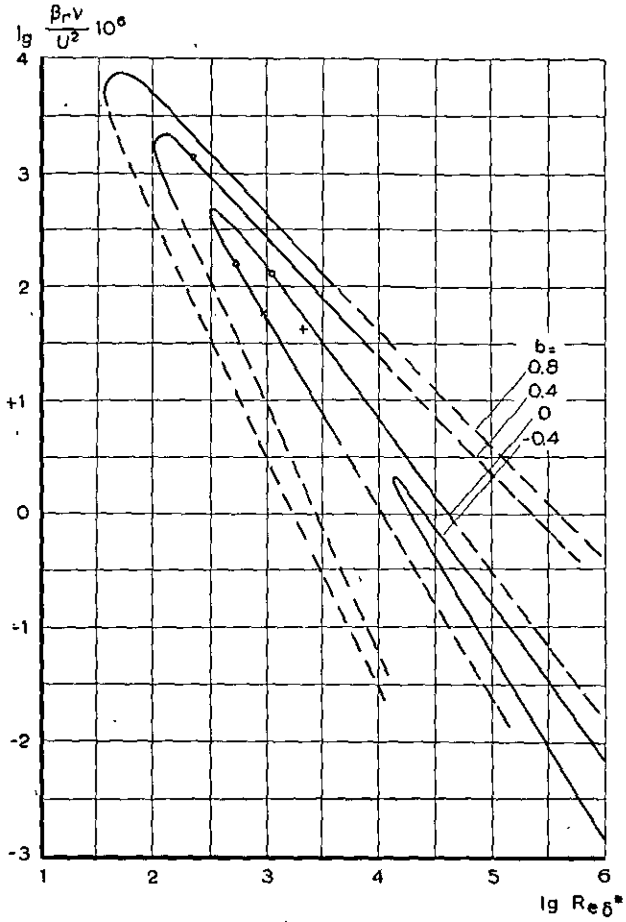

Fig. 3. *Indifference curves for the disturbing frequency β_r of the laminar boundary layer profiles with increasing and decreasing pressure gradient, as a function of* REYNOLDS' *number.*

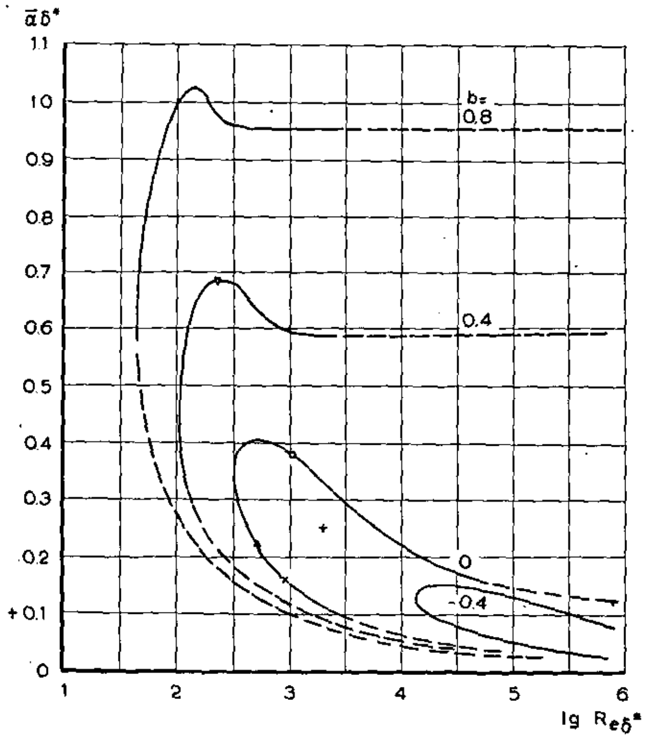

Fig. 2 *Indifference curves for the disturbing wave length $\bar{\alpha}\delta^*$ of the laminar boundary layer profiles with increasing and decreasing pressure gradient, as a function of* REYNOLDS' *number.*

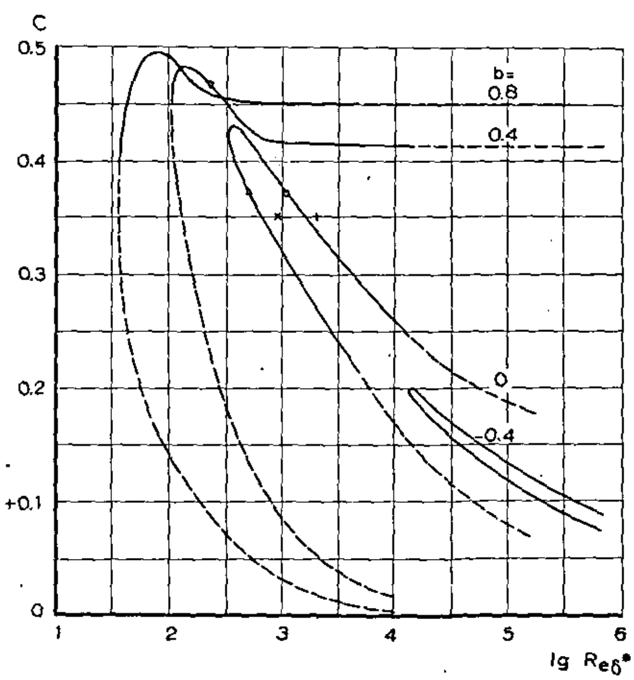

Fig. 4. *The indifference curves of the velocity of wave-propagation for laminar boundary layer profiles with increasing and decreasing pressure gradient, as a function of the* REYNOLDS' *number.*

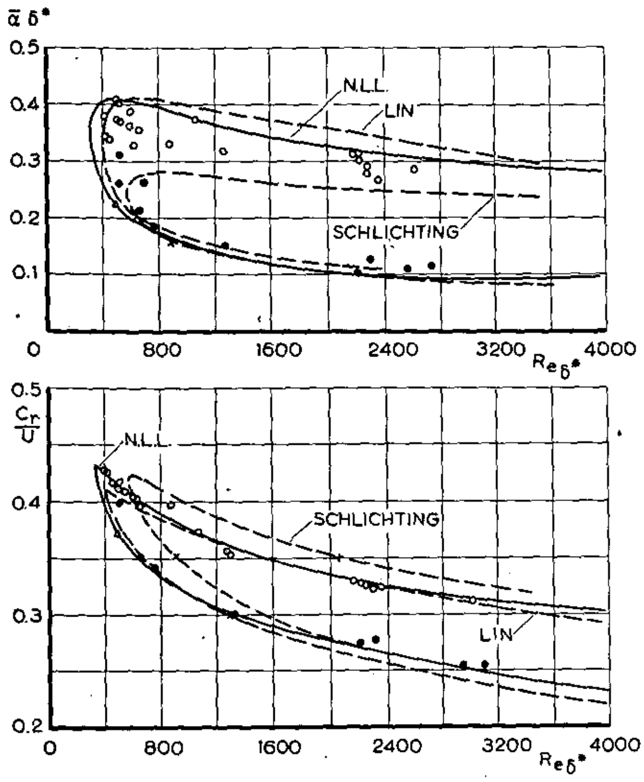

Fig. 5 A comparison between the various calculated indifference curves for the wave length and the velocity of wave propagation of the neutral disturbances in the case of the BLASIUS' profile. The heavy lines are theoretically computed. The experimental values are indicated by dots and open circles.

The critical values are:

$Re_{\delta^*_{krit}} = 321$ NLL, 420 LIN, 575 SCHLICHTING.

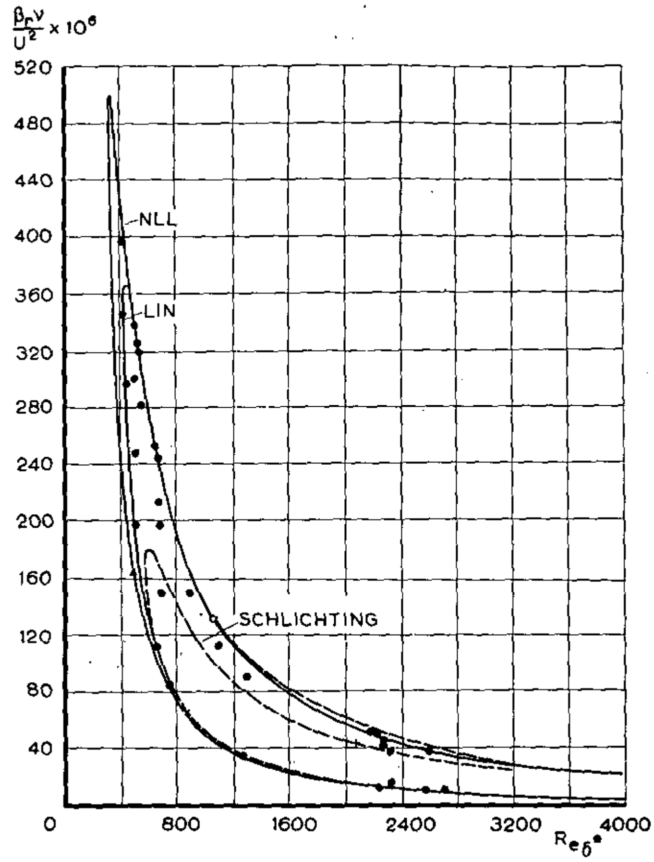

Fig. 6 A comparison between the various numerically calculated frequencies of the neutral disturbances in the case of the BLASIUS profile, and the values measured by SCHUBAUER and SKRAMSTAD. These latter values are indicated by means of dots.

For the lower limit of the critical REYNOLDS' number SCHLICHTING calculates $Re_{\delta^*} = 575$, LIN obtains 420 and from the curve here the value 321 is derived.

The velocity profile of the disturbance is calculated for the value $b = 0$, corresponding to main flow along a flat plate (BLASIUS-profile) for two points, (indicated by $\triangle$ and $\odot$) and for one point of the profile, corresponding to $b = 0{,}4$ (indicated by ∇ in fig. 1). The values

$$\varphi(\eta) = \varphi_1(\eta) + A_3\varphi_3(\eta) \tag{2}$$

and

$$\frac{d\varphi}{d\eta} = \frac{d\varphi_r}{d\eta} + i\,\frac{d\varphi_i}{d\eta}$$

are plotted as functions of η in fig. 7. This yields the amplitudes $k\,|\varphi|$ and $k\,\left|\frac{d\varphi}{d\eta}\right|$ from the disturbances inside the boundary layer.

Theoretical values of $u = \frac{\partial\psi}{\partial\eta}$ are plotted as functions of y/δ^* in fig. 8 and compared with experimental values from ref. 6, p. 21. Although the conditions in the measured values ($+$ and $\times$ in fig. 2) do not correspond exactly to the conditions in the calculated points (∇, $\odot$ in fig. 2) the results show a reasonable agreement.

In the region of retarded flow the shape of the amplitude distribution is preserved.

Finally, in fig. 9 the critical REYNOLDS' number for velocity profiles with pressure gradient is plotted as a function of the form-parameter.

$$\lambda = \frac{\delta^2}{\nu}\,,\ \frac{dU}{dx} = -\left(\frac{d^2f}{d\eta^2}\right)_{y=0} = \frac{5}{7}\,b^2 - \frac{12}{7}\,b.$$

This gives a means for obtaining directly the critical REYNOLDS' number from simple boundary layer calculations.

7 References.

1 TIMMAN, R. A one parameter method for the calculation of laminar boundary layers. NLL Report F. 35 (1949).

2 SCHLICHTING, H. Grenzschichttheorie, Verlag G. Braun. Karlsruhe (1950) p. 273—303 with references.

3 LIN, C. C. On the stability of two-dimensional parallel flows. Quarterly Appl. Math. Vol. 3 (July 1945, p. 117—142), Vol. 3 (Oct. 1945, p. 218—234), Vol. 3 (Jan. 1946, p. 277—301).

4 DRYDEN, H. L. Recent advances in the mechanics of boundary layer flow. Adv. in Appl. Mech. Vol. 1 (1948) p. 8—23 with references.

5 HOLSTEIN, H. Ueber die äussere und innere Reibungsschicht bei Störungen laminarer Strömungen. Z.A.M.M. Bd 30 no. 1/2, Jan./Febr. 1950, p. 25—49.

6 SCHUBAUER, G. B. and SKRAMSTAD, H. K. Laminar boundary layer oscillations and transition on a flat plate. NACA Report no. 909 (1948).

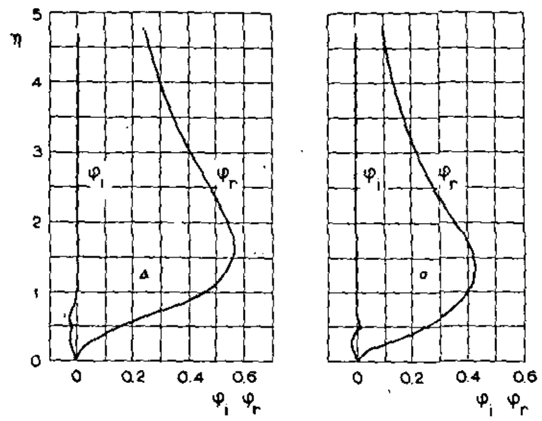

	b	η_0	Re_{δ^*}	c_r/u	$\bar{\alpha}\,\delta^*$	$\frac{\beta_r \nu}{u^2}10^6$
△	0	0.50	507	0.372	0.224	164
⊙	0	0.50	1070	0.372	0.371	131
▽	0.4	0.75	226.5	0.466	0.685	1409

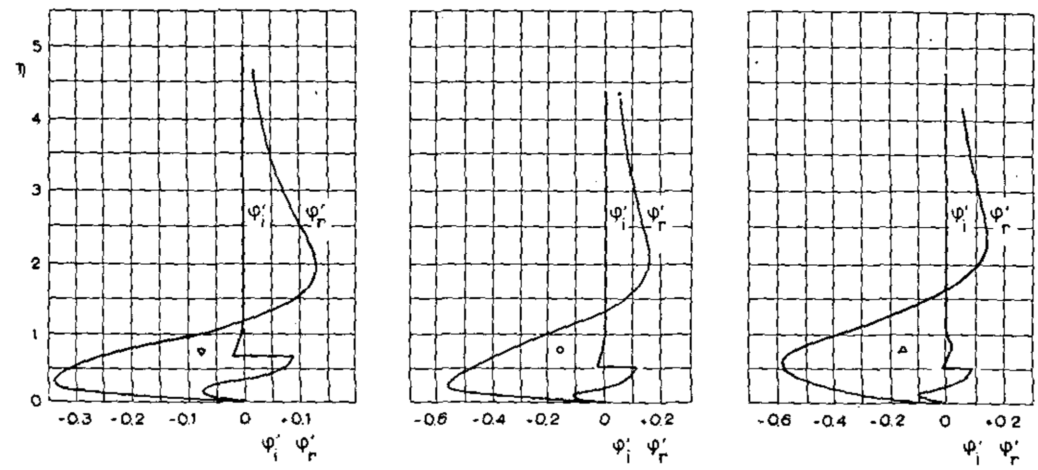

Fig. 7. The functions $\varphi_i(\eta), \varphi_r(\eta), \varphi_i'(\eta)$ and $\varphi_r'(\eta)$ for the points of the profiles △, ⊙ and ▽ in the figures 1 through 4.

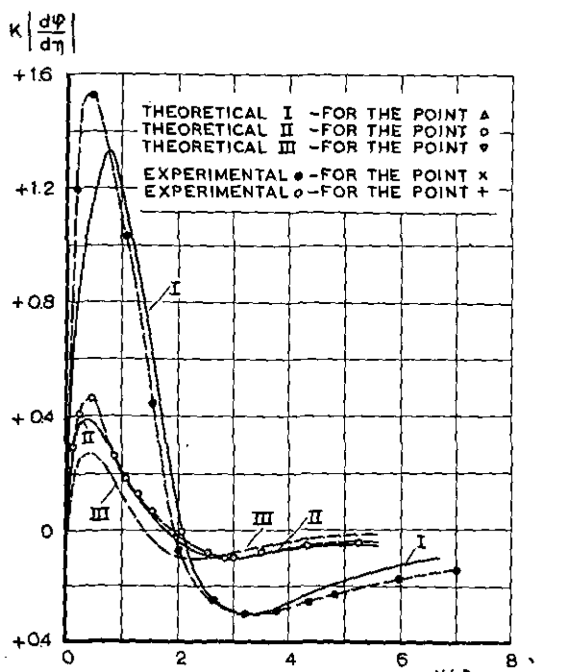

Fig. 8. Distribution of the amplitudes of disturbances in the boundary layer for the points △, ⊙, ▽, × and + in the fig. 2.

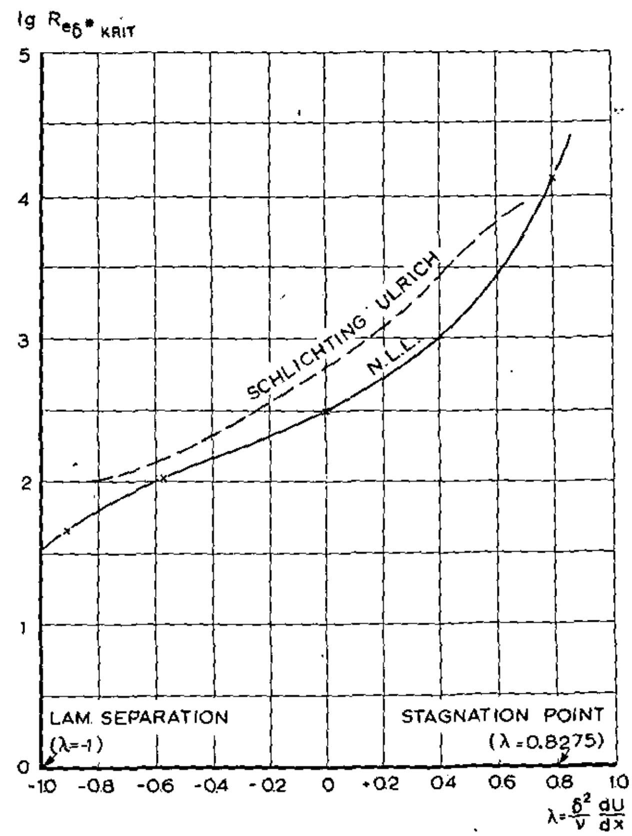

Fig. 9. The critical REYNOLDS' number of the boundary layer profiles with a pressure-gradient as a function of the shape parameter

APPENDIX A.

A method of integration using analytical continuation.

The function $f(\eta)$ which is used for the description of the velocity profile, is regular along the entire real axis. The function which is continued into the complex plane is given by $f(\zeta)$, where $\zeta = \eta + i\nu$.

Putting $\varphi = \chi + i\psi$ the differential equation for the inviscid solutions changes into:

$$\frac{\partial^2\varphi}{\partial\eta^2} - [\alpha^2 + G(\zeta)]\,\varphi(\zeta) = 0 \quad (\nu = \text{const.}) \tag{1}$$

$$\frac{\partial^2\varphi}{\partial\nu^2} + [\alpha^2 + G(\zeta)]\,\varphi(\zeta) = 0 \quad (\eta = \text{const.}) \tag{2}$$

The path of integration in the complex plane is indicated below.

It starts at infinity, passes along the real axis, then turns around the pole along the sides of a rectangle and subsequently terminates at the origin.

The initial conditions in the case of a change of direction, which are to be used for the numerical computation, follow from the relations of CAUCHY-RIEMANN:

$$\chi_\eta = \psi_\nu \qquad \psi_\eta = -\chi_\nu$$
$$\chi_{\eta\eta} = -\chi_{\nu\nu} \qquad \psi_{\eta\eta} = -\psi_{\nu\nu}$$
$$\chi_{\eta\eta\eta} = -\psi_{\nu\nu\nu} \qquad \psi_{\eta\eta\eta} = \chi_{\nu\nu\nu}, \text{ etc.}$$

The advantage of this method is that the function $G(\zeta)$ is regular along the entire path of integration. Difficult developments into series such as in sect. 4, are avoided in this way. If the path of integration is kept at a sufficient distance from the pole, the steps of integration generally need not to be diminished compared with that occurring along the real part of the integration path.

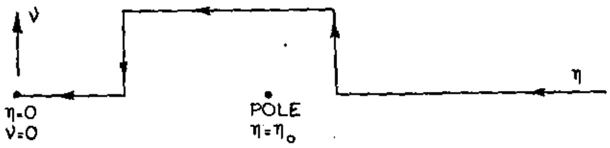

Fig. 10. The path of integration in the complex plane.

C. C. L. Class. D 050 : D 340

BERICHT F. 202

Nachprüfung der einfachen Rechenmethode für dreidimensionale laminare Grenzschichten mit Hilfe von exakten Lösungen

von

J. A. ZAAT.

Übersicht: Besondere dreidimensionale Grenzschichtströmungen sind exakt und mit Hilfe einer einfachen Näherungsmethode gelöst. Die Ergebnisse sind ausführlich mit einander verglichen. Eine gute Übereinstimmung ist erreicht worden, falls die Näherungslösungen auf eine sehr einfache — in dieser Arbeit beschriebene — Weise korrigiert werden.

Gliederung

Diese Arbeit wurde ausgeführt im Auftrag des Niederländischen Institutes für Flugzeugentwicklung (N. I. V.).

Bezeichnungen.

x, y, z	orthogonale (kartesische) Koordinaten.
u, v, w	Geschwindigkeitskomponenten in der Grenzschicht im x, y, z-System.
U, V, W	Geschwindigkeitskomponenten der freien Aussenströmung im x, y, z-System.
η	$z\sqrt{\dfrac{(m+1)U}{2\nu x}}$.
$F(\eta)$, $G(\eta)$	siehe Gl. (2.7).
$\beta\pi$	$\dfrac{2m}{m+1}\pi$ Öffnungswinkel.
u_t, u_n	Geschwindigkeitskomponenten in der Grenzschicht in Stromlinienrichtung und Querrichtung.
T	Quadrat der freien Stromgeschwindigkeit.
ϑ	$\operatorname{arc\,tg} \dfrac{V}{U}$.
$H(\eta)$	$\dfrac{dF}{d\eta} - \dfrac{dG}{d\eta}$.
λ	$\dfrac{B}{A}$ Parameter.
$f_{2n+1}(\eta), F_i, F_{ij}, F_{ijk}$	siehe Gl. (2.18).
σ	Parameter für die Profile in der Hauptströmungsrichtung.
Ω, K	Parameter für die Profile in der Querströmungsrichtung.
a_i, $a_i^* = \dfrac{a_i}{U_0}$	Koeffizienten.
$P_i(\eta)$	siehe Gl. (2.27).
u_1	$\dfrac{u_t}{\sqrt{T}}$.
u_2	$\dfrac{u_n}{\sqrt{T}}$.
$\bar{\zeta}$	$\dfrac{z}{\sqrt{\sigma\nu}}$.
f, g, h	siehe Gl. (3.6).
Λ, N, M, K	siehe die Gleichungen (3.3), (3.4) und (3.9).
ρ	$\dfrac{\partial}{\partial\varphi}\, ln\, \rho(1+z_x^2+z_y^2) = -\dfrac{2}{T}\left(\dfrac{\delta U}{\delta x} + \dfrac{\delta V}{\delta y}\right)$.
$\dfrac{\delta}{\delta x} = \dfrac{\partial}{\partial x} + z_x\dfrac{\partial}{\partial z}$, $\dfrac{\delta}{\delta y} = \dfrac{\partial}{\partial y} + z_y\dfrac{\partial}{\partial z}$	Differentiationen wo x oder y konstant bleiben, und z als Funktion von x und y genommen wird.
g	$g = 1 + z_x^2 + z_y^2$.
Δ_1	Verdrängungsdicke.
θ_{11}, θ_{21}	Impulsverlustdicke.
p, q, r / P, Q, R	siehe Gl. (3.11) und Tabelle 1.
Σ	$\left(\dfrac{A}{B}\operatorname{tg}\vartheta\right)^{\frac{l-m}{m}} A\sigma$.

1 Einleitung.

Eine einfache Methode zur Berechnung dreidimensionaler, laminarer, inkompressibler Grenzschichten wird in der Arbeit [1] beschrieben. Inwiefern diese einfache Berechnungsmethode noch einer Korrektur nötig hat wird in der vorliegenden Arbeit, an Hand exakter Lösungen der Differentialgleichungen für dreidimensionale Grenzschichten, nachgeprüft. Dazu werden, mit Hilfe von exakten Lösungen, die Geschwindigkeitsprofile der Grenzschichten in der Richtung der Stromlinien der freien Aussenströmung und in der senkrechten Querrichtung zusammengesetzt. Die Daten für diese Grenzschichtprofile sind zum Teil den Arbeiten von Howarth [2], Görtler [3] und Hansen [4] entnommen und zum Teil berechnet.

Es handelt sich um die exakten Lösungen der dreidimensionalen Reibungsschichten bei schräger Anströmung an Keilen, rechten und scharfen Ecken, die Strömung in der Umgebung des Staupunktes und die Strömung an dem schiebenden Zylinder.

Die Strömung an dem schiebenden Zylinder liefert wegen Konvergenzschwierigkeiten keine genaue Aussage mehr über die Sekundär-Strömungen bei dem Übergang von der beschleunigten zu der verzögerten Strömung. Neben dieser Strömung betrachten wir deshalb auch noch die exakte Lösung einer Grenzschicht ohne wirbelfreie Aussenströmung. Wir wählen dazu die Strömung über einer ebenen Fläche mit einer scharfen Vorderkante, wobei die parallelen Stromlinien der freien Aussenströmung durch ein Polynom dargestellt werden können.

Aus den Ergebnissen der exakten Lösungen und Näherungslösungen geht hervor, dass die einfache Berechnungsmethode für dreidimensionale laminare Grenzschichten in zweierlei Weisen verbessert werden kann. Erstens durch Veränderung des gewählten Geschwindigkeitsprofils der Querströmung in dem Übergangsgebiet von der beschleunigten zu der verzögerten Strömung mittels eines Korrekturgliedes. Dadurch erhält man in diesem Gebiet eine bessere Übereinstimmung mit der Gestalt der exakten Querstrom-Geschwindigkeitsprofile, und beugt man möglichen Schwierigkeiten vor, bei der Berechnung des Profilparameters der Querströmung.

Zweitens wird der Anfangswert des Hauptprofilparameters mit dem Anfangswert, folgend aus den vollständigen Impulsgleichungen, in Übereinstimmung gebracht; und der Verlauf dieses Parameters, der aus der einfachen Methode entsteht, bis zur Druckgradienten Null mehr oder wenig abgeändert.

Durch diese Ergänzung stimmen die Ergebnisse der einfachen Berechnungsmethode mit den exakten Lösungen der Differentialgleichungen für die dreidimensionalen Grenzschichten gut überein.

2 Exakte Grenzschichtlösungen.

Unter exakten Grenzschichtlösungen werden die Lösungen verstanden, wobei keine weiteren — als die bei der Grenzschichttheorie vorhandenen — Beschränkungen gemacht sind. In diesem Sinne sind die Lösungen der Impulsgleichungen nicht exakt.

Exakte Grenzschichtlösungen sind im Falle dreidimensionaler Grenzschichten nur sehr wenig vorhanden. Sie werden hier gebraucht, um die Ergebnisse einer einfachen Näherungsmethode zur Berechnung dreidimensionaler, laminarer Grenzschichten nachzuprüfen und möglicherweise noch zu verbesseren. Folglich werden vorerst einige exakten Lösungen näher betrachtet.

2.1 *Die schrägen Keil- und Eckströmungen.*

Bei schräger Anströmung eines zweidimensionalen Keiles mit einem Öffnungswinkel $\beta\pi$ werden, in der Umgebung der Vorderkante, die Geschwindigkeitskomponenten der freien Strömung senkrecht und parallel zur Vorderkante gegeben durch (vgl. Mangler [5])

$$U = Ax^{\frac{\beta}{2-\beta}} = AX^m, \quad V = B. \tag{2.1}$$

Die Grenzschichtgleichungen sind in diesem Falle, wobei alle Gröszen unabhängig von der Koordinate y sind,

$$u\frac{\partial u}{\partial x} + w\frac{\partial u}{\partial z} = U\frac{dU}{dx} + \nu\frac{\partial^2 u}{\partial z^2} \tag{2.2}$$

$$u\frac{\partial v}{\partial x} + w\frac{\partial v}{\partial z} = \nu\frac{\partial^2 v}{\partial z^2} \tag{2.3}$$

$$\frac{\partial u}{\partial x} + \frac{\partial w}{\partial z} = 0 \tag{2.4}$$

mit den Randbedingungen

$$u = v = w = 0 \qquad \text{für } z = 0 \tag{2.5}$$

$$u \to U, \; v \to V, \qquad \text{für } z \to \infty .$$

x, y, z sind die in Abb. 1 gezeichneten rechtwinklichen kartesischen Koordinaten.

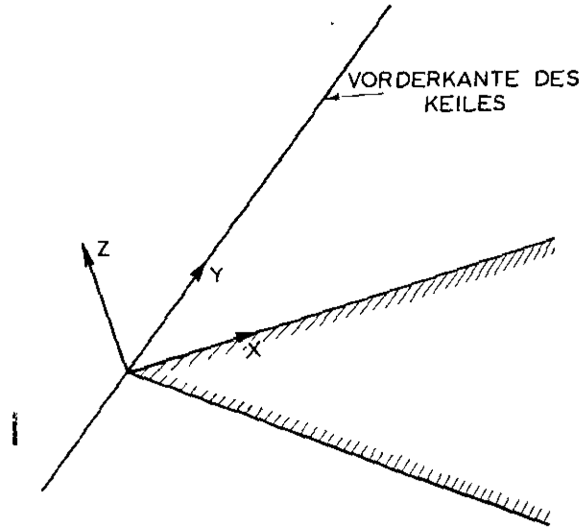

Abb. 1. Strömung um einen Keil.

u, v, w sind die Geschwindigkeitskomponenten in der Grenzschicht in den x, y, z Richtungen.

Nach Einführung von

$$\eta = z\sqrt{\frac{(m+1)U}{2\nu x}} \tag{2.6}$$

$$u = U \frac{dF(\eta)}{d\eta}$$

$$w = -\frac{U}{x}\sqrt{\frac{2\nu x}{(m+1)U}}\left(\frac{m+1}{2}F(\eta) + \right.$$
$$\left. + \frac{m-1}{2}\eta \frac{dF(\eta)}{d\eta}\right)$$

$$v = V \frac{dG(\eta)}{d\eta} \qquad (2.7)$$

gehen die Grenzschichtgleichungen (2.2) bis (2.4) über in

$$\frac{d^3F(\eta)}{d\eta^3} = -F(\eta)\frac{d^2F(\eta)}{d\eta^2} + \frac{2m}{m+1}\left[\left(\frac{dF}{d\eta}\right)^2 - 1\right] \qquad (2.8)$$

$$\frac{d^3G(\eta)}{d\eta^3} = -F(\eta)\frac{d^2G(\eta)}{d\eta^2} \qquad (2.9)$$

mit den Randbedingungen

$$F = \frac{dF}{d\eta} = \frac{dG}{d\eta} = 0 \quad \text{für } \eta = 0 \qquad (2.10)$$

$$\frac{dF}{d\eta} \to 1 \quad \frac{dG}{d\eta} \to 1 \quad \text{für } \eta \to \infty .$$

Die Gleichung (2.9) lässt sich lösen als

$$\frac{d^2G(\eta)}{d\eta^2} = \alpha_0 e^{-\int_0^\eta F(t)\,dt} .$$

Die Gleichung (2.8) ist die Differentialgleichung der ähnlichen Lösungen des ebenen Problems. Von praktischer Bedeutung ist hierbei die Potentialströmung gegen einen Keil vom Öffnungswinkel $0 < \beta\pi = \frac{2m}{m+1}\pi \leqq 2\pi$, auf welche die Geschwindigkeitsverteilung $U = Ax^m$ mit $m > 0$ führt. Vgl. Mangler [5]. Wir betrachten die folgenden Sonderfälle:

a. Die schräge Umströmung eines Keiles mit dem halben Keilwinkel $^1/_2\,\beta\pi = {^1/_4}\,\pi (m = {^1/_3})$. Die Aussenstromlinien sind dann parabelförmig

$$y = {^3/_2}\frac{B}{A}x^{2/3} + C.$$

b. Die schräge Strömung gegen eine senkrechtstehende Platte, d.h. gegen einen Keil vom rechten halben Kantenwinkel $^1/_2\,\beta\pi = {^1/_2}\,\pi (m = 1)$. Die Aussenstromlinien sind die logarithmischen Kurven

$$y = \frac{B}{A}\ln x + C.$$

c. Die schräge Eckströmung mit dem stumpfen halben Keilwinkel $^1/_2\,\beta\pi = {^4/_5}\,\pi (m = 4)$. Die Aussenstromlinien sind hyperbelförmig

$$y = -{^1/_3}\frac{B}{A}x^{-3} + C.$$

Die Lösungen der Gleichungen (2.8), für $\beta = \frac{2m}{m+1} = 0{,}5$; $1:1{,}6$, sind der Arbeit [6] entnommen. Für die Lösung der Gleichung (2.9) vergleich auch [7].

Bildet die Geschwindigkeitskomponente in der Richtung der freien Strömung einen Winkel ϑ mit der x-Achse und sind u_t, u_n die Geschwindigkeitskomponenten im Grenzschicht in der Richtung der Stromlinien der freien Strömung und senkrecht darauf, dann existieren die Beziehungen (siehe Abb. 2).

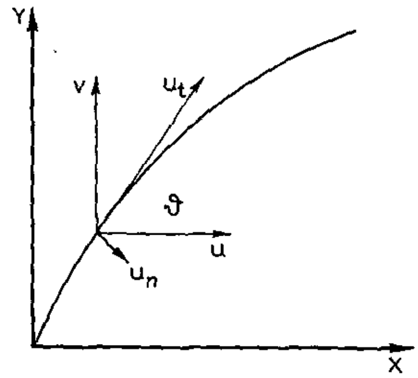

Abb. 2. Die Stromlinie und die Komponenten u, v, u_t und u_n.

$$u_t = u\cos\vartheta + v\sin\vartheta = \frac{uU + vV}{\sqrt{T}}$$

$$u_n = u\sin\vartheta - v\cos\vartheta = \frac{uV - vU}{\sqrt{T}}$$

mit

$$T = U^2 + V^2 \quad \text{und} \quad \operatorname{tg}\vartheta = \frac{V}{U}$$

oder

$$\frac{u_n}{\sqrt{T}} = \frac{uV}{T} - \frac{vU}{T} = \frac{UV}{T}\left(\frac{dF(\eta)}{d\eta} + \right.$$
$$\left. - \frac{dG(\eta)}{d\eta}\right) = {^1/_2}\sin 2\vartheta\, H(\eta) \qquad (2.11)$$

$$\frac{u_t}{\sqrt{T}} = \frac{U^2}{T}\frac{dF(\eta)}{d\eta} + \frac{V^2}{T}\frac{dG(\eta)}{d\eta} =$$
$$\frac{dF(\eta)}{d\eta} - \sin^2\vartheta\, H(\eta). \qquad (2.12)$$

Die exakten Lösungen sind für verschiedene Werte von ϑ in den Abbildungen 3a und 3b gezeichnet.

Je nachdem der Öffnungswinkel des Keiles zunimmt, nimmt auch die Querströmung zu. Trotzdem ergibt sich, dass die Sekundärströmung $\frac{u_n}{\sqrt{T}}$ für den Fall c der schrägen Eckströmung noch klein bleibt gegenüber der Hauptströmung.

2.2 *Die Strömung in der Umgebung des Staupunktes.*

Nach Howarth [2] kann die wirbelfreie Aussenströmung in der unmittelbaren Umgebung des Staupunktes eines willkürlichen Körpers von den linearen Funktionen

$$U = Ax \qquad V = By \qquad (2.13)$$

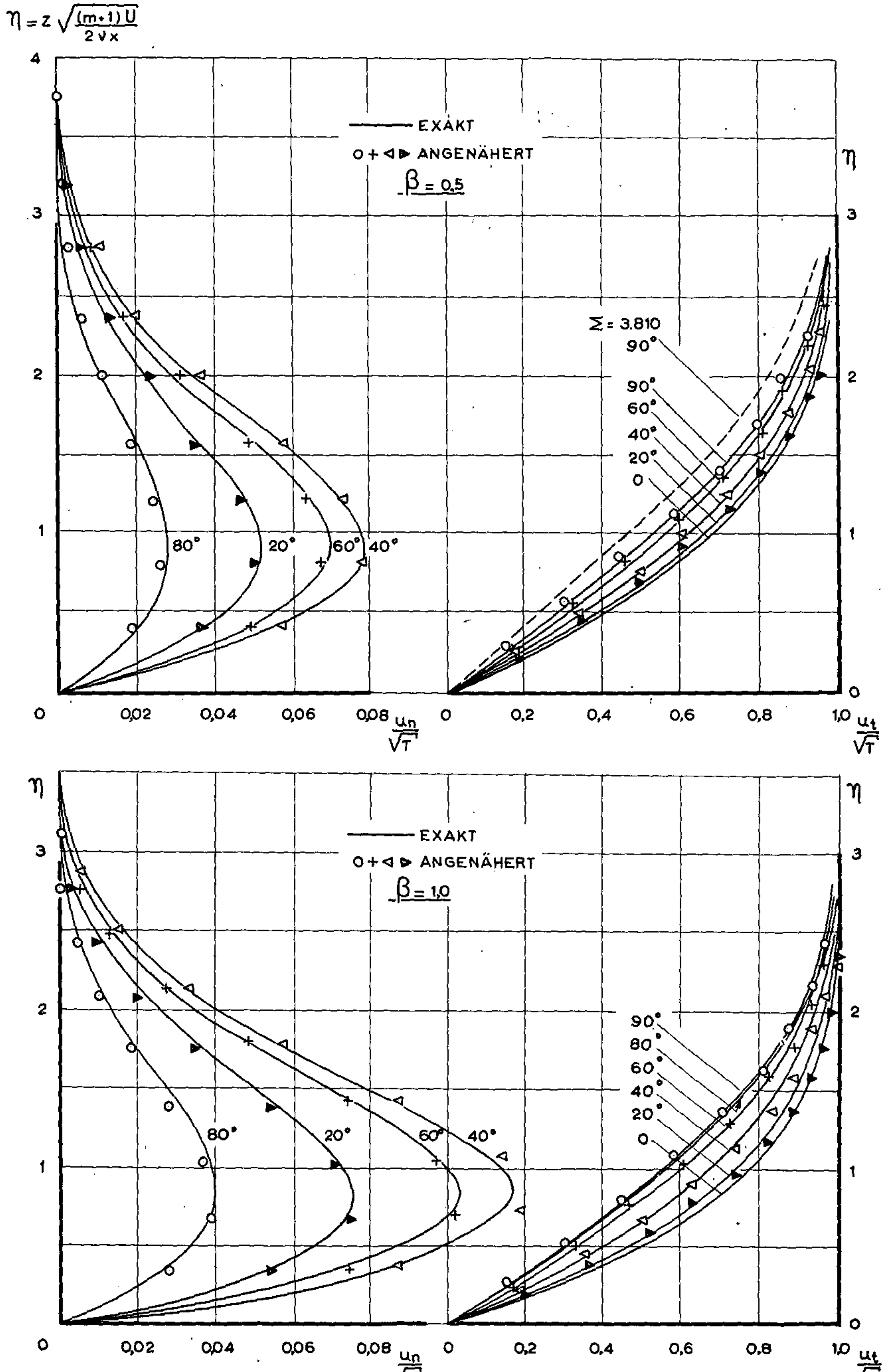

Abb. 3a. Keil- und Eckströmungen. Die Geschwindigkeitsprofile der Grenzschicht in der Richtung der Stromlinien der freien Strömung und in der senkrechten Querrichtung für verschiedene Werte von $\vartheta = \operatorname{arc\,tg} \frac{V}{U}$ und für $\beta = 0{,}5$; 1.

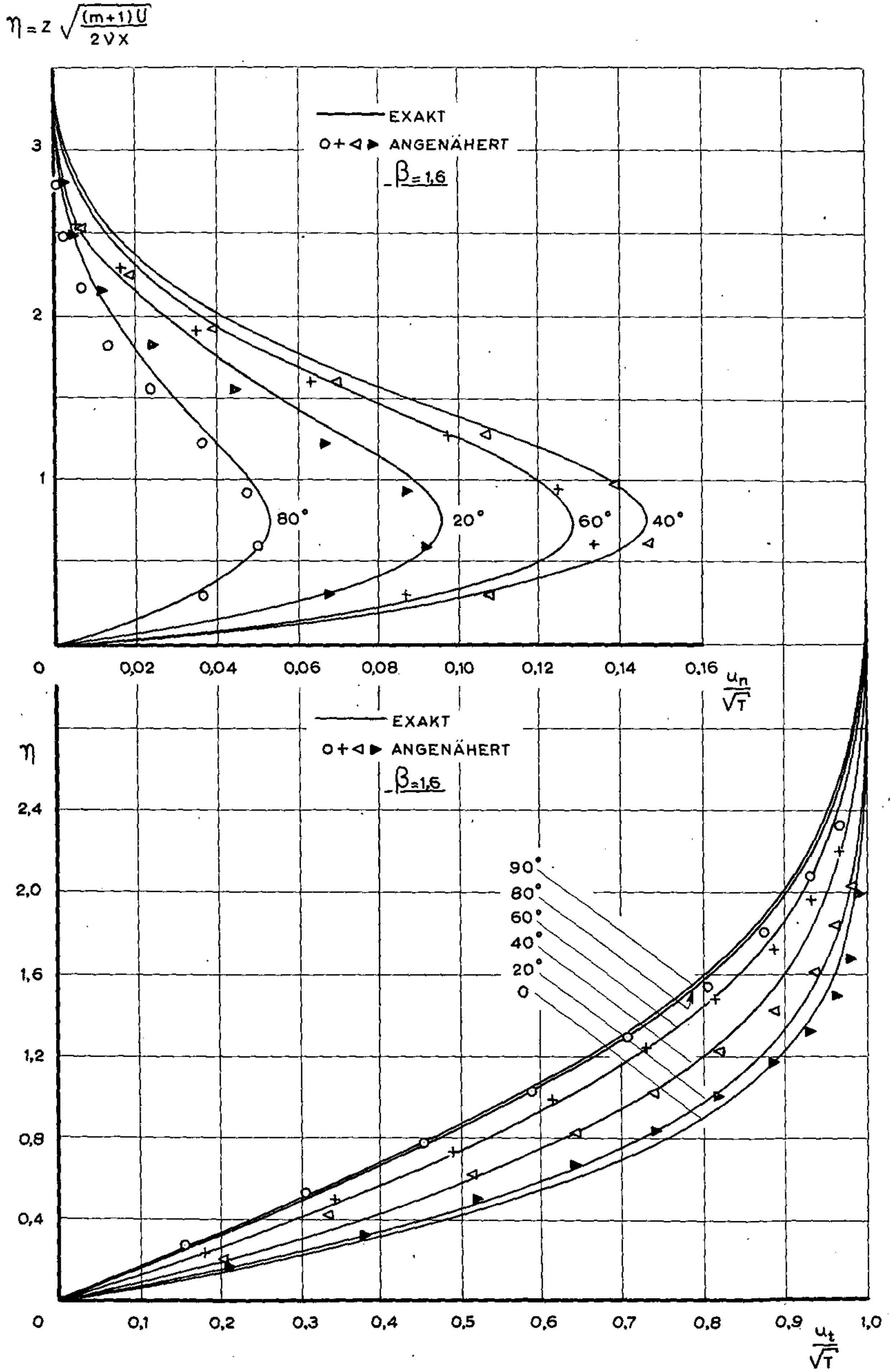

Abb. 3b. Keil- und Eckströmungen. Die Geschwindigkeitsprofile der Grenzschicht in der Richtung der Stromlinien der freien Strömung und in der senkrechten Querrichtung für verschiedene Werte von $\vartheta = \operatorname{arc\,tg} \frac{V}{U}$ und für $\beta = 1{,}6$.

dargestellt werden. Dabei wird vorausgesetzt, dass die Oberfläche in der Umgebung des Staupunktes ($x = y = z = 0$) regulär ist. Folglich können ohne Beschränkung der Allgemeinheit die metrischen Fundamentalgrössen h_i des Linienelementes

$$ds^2 = h_1{}^2 dx^2 + h_2{}^2 dy^2 + h_3{}^2 dz^2$$

in der unmittelbaren Umgebung von $x = y = 0$ durch die Werte „eins" ersetzt werden.

Damit gehen die Grenzschichtgleichungen für orthogonale krummlinige Koordinaten [Lit. 1] über in

$$\begin{aligned} u \frac{\partial u}{\partial x} + v \frac{\partial u}{\partial y} + w \frac{\partial u}{\partial z} &= U \frac{dU}{dx} + \nu \frac{\partial^2 u}{\partial z^2} \\ u \frac{\partial v}{\partial x} + v \frac{\partial v}{\partial y} + w \frac{\partial v}{\partial z} &= V \frac{dV}{dy} + \nu \frac{\partial^2 v}{\partial z^2} \\ \frac{\partial u}{\partial x} + \frac{\partial v}{\partial y} + \frac{\partial w}{\partial z} &= 0 \end{aligned} \tag{2.14}$$

mit den Randbedingungen

$$u = v = w = 0 \qquad \text{für } z = 0$$
$$u \to U \quad v \to V \qquad \text{für } z \to \infty .$$

Nach Einführung von

$$\begin{aligned} \eta &= z \sqrt{\frac{A}{\nu}} \\ u &= U \frac{dF(\eta)}{d\eta} \\ v &= V \frac{dG(\eta)}{d\eta} \\ w &= -\sqrt{A\nu}\,(F(\eta) + \lambda G(\eta)) \qquad \lambda = \frac{B}{A} \end{aligned} \tag{2.15}$$

gehen die Grenzschichtgleichungen über in

$$\begin{aligned} &\frac{d^3F(\eta)}{d\eta^3} + F(\eta) \frac{d^2F(\eta)}{d\eta^2} + \lambda\, G(\eta) \frac{d^2F(\eta)}{d\eta^2} + \\ &\qquad + 1 - \left(\frac{dF(\eta)}{d\eta}\right)^2 = 0 \\ &\frac{d^3G(\eta)}{d\eta^3} + F(\eta) \frac{d^2G(\eta)}{d\eta^2} + \lambda\, G(\eta) \frac{d^2G(\eta)}{d\eta^2} + \\ &\qquad + \lambda - \lambda \left(\frac{dG(\eta)}{d\eta}\right)^2 = 0 \end{aligned} \tag{2.16}$$

mit den Randbedingungen

$$F = G = \frac{dF}{d\eta} = \frac{dG}{d\eta} = 0 \qquad \text{für } \eta = 0$$
$$\frac{dF}{d\eta} \to 1 \quad \frac{dG}{d\eta} \to 1 \qquad \text{für } \eta \to \infty .$$

Die Lösungen dieser Gleichungen werden der Arbeit [2] entnommen.

Man braucht sich nur auf den Bereich $0 \leqq \lambda \leqq 1$ zu beschränken. Für die übrigen Parameterwerte λ können die zugehörigen Funktionen leicht mit den schon berechneten Funktionen ermittelt werden (vgl. Arbeit 2). $\lambda = 0$ stimmt mit der zweidimensionalen Strömung überein und $\lambda = 1$ mit einer Achsen-symmetrischen Strömung.

Die Stromlinien der Aussenströmung entsprechen der Gleichung $\frac{y}{y_0} = x^\lambda$. Für $\lambda > 1$ haben sie einen Berührungspunkt von der Ordnung λ mit der x-Achse, und für $0 < \lambda < 1$ einen Berührungspunkt von der Ordnung $1/\lambda$ mit der y-Achse (siehe Abb. 4). Mit Hilfe der Gleichungen (2.11) und

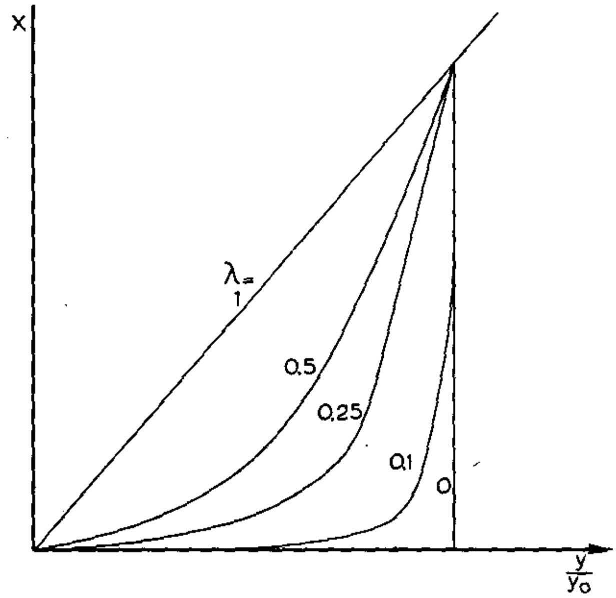

Abb. 4. Die Stromlinien einer Staupunktströmung.

(2.12) erhält man wieder die Geschwindigkeitsverteilungen innerhalb der Reibungsschicht in der Richtung der Stromlinien der freien Aussenströmung und senkrecht darauf. Diese Geschwindigkeitsverteilungen sind in der Abb. 5 für die Punkte $\operatorname{tg} \vartheta = \frac{V}{U} = \frac{\lambda y}{x} = 1$ und in der Abb. 6 für den Staupunkt $x = y = 0$ $\left(\vartheta = \frac{\pi}{2}\right)$ für verschiedene Parameterwerte λ, mit $0 < \lambda < 1$, aufgetragen. In der Abb. 6 sind statt der Nullverteilungen $\frac{u_n}{\sqrt{T}} = 0$ die Verteilungen $\frac{1}{\cos \vartheta} \frac{u_n}{\sqrt{T}} = \frac{u_n}{U}$ aufgetragen.

Es folgt aus Gl. (2.11) dass die grösste Grenzschichtquerströmung für $\vartheta = \frac{\pi}{4}$ auftritt. Aus der Abb. 5 geht folgendes hervor. Bei wirbelfreier Aussenströmung bleiben die Querstromprofile der laminaren Geschwindigkeitsgrenzschicht klein gegenüber den Hauptstromprofilen in der örtlichen Richtung der freien Aussenströmung. Diese Betrachtungen gelten also in der Umgebung des Staupunktes eines Körpers. Dabei können sehr grosse Krümmungen der Stromlinien auftreten. Folglich ist zu erwarten, dass auch bei Anströmung eines Körpers unter Anstellwinkel innerhalb der ganzen laminaren Grenzschicht, die Querstromprofile klein gegenüber den Hauptstromprofilen bleiben. Die fast immer grösseren Abweichungen der Stromlinien an der Wand mit den Aussenstromlinien, bei

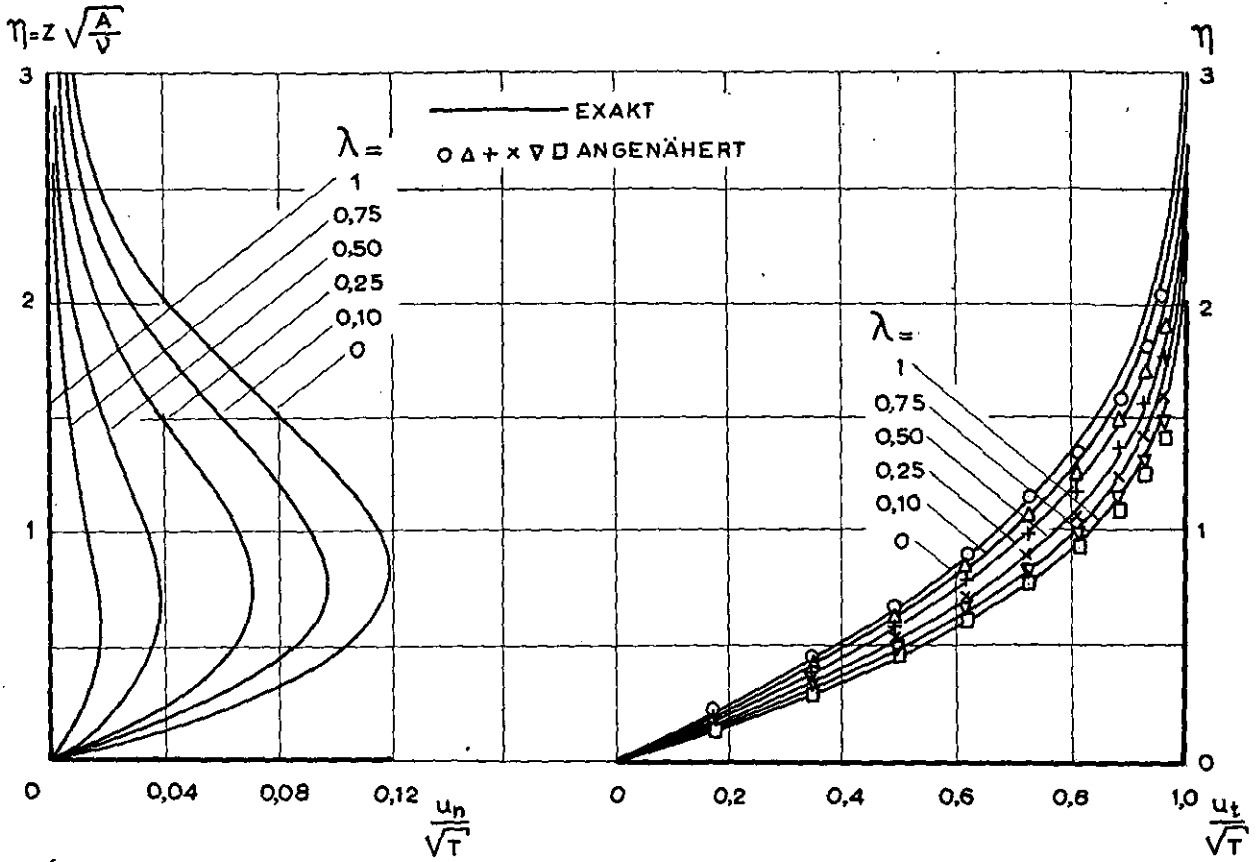

Abb. 5. *Staupunktströmung mit $U = Ax$, $V = By$. Die Grenzschichtprofile $\frac{u_t}{\sqrt{T}}$ und $\frac{u_n}{\sqrt{T}}$ sind für verschiedene Werte von $\lambda = \frac{B}{A}$ in den Punkten der Stromlinien, wo $U = V$, gezeichnet.*

zunehmenden Anstellwinkeln, finden ihre Ursache in den viel längeren Weg über den die Zentrifugalkraft auf die Sekundarströmung einwirkt. Klein bleiben der Querstromprofile gegenüber den Hauptstromprofilen bedeutet noch nicht, dass auch die Schubspannungskomponente in der Querrichtung klein gegenüber der Schubspannungskomponente der Hauptstromrichtung ist, welches bei der laminaren Ablösung ersichtlich ist.

2.3 *Die Strömung am schiebenden Zylinder.*

In der Arbeit [3] beschreibt GÖRTLER eine Methode zur Berechnung der laminaren Grenzschicht am schiebenden Zylinder. Er überträgt die allgemeine Methode der BLASIUS'schen Reihe des zweidimensionalen Problems auf den dreidimensionalen Fall des schiebenden Zylinders. Sind die Geschwindigkeitskomponenten in der Richtung des senkrechten Querschnittes, und in der Achsenrichtung des Zylinders

$$U = U(x), \quad \text{und} \quad V = \text{Konstant},$$

dann sind die Grenzschichtgleichungen und Randbedingungen in den Gleichungen (2.2) bis (2.5) gegeben.

Dabei ist x die Wandbogenlänge längs der Kontur des senkrechten Querschnittes. y ist der Abstand in der Richtung der Erzeugenden des Zylinders und z ist der Abstand in der Aussennormalrichtung.

Die BLASIUS'sche Reihe setzt die Entwickelbarkeit der äuszeren Geschwindigkeit $U(x)$ in eine Reihe nach Potenzen von x voraus. Bei symmetrischer Anströmung

$$U(x) = \sum_{n=0}^{\infty} u_{2n+1}\, x^{2n+1} \tag{2.17}$$

ergeben sich für die Geschwindigkeitskomponenten u, v, w in der Grenzschicht die folgenden Reihendarstellungen

$$u(x, \eta) = \sum_{n=0}^{\infty} (2\,n+2) u_{2n+1}\, x^{2n+1}\, f'_{2n+1}(\eta)$$

$$\sqrt{\frac{u_1}{\nu}}\; w(x, \eta) = -\sum_{n=0}^{\infty} (2\,n+2)(2\,n+1) u_{2n+1}\, x^{2n} f_{2n+1}(\eta) \tag{2.18}$$

$$\frac{v(x, \eta)}{V} = F_0(\eta) + \frac{u_3}{u_1}\, x^2 F_2(\eta) + \left[\frac{u_5}{u_1}\, F_4(\eta) + \frac{u_3^{\,2}}{u_1^{\,2}}\, F_{22}(\eta)\right] x^4 +$$

$$+ \left[\frac{u_7}{u_1}\, F_6(\eta) + \frac{u_3 u_5}{u_1^{\,2}}\, F_{24} + \frac{u_3^{\,3}}{u_1^{\,3}}\, F_{222}(\eta)\right] x^6 + \ldots\ldots$$

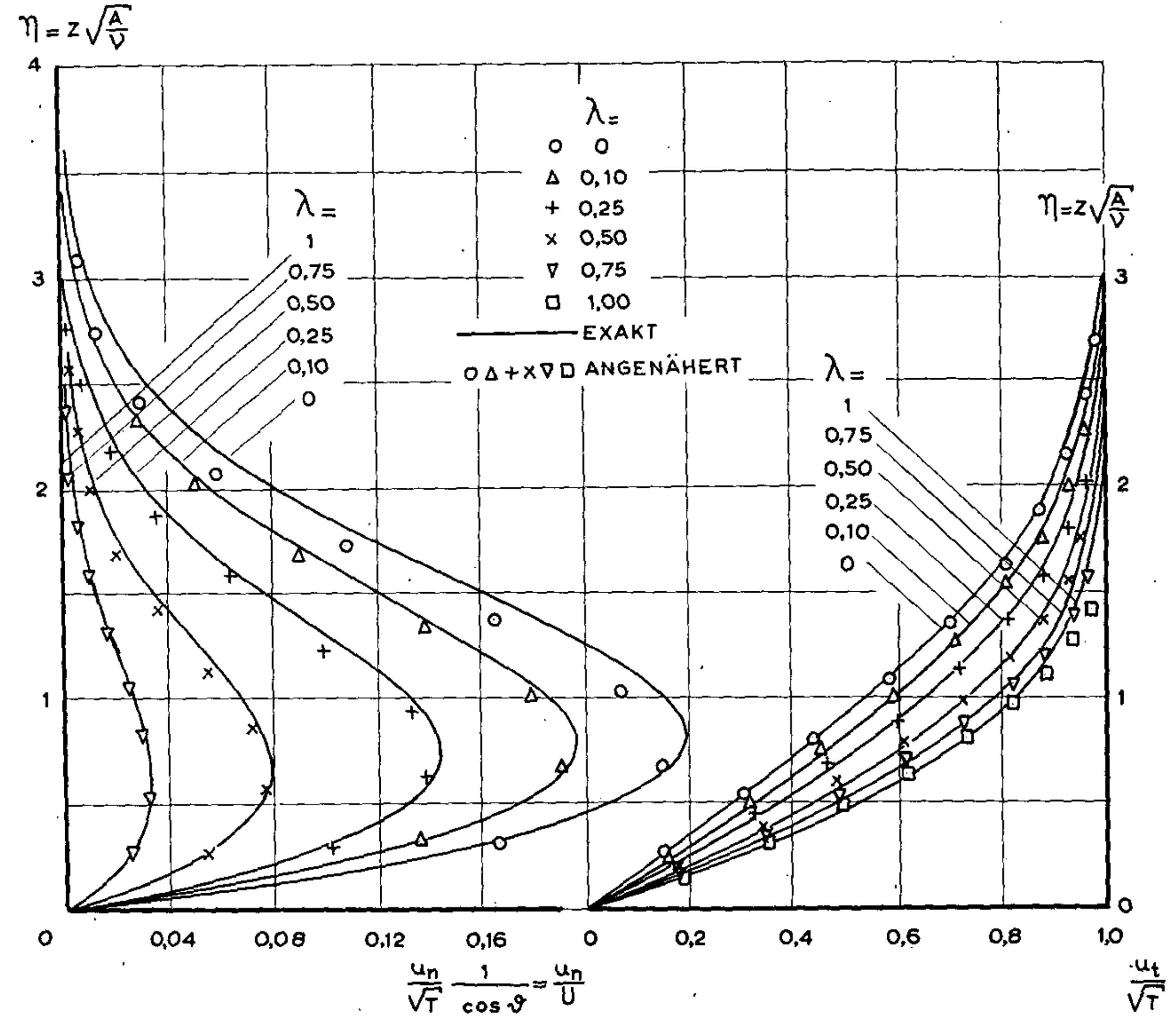

Abb. 6. Staupunktströmung mit $U = Ax$, $V = By$. Die Grenzschichtprofile $\frac{u_t}{\sqrt{T}}$ und $\frac{u_n}{U} = \frac{u_n}{\sqrt{T}} \frac{1}{\cos\vartheta}$ sind für verschiedene Werte von $\lambda = \frac{B}{A}$ in dem Staupunkt $U = V = 0$ gezeichnet.

mit

$$\eta = z\sqrt{\frac{u_1}{\nu}} \tag{2.19}$$

und den Randbedingungen

$$f_{2n+1} = f'_{2n+1} = F_0 = F_2 = \ldots = F_{222} = \ldots = 0 \text{ für } \eta = 0$$

$$f'_{2n+1} = \frac{1}{2n+2}, \; F_0 = 1, \; F_2 = \ldots = F_{222} = \ldots = 0 \text{ für } \eta \to \infty .$$

Der Strich bedeutet Differentiation nach η.

Die Zahlentafeln $f_{2n+1}(\eta)$ und $f'_{2n+1}(\eta)$ sind von Ulrich bis zum Gliede 9. Ordnung gegeben [8]. Dabei sind $2f_1(\eta)$ und $2f_1'(\eta)$ durch $f_1(\eta)$ und $f_1'(\eta)$ und $u_{2n+1}f_{2n+1}(\eta)$ durch die Funktionen von [8] innerhalb den Klammern zu ersetzen (z. B. $f_5 = g_5 + \frac{u_3^2}{u_1 u_5} h_5$). Die Zahlentafeln der Funktionen $F(\eta)$ sind in der Arbeit [3] gegeben. Leider erfolgt die Konvergenz der Rechenentwicklung nicht genügend schnell, sodass bei vorgeschriebenen Genauigkeit die Berechnungen der Grenzschichtprofile mit zunehmender Entfernung von der vorderen Staulinie $x = 0$ immer mehr Gliederen auffordern. Mit den, in Zahlentafeln vorhanden, Funktionen ist es nicht möglich um bis weiter als das Druckminimum die Grenzschichtprofile, bis auf einige Prozente, noch genau zu berechnen.

Die Geschwindigkeitsverteilungen innerhalb der Reibungsschicht in der örtlichen Richtung der freien Aussenströmung und senkrecht darauf erhält man mit Hilfe der Formeln (2.11) und (2.12) aus

$$\frac{u_n}{\sqrt{T}} = \frac{UV}{T}\left(\frac{u}{U} - \frac{v}{V}\right), \qquad \frac{u_t}{\sqrt{T}} = \frac{U^2}{T}\frac{u}{U} + \frac{V^2}{T}\frac{v}{V}.$$

In der Staulinie $x = 0$ gehen diese Geschwindigkeitsverteilungen über in (siehe Abb. 7)

$$\frac{u_t}{\sqrt{T}} = F_0(\eta) \qquad \frac{u_n}{U} = 2 f_1'(\eta) - F_0(\eta). \tag{2.20}$$

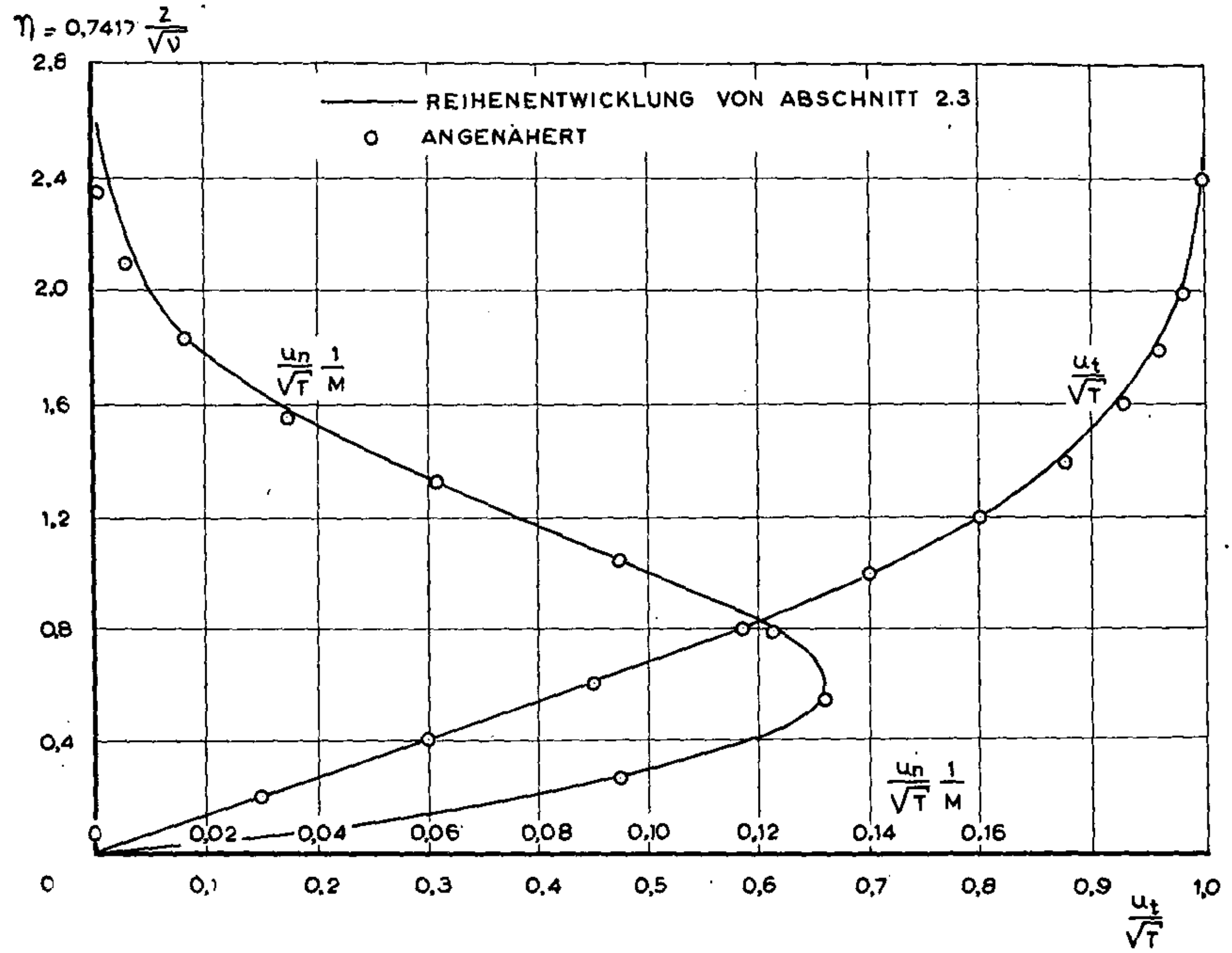

Abb. 7. Zylinderströmung mit $U = x - x^3$, $V = 1$.

Die Grenzschichtprofile $\frac{u_t}{\sqrt{T}}$ und $\frac{u_n}{\sqrt{T}}\frac{1}{M}$ für den Grenzfall $x = 0$.

Für die Zylinderströmung mit $U = x - x^3$, $V = 1$ sind für verschiedene Werte von x die Geschwindigkeitsprofile der Grenzschicht $\frac{u_n}{\sqrt{T}}$ und $\frac{u_t}{\sqrt{T}}$ mit Hilfe der abgebrochenen Reihenentwicklung berechnet und in der Abb. 8 gezeichnet. Das Druckminimum liegt in dem Punkt mit $x = \sqrt{1/3}$. Für diesen Punkt ist das Geschwindigkeitsprofil der Hauptströmung mit Abweichungen bis zu 3 % bekannt und ist die Profilform der Sekundärströmung, trotz ihrer Abweichungen, die dort schon sehr gross sind (bis etwa 50 %), noch hinreichend genau zu erkennen. Für Profile auf grösserer Entfernung können die Abweichungen sehr viel grösser sein. Folglich sind die Ergebnisse dort völlig unzuverlässig.

Die Berechnungsmethode von Görtler am schiebenden Zylinder liefert also wegen Konvergenzschwierigkeiten keine genaue Aussage mehr über die Form der Geschwindigkeitsprofile der Sekundärströmungen vorbei dem Übergang von der beschleunigten zu der verzögerten Strömung. Dazu wird der folgende Fall betrachtet.

2.4 *Eine Grenzschichtströmung ohne wirbelfreie Aussenströmung.*

Hansen und Herzig [4] betrachten die exakten Lösungen der inkompressiblen, laminaren, dreidimensionalen Grenzschichtströmung über eine ebene Platte mit scharfer Vorderseite, wobei die parallelen Stromlinien der nicht wirbelfreien Aussenströmung durch eine Potenzreihe darstellbar sind. Diese Strömung gibt eine Einsicht in den sekundären Strömungserscheinungen bei gekrümmten Kanälen. Die Grenzschichtgleichungen sind

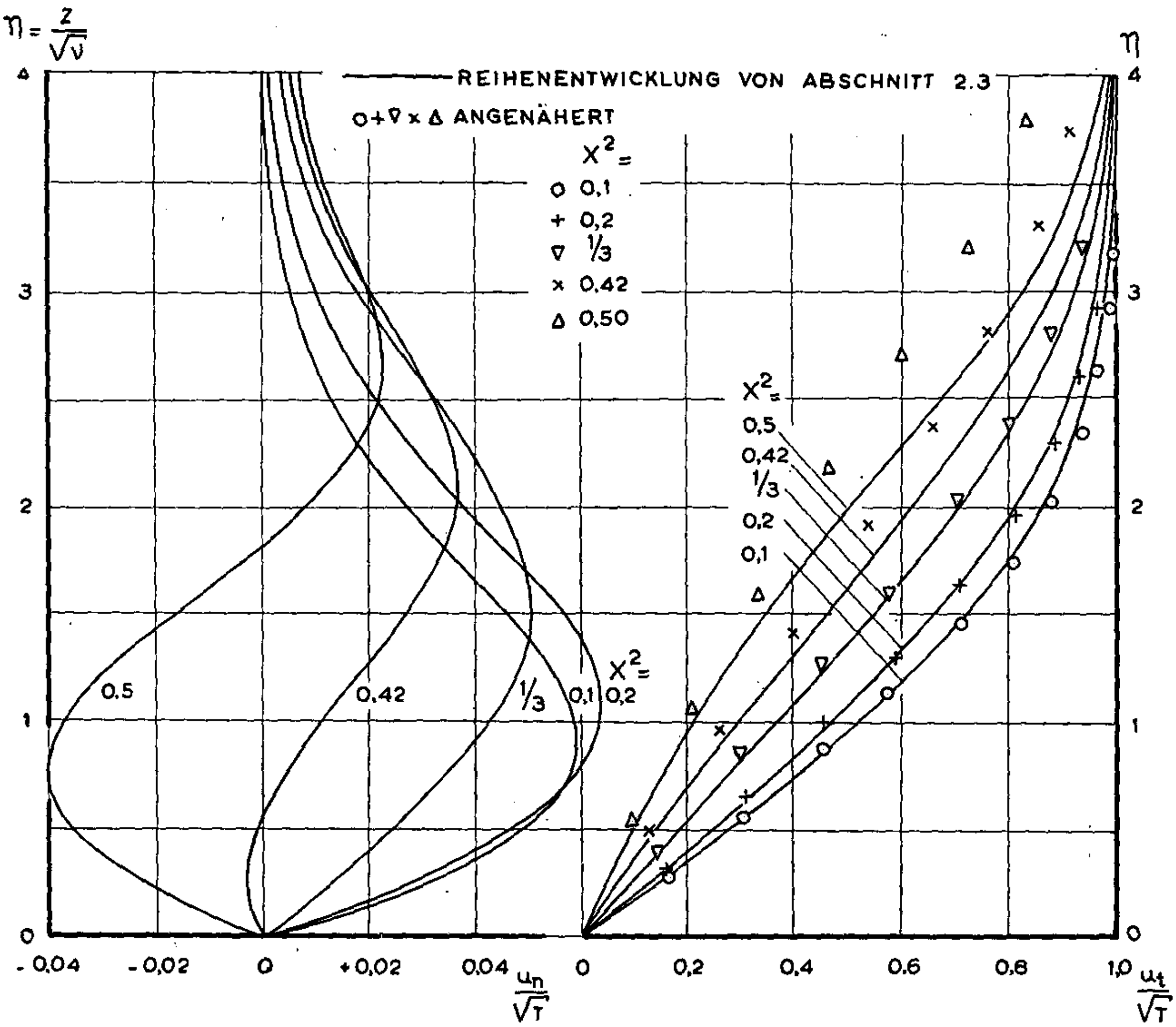

Abb. 8. Zylinderströmung mit $U = x - x^3$, $V = 1$.

Die Grenzschichtprofile $\frac{u_t}{\sqrt{T}}$ und $\frac{u_n}{\sqrt{T}}$ für verschiedene Werte von x^2.

$$
\begin{aligned}
u \frac{\partial u}{\partial x} + w \frac{\partial u}{\partial z} &= U \frac{dU}{dx} + \nu \frac{\partial^2 u}{\partial z^2} \\
u \frac{\partial v}{\partial x} + w \frac{\partial v}{\partial z} &= U \frac{dV}{dx} + \nu \frac{\partial^2 v}{\partial z^2} \qquad (2.21) \\
\frac{\partial u}{\partial x} + \frac{\partial w}{\partial z} &= 0
\end{aligned}
$$

mit

$$U = U_0 = \text{konstant}; \; V = \sum_{i=0}^{n} a_i x^i \qquad (2.22)$$

und mit den Randbedingungen

$$
\begin{aligned}
u = v = w = 0 \qquad & \text{für } z = 0 \\
u \to U, \; v \to V \qquad & \text{für } z \to \infty .
\end{aligned}
$$

Aus (2.21) folgt die bekannte Blasius-Lösung

$$u = U_0 F'(\eta)$$

$$w = {}^1/_2 \sqrt{\frac{\nu U_0}{x}} \, (\eta F' - F) \qquad 2.23)$$

wo

$$\eta = z \sqrt{\frac{U_0}{\nu x}}$$

und $F(\eta)$ die Blasius-Funktion [4] ist.

Setzt man

$$v = \sum_{i=0}^{n} a_i x^i P_i(\eta), \qquad (2.24)$$

dann entsprechen die Funktionen $P_i(\eta)$ der Differentialgleichung

$$P_i'' + \frac{F P_i'}{2} - i F' P_i + i = 0,$$

mit den Randbedingungen

$$P_i(0) = 0 \qquad \lim_{\eta = \infty} P_i(\eta) = 1.$$

Der Strich bedeutet Differentiation nach η.

Die Stromlinien erhält man aus der Beziehung

$$\frac{dy}{dx} = \frac{V}{U_0} = \frac{1}{U_0} \sum_{i=0}^{n} a_i x^i = \sum_{i=0}^{n} a_i^* x^i, \qquad (2.25)$$

wo

$$a_i^* = \frac{a_i}{U_0}.$$

Die Geschwindigkeitsverteilungen innerhalb der Reibungsschicht in der Richtung der Aussenströmung und senkrecht darauf, erhält man aus den Formeln (2.11) und (2.12), sodass

$$
\begin{aligned}
\frac{u_n}{\sqrt{T}} &= \frac{uV}{T} - \frac{vU}{T} = -\frac{U_0^2}{T} \sum_{i=0}^{n} a_i^* x^i (P_i - F') = -\frac{U_0^2}{T} \sum_{i=0}^{n} a_i^* x^i H_i(\eta) \\
\frac{u_t}{\sqrt{T}} &= \frac{U^2}{T}\,\frac{u}{U} + \frac{VU}{T}\,\frac{v}{U} = \frac{u}{U} + \frac{V}{U}\left(\frac{vU}{T} - \frac{uV}{T}\right) = F' - \frac{V}{U_0}\,\frac{u_n}{\sqrt{T}}.
\end{aligned} \tag{2.26}
$$

Für den Fall

$$a_1^* = 1 \qquad a_3^* = -1 \qquad a_i^* = 0 \text{ für } i \neq 1{,}3$$

sind

$$\frac{T}{U_0^2} = 1 + (x - x^3)^2 \tag{2.27}$$

$$\frac{u_n}{\sqrt{T}} = \frac{-xH_1 + x^3 H_3}{1 + (x - x^3)^2}\,; \qquad \frac{u_t}{\sqrt{T}} = F' - (x - x^3)\,\frac{u_n}{\sqrt{T}}. \tag{2.28}$$

Die Stromlinie ist

$$y - y_0 = \frac{x^2}{2} - \frac{x^4}{4}. \tag{2.29}$$

Die Funktionen F, H_1 und H_3 sind der Arbeit [4] entnommen. In der Abbildung 9 sind die Stromlinie (2.29) und auch die Geschwindigkeitsverteilungen $\frac{u_t}{\sqrt{T}}$ und $\frac{u_n}{\sqrt{T}}$ für verschiedene Werte von x als Funktionen von η aufgetragen. Bei dem Übergang von der beschleunigten zu der verzögerten Aussenströmung weisen die Sekundärströmungsprofile — wie auch schon aus der Abbildung 8 hervortritt — eine Rückströmung auf. Hierauf kommen wir im nächsten Abschnitt zurück.

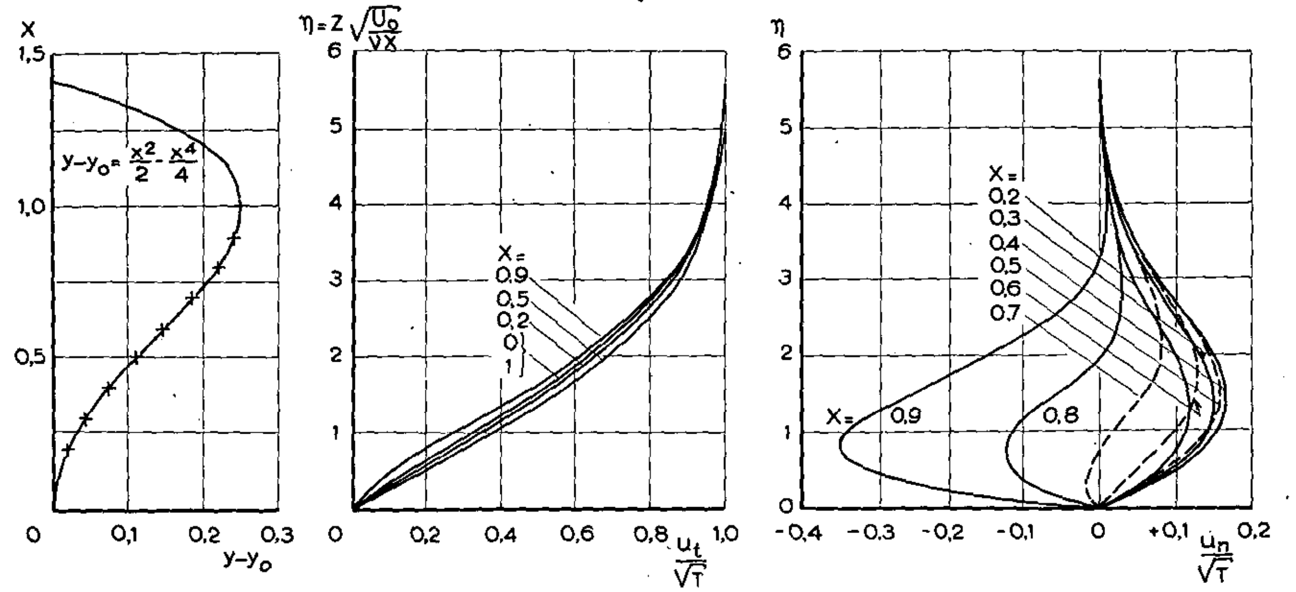

Abb. 9. Die Stromlinie der freien Aussenströmung und die exakten Geschwindigkeitsverteilungen $\frac{u_t}{\sqrt{T}}$ und $\frac{u_n}{\sqrt{T}}$ innerhalb der Grenzschicht einer ebenen Plattenströmung mit den freien Geschwindigkeitskomponenten $U = U_0$, $V = U_0(x - x^3)$.

3 Näherungslösungen.

Eine einfache Näherungsmethode zur Berechnung dreidimensionaler laminarer Grenzschichten um willkürliche Körper wird in der Arbeit [1] beschrieben. Mit Hilfe der Impulsgleichungen in Stromlinienkoordinaten werden zwei einfache Differentialgleichungen hergeleitet, die eine einfache Quadraturgleichung und Integralgleichung zur Lösung haben.

Die einfachen Differentialgleichungen (4.3) und (4.5) in der Arbeit 1, lauten

$$\frac{\partial}{\partial \varphi}\left(\frac{T^2 \sigma}{\rho}\right) = \frac{0{,}436}{a^2}\,\frac{T}{\rho} = 5{,}08\,\frac{T}{\rho} \tag{3.1}$$

$$\frac{\rho^2}{2\,\theta_{21}}\,\frac{\partial}{\partial \varphi}\left(\frac{\sigma \theta_{21}^2}{\rho^2}\right) = \rho\sqrt{\sigma}\,\frac{\partial}{\partial \varphi}\left(\frac{\sqrt{\sigma}\,\theta_{21}}{\rho}\right) = \frac{1}{T}\left(\frac{\partial u_2}{\partial \zeta}\right)_{\zeta=0} - \frac{M}{T}\,(0{,}293 + \Delta_1). \tag{3.2}$$

σ und Ω sind die Parameter der vorgegebenen Grenzschichtprofile in der Richtung der Stromlinien der freien Strömung und in der Querrichtung. T ist das Quadrat der freien Stromgeschwindigkeit.
Die Funktion ρ wird durch die Kontinuitätsgleichung — angewandt auf der Potentialströmung — bestimmt, und mit Hilfe der Gleichung (3.8) berechnet.
Die Grenzschichtprofile können dargestellt werden durch

$$u_1 = f(\bar{\zeta}) - \Lambda g(\bar{\zeta}) - Nh(\bar{\zeta}) \tag{3.3}$$

$$u_2 = -\Omega^2 Mg\left(\frac{\bar{\zeta}}{\Omega}\right) + \Omega^2 Kh\left(\frac{\bar{\zeta}}{\Omega}\right) \tag{3.4}$$

wo

$$u_1 = \frac{u_t}{\sqrt{T}}, \quad u_2 = \frac{u_n}{\sqrt{T}}, \quad \bar{\zeta} = \frac{z}{\sqrt{\sigma\nu}}, \tag{3.5}$$

und

$$1 - f(\bar{\zeta}) = 2\,g(\bar{\zeta}) + e^{-\bar{\zeta}^2} = 2\,h(\bar{\zeta}) + (1+\bar{\zeta}^2)e^{-\bar{\zeta}^2} = \frac{2}{3\sqrt{\pi}}\,\bar{\zeta}\,e^{-\bar{\zeta}^2} + \frac{2}{\sqrt{\pi}}\int_{\bar{\zeta}}^{\infty} e^{-t^2}\,dt. \tag{3.6}$$

$K=0$ liefert uns die Gleichungen der Grenzschichtprofile aus den Arbeiten [1], [9] und [10].
Die Funktionen f, g und h sind in Abbildung 11 gezeichnet und in Tabelle 2 tabelliert.
Für $\bar{\zeta}=0$ sind die Randwerten

$$f = g = h = f'' = h'' = f''' = g''' = h''' = f^{\mathrm{IV}} = 0$$

$$f' = -2\,g' = -2\,h' = \frac{4}{3\sqrt{\pi}}$$

$$g'' = 1$$

$$g^{\mathrm{IV}} = -h^{\mathrm{IV}} = -6.$$

u_t und u_n sind die Geschwindigkeitskomponenten innerhalb der Grenzschicht in der Richtung der örtlichen Stromlinien der freien Strömung und in der senkrechten Querrichtung.
$\sqrt{\sigma\nu}$ ist ein Mass für die Grenzschichtdicke. Sie hat die Dimension einer Länge. Setzt man $\sigma\nu = \bar{\sigma}l^2/Re_l$, dann ist $\bar{\sigma}$ die dimensionslose Grösse $\bar{\sigma} = U_\infty \sigma/l$ und man bekommt

$$\bar{\zeta} = \frac{z}{\sqrt{\sigma\nu}} = \frac{z}{l}\sqrt{Re_l/\bar{\sigma}}. \tag{3.7}$$

Die Grenzschichtdicke der Querströmung ist um einen Faktor Ω grösser als die Grenzschichtdicke der Hauptströmung.
Sind x, y, z die räumlichen kartesischen Koordinaten dann sind wegen den Gleichungen (5.3), und (6.3) in der Arbeit [1]

$$\frac{\partial}{\partial\varphi}\ln\rho g = -\frac{2}{T}\left(\frac{\delta U}{\delta x} + \frac{\delta V}{\delta y}\right) \quad \text{mit} \quad g = 1 + z_x^2 + z_y^2 \tag{3.8}$$

$$T\frac{\partial}{\partial\varphi} = U\frac{\delta}{\delta x} + V\frac{\delta}{\delta y} \tag{3.9}$$

$$T\sqrt{\rho g}\,\frac{\partial}{\partial\psi} = \frac{\delta\varphi}{\delta y}\frac{\delta}{\delta x} - \frac{\delta\varphi}{\delta x}\frac{\delta}{\delta y}. \tag{3.10}$$

Dabei sind

$$\frac{\delta}{\delta x} = \frac{\partial}{\partial x} + z_x\frac{\partial}{\partial z}, \quad \frac{\delta}{\delta y} = \frac{\partial}{\partial y} + z_y\frac{\partial}{\partial z}$$

Differentiationen wo y oder x konstant bleiben und z als Funktion von x und y genommen wird.
Λ und M hängen mit den Geschwindigkeitsgradienten zusammen und sind in der Arbeit [1] Gl. (3.3) gegeben

$$\Lambda = \tfrac{1}{2}\sigma\frac{\partial T}{\partial\varphi}, \quad M = \tfrac{1}{2}\sigma\sqrt{\rho}\,\frac{\partial T}{\partial\psi}. \tag{3.11}$$

Für das Grenzschichtprofil u_1 in der Hauptströmungsrichtung wird für die beschleunigte Strömung ($\Lambda > 0$) die Lösung mit $N = 0$ genommen. Für die verzögerte Strömung ($\Lambda < 0$) wird eine Lösung mit $N = \Lambda$ angesetzt. Die Schubspannung an der Wand in Strömungsrichtung $(\partial u_1/\partial \zeta)_{\bar{\zeta}=0}$ verschwindet dann für $\Lambda = -1$. Der Punkt, wo $\Lambda = -1$ ist, soll als ein Punkt der laminaren Ablösung genommen werden. Das Kriterium für laminare Ablösung $\Lambda = -1$ ist für die Stromlinienkoordinaten nicht exakt (vgl. Arbeit [1]). Sie ergibt aber meistens eine ziemlich gute Annäherung.

Für die Geschwindigkeitsprofile u_2 der Querströmung wird in der Arbeit [1] der Wert $K \equiv 0$ angesetzt. Diese Annahme ist nicht mehr richtig wenn $\frac{\partial T}{\partial \psi}$ sich von Vorzeichen ändert, d.h. wenn die Stromlinie einen Wendepunkt enthält. In diesem Falle reicht die Funktion $g\left(\frac{\bar{\zeta}}{\Omega}\right)$ nicht mehr aus, um die Profile der Sekundärströmung zu beschreiben (vgl. die Abb. 8, 9 und 11).

Folglich wird die Profilgleichung u_2 mit einem Korrekturglied $K\Omega^2 h\left(\frac{\bar{\zeta}}{\Omega}\right)$ erweitert. Das Korrekturglied $h(\bar{\zeta})$ ist so gewählt, dass die Funktion u_2, zur Beschreibung des Querstromprofils, auch das nächst höhere Glied $\bar{\zeta}^2 e^{-\bar{\zeta}^2}$ enthält, ohne dabei die Randbedingungen an der Wand

$$u_2 = \frac{\partial^3 u_2}{\partial \bar{\zeta}^3} = 0, \quad \frac{\partial^2 u_2}{\partial \bar{\zeta}^2} = -M \qquad \text{für } \bar{\zeta} = 0$$

zu verletzen. Damit wird zugleich ein neuer Profilparameter eingeführt. Zur Lösung neuer Profilparameter können die höheren Randbedingungen an der Wand ohne sehr grossen Arbeitsaufwand nicht mehr angewandt werden. Sie liefern nämlich mit der Gleichung (3.2) ein System simultaner Differentialgleichungen, dass ausserordentlich schwierig zu lösen ist. Von physischem Standpunkt aus ist aber zu erwarten, dass in dem Bereich wo der Druckgradient sich praktisch nicht mehr ändert, auch der Profilparameter Ω sich nicht stark ändert. Infolgedessen werden, falls der Parameter K auftritt, für die Funktionen K und Ω die folgenden Annahmen gemacht.

$K = 0$, $\Omega = \Omega(\varphi)$; für die beschleunigte Strömung vom Staupunkt aus bis oben auf dem Körper, wo der Druckgradient sich nicht mehr so stark ändert. $K = K(\varphi)$, $\Omega =$ Konstant; oben auf dem Körper. Die Funktion K ändert sich so lange, bis sie wieder den Wert Null annimmt. $K = 0$, $\Omega = \Omega(\varphi)$ in dem etwaigen weiteren Bereich.

Mit Hilfe dieser Annahme geht die Differentialgleichung (3.2) für die Querströmung über in die Integralgleichung

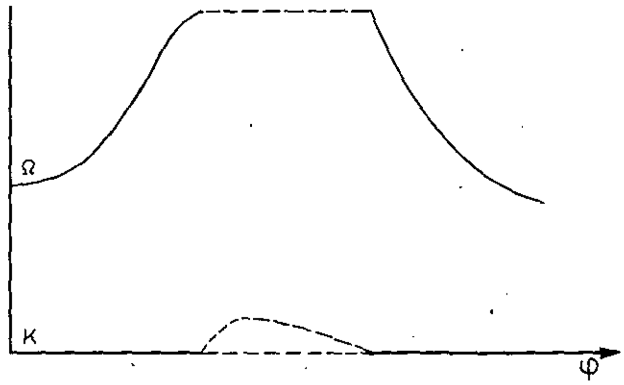

Abb. 10. Ω und K als Funktionen von φ.

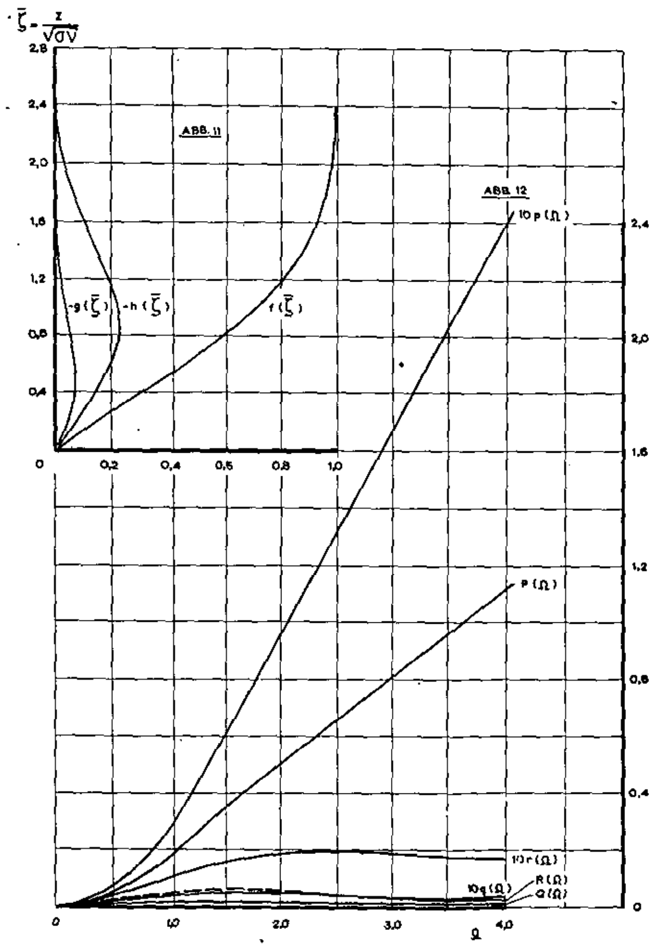

Abb. 11. f, g und h als Funktion von $\bar{\zeta} = \frac{z}{\sqrt{\sigma\nu}}$.

Abb. 12. p, q, r, P, Q und R als Funktion von Ω.

$$\frac{\theta_{21}\sqrt{\sigma}}{\rho} = c_1(\varphi_0) + \int_{\varphi_0}^{\varphi} \frac{1}{T\rho\sqrt{\sigma}} \left[M\left(\frac{2}{3\sqrt{\pi}}\ \Omega - 0{,}293 - \Delta_1\right) - \frac{2}{3\sqrt{\pi}}\ \Omega K\right] d\varphi. \tag{3.12}$$

Die Verdrängungsdicke Δ_1 und Impulsverlustdicke θ_{21} sind gegeben durch

TABELLE 1

Die Funktionen $f(\bar{\zeta})$, $g(\bar{\zeta})$, $h(\bar{\zeta})$ der Grenzschichtprofile und die Funktionen p, q, r, P, Q, R zur Beschreibung der Impulsverlustdicke θ_{21}.

$\bar{\zeta}$	$f(\bar{\zeta})$	$g(\bar{\zeta})$	$h(\bar{\zeta})$	Ω	$p(\Omega)$	$q(\Omega)$	$r(\Omega)$	$P(\Omega)$	$Q(\Omega)$	$R(\Omega)$
0	0	0	0	0	0	0	0	0	0	0
0,2	0,15043	— 0,05561	— 0,07482	0,25	0,00196	0,00072	0,00097	0,01368	0,00418	0,00666
0,4	0,30019	— 0,07617	— 0,14434	0,50	0,00780	0,00204	0,00369	0,05367	0,00921	0,02276
0,6	0,44641	— 0,07204	— 0,19762	0,75	0,01729	0,00313	0,00740	0,11447	0,01118	0,03842
0,8	0,58344	— 0,05537	— 0,22410	1,00	0,02983	0,00380	0,01108	0,18762	0,01108	0,04774
1,0	0,70433	— 0,03611	— 0,22005	1,25	0,04460	0,00412	0,01409	0,26621	0,01021	0,05106
1,2	0,80338	— 0,02015	— 0,19074	1,50	0,06085	0,00421	0,01624	0,34640	0,00918	0,05066
1,4	0,87811	— 0,00949	— 0,14753	1,75	0,07802	0,00418	0,01763	0,42648	0,00822	0,04845
1,6	0,92983	— 0,00357	— 0,10252	2,00	0,09571	0,00407	0,01842	0,50583	0,00739	0,04552
1,8	0,96258	— 0,00087	— 0,06432	2,25	0,11368	0,00393	0,01878	0,58429	0,00668	0,04244
2,0	0,98154	+ 0,00007	— 0,03656	2,50	0,13179	0,00377	0,01884	0,66192	0,00608	0,03949
2,2	0,99160	+ 0,00025	— 0,01745	2,75	0,14993	0,00361	0,01869	0,73880	0,00557	0,03676
2,4	0,99647	+ 0,00019	— 0,00888	3,00	0,16805	0,00345	0,01841	0,81506	0,00513	0,03428
2,6	0,99863	+ 0,00011	— 0,00381	3,25	0,18613	0,00330	0,01805	0,89078	0,00475	0,03205
3,0	0,99984	+ 0,00002	— 0,00054	3,50	0,20416	0,00316	0,01764	0,96607	0,00443	0,03005
3,4	0,99999	+ 0,00000	— 0,00005	3,75	0,22211	0,00303	0,01719	1,04097	0,00414	0,02826
				4,00	0,24000	0,00290	0,01673	1,11556	0,00389	0,02664

$$\left.\begin{aligned}\Delta_1 &= \int_0^\infty (1-u_1)\,d\bar{\zeta} = 0{,}75225 - 0{,}06699\,\Lambda - 0{,}28854\,N \\ \theta_{21} &= -\int_0^\infty u_1 u_2\,d\bar{\zeta} \\ &= -M\Omega^2[p(\Omega)+\Lambda\,q(\Omega)+Nr(\Omega)]+K\Omega^2[P(\Omega)+\Lambda Q(\Omega)+NR(\Omega)].\end{aligned}\right\} \tag{3.13}$$

Die Funktionen $p(\Omega)$ bis $R(\Omega)$ sind in Tabelle 1 und in der Abbildung 12 gegeben.

Durch ein Iterationsverfahren werden, sowohl in dem Bereich wo $K=0$ und $\Omega=\Omega(\varphi)$, als in dem Bereich wo $K=K(\varphi)$ und Ω konstant ist, Ω und K mit Hilfe der Gleichungen (3.12) und (3.13) bestimmt.

Aus (3.1) folgt die Quadraturgleichung

$$\sigma = 5{,}08\,\frac{\rho}{T^2}\left(c_0(\varphi_0) + \int_{\varphi_0}^{\varphi} \frac{T}{\rho}\,d\varphi\right). \tag{3.14}$$

Den Stromlinien entlang gilt

$$\frac{dx}{U} = \frac{dy}{V} = \frac{dz}{W} = \frac{d\varphi}{T}. \tag{3.15}$$

Sind $z=z(x)$, $U=U(x)$, $V=V(x)$ Funktionen von x allein, dann sind alle Grenzschichtgrössen unabhängig von der Koordinate y.

Folglich gehen die Gleichungen (3.8) bis (3.11) über in

$$\left.\begin{aligned}&\rho = \frac{c}{U^2(1+z_x^2)}\,;\quad T\frac{\partial}{\partial\varphi} = U\frac{d}{dx},\quad T\frac{\partial}{\partial\psi} = \frac{UV}{\sqrt{c}}\,\frac{d}{dx} \\ &\Lambda = \tfrac{1}{2}\,\sigma\,\frac{U}{T}\,\frac{dT}{dx},\quad M = \tfrac{1}{2}\,\frac{\sigma}{\sqrt{1+z_x^2}}\,\frac{V}{T}\,\frac{dT}{dx}\end{aligned}\right. \tag{3.16}$$

und die Quadraturgleichung (3.14) in

$$\sigma = \frac{5{,}08}{T^2U^2(1+z_x^2)}\int_0^x T^2U\sqrt{1+z_x^2}\,dx \tag{3.17}$$

im Anfangspunkt $x=0$, wo $U=0$, ist $c_0(\varphi)=0$.

4 Spezielle Lösungen.

Bei den schrägen *Keil-* und *Eck-Strömungen* mit

$$U = Ax^m,\quad V = B = U\operatorname{tg}\vartheta \tag{4.1}$$

gelten die folgenden Beziehungen

$$T = U^2 + V^2 = B^2(1+\operatorname{cotg}^2\vartheta)$$

$$\Lambda = M\operatorname{cotg}\vartheta = \frac{\sigma U m}{x}\cos^2\vartheta = m\left(\frac{A}{B}\right)^{\frac{1}{m}} B\sigma(\operatorname{tg}\vartheta)^{\frac{1-m}{m}}\cos^2\vartheta \tag{4.2}$$

$$\bar{\zeta} = \frac{z}{\sqrt{\sigma\nu}} = \frac{\eta}{\sqrt{\dfrac{(m+1)U\sigma}{2x}}} = \frac{\eta\cos\vartheta}{\sqrt{\dfrac{m+1}{2m}\Lambda}}.$$

Folglich gehen die Gleichungen (3.16) und (3.12) mit $K\equiv 0$ über in

$$\left(\frac{A}{B}\right)^{\frac{1}{m}} B\sigma = 5{,}08\,(\operatorname{tg}\vartheta)^{\frac{m-1}{m}}\cos^4\vartheta\left[\frac{1}{5m+1} + \frac{2}{3m+1}\operatorname{tg}^2\vartheta + \frac{1}{m+1}\operatorname{tg}^4\vartheta\right] \tag{4.3}$$

$$\theta_{21} = -\frac{1}{\sqrt{\sigma}U^2}\int_{\frac{\pi}{2}}^{\vartheta}\sqrt{\sigma}U^2\left(\frac{2}{3\sqrt{\pi}}\Omega - 0{,}293 - \Delta_1\right)d\vartheta. \tag{4.4}$$

Der Grenzübergang $x \to 0$ bzw $\vartheta \to \frac{\pi}{2}$ liefert die Gleichungen

$$\left(\frac{A}{B}\operatorname{tg}\vartheta\right)^{\frac{1-m}{m}} A\vartheta = \frac{5{,}08}{m+1} \tag{4.5}$$

$$\frac{\theta_{21}}{M} = -\Omega^2 p(\Omega) = \frac{m+1}{2{,}54(1+5m)}(0{,}37613\,\Omega - 1{,}04525)$$

und damit die Anfangswerte für σ und Ω.

Bei der *Staupunktströmung* mit

$$U = Ax, \quad V = By = U\operatorname{tg}\vartheta$$
$$T = U^2 + V^2 = A^2x^2(1 + \operatorname{tg}^2\vartheta) \tag{4.6}$$

entsprechen die Stromlinien der Aussenströmung den Gleichungen

$$y = \alpha x^\lambda \quad \text{mit} \quad \lambda = \frac{B}{A}. \tag{4.7}$$

Den Stromlinien entlang gelten die nachfolgenden Beziehungen. Es ist

$$\alpha\lambda x^{\lambda-1} = \operatorname{tg}\vartheta, \tag{4.8}$$

Wegen

$$\frac{\partial}{\partial\varphi} \ln\rho = -\frac{2}{T}\left(\frac{\partial U}{\partial x} + \frac{\partial V}{\partial y}\right) = -\frac{2A(1+\lambda)}{T}$$

ist

$$\rho = \frac{c_1}{x^{2+2\lambda}}.$$

Die Differentialgleichung (3.1) hat die Lösung

$$A\sigma = 5{,}08\frac{\rho}{T^2}\int_0^x \frac{AT^2}{\rho U}dx = \frac{5{,}08}{6+2\lambda}\cos^4\vartheta + \frac{5{,}08}{2+2\lambda}\cos^2\vartheta\sin^2\vartheta + \frac{5{,}08}{2+6\lambda}\sin^4\vartheta. \tag{4.9}$$

Unter Benutzung der Gleichungen (3.9) bis (3.11) sind

$$\Lambda = \frac{\sigma}{2}\frac{\partial T}{\partial\varphi} = \frac{1}{2}\frac{\sigma}{T}\left(U\frac{\partial T}{\partial x} + V\frac{\partial T}{\partial y}\right) = A\sigma(\cos^2\vartheta + \lambda\sin^2\vartheta)$$

$$M = \frac{\sigma}{2}\sqrt{\rho}\frac{\partial T}{\partial\psi} = \frac{1}{2}\frac{\sigma}{T}\left(V\frac{\partial T}{\partial x} - U\frac{\partial T}{\partial y}\right) = A\sigma(1-\lambda)\sin\vartheta\cos\vartheta.$$

Die Integralgleichung (3.12) lautet für $K \equiv 0$

$$\theta_{21} = -\left\{\sqrt{A\sigma}(\operatorname{tg}\vartheta)^{\frac{2\lambda+2}{\lambda-1}}\right\}^{-1}\int_{\vartheta_0}^{\vartheta}\sqrt{A\sigma}(\operatorname{tg}\vartheta)^{\frac{2\lambda+2}{\lambda-1}}\left(\frac{2}{3\sqrt{\pi}}\Omega - 0{,}293 - \Delta_1\right)d\vartheta \tag{4.10}$$

wo

$$\vartheta_0 = 0 \text{ für } \lambda > 1 \text{ und } \vartheta_0 = \frac{\pi}{2} \text{ für } \lambda < 1.$$

Dazu ist noch

$$\zeta = \frac{z}{\sqrt{\sigma\nu}} = \frac{\eta}{\sqrt{A\sigma}}. \tag{4.11}$$

Der Anfangswert Ω für $x \to 0$ und $0 < \lambda < 1$ folgt aus

$$\frac{\theta_{21}}{M} = -\Omega^2 p(\Omega) - \Lambda\,\Omega^2 q(\Omega) = \frac{1}{2{,}54}\,\frac{1+3\lambda}{3+\lambda}\left(\frac{2}{3\sqrt{\pi}}\Omega - 0{,}293 - \Delta_1\right). \tag{4.12}$$

5 **Geeignetere Anfangswerte und Staupunktwerte** (mit Beispiel).

Die vollständigen Impulsgleichungen (2.8) in der Arbeit [1] liefern für die *Keil-* und *Eck-Strömungen*, mit

$$U = Ax^m \qquad V = B$$

nach Einführung von

$$\frac{A\sigma}{x^{1-m}} = \left(\frac{A}{B}\right)^{1/m} B\sigma(\operatorname{tg}\vartheta)^{\frac{1-m}{m}} = \Sigma$$

und mittels des Grenzübergangs $x \to 0$, die Gleichungen

$$\frac{m(1+m)}{2}(\Omega^2 p(\Omega) - 0{,}06699\,\Omega^3)\Sigma^2 - 0{,}14471\,(1+m)\Sigma + 0{,}75225 = 0 \tag{5.1}$$

$$0{,}0019\,m(1+3\,m)\Omega^5\Sigma^2 + \frac{1+5\,m}{2}\,\Omega^2 p(\Omega)\Sigma + 0{,}37613\,\Omega - 1{,}04168 = 0.$$

Für die *Staupunktströmung* mit

$$U = Ax, \quad V = By \qquad 0 < \frac{B}{A} = \lambda < 1$$

lauten diese Grenzübergangs-Gleichungen, nach Einführung von $A\sigma = \Sigma$, für den Punkt $x = y = 0$

$$-(1-\lambda)\,[\Omega^2 p(\Omega) - 0{,}06699\,\Omega^3 + \Lambda\,\Omega^2 q(\Omega)]\,\Sigma^2 + [(1+2\,\lambda)\theta_{11} + \lambda\Delta_1]\,\Sigma - \frac{2}{3\sqrt{\pi}}(2+\Lambda) = 0$$

$$0{,}0076\,(1-\lambda)\Omega^5\Sigma^2 + (3+\lambda)\,[\Omega^2 p(\Omega) + \Lambda\,\Omega^2 q(\Omega)]\Sigma - (\theta_{11} + \Delta_1) + \frac{2}{3\sqrt{\pi}}\,\Omega = 0 \tag{5.2}$$

wo

$$\Lambda = \lambda(A\sigma) = \lambda\Sigma.$$

Die Funktionen θ_{11} und Δ_1 sind in den Arbeiten [9] und [10] und die Funktionen $p(\Omega)$ und $q(\Omega)$ in Tabelle 1 gegeben.

In Abb. 13 sind die Staupunktwerte Ω und $\Sigma = A\sigma$ über λ ausgesetzt.

Hat die Strömung einen Staupunkt, dann können die Anfangswerte Ω und Σ in diesem Punkt unmittelbar aus der Abb. 13 abgelesen werden. Dazu benötigt man die linearen Glieder der Reihenentwicklung der Geschwindigkeitskomponenten in der Richtung von zwei orthogonalen Koordinaten in der Tangentialebene im Staupunkt.

Als Beispiel wird die Staupunktströmung an einem dreiachsigen Ellipsoid

$$\frac{x^2}{a^2} + \frac{y^2}{b^2} + \frac{z^2}{c^2} = 1 \qquad a \geq b \geq c \tag{5.3}$$

gewählt. Wird dieses Ellipsoid in einer seiner Symmetrieebenen (x, y-Ebene) angeströmt, dann ist das Geschwindigkeitspotential φ auf der Oberfläche in den Oberflächenkoordinaten x und y gegeben durch [11] [12]

$$\varphi = -px - qy. \tag{5.4}$$

Hier ist

$$p = \frac{2\,U_0}{2-\alpha_0} \qquad q = \frac{2\,V_0}{2-\beta_0} \tag{5.5}$$

und

$$\alpha_0 = abc\int_0^\infty \frac{d\zeta}{(a^2+\zeta)L}\;;\quad \beta_0 = abc\int_0^\infty \frac{d\zeta}{(b^2+\zeta)L},\quad L = \sqrt{(a^2+\zeta)(b^2+\zeta)(c^2+\zeta)}\,. \tag{5.6}$$

$-U_0$, $-V_0$, 0 sind die ungestörten Geschwindigkeitskomponenten im Unendlichen.

Sind U, V, W die Geschwindigkeitskomponenten in dem orthogonalen kartesischen x, y, z-Koordinatensystem, dann gilt auf der Oberfläche

$$\begin{aligned}
\frac{\delta\varphi}{\delta x} &= -p = \frac{\partial\varphi}{\partial x} + \frac{\partial z}{\partial x}\,\frac{\partial\varphi}{\partial z} = U + Wz_x = U(1+z_x^2) + Vz_xz_y \\
\frac{\delta\varphi}{\delta y} &= -q = \frac{\partial\varphi}{\partial y} + \frac{\partial z}{\partial y}\,\frac{\partial\varphi}{\partial z} = V + Wz_y = Uz_xz_y + V(1+z_y^2) \\
W &= Uz_x + Vz_y\,.
\end{aligned} \tag{5.7}$$

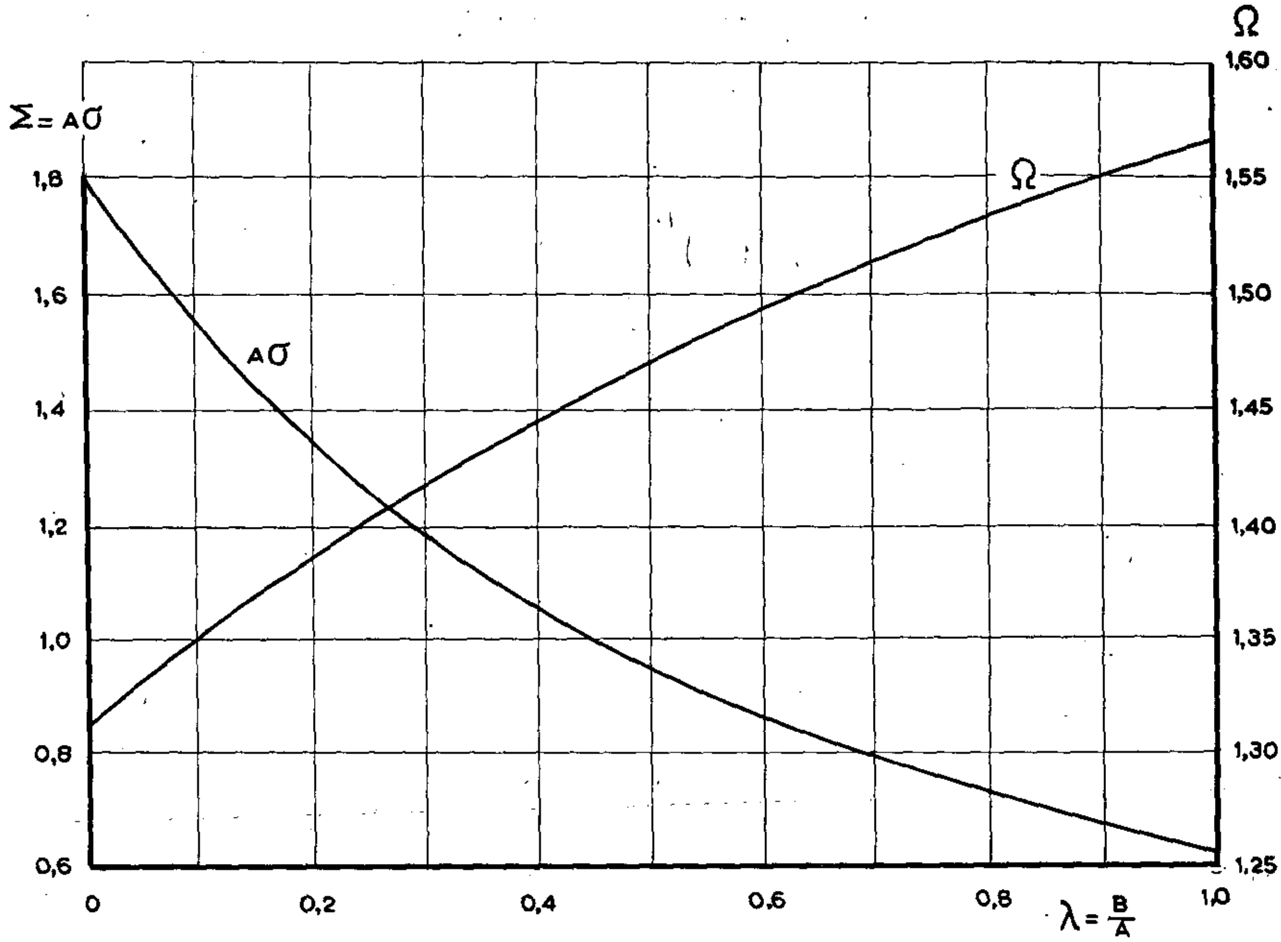

Abb. 13. Die Staupunktswerte $\Sigma = A\sigma$ und Ω über $0 < \lambda = \frac{B}{A} < 1$, berechnet mit Hilfe der vollständigen Impulsgleichungen für die Staupunktströmung mit den Geschwindigkeitskomponenten der freien Strömung $U = Ax$, $V = By$.

In dem Staupunkt ist $U = V = W = 0$. Folglich ist in diesem Punkt

$$z = 0, \quad \frac{qx}{a^2} - \frac{py}{b^2} = 0 \tag{5.8}$$

sodass in dem vorderen Staupunkt

$$\frac{x}{a^2} = \frac{p}{l}, \quad \frac{y}{b^2} = \frac{q}{l}, \quad l = \sqrt{a^2p^2 + b^2q^2}. \tag{5.9}$$

In der Tangentialebene im Staupunkt führen wir jetzt die orthogonalen Koordinaten [9] [10]

$$\eta_2 = \frac{ab}{l}\left(\frac{qx}{a^2} - \frac{py}{b^2}\right) \tag{5.10}$$

$$\eta_3 = \frac{z}{c}$$

ein. Die Gleichungen für die Stromlinien bezeichnen, dass sie überall auf der Oberfläche tangential zu dem Geschwindigkeitsvektor sind, sodass wegen (5.10)

$$\frac{dx}{U} = \frac{dy}{V} = \frac{dz}{W} = \frac{d\eta_3}{W/c} = \frac{d\eta_2}{\frac{bq}{al}U - \frac{ap}{bl}V} = \frac{d\eta_3}{U^3} = \frac{d\eta_2}{U^2}. \tag{5.11}$$

Im Staupunkt ($\eta_2 = \eta_3 = 0$) sind die kontravarianten Geschwindigkeitskomponenten U^2 und U^3 wegen (5.7)

$$U^3 = W/c = \frac{l}{c^2}\,\eta_3 = A\eta_3$$

$$U^2 = \frac{bq}{al}U - \frac{ap}{bl}V = \frac{l^3}{(p^2+q^2)a^2b^2}\,\eta_2 = B\eta_2. \tag{5.12}$$

Damit ist

$$\lambda = \frac{B}{A} = \frac{l^2 c^2}{(p^2+q^2)a^2b^2} = \frac{(a^2p^2+b^2q^2)c^2}{(p^2+q^2)a^2b^2}\,. \tag{5.13}$$

Nach (12, S. 301) werden α_0 und β_0 berechnet mit Hilfe der Formeln

$$\alpha_0 = \frac{2\,abc}{\sqrt{(a^2-c^2)^3}}\,\frac{1}{k^2}\,[F(s)-E(s)] = \frac{2\sqrt{(1-s^2)(1-k^2s^2)}}{s^3k^2}[F(s)-E(s)]$$

$$\beta_0 = \frac{2\,abc}{\sqrt{(a^2-c^2)^3}};\frac{1}{k^2(1-k^2)}\left[E(s)-(1-k^2)F(s)-\frac{c}{b}k^2\right] \tag{5.14}$$

$$= \frac{2\sqrt{(1-s^2)(1-k^2s^2)}}{s^3k^2(1-k^2)}\left[E(s)-(1-k^2)F(s)-k^2s\sqrt{\frac{1-s^2}{1-k^2s^2}}\right]$$

wo

$$0 < k^2 = \frac{a^2-b^2}{a^2-c^2} < 1 \qquad 0 < s = \sqrt{1-c^2/a^2} < 1 \tag{5.15}$$

und die elliptischen Integralen

$$F(s) = \int_0^s \frac{dt}{\sqrt{(1-t^2)(1-k^2t^2)}} \tag{5.16}$$

$$E(s) = \int_0^s \sqrt{\frac{1-k^2t^2}{1-t^2}}\,dt \tag{5.17}$$

in vorhandenen Tabellen gegeben sind.

Für das Rotationsellipsoid ($c = b$) ist $k = 1$ und man erhält durch den Grenzübergang $\lim k = 1$

$$\alpha_0 = \frac{2(1-s^2)}{s^3}\left[\frac{1}{2}\ln\frac{1+s}{1-s}-s\right] \tag{5.18}$$

$$\beta_0 = \frac{2(1-s^2)}{s^3}\left[\frac{s}{2(1-s^2)}-\frac{1}{4}\ln\frac{1+s}{1-s}\right].$$

Nachdem für ein bestimmtes Achsenverhältnis (a, b, c) λ bestimmt ist, können die Staupunktwerte $A\sigma$ und Ω aus dem Bild 13 abgelesen werden.

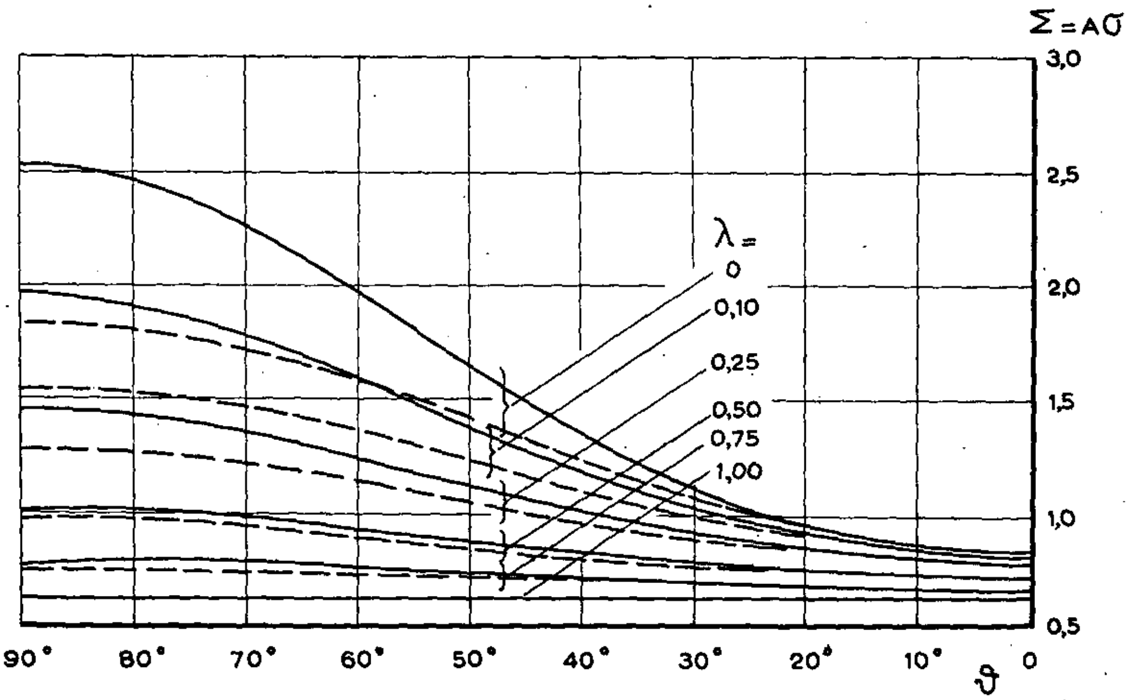

Abb. 14. Staupunktströmung mit $U = Ax$, $V = By$.

Die Funktionen $\Sigma = A\sigma$ über $\vartheta = \mathrm{arc\,tg}\frac{V}{U}$ für verschiedene Werte von $\lambda = \frac{B}{A}$ ($U = Ax$, $V = By$).

——— angenähert mit Gl. (4.9).

– – – – Korrektion mit Hilfe der Anfangswerte (aus Gl. (5.2)) der vollständigen Impulsgleichungen.

6 Ergebnisse.

Die Grenzschichtberechnungen werden für die schägen Keil- und Eck-Strömungen und für die Strömungen in der Umgebung des Staupunktes sowohl exakt mit den Grenzschichtdifferentialgleichungen, wie auch mit der einfachen Näherungsmethode ausgeführt. Gemäsz der in den Abschnitten 2.1 und 2.2 angegebenen exakten Lösungen sind die Geschwindigkeitsprofile, in der dort angewandten rechtwinklichen kartesischen Koordinaten, im Falle solcher Strömungen ähnlich. Die Ähnlichkeit der Geschwindigkeitsprofile gilt nur für diese

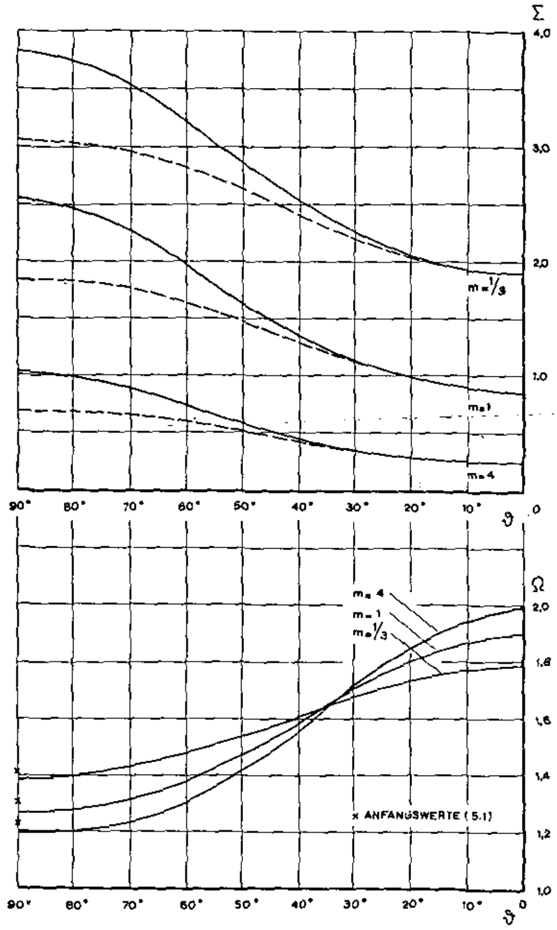

Abb. 15. Keil- und Eckströmungen ($U = Ax^m$, $V = B$).
Die Funktionen $\Sigma = \left(\frac{A}{B}\,\mathrm{tg}\,\vartheta\right)^{\frac{1-m}{m}} A\sigma = \frac{U\sigma}{x}$ und Ω über $\vartheta = \mathrm{arc\,tg}\,\frac{V}{U}$, für $m = \frac{1}{3}$; 1; 4.
——— angenähert mit Hilfe der Gleichungen aus (4.3) und (4.4).
– – – – Korrektion mit Hilfe der Anfangswerte (aus Gl. (5.1)) der vollständigen Impulsgleichungen.

Wahl des Koordinatensystems und besteht daher nicht bei der Verwendung von Stromlinienkoordinaten. Anwendung der einfachen Berechnungsmethode liefert mittels Gleichungen (4.3) und (4.9) die Parameter σ für die Grenzschichtprofile in der Richtung der Stromlinien der freien Strömung. Die Parameter Ω der Querströmungen werden mit Hilfe der Integralgleichungen (4.4) und (4.10) durch ein Iterationsverfahren berechnet. Die Berechnung der Keil- und Eckströmungen werden für $m = {}^1/_3$, 1, 4 bzw. $\beta = \frac{2m}{m+1} = 0{,}5$; 1; 1,6 ausgeführt. Die Funktionen $\Sigma = \left(\frac{A}{B}\,\mathrm{tg}\,\vartheta\right)^{\frac{1-m}{m}} A\sigma$ und Ω sind in der Abbildung 15 gegeben. Die Anfangswerte der vollständigen Impulsgleichungen folgen aus (5.1).

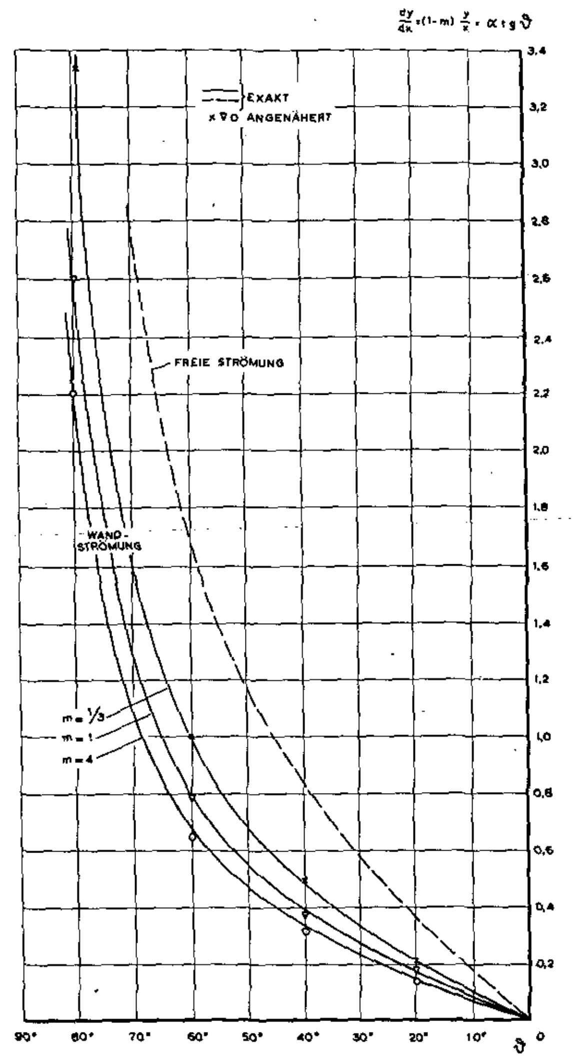

Abb. 16. Keil- und Eckströmungen mit $U = Ax^m$, $V = B$.
Die Richtungskoeffizienten $\frac{dy}{dx}$ und die Funktionen für die freien Stromlinien und die Stromlinien $y = y(x)$ an der Wand über $\vartheta = \mathrm{arc\,tg}\,\frac{V}{U}$ für $m = \frac{1}{3}$, 1 und 4.

Sie sind für $\vartheta = \frac{\pi}{2}$, also an der Vorderkante

m	β	Σ	Ω	
${}^1/_3$	0,5	3,0477	1,4128	
1	1,0	1,8181	1,3107	(6.1)
4	1,6	0,6719	1,2284	

Die Anfangswerte Σ der vollständigen Impulsgleichungen sind bedeutend verschieden von den Anfangswerten von Σ, die aus der einfachen Methode folgen (vgl. Abb. 15). Diese Verschiedenheit findet ihre Ursache darin, dass im Anfang, also für $\vartheta \rightarrow \pi/2$

$$\sqrt{\rho}\,\frac{\partial}{\partial\psi} = \frac{V}{U}\,\frac{\partial}{\partial\varphi} = \operatorname{tg}\vartheta\,\frac{\partial}{\partial\varphi} \gg \frac{\partial}{\partial\varphi}\,.$$

Deshalb sollen, um eine bessere Übereinstimmung mit den Ergebnissen der vollständigen Impulsgleichungen zu erhalten, die Resultaten der einfachen Methode, *nachdem* sie berechnet sind, korrigiert werden. Bedenkt man, dass auf grössere Entfernung der Vorderseite, unter Einwirkung des Druckgradienten, die Unterschiede zwischen den Werten σ der vereinfachten Methode und der vollständigen Impulsgleichungen sich meistens ausgleichen, dann können in der Abbildung 15 die gezogenen σ-Kurven durch die gestrichelten Kurven ersetzt werden. Die Ω-Kurven brauchen gewöhnlich nicht korrigiert zu werden, weil die Anfangswerte von Ω, folgend aus den vollständigen Impulsgleichungen, im allgemeinen nur wenig verschieden sind von den Anfangswerten Ω der einfachen Methode.

Die Geschwindigkeitsprofile in der Richtung der Stromlinie und in der Querrichtung werden für die exakten Grenzschichtlösungen mit Hilfe der Formeln (2.11) und (2.12) erhalten. Für die Näherungslösungen werden sie mit Hilfe der Formeln (3.3) und (3.4) berechnet. Die Werte für Λ und M befriedigen die Gleichungen von (3.11), während die zugehörigen Werte σ den gestrichelten Kurven der Abbildung 15 entnommen sind. Zum Vergleich sind die axakt und näherungsweisen berechneten Profile für $m = 1/3$, $m = 1$, $m = 4$ in den Abbildungen 3a und 3b gezeichnet.

Für $m = 1/3$ ist ausserdem noch eine gestrichelte Kurve mit dem Anfangswert $\Sigma = 3{,}813$ gezeichnet.

Die Profilkoordinaten in der z-Richtung sind dabei alle auf die uniforme Länge

$$\eta = z\sqrt{\frac{(m+1)U}{2\,\nu x}}$$

normiert. Die Winkel ϑ geben die Punkte der Stromlinien der freien Strömung an, wofür die Profile berechnet sind.

In der Abb. 16 sind die Richtungskoeffizienten $\dfrac{dy}{dx}$ der Stromlinien an der Wand über $\vartheta = \operatorname{arc\,tg}\dfrac{V}{U}$ ausgesetzt. Für die exakten Lösungen gilt (vgl. Abschnitt 2.1)

$$\left(\frac{dy}{dx}\right)_{\text{Wand}} = \lim_{\eta\to 0}\frac{v}{u} = \frac{V\,G_{\eta\eta}(0)}{U\,F_{\eta\eta}(0)} = \frac{G_{\eta\eta}(0)}{F_{\eta\eta}(0)}\operatorname{tg}\vartheta = \alpha\operatorname{tg}\vartheta. \tag{6.2}$$

Aus der Arbeit [6] und eigenen Berechnungen folgen die Werte

m	β	$F_{\eta\eta}(0)$	$G_{\eta\eta}(0)$	α
$1/3$	0,5	0,92768	0,53906	0,5811
1	1,0	1,23259	0,57058	0,4629
4	1,6	1,52151	0,59404	0,3904

Für die Näherungslösungen gilt, wegen (3.3), (3.4) und

$$u = u_t\cos\vartheta + u_n\sin\vartheta \qquad v = u_t\sin\vartheta - u_n\cos\vartheta,$$

$$\left(\frac{dy}{dx}\right)_{\text{Wand}} = \lim_{\eta\to 0}\frac{v}{u} = \lim_{\zeta\to 0}\frac{u_t\operatorname{tg}\vartheta - u_n}{u_t + u_n\operatorname{tg}\vartheta} = \frac{(2+\Lambda)\operatorname{tg}\vartheta - \Omega(M-K)}{2+\Lambda+\Omega(M-K)\operatorname{tg}\vartheta}\,.$$

Die zugehörigen Werte σ sind den gestrichelten Kurven der Abb. 15 entnommen.

Wegen $\operatorname{tg}\vartheta = \dfrac{V}{U} = \dfrac{B}{A}\,x^{-m}$ geht (6.2) nach Integration über in

$$\frac{dy}{dx} = (1-m)\frac{y}{x} = \alpha\,\frac{B}{A}\,x^{-m} = \alpha\operatorname{tg}\vartheta.$$

Sie gibt die Beziehung zwischen den freien Stromlinien und den Stromlinien an der Wand (siehe Abb. 16).

In den Abbildungen 5 und 6 sind für die Staupunktströmung sowohl exakte Lösungen, als Näherungslösungen der Grenzschicht-Geschwindigkeitsprofile in der Richtung der freien Aussenströmung und in der senkrechten Querrichtung als Funktionen von $\eta = z\sqrt{\dfrac{A}{\nu}}$ ausgesetzt; und zwar für $\vartheta = \dfrac{\pi}{4}$ und in dem Staupunkt $\vartheta = \dfrac{\pi}{2}$ für verschiedene Werte von λ, mit $0 \leqq \lambda \leqq 1$. Statt $\dfrac{u_n}{\sqrt{T}}$ wird in dem Staupunkt die Funktion $\dfrac{u_n}{\sqrt{T}}\;\dfrac{1}{\cos\vartheta}$ betrachtet. Die Werte $A\sigma$ werden den gestrichelten Kurven der Abb. 14 entnommen.

Bei der Betrachtung des schiebenden Zylinders werden die exakten Lösungen der Grenzschichtprofile $\dfrac{u_t}{\sqrt{T}}$ und $\dfrac{u_n}{U}$ für die Staulinie $x = 0$ in der Gleichung (2.20) gegeben.

Die mit der Impulsmethode eingeführten Grenzschichtprofile sind in (3.3) und (3.4) gegeben. Die vollständigen Impulsgleichungen (2.8) in der Arbeit [1], haben für den schräg angeströmten Zylinder, für $x=0$, die Lösungen (vgl. auch (5.1) und (6.1) für $m=1$)

$$\sigma \sqrt{\frac{1}{2} \frac{d^2T}{dx^2}} = \sigma \frac{dU}{dx} = 1{,}818 + 0(x^2)\,; \quad \Omega = 1{,}3107 + 0(x^2).$$

Damit gilt

$$M = \frac{\sigma}{2} \frac{V}{T} \frac{dT}{dx} = \frac{\sigma}{V} U \frac{dU}{dx} = 1{,}818 \frac{U}{V} + 0(x^3)$$

$$\Lambda = \frac{\sigma}{2} \frac{U}{2} \frac{dT}{dx} = 0(x^2).$$

Die exakten Grenzschichtprofile sind für $x=0$, vgl. (2.20).

$$\frac{u_t}{\sqrt{T}} = F_0(\eta)$$

$$\frac{u_n}{\sqrt{T}} \frac{1}{M} = -\frac{1}{1{,}818} \{ F_0(\eta) - 2 f_1'(\eta) \}.$$

Die Näherungsprofile sind für $x=0$

$$\frac{u_t}{\sqrt{T}} = f(\bar{\zeta})$$

$$\frac{u_n}{\sqrt{T}} \frac{1}{M} = -\Omega^2 g\left(\frac{\bar{\zeta}}{\Omega}\right)$$

mit

$$\bar{\zeta} = \frac{z}{\sqrt{\sigma\nu}} = \frac{1}{\sqrt{1{,}818}} z \sqrt{\frac{u_1}{\nu}} = 0.7417\,\eta.$$

Die exakten Lösungen und Näherungslösungen sind in der Abbildung 7 aufgetragen. Sie stimmen sehr gut überein.

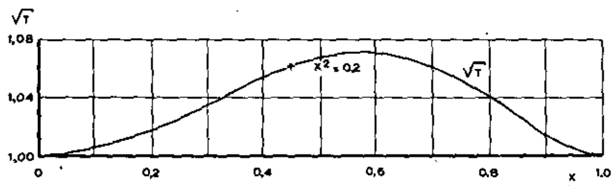

Abb. 17. Zylinderströmung mit $U = x - x^3$, $V = 1$. Die Geschwindigkeitsverteilung.

Weiter sind mit Hilfe der Quadraturgleichung (3.17) und der Integralgleichung (3.12) die Profilparameter σ, Ω und K für eine Zylinderströmung, mit den freien Geschwindigkeitskomponenten $U = x - x^3$, $V = 1$ berechnet. Dabei ist x die Wandbogenlänge längs der Kontur des senkrechten Querschnittes, y der Abstand in der Richtung der Zylinderachse. Der Abstand in der Aussennormalrichtung wird mit z angedeutet $\left(\bar{\zeta} = \frac{z}{\sqrt{\sigma\nu}}\right)$.
Aus den vollständigen Impulsgleichungen folgt der Anfangswert $\sigma = 1{,}818$. Damit wird, nachdem die einfachen Grenzschichtberechnungen ausgeführt sind, die Funktion σ korrigiert (Abb. 18).

Für den schiebenden Zylinder, mit $U = x - x^3$, $V = 1$, sind für verschiedene Werte von x die Geschwindigkeitsprofile der Grenzschicht in der Richtung der Stromlinienkoordinaten mit Hilfe der abgebrochenen Reihenentwicklung und mit der einfachen Methode berechnet. Sie sind in den Abbildungen 8 und 21 gezeichnet. Die, mit der abgebrochenen Reihenentwicklung berechneten, Querstromprofile werden mit zunehmender Entfernung

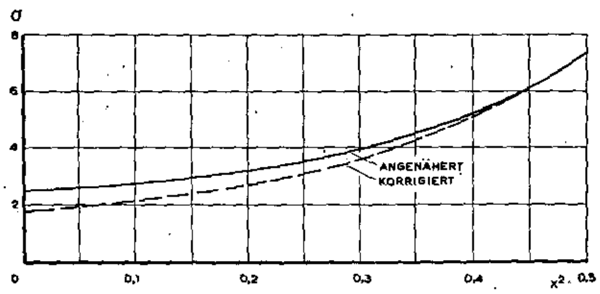

Abb. 18. Zylinderströmung mit $U = x - x^3$, $V = 1$. Die Funktion σ.

von der vorderen Staulinie $x=0$ stets unzuverlässiger. Im Anfang wird der Fehler nicht mehr als einige Prozenten sein. Nach dem Druckminimum $(x = \sqrt{1/3})$ sind die berechneten Profile schon völlig unzuverlässig. Für die einfache Berechnungsmethode ist der Startpunkt des Profilparameters K nicht einwandfrei bestimmt. Bei unserer Berechnung wählen wir dafür den Punkt mit $x^2 = 0.20$, weil von dort ab bis zum Druckminimum die Geschwindigkeitsverteilung U sich nicht mehr stark ändert (Abb. 17).

Für den Verlauf der Profilparameter Ω und K und des Schubspannungskomponenten τ_{0n} an der Wand vergleiche man die Abbildungen 19 und 20.

Die Profile der Querströmung sind in Abb. 21 mit einander verglichen. Dort, wo die abgebrochene

Reihenentwicklung noch brauchbar ist wird eine Übereinstimmung erreicht. In dem Gebiet der verzögerten Strömung treten Rückstromprofile auf. Obwohl diese Profile auch in der Abbildung 8, bei der Berechnung mit der abgebrochenen Reihenentwicklung auftreten, sind sie dort sehr ungenau.

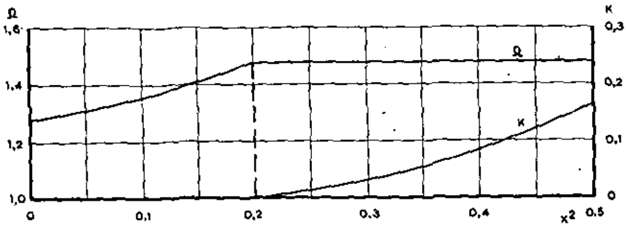

Abb. 19. Zylinderströmung mit $U = x - x^3$, $V = 1$. Die Funktionen Ω und K.

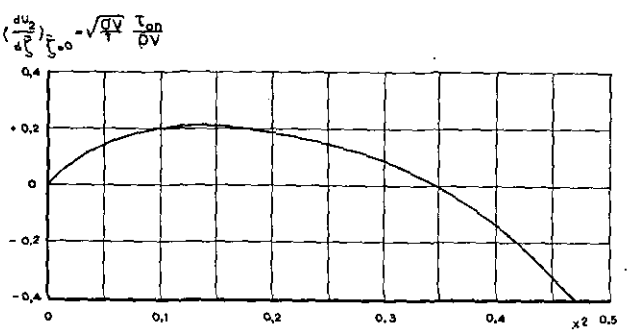

Abb. 20. Zylinderströmung mit $U = x - x^3$, $V = 1$. Der Schubspannungs-Komponent in Querrichtung.

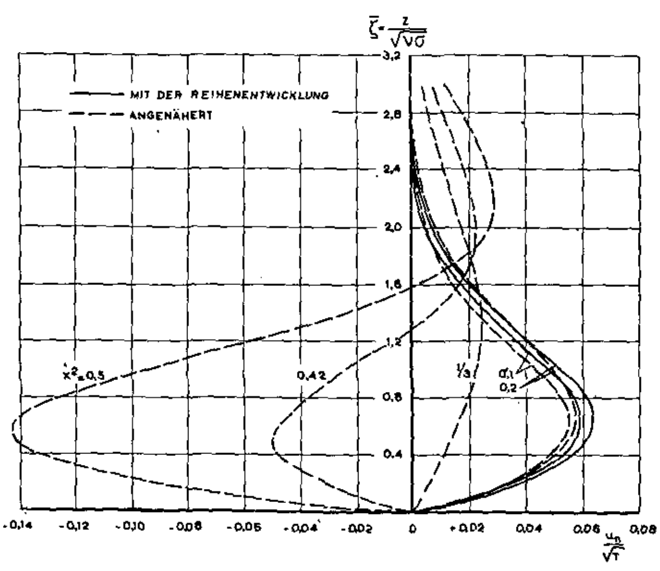

Abb. 21. Zylinderströmung mit $U = x - x^3$, $V = 1$. Die Geschwindigkeitsverteilungen $\frac{u_n}{\sqrt{T}}$ innerhalb der Grenzschicht in der senkrechten Querrichtung der Stromlinien der freien Strömung, für verschiedene Werte von x^2.

Ähnliche Rückstromprofile sind auch schon in der Arbeit [13] gefunden, wo Grenzschichtberechnungen an dem schräg angestromten elliptischen Zylinder ausgeführt sind, und die Querstromprofile aus Berechnungen in der Achsenrichtung und senkrecht darauf zusammengesetzt sind (vgl. Abb. 22).

Für die nicht-wirbelfreie Aussenströmung, beschrieben in Abschnitt 2.4, sind die exakten Grenzschichtprofile in der Abbildung 9 gegeben. Auch dort treten bei der Sekundärströmung ebenfalls Rückstromprofile auf.

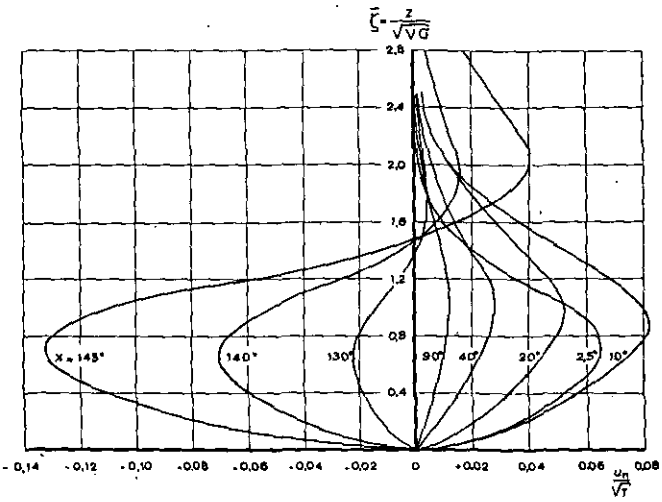

Abb. 22. Die Geschwindigkeitsverteilungen $\frac{u_n}{\sqrt{T}}$ innerhalb der Grenzschicht für den schräg angeströmten elliptischen Zylinder $\frac{x^2}{a^2} + \frac{y^2}{b^2} = 1$ aus der Arbeit 13. Die Profile $\frac{u_n}{\sqrt{T}}$ sind zusammengesetzt aus Profilen in der Richtung der Zylinderachse und senkrecht darauf $\left(\frac{x}{a} = \cos \chi\right)$.

7 Schlussfolgerungen.

Näherungslösungen der dreidimensionalen, laminaren Grenzschichten, — mit Hilfe einer sehr vereinfachten Impulsgleichungsmethode — werden mit exakten Lösungen, folgend aus den Grenzschichtdifferentialgleichungen, verglichen. Es handelt sich dabei um schräge Keil- und Eckströmungen, Strömungen in der Umgebung des Staupunktes und Strömungen an dem schiebenden Zylinder. Bei der Impulsgleichungsmethode sind sowohl in der Richtung der Stromlinien der freien Strömung als in der Querrichtung die Geschwindigkeitsprofile in der Grenzschicht gegeben, und zwar je mit einem Parameter σ und Ω bezw. K. Die Profilparameter σ und Ω, die die Grenzschichtdicken in der Hauptrichtung $(\sqrt{\sigma\nu})$ und in der Querrichtung $(\Omega\sqrt{\sigma\nu})$ bestimmen, werden mit den Näherungsformeln (3.1) und (3.2) einfach berechnet.

Im Anfangspunkt (Staupunkt, Staulinie, scharfe Vorderseite einer Fläche) können die, mit den vollständigen Impulsgleichungen berechneten, Werte σ bedeutend verschieden sein von den Anfangswerten σ, die aus der einfachen Methode folgen (vgl. Abschnitt 4). In diesem Falle muss der Verlauf von σ etwa bis zum Druckminimum korrigiert werden und in Übereinstimmung mit den Ergebnissen der vollständigen Impulsgleichungen gebracht werden. Man vergleicht dazu in den Abbildungen 14, 15 und 18 die gestrichelten Kurven mit den ausgezogenen Kurven. Ist der, mit den vollständigen Impulsgleichungen berechnete, Anfangswert σ bekannt, dann kann die korrigierte Kurve aus freier Hand gezogen werden, falls man die Gestalt einer affinen Verzerrung beibehält.

Die Ω-Kurven brauchen meistens nicht mehr korrigiert zu werden. Die Korrektion von σ wird erst nachträglich ausgeführt, nachdem die einfachen Grenzschichtgleichungen (3.1) und (3.2) gelöst sind. Auch die für die Grenzschichtprofile nötigen Werte Λ und M werden dann mit den korrigierten Werten von σ berechnet.

Wie die Abbildungen 3, 5, 6, 7 und 8 zeigen, stimmen — unter Anwendung der korrigierten Werte σ — die Näherungslösungen der Geschwindigkeitsprofile ziemlich gut mit den exakten Lösungen überein. Für die Stromlinien an der Wand ist die Übereinstimmung ausserordentlich gut (Bild 16).

Wird dort, wo es nötig ist, die Korrektion in σ nicht angebracht, dann ist im allgemeinen keine gute Übereinstimmung mit der exakten Lösung zu erwarten (siehe Abb. 3a).

In Abb. 9 sind die exakten Lösungen der Grenzschichtprofile in dem Übergangsgebiet von der beschleunigten zu der verzögerten freien Strömung gegeben. Obwohl die Aussenströmung dabei nicht wirbelfrei ist, gibt die Sekundärströmung doch eine Aussage über die Gestalt der Querstromprofile. Enthält die Stromlinie der freien Aussenströmung einen Wendepunkt, dann ergibt sich, dass das frühere gegebene Querstromprofil $u_2 = -\Omega^2 Mg\left(\frac{\zeta}{\Omega}\right)$ in dem Übergangsgebiet *von der beschleunigten zu* der verzögerten Strömung mittels eines Zusatzglieds korrigiert werden muss. Dadurch verschwindet auch der frühere Schönheitsfehler des unendlich werden von Ω in diesem Gebiet. Diese Korrektion ist in Abschnitt 3 beschrieben und auf den Fall des schiebenden Zylinders angewandt (vgl. Abschnitt 6). Ein genaues Kriterium für die Wahl des Startpunktes des Korrekturprofils fehlt noch, weil kein Vergleich mit exakten Lösungen vorhanden ist. Vorläufig wird als Startpunkt des Korrekturprofils ein Punkt gewählt, von wo bis zu dem Druckminimum die Geschwindigkeitsverteilung sich nur wenig ändert.

Hat die Strömung einen Staupunkt, dann können die Anfangswerte σ und Ω in diesem Punkt, berechnet mit den vollständigen Impulsgleichungen, unmittelbar aus der Abbildung 13 abgelesen werden. Dazu benötigt man die linearen Glieder der Reihenentwicklung der Geschwindigkeitskomponenten in der Richtung von zwei orthogonalen Koordinaten in der Tangentialebene im Staupunkt (vgl. Abschnitt 5).

Schliesslich wird an dieser Stelle nochmals hingewiesen auf die Bemerkung am Ende des Abschnitts 2.2, wobei die Erwartung ausgesprochen wird, dass auch bei Anströmung eines Körpers unter Anstellwinkel die Querstromprofile stets klein gegenüber den Hauptstromprofilen bleiben. Folglich ist offenbar auch hier die vereinfachte Impulsgleichungsmethode für Grenzschichtberechnungen ohne weiteres anwendbar.

8 Literatur.

1. ZAAT, J. A. A simplified method for the calculation of three-dimensional laminar boundary layers. NLL Report F. 184 (1956).
2. HOWARTH, L. The boundary layer in three-dimensional flow. Part II. The flow near a stagnation point. Phil. Mag., Series 7, *Vol.* 42, *pp.* 1433—1440, 1951.
3. GÖRTLER, H. Zur laminaren Grenzschicht am schiebenden Zylinder. Teil 1. Archiv der Math., Vol. III, S. 216—231, 1952.
4. HANSEN, A. und HERZIG, H. Cross flows in laminar incompressible boundary layers. NACA T. N. 3651 (1956).
   Experimental and analytical investigation of secondary flows in ducts. Journal of the Aeron. Sciences, Vol. 24, No. 3, pp. 217—231, March, 1957.
5. MANGLER, W. Die ähnlichen Lösungen der Prandtlschen Grenzschichtgleichungen. Z. angew. Math. Mech. Bd. 23, S. 241—251, 1943.
6. SMITH, A. M. O. Method of computing general laminar boundary layer flows by piecewise application of the Falkner-Skan solutions. Douglas Aircraft Company, California, June 1954.
7. COOKE, J. C. The boundary layer of a class of infinite yawed cylinders. Proc. of the Cambr. Phil. Soc. 46, S. 645—648 (1950).
8. ULRICH, A. Die laminare Reibungsschicht am Kreiszylinder. Aerodyn. Inst. der T. H., Braunschweig, 1943.
9. TIMMAN, R. und ZAAT, J. A. Eine Rechenmethode für dreidimensionale laminare Grenzschichten. 50 Jahre Grenzschichtforschung, Friedr. Vieweg u. Sohn, Braunschweig, S. 432—445, 1955.
10. ZAAT, J. A., SPIEGEL, E. VAN, TIMMAN, R. The three-dimensional laminar boundary layer flow about a yawed ellipsoid at zero incidence. NLL Report F. 165, 1955. Transactions of the Nat. Aero. Res. Inst. A'dam S. 1—16, 1955.
11. LAMB, H. Hydrodynamics, 5th Ed., 1935. Cambridge University Press.
12. MUNK, M. Durand: Aerodynamic Theory I, 1934. *Springer, Berlin.*
13. ZAAT, J. A. Anwendung der Stromlinienkoordinaten für die Grenzschichtberechnung am schräg angeströmten Zylinder. NLL Report F. 194, 1956.

C.C.L. Class. D 023; D 421

REPORT TR F. 206.

Linearized theory of lifting sweptback wings at sonic speed

by

W. ECKHAUS and E. M. DE JAGER.

Summary.

A linearized theory is presented for the determination of the load distribution on sweptback wings at sonic speed. The method is valid for any given camber and twist of the wing, with the only restriction that the downwash on the wing is assumed to be symmetrical with respect to the axis of symmetry of the wing; the case of antisymmetrical downwash can be treated, with some modifications, in the same way. The theory is applied to two flat sweptback wings at incidence, one without taper and the other with taper.

Comparisons have been made with other theories in which the same problem is treated.

Contents.

This investigation has been sponsored by the Netherlands Aircraft Development Board (N.I.V.).

Symbols.

a_i	$i = 0,1, \dots 5$ coefficients of development of $g(\eta)$.
a_i^*	$i = 0,1 \dots 5$ coefficients of another development of $g(\eta)$.
$\bar{a}_i =$	$\left(\frac{b}{t}\right)^i a_i^* \quad i = 1, 2, \dots 5$.
b	wing-semispan at the cross-section through the kink of the trailing edge.
c	semi-chord of the centre-section of the wing.
d	abscis of the most forward point of the wing-tip.
e	abscis of the most rearward point of the wing.
$g(\eta)$	vorticity in the wake; η is spanwise coordinate.
k	$\sqrt{1 - y_t'^2/y_l'^2}$
k'	$\sqrt{1-k^2} = y_t'/y_l'$
$\bar{k}$	$k'\sqrt{\dfrac{s^2 - y_l^2}{s^2 - y_t^2}}$
$\bar{k}'$	$\sqrt{1-\bar{k}^2}$
$p(x, y)$	load distribution on the wing.
q	dynamic pressure $\frac{1}{2}\rho V^2$.
s	wing semi-span.
t	some parameter larger than s.
$w(x, y)$	down-wash, taken positive in downward direction.
x, y, z	cartesian-coordinates (see sketch a.).
$y_l(x)$	y coordinate of leading edge.
$y_t(x)$	y coordinate of trailing edge.
y_l'	slope of leading edge of right semi-wing.
y_t'	slope of trailing edge of right semi-wing.
C	coefficient of the singular term of $g(\eta)$.
C_L	aerodynamic lift-coefficient.
$E(\psi, k)$	incomplete elliptic function of the second kind; $E(k)$ complete elliptic function of the second kind.
$F(\psi, k)$	incomplete elliptic function of the first kind.

$$F_n(k') = \frac{J_n}{\left(\frac{y_l}{b}\right)^n}$$

$$F_n'(k') = \frac{J_n'}{y_t^2\left(\frac{y_l}{b}\right)^n}$$

$I_1(x, y; \eta') = \frac{1}{2} \frac{1}{y^2 - \eta'^2} \sqrt{\frac{y_l^2 - \eta'^2}{y_t^2 - \eta'^2}}$

$I_2(x, y) = \frac{1}{4} \pi \sqrt{\frac{y_l^2 - y^2}{y^2 - y_t^2}}$

$I_3(x, y; \eta) = \int_{y_t}^{y} \sqrt{\frac{\eta'^2 - y_t^2}{y_l^2 - \eta'^2}} \frac{d\eta'}{\eta'^2 - \eta^2}$

with $y_t \leqq \eta < y_l$ and $y_t < y < y_l$.

$\overline{I}_3(x, y; \eta) = \int_{y_t}^{y} \sqrt{\frac{\eta'^2 - y_t^2}{y_l^2 - \eta'^2}} \frac{d\eta'}{\eta'^2 - \eta^2}$

with $0 \leqq \eta \leqq y_t < y < y_l$.

J_n — $\frac{1}{b^n} \int_0^{y_t} \frac{\eta^{n+1}}{\sqrt{(y_l^2 - \eta^2)(y_t^2 - \eta^2)}} d\eta$

J_n' — $\frac{1}{b^n} \int_0^{y_t} \frac{d}{d\eta} \left\{ \eta^{n+1} \sqrt{y_l^2 - \eta^2} \right\} \frac{\eta d\eta}{\sqrt{y_t^2 - \eta^2}}$

$K(k)$ — complete elliptic function of the first kind with modulus k.

L — $\int_0^{y_t} \frac{1 - \frac{\eta}{b}}{ln \frac{\eta}{b}} \frac{\eta d\eta}{\sqrt{(y_l^2 - \eta^2)(y_t^2 - \eta^2)}}$

L' — $\int_0^{y_t} \frac{d}{d\eta} \left\{ \frac{1 - \frac{\eta}{b}}{ln \frac{\eta}{b}} \eta \sqrt{y_l^2 - \eta^2} \right\} \frac{\eta d\eta}{\sqrt{y_t^2 - \eta^2}}$

L — total lift on the wing, taken positive in upward direction.

$\frac{dL}{dx}$ — lift distribution per unit chord.

M — $\int_0^{y_t} \frac{\eta^2 d\eta}{\sqrt{(s^2 - \eta^2)(y_l^2 - \eta^2)(y_t^2 - \eta^2)}}$

M' — $\int_0^{y_t} \frac{d}{d\eta} \left\{ \eta^2 \sqrt{\frac{y_l^2 - \eta^2}{s^2 - \eta^2}} \right\} \frac{\eta d\eta}{\sqrt{y_t^2 - \eta^2}}$

M — MACH number.

P — polynomial of the fifthdegree.

$S(y_t, y_l)$ — $\int_0^{y_t} \frac{g(\eta) \cdot \eta}{\sqrt{(y_l^2 - \eta^2)(y_t^2 - \eta^2)}} d\eta.$

$S^*(y_t, y_l)$ — $1 + \frac{S(y_t, y_l)}{\alpha V \pi}$

$T(y_t, y_l)$ — $\int_0^{y_t} \frac{d}{d\eta} \left\{ g(\eta) \cdot \eta \cdot \sqrt{y_l^2 - \eta^2} \right\} \frac{\eta d\eta}{\sqrt{y_t^2 - \eta^2}}$

U — free stream velocity.

V — velocity of sound.

$W(x, y)$ — $-\frac{4\rho V}{\pi} \int_{y_t}^{y_l} w(x, \eta) \sqrt{\frac{y_l^2 - \eta^2}{\eta^2 - y_t^2}} \cdot \eta \cdot I_3(x, y; \eta) d\eta.$

$Z(x, y)$ — $-\frac{2\rho V}{\pi} \int_0^{y_t} g(\eta) \sqrt{\frac{y_l^2 - \eta^2}{y_t^2 - \eta^2}} \cdot \eta \cdot \overline{I}_3(x, y; \eta) d\eta.$

α — angle of incidence, taken positive in clockwise direction.

β — $\sqrt{1 - M^2}$.

γ — $\frac{y_t'}{y_l'}$

γ_x — x-component of the vorticity vector.

η, η' — integration variable in spanwise direction.

ξ — integration variable in x direction.

ρ — density.

ψ — $\sin^{-1} \sqrt{\frac{y_l^2 - y^2}{y_l^2 - y_t^2}}$

$\Lambda_0(\psi, \bar{k})$ — HEUMAN's lambda function with argument ψ and modulus $\bar{k}$.

1 Introduction.

In order to calculate the forces on air-ships in low-speed flight, in 1924 MUNK developed an approximate theory of the flow past slender bodies, elongated in the direction of flight (ref. 1).

In this theory the flow pattern near the body in any transverse section is assumed to be the same as in two-dimensional incompressible flow.

In 1946 R. T. JONES extended MUNK's theory to low-aspect-ratio pointed wings (ref. 2) and this extension gave rise to many publications on the subject of calculating the flow about slender wings, slender bodies and slender wing-body combinations (see e. g. ref. 3 and ref. 4).

The assumption that the flow pattern near the body or the wing in any transverse section is the same as in two-dimensional incompressible flow means mathematically, that in the PRANDTL-GLAUERT equation for the perturbation velocity potential the term $(1 - M^2)\varphi_{xx}$ is neglected (M denotes the free-stream MACH number). This approximation is allowed when the body or the wing is elongated in the direction of the flow but also in the case of wings, not necessarily slender, without thickness, when M equals unity (see ref. 5).

By aid of slender body- and slender wing-theory a first approximation is obtained for the flow about wings without thickness and not necessarily slender at sonic speed. The slender-wing theory gives the flow around wings in a simple and elegant way, when the two-dimensional cross-flow contains no shed vortex sheet, as e. g. for a delta wing. However when in the two-dimensional cross-flow a shed vortex sheet is present, as is the case for wings with a swept trailing edge, the determination of the flow around the wing and hence of the pressure on the wing is much more complicated.

In ref. 6 LOMAX and HEASLET considered the inverse problem, where the assumption was made, that there is no vortex sheet present behind the swept wing and where consecutively the form of the trailing edge is calculated, which would give rise to the absence of a vortex sheet behind the wing. The direct problem, where the wing planform and the downwash on the wing is completely specified, is of course much more difficult to solve.

In ref. 7 ROBINSON has treated the lift problem for a wing of given planform with swept trailing edge; his solution however is only valid, when the trailing edge is slightly swept (see ref. 8).

In ref. 9 EICHELBRENNER has succeeded in deriving *an integral equation for the unknown vorticity in the wake of the wing*; this integral equation is very complicated and according to the authors' knowledge it has never been solved up to now; when this integral equation would have been solved, the perturbation velocity potential and the wing pressure could be determined.

Finally, MANGLER in ref. 10 and MIRELS in ref. 11 have treated the swept wing completely and they have determined the load distribution on flat swept wings at incidence, in steady roll and in steady pitch.

These solutions of MANGLER and MIRELS *are not valid for a general prescribed downwash on the wing*, but MANGLER *has also given* (see ref. 12) a new method for calculating the wing pressure on swept wings for arbitrary downwash, provided the downwash distribution is continuous in streamwise direction, the case of deflected flaps being outside the scope of his paper. MANGLER has applied this method only to the case of cropped deltawings; the case of sweptback wings will lead to rather cumbersome numerical calculations.

Whereas MANGLER starts from the integral equation, relating the downwash to the load distribution, *in the present report the integral equation, relating the downwash to the vorticity component in streamwise direction, has been taken as the starting point.* The formulae which now determine the load distribution on the wing seem somewhat simpler than those of MANGLER and it may be, that they are *a more appropriate starting point for the determination of the load distribution on swept swings for general prescribed downwash*; moreover by aid of this method some knowledge about the behaviour of the vorticity in the wake is obtained, which is an interesting additional result especially for the vorticity in the neighbourhood of the kink of the trailing edge.

In this paper the downwash is assumed to be symmetrical with respect to the axis of symmetry of the wing. The case of antisymmetrical downwash can be treated with some modifications in the same way as for symmetrical downwash, and will be presented in a subsequent paper.

All the derivations and deductions which are not strictly necessary for the understanding of the contents of this report are presented in a separate report, viz.: NLL report F. 206a "Linearized theory of lifting swept back wings at sonic speed; (derivations of formulae)."

After this report was finished, the authors received a paper of E. TRUCKENBRODT, where the same problem is treated and where a numerical calculation of the lift distribution for sweptback wings with arbitrary camber and twist is presented. (see lit. 18).

The authors wish to thank Mr. J. G. WOUTERS, under whose direction the numerical computations have been performed.

2 Basic concepts and formulation of the problem.

In keeping with the concepts of linear theory the wing is considered an impenetrable surface, which lies nearly in the (x, y) plane, and the downwash $w(x, y)$, taken positive in downward direction, is prescribed in the region A, the projection of the wing on the (x, y) plane (see sketch a). The coordinate

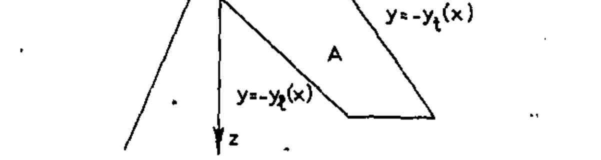

Sketch a.

system and the surface A are assumed to move in the direction of the negative x-axis at a uniform velocity U. The lift distribution $p(x, y)$ on the wing, taken positivily in upward direction, is now determined by the following well known integral equation:

$$w(x,y) = -\frac{1}{4\pi\rho U} \iint_A \frac{1}{(y-\eta)^2} \left\{ 1 + \frac{x-\xi}{\sqrt{(x-\xi)^2 + \beta^2 (y-\eta)^2}} \right\} p(\xi,\eta)\, d\xi d\eta \tag{2.1}$$

ρ denoting air density and $\beta = \sqrt{1 - M^2}$, with M as MACH number; the integral is taken in the sense of HADAMARD.

When the velocity of the wing equals the velocity of sound the integral equation (2.1) can be reduced to a much simpler form by putting β equal to zero and U equal to the velocity of sound V; doing this one obtains:

$$w(x,y) = -\frac{1}{2\pi\rho V} \times\!\!\!\!\int_{-y_l(x)}^{+y_l(x)} \frac{1}{(y-\eta)^2} \left\{ \int_{-c}^{x} p(\xi,\eta)d\xi \right\} d\eta \tag{2.2}$$

where $y = y_l(x)$ is the equation of the leading edge of the wing and $-c$ the x-coordinate of the most forward point of the wing; the cross in the integral sign denotes that the finite part has to be taken.

Using the relation between the pressure distribution and the x-component $\gamma_x(x,y)$ of the vorticity vector, viz.:

$$\frac{\partial}{\partial y} p(x,y) = -\rho V \frac{\partial \gamma_x(x,y)}{\partial x} \tag{2.3}$$

and integrating (2.2) by parts one obtains the well known integral equation of slender wing theory:

$$w(x,y) = \frac{1}{2\pi} \int_{-y_l(x)}^{+y_l(x)} \frac{\gamma_x(x,\eta)}{\eta - y} d\eta \tag{2.4}$$

where the flow in some plane $x = \text{constant}$ is treated as a two-dimensional incompressible flow, with given downwash along the intersection of the wing and the plane $x = \text{constant}$.

For some literature about slender wing theory the reader is referred to refs. 1, 2, 3, 4 and 13.

A formula for the lift distribution on the wing, which expresses $p(x,y)$ in the x-component of the vorticity vector, can be obtained by integrating (2.3) with respect to y, viz:

$$p(x,y) = \rho V \times\!\!\!\!\int_{y}^{y_l(x)} \frac{\partial \gamma_x(x,\eta)}{\partial x} d\eta = \rho V \frac{\partial}{\partial x} \int_{y}^{y_l(x)} \gamma_x(x,\eta) d\eta \tag{2.5}$$

Hence for the determination of the lift distribution on the wing, equation (2.4) is inverted and the result is substituted into equation (2.5); this process will be carried out in the following sections 3 and 4.

In this report the downwash will be assumed symmetrical with respect to the x-axis; the deductions for antisymmetrical downwash run along the same lines as those given below for symmetrical downwash and similar results which will be presented in a subsequent paper can easily be obtained.

3 Solution of the integral equation.

The solutions of singular integral equations of the type (2.4), where the integral must be taken in the sense of CAUCHY, are well known today in theoretical aerodynamics; the form of the various possible solutions depends on the conditions, which are to be imposed on the unknown function $\gamma_x(x,y)$, as whether this function becomes integrable infinite or zero at one or both limits of the integration interval.

The solutions, necessary in this section, have been given already by SÖHNGEN in 1939, ref. (14), and a full account of the theory of this type of singular integral equations has been given in textbooks, such as ref. (15) and ref. (16). When $+c$ is the x-coordinate of the most forward point of the trailing edge, two cases have to be considered, according as the value of x is larger or smaller than c.

3.1 *Solution of the integral equation for $-c \leqq x \leqq +c$.*

For $x \leqq c$ the downwash is a given function of x and y along the whole integration interval and $\gamma_x(x,y)$ remaining of course integrable becomes infinite for $y = \pm y_l(x)$.

The solution of equation (2.4) is now

$$\gamma_x(x,y) = \frac{2}{\pi} \frac{1}{\sqrt{\{y_l(x)\}^2 - y^2}} \int_{-y_l(x)}^{+y_l(x)} \frac{w(x,\eta)}{y-\eta} \sqrt{\{y_l(x)\}^2 - \eta^2}\, d\eta + \frac{1}{\pi} \frac{1}{\sqrt{\{y_l(x)\}^2 - y^2}} \int_{-y_l(x)}^{+y_l(x)} \gamma_x(x,\eta) d\eta$$

(see refs. 14, 15, 16), which according to HELMHOLTZ's law of conservation of vorticity reduces to

$$\gamma_x(x,y) = \frac{2}{\pi} \frac{1}{\sqrt{\{y_l(x)\}^2 - y^2}} \int_{-y_l(x)}^{+y_l(x)} \frac{w(x,\eta)}{y-\eta} \sqrt{\{y_l(x)\}^2 - \eta^2}\, d\eta. \tag{3.1}$$

In the case of a flat plate at an angle of attack this formula reduces to

$$\gamma_x(x,y) = 2\,\alpha\, V \frac{y}{\sqrt{y_l^2 - y^2}} \tag{3.2}$$

Substitution of (3.1) into equation (2.5) yields, after interchanging the order of integration and remembering the symmetry of $w(x, \eta)$, for the lift distribution on the wing for $-c \leqq x \leqq +c$

$$p(x, y) = \frac{2\rho V}{\pi} \frac{\partial}{\partial x} \left[\int_0^{y_l(x)} w(x, \eta) \sqrt{y_l^2 - \eta^2} \left\{ \int_y^{y_l(x)} \frac{2y'}{y'^2 - \eta^2} \frac{dy'}{\sqrt{y_l^2 - y'^2}} \right\} d\eta \right] =$$

$$\frac{2\rho V}{\pi} \frac{\partial}{\partial x} \left[\int_0^{y_l(x)} w(x, \eta) \log \left| \frac{\sqrt{y_l^2 - \eta^2} + \sqrt{y_l^2 - y^2}}{\sqrt{y_l^2 - \eta^2} - \sqrt{y_l^2 - y^2}} \right| d\eta \right]. \tag{3.3}$$

Substitution of (3.2) in equation (2.5) yields the lift distribution on the flat plate at incidence for $-c \leqq x \leqq +c$ and the result is:

$$p(x, y) = 2\alpha\rho V^2 \frac{y_l \frac{dy_l}{dx}}{\sqrt{y_l^2 - y^2}} = 4\alpha q \frac{y_l \frac{dy_l}{dx}}{\sqrt{y_l^2 - y^2}} \tag{3.4}$$

where q denotes the dynamic pressure which equals $\frac{1}{2}\rho V^2$; formula (3.4) is a well known result of slender wing theory, already found by R. T. Jones in ref. 2.

3.2 *Solution of the integral equation for $x > c$.*

For $x > c, w(x, y)$ is no longer a given function of x and y along the whole integration interval, but is in fact unknown for $-y_t(x) < y < +y_t(x)$, $y = y_t(x)$ being the equation of the trailing edge of the wing; the solution is now more complicated than in the case of $x \leqq c$. Equation (2.4) can be written as:

$$w(x, y) = \frac{1}{2\pi} \left\{ \int_{-y_l}^{-y_t} \frac{\gamma_x(x, \eta)}{\eta - y} d\eta + \int_{-y_t}^{0} \frac{\gamma_x(x, \eta)}{\eta - y} d\eta + \int_0^{y_t} \frac{\gamma_x(x, \eta)}{\eta - y} d\eta + \int_{y_t}^{y_l} \frac{\gamma_x(x, \eta)}{\eta - y} d\eta \right\}.$$

Replacing in the first two integrals η by $-\eta$ and using $\gamma_x(x, y) = -\gamma_x(x, -y)$, which is true due to the symmetry of $w(x, y)$, the last expression can also be written as:

$$\pi w(x, y) = \int_0^{y_t} \frac{\gamma_x(x, \eta)}{\eta^2 - y^2} \eta \, d\eta + \int_{y_t}^{y_l} \frac{\gamma_x(x, \eta)}{\eta^2 - y^2} \eta \, d\eta$$

by which the problem of solving $\gamma_x(x, y)$ is reduced to a problem for the right semi-wing only; $\gamma_x(x, y)$ for the left semi-wing can of course be obtained by considerations of symmetry.

As $p(x, y)$ is zero in the wake, it follows immediately from eq. (2.3) that $\gamma_x(x, y)$ is a function of y only, when $-y_t < y < +y_t$. Hence it is allowed to replace in the first integral $\gamma_x(x, \eta)$ by $g(\eta)$ and the last equation becomes equivalent with

$$\pi w^*(x, y) = \int_{y_t}^{y_l} \{ \gamma_x(x, \eta) - \gamma_x(x, y_t) \} \frac{\eta d\eta}{\eta^2 - y^2} \tag{3.5}$$

where

$$\pi w^*(x, y) = \pi w(x, y) - \tfrac{1}{2} \gamma_x(x, y_t) \ln \frac{y_l^2 - y^2}{y^2 - y_t^2} - \int_0^{y_t} g(\eta) \frac{\eta d\eta}{\eta^2 - y^2} \tag{3.6}$$

Equation (3.5) will now be solved for $\gamma_x(x, y)$ which in this way will be expressed in the known downwash at the wing and the as yet unknown vorticity $g(y)$ in the wake. Substituting $\lambda = \eta^2$, eq. (3.5) becomes:

$$2\pi w^*(x, y) = \int_{y_t^2}^{y_l^2} \{ \gamma_x(x, \sqrt{\lambda}) - \gamma_x(x, y_t) \} \frac{d\lambda}{\lambda - y^2} \quad y_t < y < y_l. \tag{3.7}$$

This is again an integral equation of the Cauchy type, containing the unknown function $\{ \gamma_x(x, \eta) - \gamma_x(x, y_t) \}$ which is integrable infinite at the upper limit and zero at the lower limit of the integration interval; the purpose of the substraction of $\gamma_x(x, y_t)$ from $\gamma_x(x, \eta)$ was of course to get the zero condition at one of the limits of the integration interval. The solution of (3.7) is according to refs. 14, 15 and 16:

$$\gamma_x(x, y) - \gamma_x(x, y_t) = \frac{2}{\pi}\sqrt{\frac{y^2 - y_t^2}{y_l^2 - y^2}} \int_{y_t^2}^{y_l^2} \frac{w^*(x, \sqrt{\lambda})}{y^2 - \lambda}\sqrt{\frac{y_l^2 - \lambda}{\lambda - y_t^2}}\, d\lambda \tag{3.8}$$

Putting again $\lambda = \eta^2$, substituting (3.6) into (3.8) and reversing the order of integration in the double integral which originates from the third term of (3.6) one obtains finally:

$$\gamma_x(x, y) - \gamma_x(x, y_t) = \frac{4}{\pi}\sqrt{\frac{y^2 - y_t^2}{y_l^2 - y^2}} \left\{ \int_{y_t}^{y_l} \frac{w(x, \eta)}{y^2 - \eta^2}\sqrt{\frac{y_l^2 - \eta^2}{\eta^2 - y_t^2}}\, \eta d\eta + \int_0^{y_t} g(\eta')\eta' I_1(x, y; \eta')d\eta' - \gamma_x(x, y_t)\, I_2(x, y) \right\} \tag{3.9}$$

where

$$I_1(x, y; \eta') = \frac{1}{\pi}\int_{y_t}^{y_l} \sqrt{\frac{y_l^2 - \eta^2}{\eta^2 - y_t^2}} \frac{\eta d\eta}{(y^2 - \eta^2)(\eta^2 - \eta'^2)} = +\tfrac{1}{2}\, \frac{1}{y^2 - \eta'^2}\sqrt{\frac{y_l^2 - \eta'^2}{y_t^2 - \eta'^2}} \tag{3.10}$$

$$I_2(x, y) = \frac{1}{\pi}\int_{y_t}^{y_l} \left\{ \ln \sqrt{\frac{y_l^2 - \eta^2}{\eta^2 - y_t^2}} \right\} \sqrt{\frac{y_l^2 - \eta^2}{\eta^2 - y_t^2}} \frac{\eta d\eta}{y^2 - \eta^2} = \tfrac{1}{4}\pi \sqrt{\frac{y_l^2 - y^2}{y^2 - y_t^2}} \tag{3.11}$$

For the reduction of both integrals the reader is referred to lit. 17 (sections 1 and 2). Substitution of (3.10) and (3.11) in (3.9) finally yields for the x-component of the vorticity vector on the wing:

$$\gamma_x(x, y) = \frac{4}{\pi}\sqrt{\frac{y^2 - y_t^2}{y_l^2 - y^2}} \left\{ \int_{y_t}^{y_l} \frac{w(x, \eta)}{y^2 - \eta^2}\sqrt{\frac{y_l^2 - \eta^2}{\eta^2 - y_t^2}}\, \eta d\eta + \tfrac{1}{2}\int_0^{y_t} g(\eta)\sqrt{\frac{y_l^2 - \eta^2}{y_t^2 - \eta^2}}\, \frac{\eta d\eta}{y^2 - \eta^2} \right\}$$

$$y_t < y < y_l;\ x > c. \tag{3.12}$$

When y_t tends to zero, the righthand side of this equation becomes equal to the righthand side of equation (3.1), if in equation (3.1) symmetry is also introduced. Hence $\gamma_x(x, y)$ is continuous in x along the line $x = c$, as could be expected from physical considerations.

Substituting the relation (3.12) into equation (2.5) one obtains after interchanging the order of integration the lift distribution $p(x, y)$ on the wing:

$$p(x, y) = -\frac{4\rho V}{\pi}\, \frac{\partial}{\partial x}\left[\int_{y_t}^{y_l} w(x, \eta)\sqrt{\frac{y_l^2 - \eta^2}{\eta^2 - y_t^2}}\, \eta\, I_3(x, y; \eta)d\eta + \tfrac{1}{2}\int_0^{y_t} g(\eta)\sqrt{\frac{y_l^2 - \eta^2}{y_t^2 - \eta^2}}\, \eta\, \bar{I}_3(x, y; \eta)d\eta \right]$$

$$y_t < y < y_l;\ x > c \tag{3.13}$$

where

$$\left.\begin{aligned} I_3(x, y; \eta) &= -\int_y^{y_l} \sqrt{\frac{\eta'^2 - y_t^2}{y_l^2 - \eta'^2}}\, \frac{d\eta'}{\eta'^2 - \eta^2} \quad \text{with } y_t \leqq \eta \leqq y_l \text{ and } y_t < y < y_l \\ &\text{and} \\ \bar{I}_3(x, y; \eta) &= -\int_y^{y_l} \sqrt{\frac{\eta'^2 - y_t^2}{y_l^2 - \eta'^2}}\, \frac{d\eta'}{\eta'^2 - \eta^2} \quad \text{with } 0 \leqq \eta \leqq y_t < y < y_l \end{aligned}\right\} \tag{3.14}$$

From equation (3.13) it is seen that the lift distribution on the wing consists of two terms, one containing the downwash on the wing, which is a known function of x and y and the other containing the vorticitiy $g(\eta)$ in the wake which is as yet an unknown function of η.

Equation (3.13) is still rather complicated; it is however possible to simplify the formula considerably by performing in the right hand side the differentiation with respect to x in an appropriate way. This will be done in the next chapter.

4 The lift-distribution on the wing.

The righthand side of the expression (3.13) for the lift distribution on the wing consists of two terms, which will be denoted by $\frac{\partial W(x,y)}{\partial x}$ and $\frac{\partial Z(x,y)}{\partial x}$, where

$$W(x,y) = -\frac{4\rho V}{\pi}\int_{y_t}^{y_l} w(x,\eta)\sqrt{\frac{y_l^2-\eta^2}{\eta^2-y_t^2}}\,\eta\, I_3(x,y;\eta)\,d\eta \tag{4.1}$$

and

$$Z(x,y) = -\frac{2\rho V}{\pi}\int_{0}^{y_t} g(\eta)\sqrt{\frac{y_l^2-\eta^2}{y_t^2-\eta^2}}\,\eta\,\overline{I}_3(x,y;\eta)\,d\eta \tag{4.2}$$

Hence

$$p(x,y) = \frac{\partial}{\partial x}\,[W(x,y) + Z(x,y)] \tag{4.3}$$

The first term $\frac{\partial}{\partial x}W(x,y)$ can always be calculated either exactly or numerically, since $w(x,y)$ is a given function of x and y on the wing. The operation

$$\frac{\partial}{\partial x} = \frac{dy_l}{dx}\left(\frac{\partial}{\partial y_l}\right) + \frac{dy_t}{dx}\left(\frac{\partial}{\partial y_t}\right)$$

has been applied to the function $Z(x,y)$ in lit. 17, section 3. The result is

$$\frac{\partial Z(x,y)}{\partial x} = \frac{2\rho V}{\pi y_l}\left[\left\{y\sqrt{\frac{y^2-y_t^2}{y_l^2-y^2}} + y_l\,E(\psi,k)\right\}\frac{dy_l}{dx}\int_0^{y_t} g(\eta)\frac{\eta\,d\eta}{\sqrt{(y_l^2-\eta^2)(y_t^2-\eta^2)}} + \right.$$

$$\left. + \frac{F(\psi,k)}{y_t}\,\frac{dy_t}{dx}\int_0^{y_t}\frac{d}{d\eta}\left\{g(\eta)\,.\,\eta\sqrt{y_l^2-\eta^2}\right\}\frac{\eta\,d\eta}{\sqrt{y_t^2-\eta^2}}\right] \tag{4.4}$$

where $F(\psi,k)$ and $E(\psi,k)$ respectively are incomplete elliptic functions of the first and second kind with argument

$$\psi = \sin^{-1}\sqrt{\frac{y_l^2-y^2}{y_l^2-y_t^2}} \text{ and modulus } k = \sqrt{1-y_t^2/y_l^2}.$$

Putting

$$\int_0^{y_t} g(\eta)\frac{\eta\,d\eta}{\sqrt{(y_l^2-\eta^2)(y_t^2-\eta^2)}} = S(y_t,y_l) \tag{4.5}$$

and

$$\int_0^{y_t}\frac{d}{d\eta}\left\{g(\eta)\,.\,\eta\,.\sqrt{y_l^2-\eta^2}\right\}\frac{\eta\,d\eta}{\sqrt{y_t^2-\eta^2}} = T(y_t,y_l) \tag{4.6}$$

the formula for the lift distribution becomes:

$$p(x,y) = \frac{\partial}{\partial x}\{W(x,y)\} + \frac{2\rho V}{\pi y_l}\left[\left\{y\sqrt{\frac{y^2-y_t^2}{y_l^2-y^2}} + y_l E(\psi,k)\right\}\frac{dy_l}{dx}\,S(y_t,y_l) + \right.$$

$$\left. + \frac{dy_t}{dx}\,\frac{F(\psi,k)}{y_t}\,T(y_t,y_l)\right]. \tag{4.7}$$

Applying the KUTTA condition at the trailing edge of the wing gives a relation between S and T which enables the elimination of $T(y_t,y_l)$.
The KUTTA condition follows from eq. (4.7) by setting $y = y_l$ and $p(x,y) = 0$, viz.:

$$y_l\frac{dy_l}{dx}E(k)S(y_t,y_l) + \frac{1}{y_t}\,\frac{dy_t}{dx}K(k)T(y_t,y_l) = -\frac{\pi y_l}{2\rho V}\left[\frac{\partial}{\partial x}W(x,y)\right]_{y=y_l}. \tag{4.8}$$

Eliminating $T(y_t, y_l)$ from equations (4.7) and (4.8) finally yields for the lift distribution on the wing the formula:

$$p(x,y) = \frac{2\rho V}{\pi} \frac{dy_l}{dx} S(y_t, y_l) \left\{ E(\psi,k) - \frac{E(k)}{K(k)} F(\psi,k) + \frac{y}{y_l} \sqrt{\frac{y^2 - y_t^2}{y_l^2 - y^2}} \right\} + \\ + \frac{\partial W(x,y)}{\partial x} - \frac{F(\psi,k)}{K(k)} \left[\frac{\partial W(x,y)}{\partial x} \right]_{y=y_t} ; \; y_t < y < y_l \text{ and } x > c. \tag{4.9}$$

Formula (4.9) is valid for arbitrary forms of leading and trailing edges, provided $\frac{dy_l}{dx} \geqq 0$, and for arbitrary symmetrical downwash distributions. This general formula contains still one unknown function, viz. $S(y_t, y_l)$ which appears as a factor and which is moreover a function of x only.

Thus for the determination of the wing pressure it is not required to know exactly the complete vorticity distribution in the wake, represented by the function $g(\eta)$, but the knowledge of the function $S(y_t, y_l)$ is already sufficient. Formula (4.9) yields also the following important result: for the part of the wing with $x > c$ and $\frac{dy_l}{dx} = 0$ the lift distribution is given by the simple formula:

$$p(x,y) = \frac{\partial W(x,y)}{\partial x} - \frac{F(\psi,k)}{K(k)} \left[\frac{\partial W(x,y)}{\partial x} \right]_{y=y_t}, \tag{4.10}$$

this formula being valid for arbitrary symmetrical downwash distribution and arbitrary shape of the trailing edge. Here, the pressure is completely independent of the vorticity distribution in the wake.

For any given symmetrical downwash the two terms, appearing in (4.10), can easily be calculated by aid of (4.1). Hence the lift distribution on swept wings is now known in the region of the tip, when the tip has a straight edge with $\frac{dy_l}{dx} = 0$; in particular the lift distribution on swept wings for which the foremost point of the tip is lying ahead of the most forward point of the trailing edge (see sketch b) is now determined on the whole wing.

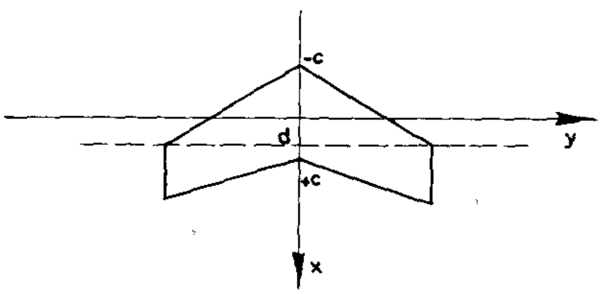

Sketch b.

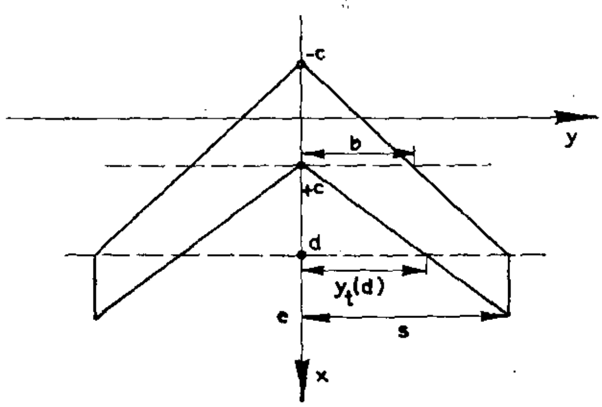

Sketch c.

It is given by equation (3.3) if $x \leqq c$ and by equation (4.10) if $x \geqq c$. For wings of the type of sketch c, foremost point of the tip aft of the most forward point of the trailing edge, the lift distribution for $x < c$ is given by (3.3), for $x > d$ by (4.10), and for $c < x < d$ by formula (4.9). In order to calculate the lift distribution in the latter region, it is necessary to determine the function $S(y_t, y_l)$.

5 Method of determination of the function $S(y_t, y_l)$.

Substituting the expressions (4.5) and (4.6) for the functions $S(y_t, y_l)$ and $T(y_t, y_l)$ into the KUTTA condition (4.8) one obtains:

$$y_l \frac{dy_l}{dx} E(k) \int_0^{y_t} g(\eta) \frac{\eta d\eta}{\sqrt{(y_l^2 - \eta^2)(y_t^2 - \eta^2)}} + \frac{1}{y_l} \frac{dy_l}{dx} K(k) \int_0^{y_t} \frac{d}{d\eta} \left\{ g(\eta) \cdot \eta \cdot \sqrt{y_l^2 - \eta^2} \right\} \frac{\eta d\eta}{\sqrt{y_t^2 - \eta^2}} = \\ - \frac{\pi y_l}{2\rho V} \left\{ \frac{\partial}{\partial x} W(x,y) \right\}_{y=y_t} \tag{5.1}$$

The function $\left\{ \frac{\partial}{\partial x} W(x,y) \right\}_{y=y_t}$ is a known function of x which can be calculated either exactly or numerically and hence the right hand side of (5.1) is known for any given downwash.

The unknown function $g(\eta)$ can be approximated for very small values of η by aid of an asymptotic evaluation of the left and right hand sides of equation (5.1) for y_t tending to zero; this is performed in lit. 17 (section 4). The behaviour of $g(\eta)$ in the neighbourhood of the kink in the trailing edge appears to be:

$$g(\eta) = C\,\frac{1}{\log\eta} + 0\left\{\frac{1}{(\log\eta)^2}\right\} \tag{5.2}$$

with

$$C = \frac{\pi}{2\,\rho V}\left[\frac{\left\{\dfrac{\partial W(x,y)}{\partial x}\right\}_{y=y_t}}{\dfrac{dy_t}{dx}}\right]_{x=c} \tag{5.3}$$

c being the abscis of the kink in the trailing edge.

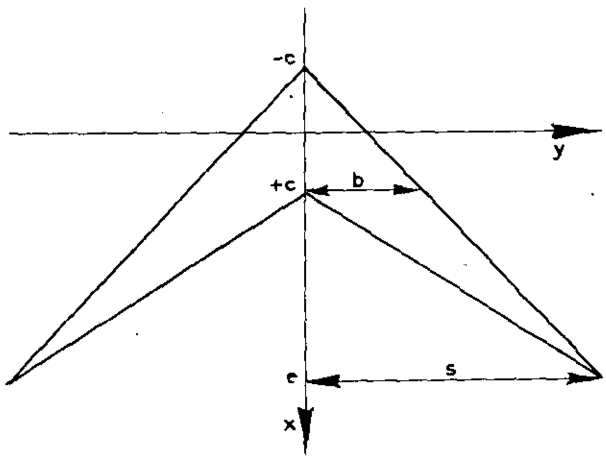

Sketch d.

The behaviour of $g(\eta)$ in the neighbourhood of the tip at $\eta = s$ (see sketch c or d) is given by:

$$g(\eta) = \frac{a_0\eta}{\sqrt{s^2-\eta^2}} + 0(1) \tag{5.4}$$

as is shown in lit. 17, section 5; a_0 is a coefficient, which has to be determined later on. With the knowledge of the asymptotic behaviour of $g(\eta)$ near the ends of the interval $o < \eta < s$, the function $g(\eta)$ in the whole interval can now be approximated by the formula

$$g(\eta) = C\,\frac{1-\dfrac{\eta}{b}}{\log\dfrac{\eta}{b}} + a_0\,\frac{\dfrac{\eta}{b}}{\sqrt{\left(\dfrac{s}{b}\right)^2-\left(\dfrac{\eta}{b}\right)^2}} + P\left(\frac{\eta}{b}\right) \tag{5.5}$$

where $P\left(\dfrac{\eta}{b}\right)$ is some polynomial in $\dfrac{\eta}{b}$.

The semispan b of the wing at $x = c$ is taken as length of reference. In order to avoid a singularity at $\eta = b$ in the logarithmic term of $g(\eta)$, which in reality does not exist, this term is written as $C\,\dfrac{1-\dfrac{\eta}{b}}{\log\dfrac{\eta}{b}}$ which is asymptotically equal to $\dfrac{C}{\log\eta}$ for $\eta \to 0$.

The polynomial $P\left(\dfrac{\eta}{b}\right)$ is written as:

$$P\left(\frac{\eta}{b}\right) = \sum_{n=1}^{m} a_n\left(\frac{\eta}{b}\right)^n \tag{5.6}$$

the constant term being omitted, since $g(\eta)$ equals zero for $\eta = 0$.

Substituting now (5.5) into equation (5.1) and dividing by y_l one obtains:

$$y_l' E(k) \left\{ C L + a_0 M + \sum_{n=1}^{m} a_n J_n \right\} + y_t' k' K(k) \frac{1}{y_t^2} \left\{ CL' + a_0 M' + \sum_{n=1}^{m} a_n J_n' \right\} = \frac{-\pi}{2\rho V} \left\{ \frac{\partial}{\partial x} W(x,y) \right\}_{y=y_t} \tag{5.7}$$

where $k' = \frac{y_t}{y_l}$, $y_t' = \frac{dy_t}{dx}$ and $y_l' = \frac{dy_l}{dx}$, and

$$\left.\begin{aligned}
L &= \int_0^{y_t} \frac{1-\frac{\eta}{b}}{\log\frac{\eta}{b}} \frac{\eta d\eta}{\sqrt{(y_l^2-\eta^2)(y_t^2-\eta^2)}}; \quad L' = \int_0^{y_t} \frac{d}{d\eta}\left\{ \frac{1-\frac{\eta}{b}}{\log\frac{\eta}{b}} \eta \sqrt{y_l^2-\eta^2} \right\} \frac{\eta d\eta}{\sqrt{y_t^2-\eta^2}} \\
M &= \int_0^{y_t} \frac{\eta^2 d\eta}{\sqrt{(s^2-\eta^2)(y_l^2-\eta^2)(y_t^2-\eta^2)}}; \quad M' = \int_0^{y_t} \frac{d}{d\eta}\left\{ \frac{\eta^2\sqrt{y_l^2-\eta^2}}{\sqrt{s^2-\eta^2}} \right\} \frac{\eta d\eta}{\sqrt{y_t^2-\eta^2}} \\
J_n &= \frac{1}{b^n}\int_0^{y_t} \frac{\eta^{n+1}}{\sqrt{(y_l^2-\eta^2)(y_t^2-\eta^2)}} d\eta; \quad J_n' = \frac{1}{b^n}\int_0^{y_t} \frac{d}{d\eta}\left\{ \eta^{n+1}\sqrt{y_l^2-\eta^2} \right\} \frac{\eta d\eta}{\sqrt{y_t^2-\eta^2}}
\end{aligned}\right\} \tag{5.8}$$

The integrals M, M', J_n and J_n' can be calculated exactly (see lit. 17, section 6); for the determination of the integrals L and L', however, a numerical procedure must be used; this is performed in lit. 17 section 7). The results of the reduction of the integrals M, M', J_n and J_n' are given in table 1. Equation (5.7) contains x as the only variable and is valid for any x with $x > c$.

By satisfying equation (5.7) in $(m+1)$ points of the x-axis, a system of $(m+1)$ linear algebraic equations are obtained for the unknown constants $a_0, a_1, \ldots a_m$; solving this system one gets the constants $a_0, a_1, \ldots a_m$ and finally the functions $S(y_t, y_l)$ given by:

$$S(y_t, y_l) = a_0 M + \sum_{n=1}^{m} a_n J_n + CL. \tag{5.9}$$

The $(m+1)$ points of the x-axis in which equation (5.7) should be satisfied must of course be chosen in an appropriate way; the solution can be checked by substituting the values obtained for $a_0 \ldots a_m$ in equation (5.7) and comparing left and right hand sides of this equation for arbitrary values of x.

6 Solution of the system of equations.

6.1 *The system of equations.*

The system of linear algebraic equations for the unknown constants $a_0, \ldots a_m$ which is obtained by satisfying equation (5.7) in $(m+1)$ points of the x-axis can be written in the form:

$$a_0 \left\{ y_l' E(k) M + y_t' k' K(k) \frac{1}{y_t^2} M' \right\} + \sum_{n=1}^{m} a_n \left\{ y_l' E(k) J_n + y_t' k' K(k) \frac{1}{y_t^2} J_n' \right\} =$$
$$- \frac{\pi}{2\rho V} \left\{ \frac{\partial}{\partial x} W(x,y) \right\}_{y=y_t} - C \left\{ y_l' E(k) L + y_t' k' K(k) \frac{1}{y_t^2} L' \right\}; \; x > c. \tag{6.1}$$

It appears in lit. 17 (sections 6 and 7) that the integrals M', L' and J_n' contain a factor y_t^2 and hence the factor $\frac{1}{y_t^2}$ occurring in equation (6.1) is cancelled.

The integrals J_n and J_n' can be written according to table 1 as

$$J_n = \left(\frac{y_l}{b}\right)^n F_n(k') \text{ and } J_n' = y_t^2 \left(\frac{y_l}{b}\right)^n F_n'(k'). \tag{6.2}$$

Here the planform of the wing is represented only by the factor $\left(\frac{y_l}{b}\right)^n$; hence for wings with different planforms the functions $F_n(k')$ and $F_n'(k')$ remain the same. This means a reduction of the amount of calculations, which has to be performed, when another wing-planform is considered. Therefore numerical values of $F_n(k')$ and $F_n'(k')$ for $k' = 0(0.1)1$ and $n = 1(1)5$ are given in table 2.

For wings with straight edges $\frac{y_l}{b}$ can simply be expressed into the parameter k' and into the sweep-ratio γ, denoting the ratio of the slopes of the trailing and leading edges, viz:

$$\frac{y_l}{b} = \frac{\gamma}{\gamma - k'}, \text{ where } \gamma = \frac{y_t'}{y_l'}. \tag{6.3}$$

From, the formulae (6.1), (6.2), (6.3) and the expressions for M, M', L and L', derived in lit. 17 (sections 6 and 7) it is seen that in equation (6.1) the use of k' as cross-sectional parameter is preferable to x and therefore equation (6.1) will be considered as an equation in k'. When $x=e$ is the abscis of the most back-ward point of the wing (see sketches c and d), the interval $c < x < e$ corresponds to the interval $0 < k' < 1$.

6.2 *Tapered wings with straight edges.*

For tapered wings with straight edges whose sweep ratio γ is larger than one and not nearly one the method of calculation of $S(y_t, y_l)$, as described in section 5, can simply be applied.

In section 7 the theory is applied to a flat fully tapered swallow-tail wing at incidence with a sweep ratio $\gamma=2$; the degree of the polynomial $P\left(\frac{\eta}{b}\right)$ is taken equal to 5. After the determination of the constants $a_0, a_1 \ldots a_5$ the function $S(y_t, y_l)$ is calculated in the interval $0 < k' < 1$ by aid of formula (5.9).

6.3 *Wings without taper or with small taper and with straight edges.*

For wings without taper ($\gamma=1$) or with small taper (γ nearly one), the method for numerically calculating $S(y_t, y_l)$ is somewhat different from that described in 6.2.

For untapered wings the term $a_0 \dfrac{\frac{\eta}{b}}{\sqrt{\left(\frac{s}{b}\right)^2-\left(\frac{\eta}{b}\right)^2}}$ used in the approximation (5.5) of $g(\eta)$ can be omitted, because the function $g(\eta)$ remains the same within the interval $0 \leqq \eta \leqq y_t(d)$, when the wing

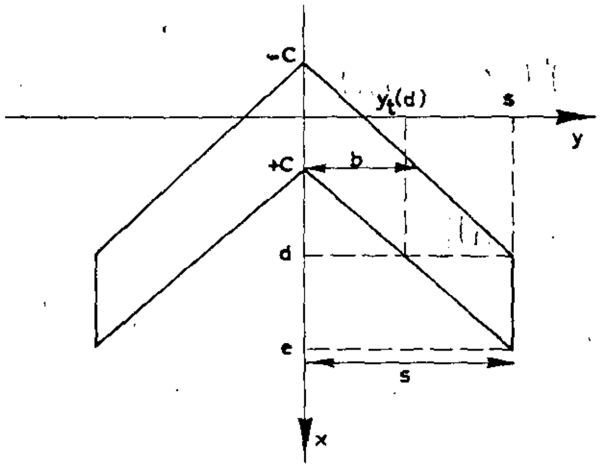

Sketch e.

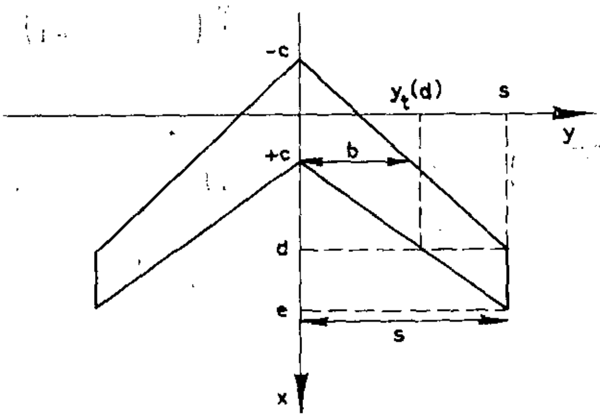

Sketch f.

is not cut off at the tip, but stretches outward to infinity (see sketch e). Also for wings with a small taper (see sketch f) the term

$$a_0 \frac{\frac{\eta}{b}}{\sqrt{\left(\frac{s}{b}\right)^2-\left(\frac{\eta}{b}\right)^2}}$$

can mostly be omitted, because the singularity in $g(\eta)$ at $\eta=s$ cannot strongly influence the function $g(\eta)$ for $0 \leqq \eta \leqq y_t(d)$, since $y_t(d)$ is mostly much smaller than the ordinate $\eta=s$ of the singular point.

Hence for untapered wings and for wings with small taper a simplification of equation (6.1) can be made, since it is allowed to omit the first term and equation (6.1) becomes:

$$\sum_{n=1}^{m} a_n \left\{ y_l' E(k) J_n + y_t' k' K(k) \frac{1}{y_t^2} J_n' \right\} = -\frac{\pi}{2\rho V} \left\{ \frac{\partial}{\partial x} W(x,y) \right\}_{y=y_t} - C \left\{ y_l' E(k) L + y_t' k' K(k) \frac{1}{y_t^2} L' \right\} \qquad (6.4)$$

The coefficients of the unknown constant a_n, however, contain the factor $\left(\frac{y_l}{b}\right)^n = \left(\frac{\gamma}{\gamma - k'}\right)^n$ and hence they become very large in comparison with the known right hand side of equation (6.4), even when k' is not near to the value 1.

In this case it is very difficult to satisfy approximately equation (6.4) in the interval $0 < k' < \frac{y_t(d)}{s}$ by satisfying this equation exactly for m chosen values of k'.

Instead of the polynomial $P\left(\frac{\eta}{b}\right)$, used in the approximation (5.5) of $g(\eta)$, the following polynomial will be used now:

$$P^*\left(\frac{\eta}{t}\right) = \left(1 - \frac{\eta}{t}\right) \sum_{n=1}^{m-1} a_n^* \left(\frac{\eta}{t}\right)^n$$

where t is some parameter which has to be chosen properly.

The approximation (5.5) of the function $g(\eta)$ becomes now:

$$g(\eta) = C \frac{1 - \frac{\eta}{b}}{\log \frac{\eta}{b}} + \left(1 - \frac{b}{t} \frac{\eta}{b}\right) \sum_{n=1}^{m-1} \overline{a}_n \left(\frac{\eta}{b}\right)^n \tag{6.5}$$

where

$$\overline{a}_n = \left(\frac{b}{t}\right)^n a_n^*.$$

Instead of the integrals J_n and J_n' occurring in (6.4), a linear combination of J_n and J_{n+1}, respectively J_n' and J'_{n+1}, will now appear; viz:

$$\left(\frac{b}{t}\right)^n \left(J_n - \frac{b}{t} J_{n+1}\right) \quad \text{and} \quad \left(\frac{b}{t}\right)^n \left(J_n' - \frac{b}{t} J'_{n+1}\right) \tag{6.6}$$

and equation (6.4) becomes:

$$\sum_{n=1}^{m-1} \overline{a}_n \left\{ y_l' E(k) \left(J_n - \frac{b}{t} J_{n+1}\right) + y_t' k'K(k) \frac{1}{y_t^2} \left(J_n' - \frac{b}{t} J'_{n+1}\right)\right\} =$$

$$= - \frac{\pi}{2\rho V} \left\{\frac{\partial}{\partial x} W(x, y)\right\}_{y=y_t} - C \left\{ y_l' E(k) L + y_t' k'K(k) \frac{1}{y_t^2} L' \right\} \tag{6.7}$$

$\frac{b}{t}$ has now to be chosen in such a manner, that the coefficients of $\overline{a}_n$ do not become very large in comparison with the known right hand side of equation (6.7).

By satisfying (6.7) for $(m-1)$ values of k' the constants $\overline{a}_n$ can be calculated and consecutively the function $S(y_t, y_l)$ is determined by the formula

$$S(y_t, y_l) = \sum_{n=1}^{m-1} \overline{a}_n \left(J_n - \frac{b}{t} J_{n+1}\right) + C L. \tag{6.8}$$

This procedure for the determination of $S(y_t, y_l)$ is used in section 7, where the theory is applied to a flat untapered wing at incidence, with wing semi-span equal to 2b. In this case the parameter $\frac{b}{t}$ is chosen equal to $^1/_3$ and m is taken equal to 5.

7 Application of the theory to swept flat wings at given angle of attack.

The theory of the preceding section will now be applied to two swept flat wings at a given angle of attack α; the wings have straight edges, one without taper and the other with taper. The wing without taper has a semispan equal to 2b and the wing with taper is a so called "swallow tail" for which the sweep ratio γ is taken equal to 2. The slope of the leading edge $\frac{dy_l}{dx}$, denoted by y_l', is not fixed, so that strictly speaking two families of wing planforms are considered; a member of both families is shown in figure 1.

7.1 *The lift distribution.*

The downwash $w(x, y)$, prescribed on the wings, is given by $w = \alpha V$. For $-c < x < +c$ the lift distribution on both wings is given by formula (3.4) viz:

$$p(x, y) = 4\,\alpha\, q\, y_l' \frac{y_l}{\sqrt{y_l^2 - y^2}}, \tag{7.1}$$

where q denotes the dynamic pressure and equals $\frac{1}{2}\rho V^2$.

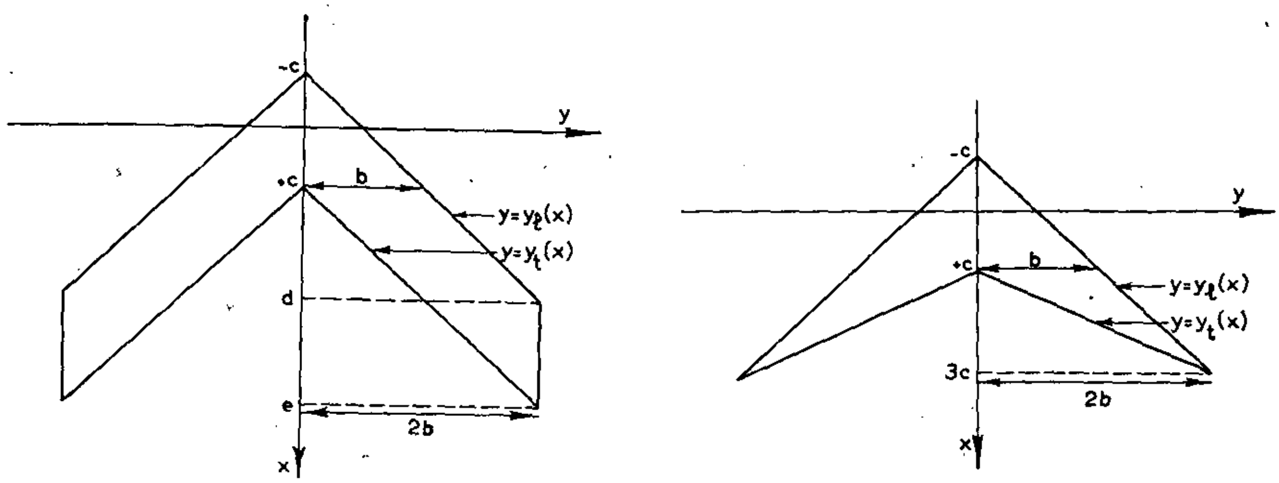

Untapered wing; $\gamma = 1$. Tapered wing; $\gamma = 2$.

Fig. 1

For $x > c$ the influence of the wake must be taken into account and formula (4.9) has to be used; therefore the function $\dfrac{\partial W(x, y)}{\partial x}$ has to be determined first. In accordance with the formulae (3.14) and (4.1) $W(x, y)$ becomes

$$W(x, y) = + \frac{4\,\alpha\rho V^2}{\pi} \int\limits_{y_t}^{y_l} \sqrt{\frac{y_l^2 - \eta^2}{\eta^2 - y_t^2}}\, \eta \left\{ \int\limits_{y}^{y_l} \sqrt{\frac{\eta'^2 - y_t^2}{y_l^2 - \eta'^2}}\, \frac{d\eta'}{\eta'^2 - \eta^2} \right\} d\eta.$$

In lit. 17 (section 8) this expression is reduced to the simple form:

$$W(x, y) = 4\,\alpha q\, y_l \left\{ E(\psi, k) - k'^2 F(\psi, k) \right\} \tag{7.2}$$

where

$$\psi = \sin^{-1} \sqrt{\frac{y_l^2 - y^2}{y_l^2 - y_t^2}} \quad \text{and} \quad k' = \frac{y_t}{y_l}.$$

Differentiation with respect to x yields:

$$\frac{\partial W(x, y)}{\partial x} = 4\,\alpha q \left[y_l' \left\{ E(\psi, k) + \frac{y}{y_l} \sqrt{\frac{y^2 - y_t^2}{y_l^2 - y^2}} \right\} - y_t' k' F(\psi, k) \right]. \tag{7.3}$$

Putting $y = y_t$ gives

$$\left[\frac{\partial W(x, y)}{\partial x} \right]_{y = y_t} = 4\,\alpha q \left\{ y_l' E(k) - y_t' k' K(k) \right\}. \tag{7.4}$$

Substitution of (7.3) and (7.4) into (4.9) gives finally the pressure on the wings, viz:

$$p(x, y) = 4\,\alpha q\, y_l' \left\{ 1 + \frac{S(y_t, y_l)}{\alpha V \pi} \right\} \left\{ E(\psi, k) - \frac{E(k)}{K(k)} F(\psi, k) + \frac{y}{y_l} \sqrt{\frac{y^2 - y_t^2}{y_l^2 - y^2}} \right\} \tag{7.5}$$

which is the same expression as found by Mangler in ref. (10) and by Mirels in ref. (11).
Putting

$$1 + \frac{S(y_t, y_l)}{\alpha V \pi} = S^*(x), \tag{7.6}$$

$S^*(x)$ corresponds with the function $H(x)$ of Mangler and the function $S(x)$ of Mirels.

7.2 The untapered wing.

For the wing without taper the function $S(y_t, y_l)$ is needed only for $0 < k' < \frac{1}{2}$ (see fig. 1) and is determined by aid of the procedure described in section (6.3). After substitution of (7.4) in equation (6.7) it appears that both sides of this equation can be divided by $y_t' = y_l'$ and equation (6.7) is independent of the angle of sweep of the wing. Hence $S(y_t, y_l)$ is also independent of the angle of sweep. By aid of (5.3) the coefficient C in the right hand side of (6.7) appears to be $\alpha V\pi$. By satisfying equation (6.7) with $m = 5$ and $\frac{b}{t} = {}^1/_3$ for $k' = 0.1$; 0.2; 0.4 and 0.5 a system of four linear equations for the constants $\bar{a}_1$, $\bar{a}_2$, $\bar{a}_3$ and $\bar{a}_4$ is obtained. After solving $\bar{a}_1$, $\bar{a}_2$, $\bar{a}_3$ and $\bar{a}_4$ their numerical values have been substituted again into equation (6.7) and both sides of this equation were calculated for $k' = 0.3$; the error appears to be $4\frac{1}{2}\,\%$.

Consecutively $S(y_t, y_l)$ is calculated by aid of formula (6.8). In figure 2 the function $S^*(k') = 1 + \dfrac{S(y_t, y_l)}{\alpha V\pi}$ is plotted against $\dfrac{y_l}{b} = \dfrac{1}{1-k'}$ (see form. (6.3)).

In the same figure the values of $S^*(k')$ as found by MANGLER (ref. 10) and MIRELS (ref. 11) have been inserted and moreover also the asymptotic values of $S^*(k')$ for small values of k' or what is the

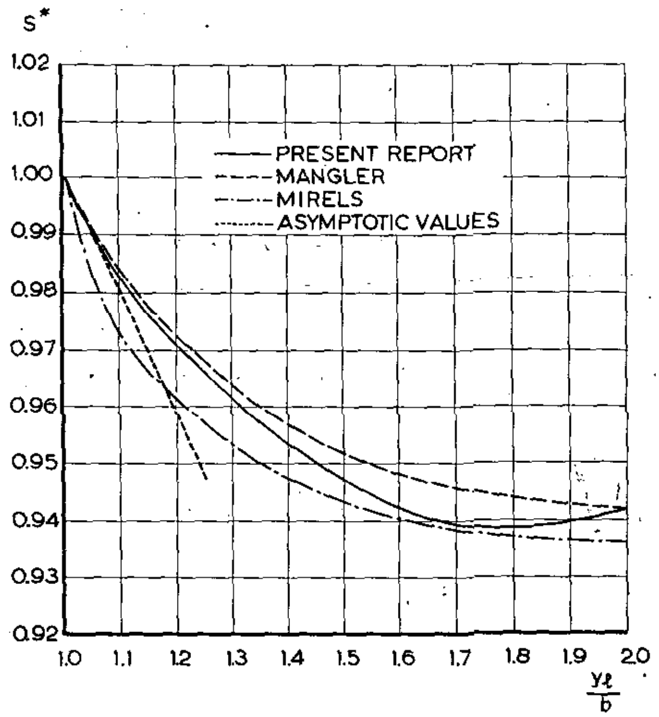

Fig. 2. The function $S^*(k')$; $\gamma = 1$.

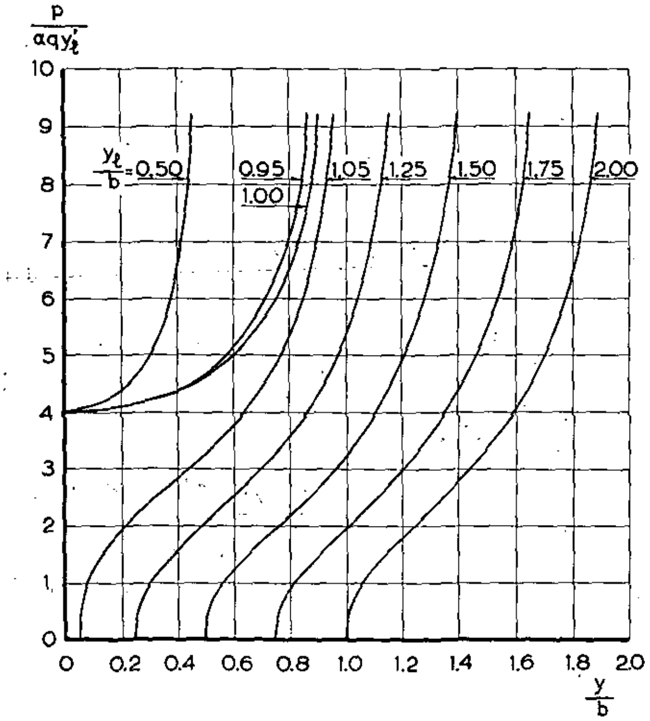

Fig. 3. Lift-distribution on the wing; $\gamma = 1$.

same, for x in the neighbourhood of $x = c$, i. e. the abscis of the kink in the trailing edge. The asymptotic approximation of $S^*(k')$ is given by the expression:

$$S^*(k') = 1 + \frac{S(y_t, y_l)}{\alpha V\pi} = 1 + 4\int_0^{\frac{k'}{4}} \frac{d\tau}{ln\,\tau} + 0(k'^2) = 1 + 4\,li\left(\frac{k'}{4}\right) + 0(k'^2). \tag{7.7}$$

This formula has been derived from formula (4.9) of section 4 of lit. 17, where the asymptotic expression for $S(y_t, y_l)$ is determined for arbitrarily given downwash.

Comparing the three curves for $S^*(k')$ it appears that the values of $S^*(k')$, presented in this report, agree quite well with the results of MANGLER and MIRELS. The values, obtained by MANGLER and by the present authors, approximate very good the asymptotic values, which approximation is not so good for MIRELS's results.

Substitution of the numerical values of $S^*(k')$ in (7.5) yields at last the pressure distribution on the wing for $x > c$.

When x is larger than the abscis d of the most forward point of the tip y_l' equals zero and hence the pressure on the wing vanishes.

In figure 3 the lift distribution $\dfrac{p(x, y)}{\alpha q y_l'}$ in several cross sections of the wing, denoted by several values of $\frac{y_l}{b} = \frac{1}{1-k'}$, is plotted against the spanwise coordinate $\frac{y}{b}$. Since the angle of sweep of the wing can still be arbitrarily chosen, figure 3 gives the lift distribution for a family of untapered wings.

The wing section at $x=c$ is an important section from the theoretical point of view, as for $x<c$ the lift distribution is given by (7.1) and for $x>c$ by (7.5); therefore the right hand side of formula (7.5) will be investigated for x going to c, or what is the same for y_t or k' going to zero.

The limit of the right hand side of equation (7.5) for k tending to 1 and $y \neq 0$ is

$$\lim_{y_t \to 0}\left[4\,\alpha q\, y_l' \left\{\sin\psi + \frac{y}{y_t}\sqrt{\frac{y^2-y_t^2}{y_l^2-y^2}}\right\}\right] = 4\,\alpha q\, y_l' \left\{\frac{1}{b}\sqrt{b^2-y^2} + \frac{y^2}{b}\,\frac{1}{\sqrt{b^2-y^2}}\right\} =$$

$$+\,4\,\alpha q\, y_l' \frac{b}{\sqrt{b^2-y^2}}, \text{ and hence } p(c^+,y) = 4\,\alpha q\, y_l' \frac{b}{\sqrt{b^2-y^2}}, \text{ provided } y \neq 0. \tag{7.8}$$

Comparing (7.8) and (7.1) leads to the conclusion, that the lift distribution in the cross-section $x=c$ is continuous in x, provided $y \neq 0$.

For $y=0$ and $x=c$, i.e. at the kink of the trailing edge, according to (7.1), the wing pressure equals $4\,\alpha q\, y_l'$; according to (7.5), however, $\lim_{y_t \to 0} p(x, y_t) = 0$, since the KUTTA condition is satisfied at the trailing edge; hence the kink of the trailing edge is a singular point for the lift distribution on the wing.

The behaviour of the pressure distribution in the neighbourhood of the section $x=c$ is illustrated by sketch g. Integrating the expressions (7.1) and (7.5) to the spanwise coordinate y over the wing surface yields the lift distribution per unit chord, denoted by $\frac{dL}{dx}$ and hence:

$$\frac{dL}{dx} = 8\,\alpha q\, y_l'\, y_l \int_0^{y_l} \frac{dy}{\sqrt{y_l^2-y^2}} = 4\,\pi\alpha\, y_l'\, q b\, \frac{y_l}{b} \tag{7.9}$$

for $-c \leqq x \leqq +c$ and

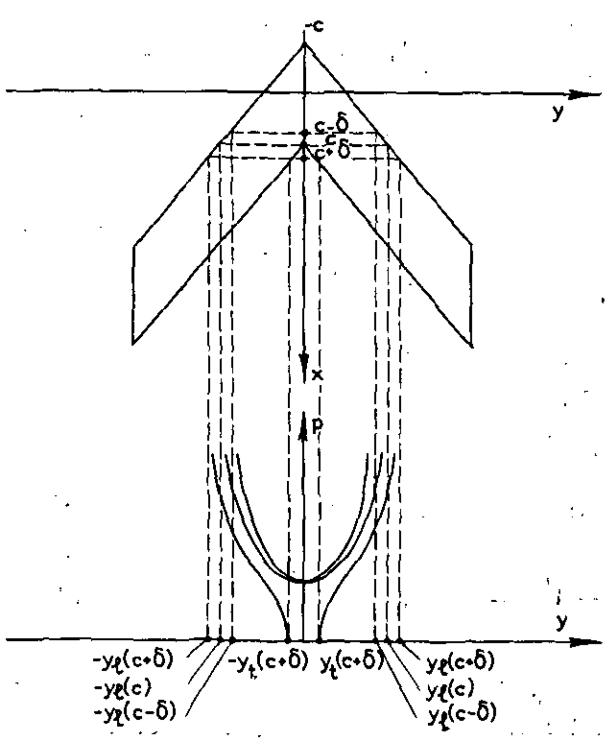

Sketch g.

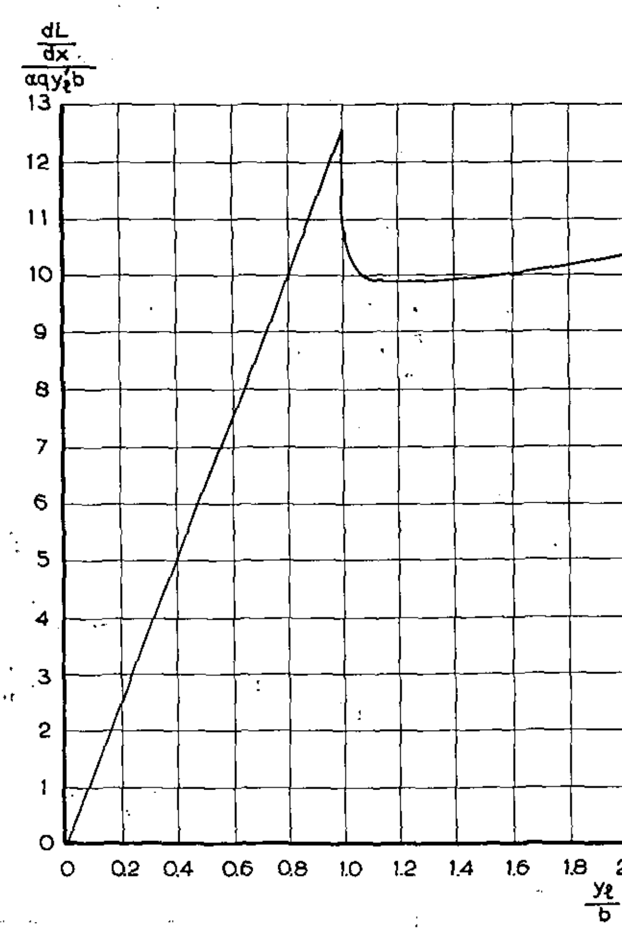

Fig. 4. Lift distribution per unit chord; $\gamma = 1$.

$$\frac{dL}{dx} = 8\,\alpha q\, y_l'\, S^*(k') \cdot \int_{y_t}^{y_l} \left\{ E(\psi, k) - \frac{E(k)}{K(k)}\, F(\psi, k) + \frac{y}{y_l} \sqrt{\frac{y^2 - y_t^2}{y_l^2 - y^2}} \right\} dy$$

for $c \leqq x \leqq d$.

In lit. 17 (section 9) the integral is reduced to the simple form:

$$\frac{\pi}{2}\, y_l \left\{1 - \frac{E(k)}{K(k)}\right\} \text{ and } \frac{dL}{dx} = 4\,\pi\,\alpha q\, y_l'\, b\, \frac{y_l}{b}\, S^*(k') \left\{1 - \frac{E(k)}{K(k)}\right\} \text{ for } c \leqq x \leqq d. \tag{7.10}$$

A plot of the function $\dfrac{\frac{dL}{dx}}{\alpha q y_l' b}$ against $\dfrac{y_l}{b}$ is given in figure 4; the lift per unit chord shows a vertical tangent at $\dfrac{y_l}{b} = 1$, i.e. at the cross section $x = c$ through the kink of the trailing edge; although the lift distribution per unit chord is continuous at the cross section $x = c$, nevertheless it falls off rapidly after this cross section; for larger values of $\dfrac{y_l}{b}$ it increases again. When the wing is not cut off at the tips but stretches outward to infinity, the limit of $\dfrac{dL}{dx}$ can be considered for k' approximating 1, i.e. for y_t and y_l tending to infinity.

Due to the fact that the vorticity vector in the wake and hence also the function $g(y)$ vanishes for y tending to infinity the function $S(y_t, y_l)$ will vanish also for y_t and y_l tending to infinity and hence $\lim\limits_{k' \to 1} S^*(k') = 1$. Therefore $\lim\limits_{k' \to 1} \dfrac{dL}{dx} = 4\,\pi\,\alpha q\, y_l' \lim\limits_{k' \to 1} y_l \left\{1 - \dfrac{E(k)}{K(k)}\right\} =$

$$2\,\pi\,\alpha q\, y_l' \lim_{k \to 0} (y_l\, k^2) = 2\,\pi\,\alpha q\, y_l' \lim_{y_l \to \infty} \frac{y_l^2 - y_t^2}{y_l}.$$

Since $y_l - y_t$ is constant and equal to b, the limit becomes

$$\lim_{k' \to 1} \frac{dL}{dx} = 4\,\pi\,\alpha q\, y_l'\, b.$$

which, incidentally, is the same value as is reached by the function $\dfrac{dL}{dx}$ for $k' = 0$. The last formula could of course also be obtained by simple two-dimensional wing theory.

Integration of $\dfrac{dL}{dx}$ with respect to x yields at last the total lift L on the wing, viz.:

$$L = \int_{-c}^{d} \frac{dL}{dx}\, dx = \frac{b}{y_l'} \int_0^2 \frac{dL}{dx}\, d\left(\frac{y_l}{b}\right) = 4\,\pi\,\alpha q\, b^2 \left[\tfrac{1}{2} + \int_1^2 \frac{y_l}{b}\, S^*\left(\frac{y_l}{b}\right)\left\{1 - \frac{E(k)}{K(k)}\right\} d\left(\frac{y_l}{b}\right)\right]. \tag{7.11}$$

The integral is calculated numerically and the result is $L = 16.431\, \alpha q b^2$. Hence the derivative $\dfrac{dC_L}{d\alpha} = 16.431\, \dfrac{b^2}{8\, bc} = 4.108\ y_l'$.

Thus for the family of untapered swept wings the aerodynamic derivative $\dfrac{dc_L}{d\alpha}$ is proportional to the slope of the leading edge y_l' and the proportionality factor equals 4.108.

The aerodynamic centre is given by the formula:

$$\frac{x_{A.c}}{c} = \frac{\int_{-c}^{d} \frac{x}{c}\, \frac{dL}{dx}\, dx}{L}.$$

After substitution of $\dfrac{x}{c} = 2\,\dfrac{y_l}{b} - 1$ the expression is evaluated in the form:

$$\frac{x_{A.c}}{c} = \frac{8\,\pi\alpha q b^2}{L} \left[{}^1/_3 + \int_1^2 \left(\frac{y_l}{b}\right)^2 S^*\left(\frac{y_l}{b}\right)\left\{1 - \frac{E(k)}{K(k)}\right\} d\left(\frac{y_l}{b}\right)\right] - 1; \tag{7.12}$$

the integral is calculated numerically and the result is $\dfrac{x_{AC}}{c} = 1.3897$. Thus for the family of untapered swept wings the location of the aerodynamic centre is independent of the angle of sweep of the wing.

7.3 *The tapered wing.*

For the swallow tail wing the function $S(y_t, y_l)$ is needed for $0 < k' < 1$ (see fig. 1) and is determined by the procedure described in sections 5 and 6.2. The expression for $\left[\frac{\partial W(x,y)}{\partial x}\right]_{y=y_t}$, given by (7.4), is substituted into equation (6.1); after dividing by y_l' it appears that this equation depends on the sweep ratio $\gamma = \frac{y_t'}{y_l'}$, but not on the angle of sweep of the wing. Hence this is also the case for $S(y_t, y_l)$.

By satisfying equation (6.1) with $m = 5$ and $\gamma = 2$ for $k' = 0.1$; 0.2; 0.4; 0.6; 0.8 and 0.9 a system of six linear equations for the constants $a_0, a_1, \ldots a_5$ is obtained. The constant C in the right hand side of equation (6.1) is determined by the formulae (5.3) and (7.4); for $\gamma = 2$ this constant is equal to $\frac{1}{2}\alpha V\pi$. After solving the constants their numerical values are substituted again into equation (6.1) and both sides of this equation are calculated for $k' = 0.3$, 0.5 and 0.7; the error appears to be 2 %, 3 % and 8 % respectively.

Consecutively the function $S(y_t, y_l)$ is calculated by aid of formula (5.9).

The asymptotical values of $S^*(k')$ for k' tending to zero are given by the formula:

$$S^*(k') = 1 + \frac{S(y_t, y_l)}{\alpha V\pi} = 1 + \frac{4}{\gamma}\int_0^{\frac{k'}{4}} \frac{d\tau}{ln\,\tau} +$$

$$+ 0(k'^2) = 1 + \frac{4}{\gamma}\; li\left(\frac{k'}{4}\right) + 0(k'^2) \qquad (7.13)$$

this expression is derived from formula (4.9) of section 4 of lit. 17.

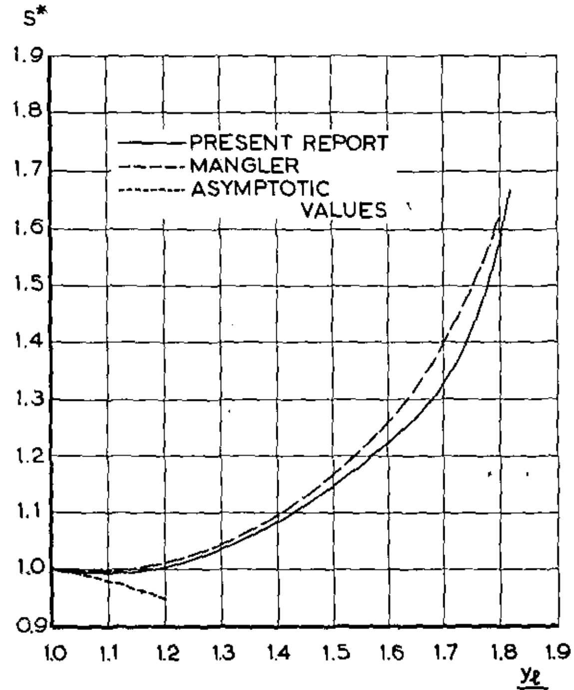

Fig. 5. The function $S^*(k')$; $\gamma = 2$.

In figure 5 the function $S^*(k')$ is plotted again against the cross sectional parameter $\frac{y_l}{b}$, which is equal to $\frac{\gamma}{\gamma - k'} = \frac{2}{2 - k'}$.

In the same figure the corresponding results of Mangler (ref. (10)) and the asymptotical values are inserted and the agreement is quite satisfactory. Because Mirels has not carried out a calculation for a tapered wing, there is no comparison possible with a corresponding result of Mirels. Substitution of the numerically obtained values of $S^*(k')$ into (7.5) finally yields the lift distribution on the wing for $x > c$.

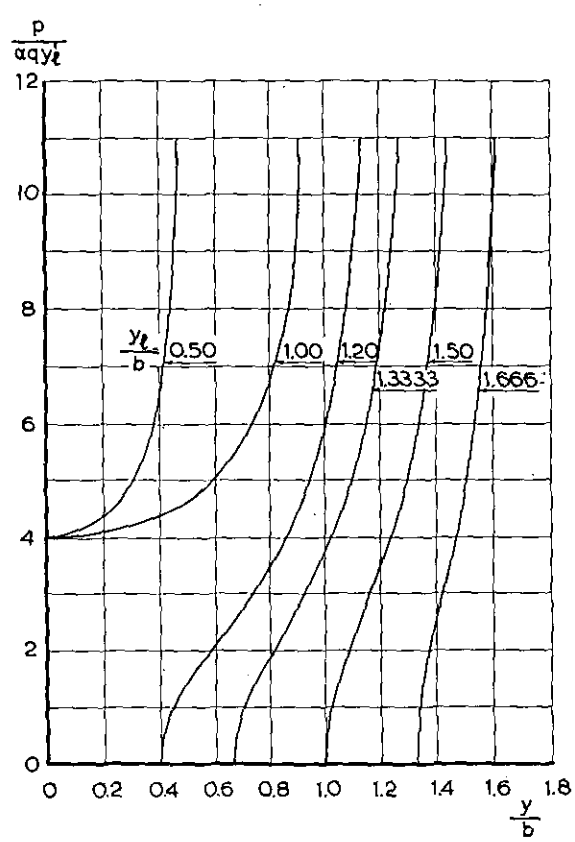

Fig. 6. The lift distribution on the wing; $\gamma = 2$.

In figure 6 the lift distribution $\frac{p(x,y)}{\alpha q\, y_l'}$ in several cross sections of the wing, denoted by several values of $\frac{y_l}{b}$, is plotted against the spanwise coordinate $\frac{y}{b}$. Since the angle of sweep of the wing can still be arbitrarily chosen, figure 6 gives in the same way as figure 3, the lift distribution for a family of swept wings with $\gamma = 2$.

Finally, figure 7 shows the plot of the lift distribution per unit chord, which is given by the same formulae as are valid for the untapered wing, viz: (7.9) and (7.10). Integration of $\frac{dL}{dx}$ with respect to x from $-c$ to $+3c$, see figure 1, yields the total lift on the wing; L is determined by aid of (7.11), where the integral is calculated numerically; the result is $L = 12.5239\, qb^2\alpha$. Hence the aerodynamic derivative $\frac{dC_L}{d\alpha}$ is equal to $12.5239\, \frac{b^2}{4\,bc} = 6.2620\; y_l'$. The aerodynamic centre is also calculated in the same way as for

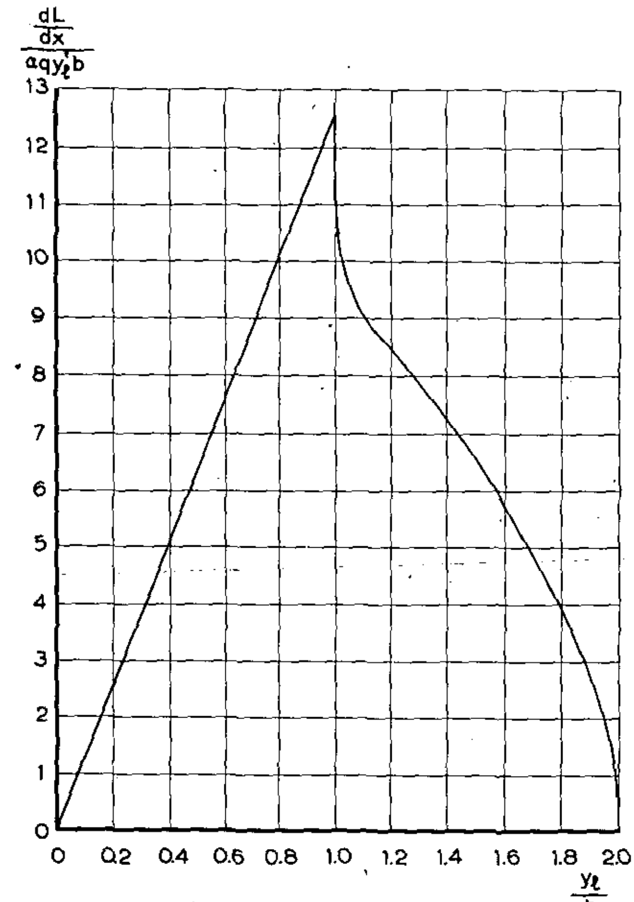

Fig. 7. Lift distribution per unit chord; $\gamma = 2$.

the untapered wing and the result, obtained by aid of formula (7.12), is $\frac{x_{A.C}}{c} = 1.0454$.

Thus also for the family of swallow tail wings the aerodynamic derivative $\frac{dC_L}{d\alpha}$ is proportional to the slope of the leading edge and the centre of pressure is independent of the angle of sweep of the wing; this result holds of course for any family of swallow tail wings with constant sweep ratio γ. The numerical values for the aerodynamic derivative $\frac{dC_L}{d\alpha}$ and for the aerodynamic centre x_{AC} agree quite well with the results of TRUCKENBRODT (lit. 18).

8 Recapitulation of the theory and conclusions.

Expressions for the lift distribution on swept-back wings without thickness have been obtained for any given symmetrical camber and twist of the wing.

In cross sections perpendicular to the direction of the undisturbed flow the lift distribution on the wing is given by formula (3.3) when there is no wake and by formula (4.9) or (4.10) when there is a wake present.

In those parts of the wing where the load distribution is given by formula (3.3) or (4.10) the determination of this load distribution involves no difficulty at all, whatever may be the given downwash distribution or the planform of the wing.

In those parts of the wing, however, where the load distribution is given by formula (4.9) the wing pressure apart from the factor $S(y_t, y_l)$ can also be calculated without much difficulties.

The determination of the function $S(y_t, y_l)$ involves the largest part of the amount of numerical calculations which has to be performed in order to obtain the lift distribution on the wing.

The determination of this function $S(y_t, y_l)$ is reduced in section 5 to the solution of a linear system of algebraïc equations, see formula (6.1). When the function $S(y_t, y_l)$ has already been calculated for some given wing planform with given downwash distribution on the wing, the determination of $S(y_t, y_l)$ for a wing with the same planform but with another given downwash distribution is readily performed, since only the first term of the right hand side of equation (6.1) is changed and hence only the known terms of the linear system of algebraïc equations have obtained other values. Thus when the load distribution for some wing with given camber and twist is already known, the determination of the load distribution on a wing with the same planform but with another camber and twist does not involve much extra numerical calculations.

When however the wing planform is also changed, the whole system of linear equations (6.1) is altered, since the coefficients of the unknowns a_0, a_1, ... a_m and the known terms have now obtained other values.

The integrals M, M', J_n, J_n', L and L' must again be calculated; the calculation of M, M', J_n and J_n' is fairly simple, since they can be calculated exactly (see table 1) and moreover J_n and J_n' can be written in the form (6.2), but the total numerical calculation of L and L' has to be carried out again.

The theory has been applied to two examples viz. a flat wing without taper and a flat wing with taper, both at constant angle of attack.

The results obtained by aid of the method presented in this report are satisfactory and show good agreement with the results obtained by aid of other methods (lit. 10 and 11).

9 List of references.

1. MUNK, M. M., The aerodynamic forces on airship hulls. NACA Report 184, 1924.
2. JONES, R. T., Properties of low-aspect-ratio pointed wings at speeds below and above the speed of sound. NACA Report 835, 1946; also NACA T. N. 1032, 1946.
3. WARD, G. N., Supersonic flow past slender pointed bodies. Quart. J. Mech. and Appl. Math. 2 (1949), 75—97.

4. ADAMS MAC C., SEARS, W. R., Slender-body theory. Review and extension. J. Aeronaut. Sci. 20 (1953), 85—98.

5. HEASLET, M. A., LOMAX, H., SPREITER, J. R., Linearized compressible-flow theory for sonic flight speeds. NACA Report 956, 1950; also NACA T. N. 1824, 1949.

6. LOMAX, H., HEASLET, M. A., Linearized lifting-surface theory for swept-back wings with slender plan forms. NACA T. N. 1992, 1949.

7. ROBINSON, A., Aerofoil theory for swallow tail wings of small aspect ratio. Aero. Quart., **IV**, part 2 (Aug. 1952), 69—82.

8. MIRELS, H., Lift of highly swept wings. J. Aeronaut. Sci., **20** (Mar. 1953), 210—211.

9. EICHELBRENNER, E. A., *Théorie des corps élancés.* O.N.E.R.A. Publ. 68, 1954.

10. MANGLER, K. W., *Calculation of the pressure distribution over a wing at sonic speeds.* R. A. E. Rep. Aero 2439, Sept. 1951.

11. MIRELS, H., *Aerodynamics of slender wings and wing-body combinations, having swept trailing edges.* NACA T. N. 3105, 1954.

12. MANGLER, K. W., Calculation of the load distribution over a wing with arbitrary camber and twist at sonic speed. R. A. E. Rep. Aero 2515, Aug. 1954.

13. ECKHAUS, W., On the theory of oscillating airfoils of finite span in subsonic flow. N.L.L. Rep. F. 153, 1954.

14. SÖHNGEN, H., Die Lösungen der Integralgleichung $g(x) = \frac{1}{2\pi} \oint_{-a}^{+a} \frac{f(\xi)}{x-\xi}\, d\xi$ *und deren Anwendung in der Tragflügeltheorie.* Math. Zeitschrift **45**, 1939.

15. MUSKHELISHVILI, N. I., Singular integral equations. Groningen, Noordhof, 1954.

16. SCHMEIDLER, W., Integralgleichungen mit Anwendungen in Physik und Technik I. Leipzig, Akademische Verlagsgesellschaft, 1950.

17. ECKHAUS, W., DE JAGER, E. M., Linearized theory of lifting sweptback wings at sonic speed (Derivations of *formulae*). N.L.L. Techn. Report F. 206a, 1957.

18. TRUCKENBRODT, E., Ein Verfahren zur Berechnung der Auftriebsverteilung an Tragflügeln bei Schallan*strömung. Jahrbuch* der Wissenschaftlichen Gesellschaft für Luftfahrt. E. V. (W. G. L.) 1956.

TABLE 1.

Expressions for the integrals M, M', J_n and J_n'.

$$M = \frac{y_l}{b} \frac{1}{\sqrt{\left(\frac{s}{b}\right)^2 - \left(\frac{y_t}{b}\right)^2}} K(\bar{k}) - \frac{\pi}{2} \Lambda_0 \left(\text{arc sin } \frac{y_t}{s}, \bar{k}\right)$$

$$M' = y_t^2 \left[\frac{y_l}{b} \frac{1}{\sqrt{\left(\frac{s}{b}\right)^2 - \left(\frac{y_t}{b}\right)^2}} \{E(\bar{k}) - K(\bar{k})\} + \frac{\pi}{2} \Lambda_0 \left(\text{arc sin } \frac{y_t}{s}, \bar{k}\right)\right]$$

where $\bar{k} = k' \sqrt{\frac{s^2 - y_l^2}{s^2 - y_t^2}}$, $k' = \frac{y_t}{y_l}$ and Λ_0 is HEUMAN's lambda-function

$$J_1 = \left(\frac{y_l}{b}\right) \{ K(k') - E(k') \}$$

$$J_2 = {}^1/_2 . \left(\frac{y_l}{b}\right)^2 - k' + {}^1/_2 (1 + k'^2) \log \frac{1 + k'}{1 - k'} \Big\}$$

$$J_3 = {}^1/_3 . \left(\frac{y_l}{b}\right)^3 \{(2 + k'^2) K(k') - 2(1 + k'^2) E(k')\}$$

$$J_4 = {}^1/_8 . \left(\frac{y_l}{b}\right)^4 \Big\{ -3 k'(1 + k'^2) + {}^1/_2 (3 + 2 k'^2 + 3 k'^4) \log \frac{1 + k'}{1 - k'} \Big\}$$

$$J_5 = {}^1/_{15} . \left(\frac{y_l}{b}\right)^5 \{(8 + 3 k'^2 + 4 k'^4) K(k') - (8 + 7 k'^2 + 8 k'^4) E(k')\}$$

$$J_1' = y_t^2 \left(\frac{y_l}{b}\right) \{ -K(k') + 2 E(k')\}$$

$$J_2' = {}^1/_2 . y_t^2 \left(\frac{y_l}{b}\right)^2 \Big\{ 3 k' + {}^1/_2 (1 - 3 k'^2) \log \frac{1 + k'}{1 - k'} \Big\}$$

$$J_3' = {}^1/_3 . y_t^2 \left(\frac{y_l}{b}\right)^3 \{(1 - 4 k'^2) K(k') - (1 - 8 k'^2) E(k')\}$$

$$J_4' = {}^1/_8 . y_t^2 \left(\frac{y_l}{b}\right)^4 \Big\{ -k'(1 - 15 k'^2) + {}^1/_2 (1 + 6 k'^2 - 15 k'^4) \log \frac{1 + k'}{1 - k'} \Big\}$$

$$J_5' = {}^1/_{15} . y_t^2 \left(\frac{y_l}{b}\right)^5 \{(2 + 7 k'^2 - 24 k'^4) K(k') - (2 + 8 k'^2 - 48 k'^4) E(k')\}.$$

TABLE 2.

Numerical values of $F_n(k')$ and $F_n'(k')$.

k'	F_1	F_2	F_3	F_4	F_5
0	0	0	0	0	0
0.1	0.00789	0.00067	0.00014	0.00001	0.00007
0.2	0.03190	0.00542	0.00103	0.00017	0.00009
0.3	0.07322	0.01869	0.00502	0.00135	0.00042
0.4	0.13406	0.04572	0.01624	0.00589	0.00220
0.5	0.21829	0.09332	0.04144	0.01883	0.00869
0.6	0.33267	0.17134	0.09155	0.05000	0.02774
0.7	0.49003	0.29614	0.18545	0.11846	0.07694
0.8	0.71895	0.50085	0.36046	0.26450	0.19675
0.9	1.10885	0.88239	0.72241	0.60160	0.50701
1.0	$+\infty$	$+\infty$	$+\infty$	$+\infty$	$+\infty$

k'	F_1'	F_2'	F_3'	F_4'	F_5'
0	1.57080	0	0	0	0
0.1	1.55897	0.19866	0.02345	0.00265	0.00030
0.2	1.52307	0.38920	0.09188	0.02082	0.00461
0.3	1.46161	0.56295	0.19981	0.06801	0.02258
0.4	1.37188	0.71015	0.33735	0.15346	0.06801
0.5	1.24917	0.81865	0.48916	0.27916	0.15504
0.6	1.08541	0.87225	0.63189	0.43536	0.29129
0.7	0.86563	0.84620	0.72878	0.59232	0.46561
0.8	0.55740	0.69465	0.71518	0.68093	0.62138
0.9	0.06285	0.29734	0.43741	0.52164	0.56962
1.0	$-\infty$	$-\infty$	$-\infty$	$-\infty$	$-\infty$